Ceramic-Carbon Nanotube Composites and Their Potential Applications

Submitted by **Hamed Parham**

to the University of Exeter as a thesis for the degree of

Doctor of Philosophy in Engineering

In December 2012

I certify that all material in this thesis which is not my own work has been identified and that no material has previously been submitted and approved for the award of a degree by this or any other University.

Signature: ……..

Abstract

Carbon nanotubes (CNTs) have been the subject of intensive research for nearly two decades, and this is due to their exceptional lightness, large aspect ratio, extraordinary mechanical, electrical, thermal properties and additional multi-functional characteristics. Ceramics have high stiffness and good thermal stability with a relatively low density, and they are an important constituent in the fabrication of advanced composites where high thermal and chemical stability are important. However, brittleness has limited their application in many structural applications. The combination of ceramic (alumina in particular) and CNTs, endeavouring to develop functional composites, offers a very attractive system for research and development. The fabrication of such alumina-CNT composites at bulk scale is therefore highly desirable for industrial applications. However, the synthesis of such composites possesses many technical challenges which need to be addressed. Poor synergy between the matrix and CNTs, potential damage to CNTs, obtaining a uniform and agglomeration-free distribution of CNTs within the matrix, and high cost of CNTs and processes involved in their composite fabrication have proved to be the significant challenges.

In this thesis, the focuses are laid on addressing these issues and on the fabrication of specially engineered composites for particular applications such as filter and composites with improved mechanical properties. In this regard, it has been tried to directly fabricate CNTs in different ceramic matrices based on the application requirements. After that, the critical issues and challenges in the fabrication of these functional materials have been clearly investigated and by introducing novel methods and approaches, it has been tried to solve these problems.

Also, a new polymer-ceramic-CNT composite has been fabricated by using two different thermoset (epoxy resin) and thermoplastic (polyamide 12) matrices. In this regard, good interfacial bonding between the composite elements along with good wettability of ceramic and CNTs with polymer had to be addressed as critical issues and

challenges in the fabrication process. If the adherence at the interface is not strong enough, the material will tear and fail easier. In contrary, a tailored functionalization of CNTs can lead to an improved wettability and as the results, strong interfacial adhesion and bonding between the composite elements. These dominating factors will improve the degree of filling which results in existence of fewer voids inside the composite. These voids will act later as stress points and reduce the composite strength. At the end, the mechanical properties of the fabricated samples have been assessed.

The CNT filters have been tested in the removal of bioorganic (yeast cells) and inorganic (heavy metal ions) contaminants from water, and of particulates from air, and they all showed very promising results. More than 99.6% of the air particles (size ranges from 0.3 to 10 μm) were filtered using 300 mm long CNT filter. A complete removal of heavy metal ions from water was reported particularly for single ion. 98% of the yeast cells were filtered. Different factors involved in the filtration efficiency such as ceramic pore size, length of filters, CNT loading and injection rates have also been discussed.

Furthermore, the mechanical properties (compression test, hardness and impact test) of the composite materials (including ceramic-CNT, epoxy resin-ceramic-CNT and polyamide-ceramic-CNT composites) have been assessed. During impact test, the epoxy resin-ceramic-CNT composite absorbed 117.2% and 32.7% more energy compared to the pure epoxy resin and epoxy resin-ceramic composite, respectively. The epoxy resin-ceramic-CNT composite sustained 40% more elastic deformation before breakage compared to the epoxy resin-ceramic composite as a result of the CNT reinforcement. The addition of CNTs to the polyamide12-ceramic composite increased its yield stress by 41%.

All of these results represent a big leap towards practical applications for the composite reported in the thesis, which may open up new opportunities for CNT engineering at industrial scales, due to the easy fabrication methods introduced and the promising performance they have exhibited.

Presentations and Publications

- Parham, H., Bates, S., Xia, Y. & Zhu, Y. A highly efficient and versatile carbon nanotube/ceramic composite filter. Carbon 54, 215-223, (2013).

- Parham H, Kennedy A, Zhu Y. Preparation of porous alumina–carbon nanotube composites via direct growth of carbon nanotubes. Composites Science and Technology. 2011;71(15):1739-45.

- Parham H, Bates S, Xia Y, Zhu Y. Carbon nanotube composite filter. 3rd International Conference on Nanotechnology: Fundamentals and Applications. Montreal, Quebec, Canada, 7-9 August 2012.

- Carbon nanotube-reinforced porous Al2O3 nanocomposites filters. Tenth international conference on materials chemistry (MC10). Manchester, UK. 4-7 July 2012.

Table of Contents

Table of Figures

Acknowledgments

I would like to express my deepest gratitude to Prof. Yanqiu Zhu for his continued support and guidance during my PhD studies. His attitude, enthusiasm and insight in the research are appreciable and will always be source of inspiration and motivations. His patience and encouragement regarding my education and personal development are greatly appreciated. I would also like to appreciate the guidance, valuable suggestions and advices from Dr. Yongde Xia.

I would like to thank the technical staff in functional material group and workshop. Special thanks to Dr L Wears and Peter Splatt for their expertise using a range of characterisation techniques, in particular SEM and μ-CT scan. I would like to thank Mr David Weightman and Mr Peter Gerry for their technical assistance. I am very grateful for the friendship and help from the group members Mrs Fang Xu, Mr Mohamed Mohamed-Hatta, Dr Hong Chang and Mrs Bahareh Yazdani.

Finally, my deepest gratitude goes to my parents and my wife for their love, caring, understanding and moral support. Admirable thanks to my dear wife for her constant patience, encouragement, and also useful discussions that were always a driving force for me to pursuit my PhD studies.

List of abbreviations

CNT	Carbon nanotube
SWCNT	Single wall carbon nanotube
MWCNT	Multiwall carbon nanotube
c-MWCNT	Concentric- multiwall carbon nanotube
h-MWCNT	Herringbone- multiwall carbon nanotube
CVD	Chemical vapour deposition
PECVD	Plasma enhanced chemical vapour deposition
AFM	Atomic force microscopy
FED	Field-emission device
LCD	Liquid crystal display
FET	Field effect transistor
SPS	Spark plasma Sintering
MPPS	Most penetrating particle size
O-CNT	Oxidized carbon nanotube
PA	Polyamide
SEM	Scanning electron microscope
TEM	Transmission electron microscope
TGA	Thermal gravimetric analysis
BSE	Back scattered electrons
SE	Secondary electron
FEG	Field emission guns
EDX	Energy dispersive x-ray spectroscopy
XRD	X-ray diffraction

Chapter 1: Introduction

Nanomaterials research has opened up a new era in advanced technology for a variety of potential engineering applications. Recent advances in nanomaterials, together with innovations in other engineering subjects, offer tremendous opportunities for the development of fundamentally new nanotechnologies. Of the wide ranges of nanomaterials synthesised so far, carbon nanotubes (CNTs) are the most appealing and versatile materials that were first observed by Iijima in early 1990s [1], and have since been the subject of intensive research for two decades, to fully exploit their properties [2]. Individual CNTs exhibit high elastic modulus of > 1 TPa [3] and tensile strength of up to 60 GPa [4, 5], which is 10-100 times higher than the strongest steel but only at a fraction of their weight. CNTs have been reported thermally stable up to 2800 °C in vacuum and up to 700 °C in air, along with good thermal conductivity (greater than 6600 W m^{-1} K^{-1} for single-walled CNTs and 3000 W m^{-1} K^{-1} for multi-walled CNTs), with negligible thermal expansion [6]. They also exhibit different electrical conductivities depending on their helicity and diameters, either being metallic or semiconductor [7]. CNTs have high aspect ratio and large specific surface area which makes them promising for applications in adsorption, filtration and separation industries in both gaseous and aqueous systems [8-10]. These features make them an ideal candidate for the fabrication of CNT-reinforced advanced nanocomposites. Different methods have been developed to utilise CNTs in broad applications, which are expected to revolutionize the technological landscape in near future, and examples include CNTs as reinforcement phase for engineering nanocomposites [11, 12], as electrode or electron collectors in solar cells [13, 14], in flat panel electron field emitters [15, 16], as absorbent in nanoporous filters [9], and thermal materials, etc [17],[18]. Other fascinating potential applications such as artificial muscles or space elevator tethered by the strongest cables, have also been proposed [19].

In the field of composite, CNTs have been introduced into polymer, ceramic and metal matrices, aiming to achieve improved thermal, mechanical and electrical properties. To date, most studies have focused on the development of CNT-reinforced polymer nanocomposites [20] advantaging from improved mechanical property, multi-functionalities, and strong interfacial connections with such matrices caused by nano-scale features and extremely large interfacial areas [6]. In contrast, there are fewer reports considering CNTs as reinforcements in metals and ceramics matrices.

Among ceramics, alumina (Al_2O_3) is one of the most common oxides, and has so far been applied in high speed cutting tools, in dental implants, as chemical and electrical insulators, wear resistant parts and various coatings [21]. High hardness, inertness, high compressive strength and excellent electrical and thermal insulating properties with relatively low density are the main reasons for the intensive engineering applications discussed above. For other applications, the low-fracture toughness and low-fracture strength of Al_2O_3 cause micro-cracks to grow readily, preventing them from being used directly as structural materials [21]. It is reported that the addition of CNTs in the matrix can inhibit the Al_2O_3 grain growth which occurs during high temperature processing [22], making the composite more resilient against thermal shocks. Furthermore, the combination of CNTs with ceramics could result in nanocomposites with outstanding toughness [23, 24], in addition to highly thermal and chemical stabilities [4, 25]. All these benefits have motivated research in the development of CNT-containing nanocomposites.

To date, most CNT-containing ceramic composites have been fabricated by *ex-situ* mixing of the ceramic powders with the pre-produced CNTs, followed by a secondary process like hot-pressing [2], or spark plasma sintering (SPS) etc.[26], resulting in dense composites targeted for use in structural engineering applications. For such procedures, synergy between the matrix and CNTs is generally poor and potential damage to CNTs remains an important issue, as both have negative effects on the

resulting properties, especially on the mechanical properties [12]. Furthermore, obtaining a uniform and agglomeration-free distribution of CNTs within the matrix has proved to be a significant challenge.

Distinct from fully densified ceramics, porous ceramics or ceramic foams with open channelled porosities have specific engineering applications, such as in thermal insulation applications, as filters/membranes and gas burners, or as bioceramics [27]. Synthesizing composites by in-situ, direct growth of CNTs inside pores of engineering ceramics offers the potential to avoid many of the drawbacks arising from *ex-situ* processing, in addition to the advantages of offering short reaction times at low cost. Among those, there are a number of reports describing the use of mesoporous silica [28], silicon [29], or anodic aluminium oxide (AAO) membrane [30], as substrates for the production of porous ceramic/CNT composites by a direct deposition of highly ordered nanotubes, in which the deposition of carbon atoms occurs on the internal pore surface, copying the simple channel structures [31]. For large random interconnected ceramic foams, the fabrication of composites with CNTs embedded in all directions remains a technical challenge. Such composites with open pore matrices used as trusses, depending on the level of porosity and degree of filling of these pores with nanotubes, can lead to the fabrication of multi-functional engineering composites, such as filters.

CNTs have received special attentions for their excellent capabilities in water treatment for filtering organic and inorganic contaminants [32]. The high efficiency of CNTs in filtration can be explained by looking at their structures in which the high surface areas and large aspect ratios lead to the formation of strong Van der Waals force attractions between individual tubes, which results in agglomeration and the formation of a mesoporous network with higher pore sizes that can immobilize contaminants including bacteria and viruses at interstitial pore spaces [32]. In addition, the microbial cytotoxicity of CNTs also plays a partial role in the filtration performance [10]. The use of such nanomaterials, either embedded in membranes or on other structural media, has been considered as an effective method toward more applicable approaches in water

treatment.

A densely packed CNTs network forming various pore sizes from micropores to mesopores, supported on ceramic matrix, can immobilize pollutants either in air or in aqueous via physisorption [32] which make them favourable as filters in devices for gas adsorption, water filtration and purification [32-35], hydrocarbon separation [9], and pollutant air filters [8, 36]. All these properties offer diverse opportunities for the development of fundamentally new CNT-containing advanced composites. However, there are several immediate technological challenges. One of them is how to convert, cost effectively, the proven excellent adsorption behaviour of loose CNT powder into a viable filter for specific applications via proper treatment, akin to the breakthrough made in CNT oil filter [37].

Furthermore, infiltration of polymers into porous ceramics is a relatively new idea, which counts as a novel class of functional materials with a great potential for industrial applications. Hardness, stiffness and wear resistance of ceramic, combined with elasticity properties of polymer can be an advantage in many commercial applications which are now limited by the poor mechanical properties of ceramics [38-40]. This type of composite materials has higher initial compressive strengths in comparison to porous ceramics and sustains larger deformations. Therefore, such composite absorbs energy more efficiently than both components separately, making it a desirable material as a part of lightweight shielding or panels for protecting objects and structures against impact loads [41, 42]. There are currently no reports available in combining CNTs in such new functional materials for the assessment of possible improvements in their mechanical properties.

In short, research towards meaningful engineering applications of CNT-containing advanced nanocomposite materials is still in its infancy. The high demands and rapid technological development for nanocomposites with added functionalities have motivated the present research project. In this thesis, more applicable approaches

toward cost effective ways for the fabrication of CNT/ceramic composites and for the assessment in filter applications against different conditions and contaminants will be studied; and also the possible property improvements will be evaluated. Additionally, a new class of functional materials fabricated by infiltrating polymer into porous ceramic/CNT composites, for the first time, will be attempted and their mechanical properties against compression and impact loads will be assessed.

Chapter 2: Literature Review

2. 1. Introduction

This chapter summarise the recent research progresses of CNTs and CNT containing nanocomposites, focusing on different fabrication methods, main properties and potential and practical applications.

2. 2. History

In the mid-1980s, Kroto and co-workers discovered a new, large and closed-caged carbon form which is composed of hexagonal and pentagonal faces [43], named as buckminster-fullerene--C_{60}. This discovery brought them the Nobel Prize in chemistry in 1996, marking a significant stimulation and recognition as the start of the global nanomaterials research. More researchers in the exciting nanoscience arena have so far achieved substantial results; most notable ones are the discovery of the 1 Dimensional CNTs, and the 2 D single atomic layered carbon, graphene (Nobel Prize in Physics 2010) [44].

CNTs are long slender fullerenes, and the walls of the tubular cylinders are composed of wrapped graphene with 6-membered carbon rings and often capped at each end, with 5 or 7-membered carbon rings [11]. Similarly, a single layered graphene can be considered as a cut opened single-walled CNT and flattened. 25 years apart from the discovery of fullerene to another Nobel Prize associated with carbon is truly astounding. The significant properties of these magic carbon materials have attracted numerous researchers all over the world, racing to explore their unique properties and to develop new applications, for a diverse engineering subjects. This thesis will focus on the research developments of CNTs.

2. 3. Morphology and Atomic structure of CNTs

The ability of bonding in different ways is a unique property of carbon which makes it so special. They can change from graphite to diamond, from fullerenes to

CNTs and to graphene (Fig. 2. 1), according to different hybridization of the carbon atoms. If the four valence electrons in carbon atoms are shared equally (sp^3 hybridisation), diamond will be formed. When three of electrons are shared covalently in a plane, whilst the fourth electron becomes delocalised among all atoms (sp^2 hybridisation), graphite is formed. This type of bonding shows very strong in-plane bonds, but weak out-of-plane bond of Van der Waals which allows for the graphene layers in graphite sliding easily against each other, forming a soft material. A fullerene is a hollow sphere, ellipsoid structure entirely composed of carbon atoms. A CNT refers to the state where a fullerene is in a cylindrical form and, base on the number of the graphene layers, it can be single-walled or multi-walled. Graphene is an allotrope of carbon where its structure is made of one-atom-thick planar sheets of sp^2 bonded and packed densely in a honeycomb crystal lattice. When the size shrinks, the structure needs to reduce overall energy by closing onto itself and eliminating the dangling bonds [37]. This phenomenal change in structure gives rise to graphite, diamond, fullerenes [43], graphene [44], and carbon nanotubes [1], allowing them possessing different properties.

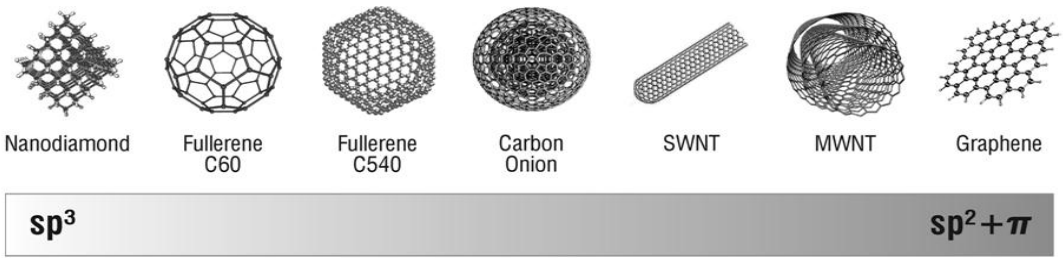

Fig. 2. 1. Different hybridization states and forms of carbon-based nanomaterials [45]

2. 3. 1. Single-walled CNTs

It is easy to imagine a single wall CNTs as one graphene layer rolled up to form a cylinder (Fig. 2. 2), whilst both ends of the cylinder are closed by hemi-fullerene caps with appropriate size. Various ways of rolling the graphene layer (direction of rolling), combined with different diameters and lengths of the rolled cylinder, determine the actual physical properties of the CNTs, which can be mathematically defined by the vector of helicity C_h and the angle of helicity θ.

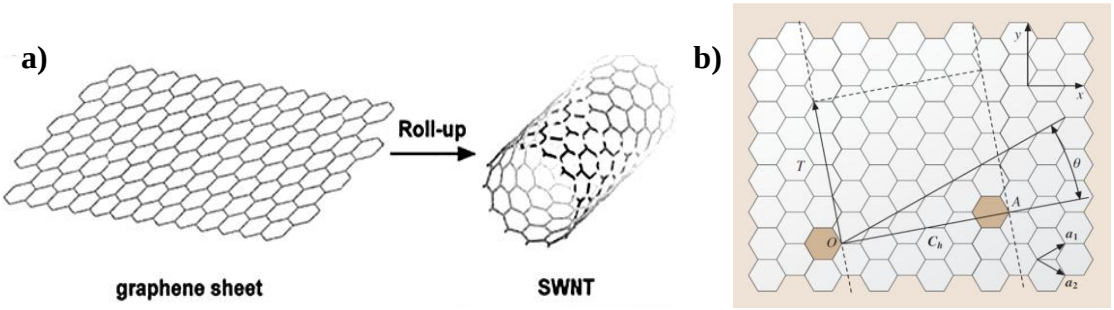

Fig. 2. 2. (a) Schematic of the fabrication of SWCNT which is a strip cut from an infinite graphene sheet rolled up to form a tube [46]. (b) Sketch of the vector of helicity C_h and angle of helicity θ [47].

The chiral vector can be described by Eq. 2. 1 [37]:

$$\boldsymbol{C_h = na_1 + ma_2} \qquad \textbf{Eq. 2. 1}$$

Where $a_1 = \frac{a\sqrt{3}}{2}x + \frac{a}{2}y$ and $a_2 = \frac{a\sqrt{3}}{2}x - \frac{a}{2}y$ and $a = 2.46\,A^0$

The angle of helicity (θ) can be described by Eq. 2. 2:

$$\cos\theta = \frac{2n+m}{2\sqrt{n^2+m^2+nm}} \qquad \textbf{Eq. 2. 2}$$

$\cos\theta = \frac{2n+m}{2\sqrt{n^2+m^2+nm}}$where n and m are the integers of the vector C_h considering the unit vectors a_1 and a_2.

By considering the mentioned equations and different methods of rolling the graphene sheet, three types of tube can be formed (Fig. 2. 3). Some of the nanotubes possess planes of symmetry both parallel and perpendicular to the tube axis (Fig. 2. 3a and 2. 3b), and some do not (Fig. 2. 3c). Tubes made from lattice translational indices of the form (n, 0) or (n, n) have got two helical symmetry operations when all other tubes have the three equivalent helical operations. Base on this, the (n, 0) sets are called zigzag nanotubes, the (n, n) are called armchair nanotubes and all other forms (n, m) will be helical [37].

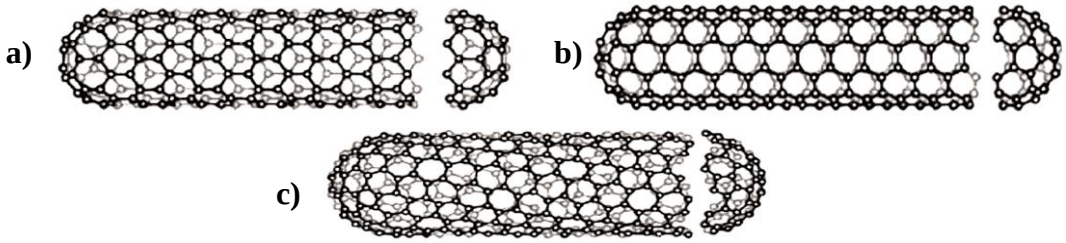

Fig. 2. 3. Sketches of three different SWCNT structures: (a) zig-zag (n, 0), (b) armchair (n, n) and (c) helical (n, m) nanotube [37].

The production of SWCNTs required very strict and controlled conditions that make the cost of final products expensive compared to the multi-walled CNTs which can be fabricated in larger quantity and cheaper approaches [37].

2. 3. 2. Multi-walled CNTs

Multi-walled carbon nanotubes (MWCNT) consist of multiple rolled layers (concentric tubes) of graphene. Understanding the morphology of MWCNT can be a little bit more complex due to the various ways graphene can be displayed and also mutually arranged within filament. The simplest MWCNT to consider is the **concentric** type (c-MWCNT), which are simply made of SWCNTs with regularly increasing diameters that are coaxially arranged and form a MWCNT similar to a Russian-doll model (Fig. 2. 4). A c-MWCNT can have any number of walls or coaxial tubes from two upwards when the intertube distance between each two layer of graphene roll in CNTs will be 0.34 nm [48].

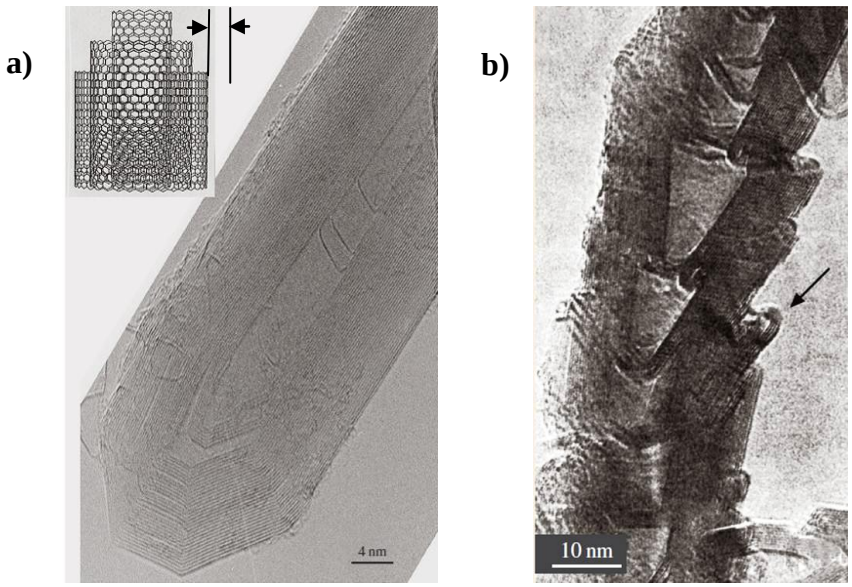

Fig. 2. 4. (a) Transmission Electron Microscopy (TEM) image of a concentric multi-walled CNT made by the electric arc-discharge method. The inset illustrates a sketch of the Russian doll like arrangement of graphene. (b) TEM images of herringbone and bamboo multi-walled CNTs (bh-MWCNT) prepared by CO disproportionation [48].

Herringbone is another frequently occurrence form of texture that a MWCNT can possess (h-MWCNTs). In this type of nanotubes, the graphene makes an angle with respect to the tube axis (Fig. 2. 4b). The amount of the following angle can vary depending on the fabrication conditions (such as the catalyst morphology or the combination of atmosphere) from 0 (in which case the texture became c-MWCNT) to 90˚ (in which the filament is more like a nanofibre rather than a nanotube) [49].

Another known structure of MWCNTs is the **bamboo** texture which happens when a limited amount of graphene oriented perpendicular to the nanotube axis. This texture cannot exist on its own and should be affected by either c-MWCNT (bc-MWCNT) or the h-MWCNT (bh-MWCNT) texture (Fig. 2. 5). This type of nanotubes is sometimes called nanofibres in the literature as their inner cavity is no longer open all the way along the filament as is in a genuine nanotube [50].

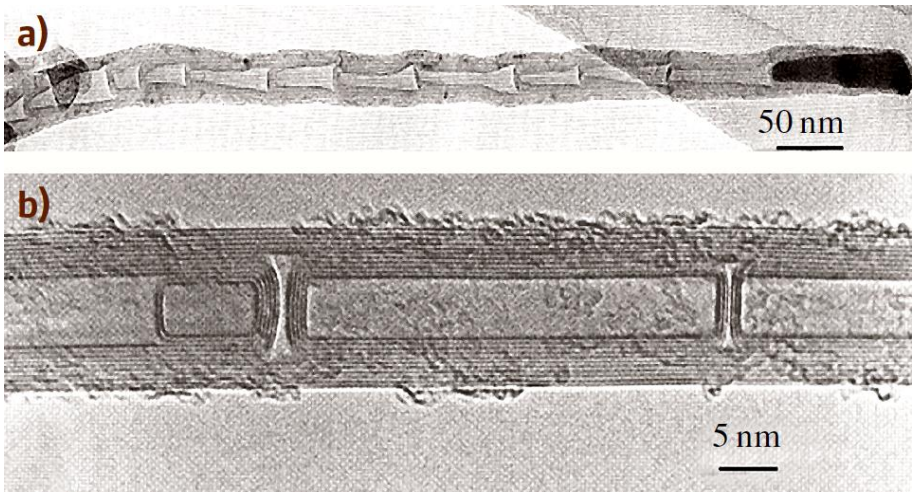

Fig. 2. 5. (a) TEM image of a bh-MWCNT which shows nearly the periodic nature of texture that happens frequently [50], (b) TEM image of a bc-MWCNT [51]

To simplify, this thesis uses CNT to represent MWCNTs, unless specified otherwise.

2. 4. Fabrication methods of CNTs

So far, various methods have been utilized to fabricate CNTs. Each method has its own advantages and drawbacks. Some seem to be easier and cheaper and some lead to better qualities. The selection of the most appropriate synthesis method depends on the required properties and feasibilities. There are currently many on-going works to reduce the manufacturing costs, towards higher yield and efficiency, which make them more feasible and practical for industries. The most important methods are:

1) Arc-discharge [52, 53]
2) Laser ablation [54, 55]
3) Chemical vapour deposition (CVD) from hydrocarbons [56-58]

In order to use CNTs in composites, large quantities production capacity is the key. Compared with CVD process, the high cost of arc discharge and laser ablation methods has made CVD the most suitable techniques for scaling up [4]. Therefore, this research will mainly focus on the CVD method.

2. 4. 1. Arc-discharge

For the first time, Iijima [1] synthesized CNTs by the arc-discharge method [5]. The principle of this technique is to vaporise a graphite, in the presence of catalysts (mostly iron, nickel or cobalt) for SWCNTs, under an inert atmosphere (argon or helium). This technique normally uses two high purity graphite rods as the anode and cathode to create the arc-discharge. The rods that are schematically shown in Fig. 2. 6 are kept under the helium atmosphere and a voltage is applied to them to produce a stable arc. After the arc was formed, a plasma consisting of the mixture of carbon vapour, catalyst vapour and inert gas will be produced. The variables of the process depend on the exact size of the graphite rods. As the anode is consumed, a constant gap between the anode and cathode should be maintained by regulating the place of the anode. At this time, the materials will be deposited on the cathode to form a build-up consisting of an outside shell of fused substance and a softer fibrous core containing CNTs with carbon particles [4].

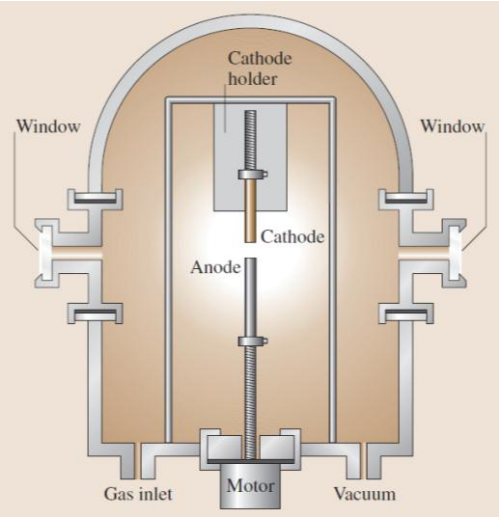

Fig. 2. 6. Schematic of an electric arc-discharge reactor [19]

In this method, the morphology and the production efficiency of nanotubes are strongly dependant of the experimental conditions [59].

2. 4. 2. Laser ablation

After the first laser was built in 1960, scientist has tried to use it as a means of concentrating a large amount of energy inside a small volume in a short time. Laser

ablation was first utilized to produce fullerenes [60], after which many researches have modified this method for the fabrication of CNTs [55, 61]. In this method, a laser beam is used to vaporise a graphite target doped with cobalt and nickel as a catalyst which produce a high temperature (1200˚C) and the CNT are collected on a water cooled target [61], as schematically shown in Fig. 2. 7.

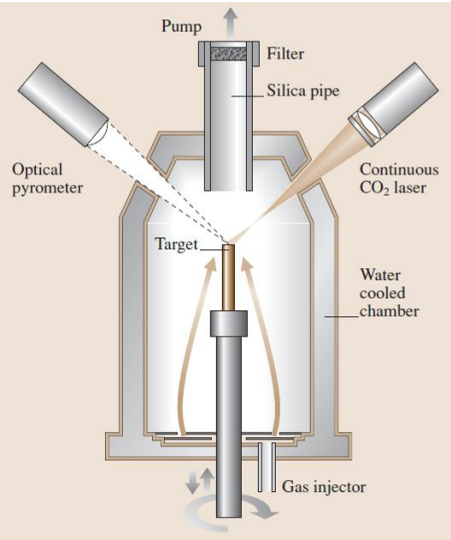

Fig. 2. 7. Schematic of the laser ablation technique with a continuous CO_2 laser device [19]

This method is capable of synthesising very clean nanotubes with limited amount of amorphous carbons with uniform diameters of 5-20 nm and tens to hundreds of micrometre length for synthesis conditions designed for high quality tubes. The ends of all the nanotubes are reported to be entirely closed with hemispherical end-caps with no evidence of catalyst and metal particles [61].

2. 4. 3. CVD technique

CVD has been a successful method in fabricating carbon fibres [62], filament [63, 64] and nanotubes [65] for more than two decades. The CVD process involves heating a catalyst material to high temperatures (500-1000 ˚C) in a tube furnace (Fig. 2. 8), and flowing a carbon source through the tube reactor over a period of time under specified atmosphere and pressure [66].

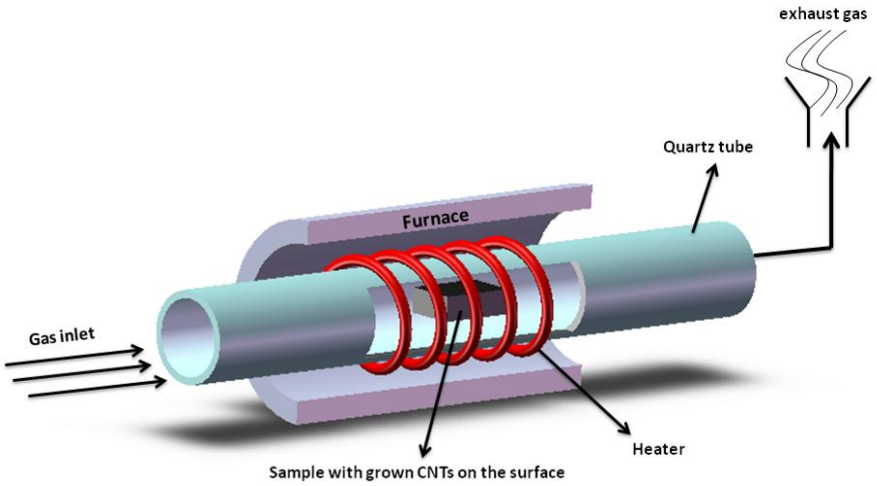

Fig. 2. 8. Schematic of the CVD process.

Catalysts used for this method are usually transition metal nanoparticles which are formed on a supporting material such as porous aluminium oxide with large surface area [66]. The most effective metals in catalytic growth of CNTs in a CVD process (also known as CCVD) are iron (Fe), nickel (Ni) and cobalt (Co) [67]. The ability of these metals to form ordered carbons are a function of several factors. Their catalytic activity for decomposing volatile carbon sources is an important issue given the fact that these carbon compounds form metastable carbide during synthesis which finally leads to the carbon diffusing through and over the catalyst particles, resulting in CNTs [68, 69]. This shows that ordered carbon is the product of diffusion and precipitation, because it is only formed near the metal surfaces. Thus, if there are significant reactions away from the metal particles, other undesired forms of carbon, e. g. amorphous carbon, will be observed [70].

The precipitation of carbon atoms from saturated catalyst particles results in the formation of tubular carbon in sp^2 structure that is favoured over other forms of carbon like graphitic sheets with open edges, as it is in a lower energy level due to the non-existence of dangling bonds [66]. Over these metallic catalysts, carbon atoms dissolve to form a solid solution and finally on the cooling process, they precipitate, in a matter of seconds, on the surface as a continuous thin film of highly crystalline perfection, as carbon atoms are tremendously mobile and can shift simply over and through the metals

[67, 70]. During the process of formation of nanotubes, the original catalyst particles remain fixed to the substrate (extrusion or root growth) or detach from the surface and remain encapsulated within the other side of tube (tip growth), as shown in Fig. 2. 9 [68, 71, 72].

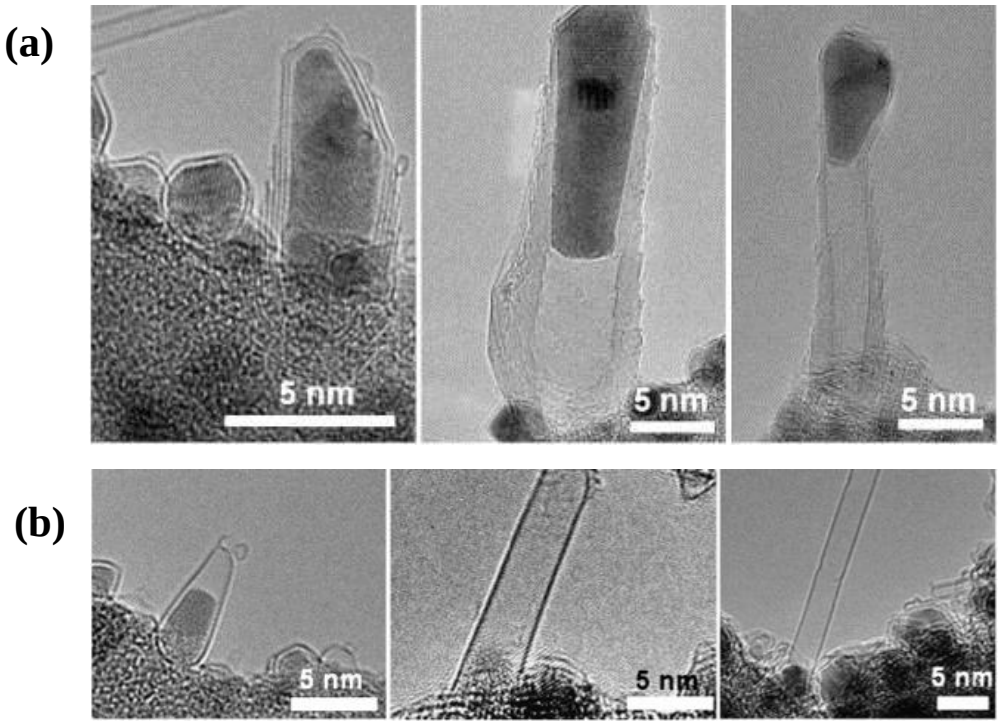

Fig. 2. 9. Growth mechanism of CNTs over metal catalyst suggesting two possible methods known as (a) "tip growth" and (b) "root growth" [73].

Using CVD along with gas carbon precursor is very popular because it forms a continuous process which allows the carbon source to be continually replaced by the flowing gas. The final product of such procedures has an acceptable purity which makes the CVD more appropriate for industrial scale production of CNTs [4]. CVD also allows for the production of CNTs at relatively low temperatures and high yields. Another unique characteristic of the CVD process is its ability to fabricate aligned arrays of CNT with controlled diameter and length, such as by using plasma enhanced vapour deposition (PECVD) where the plasma was produced by a DC source [74, 75] or microwave source [76, 77] (Fig. 2. 10).

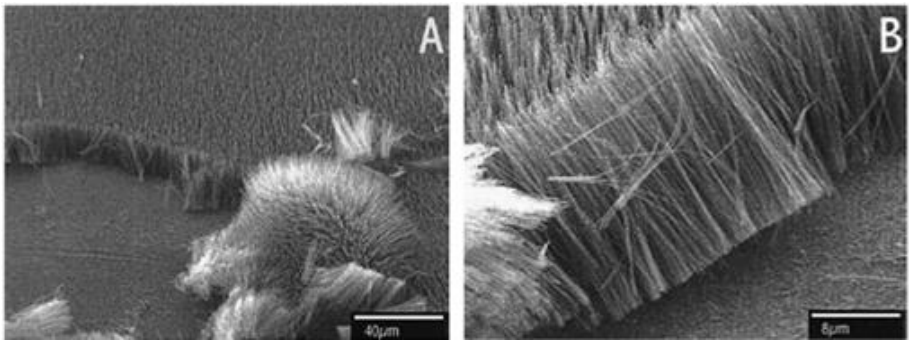

Fig. 2. 10. Well-aligned mats of CNTs grown on glass by the PECVD process [78].

The size of catalyst also plays an important role in this method as it allows engineering the diameter of nanotubes by adjusting the thickness of catalyst (Fig. 2. 11).

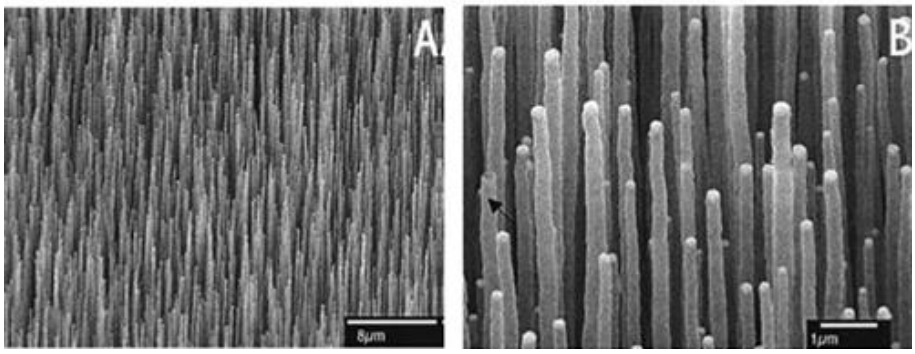

Fig. 2. 11. The effect of catalyst size on the diameters of CNTs in a CVD process [78]

2. 5. Properties of CNTs

As mentioned earlier, CNTs are a new class of materials with extraordinary properties. They possess remarkable mechanical, thermal, chemical and electronic (that can be semiconducting or metallic, depending on their chirality and diameters [66]) properties which have attracted many researchers. Table. 2. 1 summarises some of these astonishing properties.

Table. 2. 1. Unique properties of carbon nanotubes [6]

Property	CNTs	Graphite
Specific gravity	0.8 g/cm^3 for SWCNT; 1.8 g/cm^3 for MWCNT (theoretical)	2.26 g/cm^3
Elastic modulus	~1 TPa for SWCNT; ~0.3–1 TPa for MWCNT	1 TPa (in-plane)
Strength	50–500 GPa for SWCNT; 10–60 GPa for MWCNT	
Resistivity	5–50 μΩ cm	50 μΩ cm (in-plane)
Thermal conductivity	3000 W m^{-1} K^{-1} (theoretical)	3000 W m^{-1} K^{-1} (in-plane), 6 W m^{-1} K^{-1} (*c*-axis)
Magnetic susceptibility	22 × 10^6 EMU/g (perpendicular with plane), 0.5 × 10^6 EMU/g (parallel with plane)	
Thermal expansion	Negligible (theoretical)	−1 × 10^{-6} K^{-1} (in-plane), 29 × 10^{-6} K^{-1} (*c*-axis)
Thermal stability	>700 °C (in air); 2800 °C (in vacuum)	450–650 °C (in air)
Specific surface area	10–20 m^2/g	

2. 5. 1. Mechanical Strength

One of the most fascinating properties of CNTs is their mechanical strength, which justified their usage in many applications such as in composite materials. The strength of carbon bonds has made CNT one of the strongest and stiffest materials known so far. By using atomic force microscopy (AFM) (Fig. 2. 12), the axial elastic module of CNTs (on the basis of the in-plane elastic modulus of graphite) has been found to exceed 1.2 TPa (about a hundred times higher than steel), and an average bending strength of 14.2 GPa was also reported [66, 79]. The hollow structure and closed topology of CNTs have resulted in a distinct mechanical response in them, compared to other structures of graphite. CNTs can sustain very high strain (~40%) in tension without exhibiting any signs of brittleness, plastic deformation or bond crack and break [37].

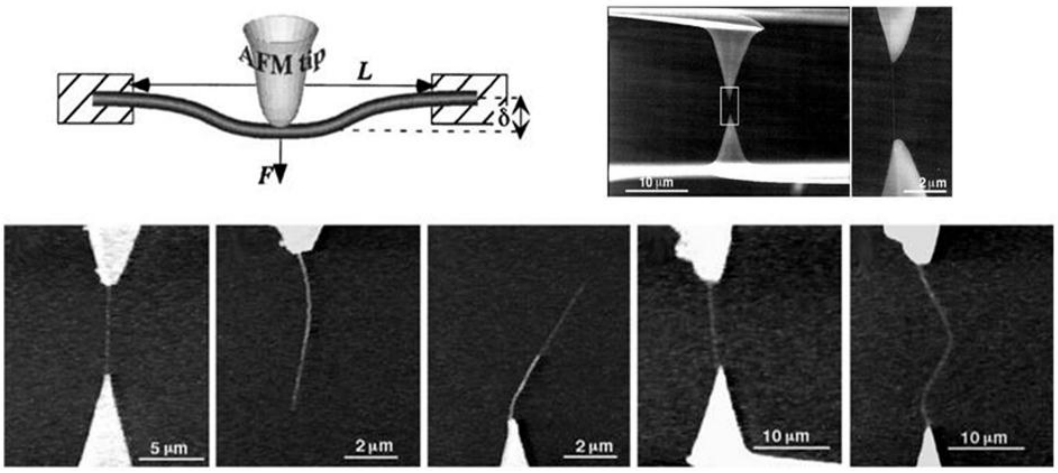

Fig. 2. 12. Tensile loading and fracture behaviour of CNTs during tests [11, 80]

To conclude, investigations have proved that CNTs hold exceptional mechanical properties such as high elastic modulus [81], large elastic strain and fracture strain sustaining capability as subjecting to stress, their inside hollow cavity should collapse (Fig. 2. 13), and this provides extra absorption of energy and increased toughness of the composite [53]. Similar conclusions have also been gained by theoretical studies [11].

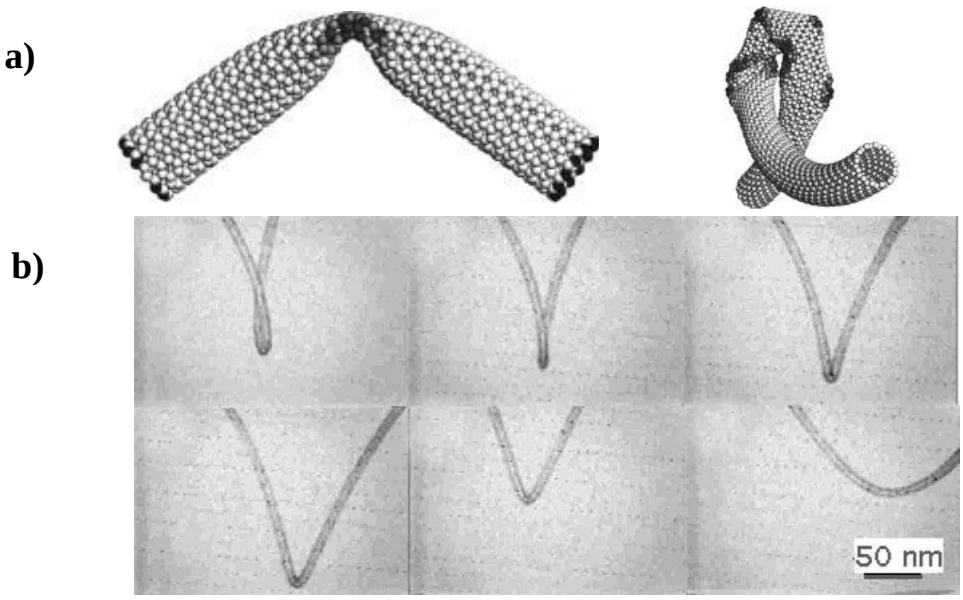

Fig. 2. 13. (a) Schematic simulation of a deformed CNT when they are loaded [37], and (b) in-situ bending sequence on a single CNT [82].

2. 5. 2. Thermal stability

CNTs exhibited superior thermal properties. High thermal stability up to 2800 ˚C in vacuum, >700 ˚C in air, and also thermal conductivity of about twice as high as diamond [83] which has the highest measured thermal conductivity of any other material [84], have been reported. The thermal conductivity of graphite is very poor along their c-axis due to the weak bound layers that are attracted to each other by the Van der Waals forces, and the in-plane thermal conductivity of graphite is about 3000 W/m· K. As CNTs reflect the in-plane properties of graphite, their thermal conductivity is very high [37], about 2-3 times larger than those of diamond or in-plane graphite [85]. It is possible to understand this high value by comparing it with a well-known highly thermal conducting metal such as copper whose conductivity is only about 400 W/m·K.

This shows why CNTs are extremely desirable for composite materials which are needed for high working temperatures such as the ones in blast furnaces. Studies shows that CNTs conduct current and heat ballistically [86]. The ballistic conduction is correlated with the large phonon mean-free path in CNTs. Thus, it is expected that CNTS can dominate the thermal conductivities of polymer/CNT composites, shifting the paradigm of heat conduction from diffusion in both polymers and CNTs to ballistic heat conduction in CNTs and diffusive heat conduction in polymers. However, researches have revealed that the thermal conductivities of polymer/CNT composites is much lower than the estimations [87]. Investigations showed that the resistance to the heat flow caused by CNT-polymer interface is responsible for the low thermal conductivities of such composites [88, 89].

2. 5. 3. Chemical reactivity

The chemical reactivity of CNTs, in comparison with a graphene sheet, is enhanced because of the curvature of the CNT surface. Reactivity of CNT is related to the pi-orbital mismatch which is caused by the increased curvature. Consequently, a distinction between the end caps and sidewalls of nanotubes must be made for more realistic understandings. Therefore, nanotubes with smaller diameter have more enhanced reactivity. The end caps of CNT are always quite reactive irrelevant of the diameter of nanotubes as they resemble a hemispherical fullerene; consequently, they have reached their maximum pyramidalization angle which is about 9.7°. Covalent chemical modification of both sidewalls and end caps are possible (functionalization), which has been widely used to facilitate the dispersion of nanotubes in solvents for the preparation of composite materials, and can also help to improve bonding between the tubes and the matrices [90].

2. 6. Applications of CNTs

Since the discovery of CNTs, research has been focused on different ways of introducing CNTs into device-oriented applications in order to use their exceptional

properties, as introduced earlier [91]. High strength, chemical stability, high aspect ratio and high conductivity of CNTs have brought much success in electron emission application [7, 92]. Strong covalent bonds makes CNTs physically inert to sputtering, which allow them to carry a huge current density before electron migration that is the main advantage of CNTs over conventional field-emission devices (FED) [93-95]. Most research activities on electronic devices have focused on utilizing nanotubes as field emission electron sources for the next generation of electron guns for electron microscopes [94], high power microwave amplifiers [96], flat panel displays [92], lamps [97] and x-ray source [98, 99]. FEDs made by CNTs have higher video rate, high power efficiency and wider operating temperature range, which make them more desirable compared to the conventional liquid crystal displays (LCDs) [99]. The metallic behaviour of CNTs, allowing for a large current density carrying capacity, has also made them a good candidate for further shrinking the size of nano-electronic devices in future integrated circuits (nanowires) [7, 100]. And finally, field effect transistors (FETs) are another nano-electronic device that CNTs show their potentials, as both metallic and semiconducting CNTs are required, dependant on their diameter and chirality, as mentioned earlier [101].

As CNTs do not reduce or oxidize over a substantial range of potentials, also the high chemically accessible surface area of their arrays, along with their high electric conductivity and high mechanical strength, they can be used as electrodes for electrochemical double-layer charge injection devices such as supercapacitors [102] and electrochemical actuators [103, 104] that may eventually use in robots [91].

CNTs have also been used widely in sensor and probe applications, as their electronic transport and thermopower are extremely sensitive to materials that affect the amount of injected charge [105]. Clearly, the main advantage of such nanosensors and probes is the small size of sensing elements and correspondingly small amounts of material needed for response. Differentiating among absorbed species in complex

mixtures, and providing rapid enough forward and reverse responses still remain to be solved in this area [91].

There are more applications for CNTs along with many other potential ones [7, 19]. The most notable ones which have already made into the applications have been briefly introduced. There are two more significant applications that will be discussed in details, due to their importance and relevancy to the current work:

i. Nanocomposites
ii. Nanofilters

2. 7. CNT-reinforced composites

One of the first realized major commercial applications of CNTs was their usage as an nanofiller in composites, due to their extraordinary mechanical strength and stiffness [82, 106-108], excellent thermal and electrical properties [109-112]. Beside the challenges which have to be overcome, the promising property enhancements of resulting nanocomposites have attracted more attentions over the last decade. Niihara has classified nanocomposites into four types based on their microstructure which are, intra, inter, intra/inter and nano-nano [113]. As shown schematically in Fig. 2. 14a, the first three types illustrate the dispersion of second-phase nanoparticles within the micro-grains of a matrix, at grain boundaries or both; whilst in the fourth type, second-phase nanoparticles are embedded within the nano-grained matrix [113]. The first three types are generally known as nanocomposites when they are more precisely referred to as micro-nano composites as suggested by Mishra and Mukherjee in a new classification [114]. In their classification, the matrix consists of continuous nanocrystalline grains (with grain sizes of less than 100 nm) where the second phase can be in the form of nanoparticles, microparticles, fibres (whiskers) or grain boundaries (nanoleyer) (Fig. 2. 14b) [114].

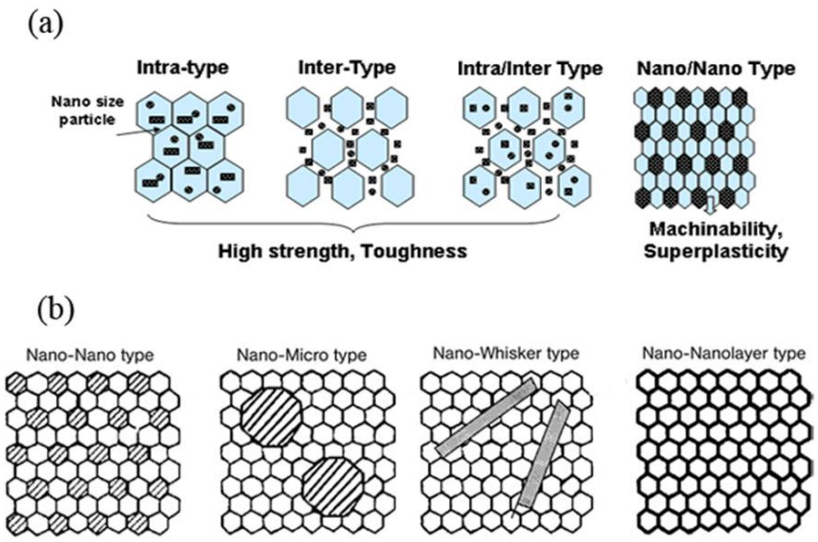

Fig. 2. 14. Schematic of four different categories of nanocomposite from the concept of new material designs based on (a) Niihara [113], and (b) Mukherjee [114] classification.

Accordingly, three different types of CNT-reinforced nanocomposites, based on their matrixes which can be polymer, metal or ceramic, have been developed. Most researches in this field have focused on polymer matrix nanocomposites [20], due to their good mechanical, surface and multi-functional properties arising from strong interactions with the matrix as a result of the nano-scale structure and extremely large interfacial area [115]. There are also other attempts on developing metal [116] and ceramic-matrix [20, 117] composites [118].

2. 7. 1. Polymer/CNT composites

A common fabrication method for polymer/nanotube composites involves mixing nanotubes dispersions with polymer solution and then evaporating the solvents in a controlled situation [119]. Solubilising CNTs are extremely important in polymer base nanocomposites, as this aqueous nanotube dispersion can be later easily mixed with proper polymer solution and then by casting the mixture and evaporating the solvent (like water), a nanocomposite is produced. For example, Qian et al. utilized a high energy ultrasonic probe for dispersing CNTs in toluene and then mixed the suspension with a dilute solution of polystyrene in toluene using ultrasonic probe again. The low viscosity of the solution allowed CNTs to move freely in the matrix. Finally they cast the mixture on glass and removed the solvent (toluene) to yield polystyrene/CNT films

(Fig. 2. 15a) [120]. The solution mixing method is appropriate for polymers which can freely dissolve in common solvents.

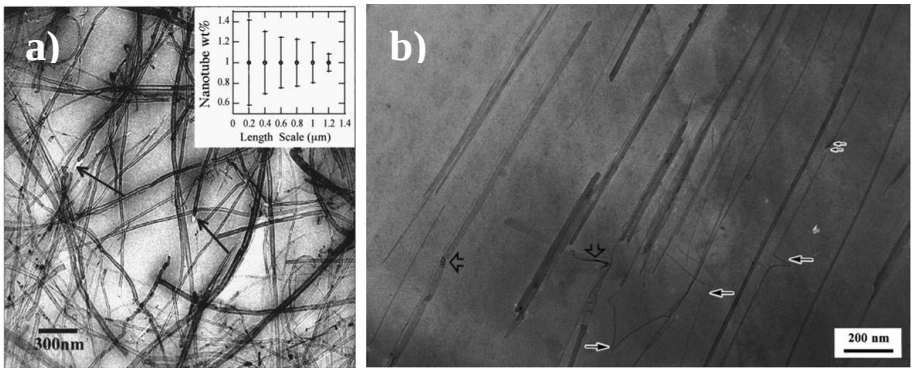

Fig. 2. 15. (a) TEM image of a Polystyrene/CNT composite (arrows show regions of polymer shrinkage and inset illustrates the length distribution of CNTs [120]. (b) Epoxy/CNT composite which shows the alignment of the nanotubes in the direction of cutting with microtome [121].

Another way to produce polymer/CNT composites is to use thermoplastic polymers (polymers which soften and melt when heated) and utilize melt processing techniques. Consequently, this method can be used to synthesis a homogenous dispersion of CNT alignment or to make artefacts in the required form by injection moulding [122]. Polyamide (PA) is an example of such thermoplastic polymers which has been used as substrate for CNTs. PA/CNTs composites have been made with improved overall mechanical properties by simple melt-compounding. Mechanical tests indicate that, compared with neat PA6, the Yong's modulus, the tensile strength, and the hardness of the composite are greatly improved by about 115%, 120%, and 67%, respectively, with incorporating only 1 wt % CNTs. SEM observation of the fracture surfaces of the composite shows a homogeneous dispersion of CNTs throughout PA6 matrix and a strong interfacial adhesion between CNTs and the matrix responsible for the significant enhancements in mechanical properties [123].

Epoxy/CNT composites have also attracted the most researchers. The earliest work was done by Ajayan et al. in 1994 [121]. They embedded purified CNTs into an epoxy resin that was then cut with a diamond knife. They found that nanotubes have become aligned in the direction of the knife movement which was a consequence of extensional or shear

flow of the matrix produced by cutting (Fig. 2. 15b). This alignment can be much more readily gained when the epoxy is in liquid state.

2. 7. 2. Metal/CNT composites

Composite materials containing carbon fibres and CNTs in metal matrix such as aluminium and magnesium are considered here. These composites have a combination of low density and high strength and modulus which makes them suitable for aerospace industries [124]. Kuzumaki et al. produced an aluminium/CNT composite in 1998 [125]. They mixed a CNT sample with a fine aluminium powder, mounted the mixture and then drew and heated the wire at 700 ˚C in a vacuum furnace. The result was a composite wire in which the nanotubes were partially aligned along its axial direction. The tensile strength of the resulting composites was very similar to the pure aluminium but it retained this strength after prolonged annealing at 600 ˚C, whilst strength of the pure aluminium decreased by about 50% after this treatment. They also fabricated composites of titanium matrix, and great improvements in hardness and modulus were observed [126]. Production of copper/CNT nanocomposite was reported by Kim et al, by utilizing spark plasma Sintering (SPS) of high energy ball milled copper nanopowders with CNTs followed by cold rolling [127]. The composite shows two regional structures, with or without CNTs (Fig. 2. 16). This inhomogeneous distribution of CNTs has resulted in a two steps yielding behaviour in the stress-strain curve of nanocomposite, in which the strength of Cu-CNT region shows 1.6 times higher compared to the CNT-free region. This result revealed the importance of homogenous distribution of CNTs in nanocomposite, which remains as a key challenge due to the high tendency for CNTs to agglomerate.

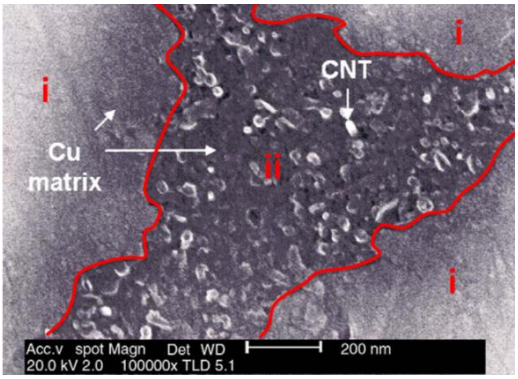

Fig. 2. 16. SEM micrograph showing two regional structures of composite consisting of CNT-free (i) and Cu-CNT (ii) parts [127].

In another experiment, Chen et al. proved that metal/CNT composites showed reduced wear rates and friction coefficient, which makes them suitable candidates for tribological applications. They have also attempted to make a CNT/Ni/P composite coating on a stainless steel substrate utilizing an electroless plating method [128].

2. 7. 3. Dense ceramic/CNT composites

The recent developments in advanced technologies in the aeronautics, space and energy areas, demand materials with high performance and superior mechanical properties along with high thermal and electrical conductivity and good wear resistance. Ceramics have good corrosion resistance, high stiffness and thermal stability with relatively low density and they have been used in industrial sectors. Alumina is one of the most popular ceramics and has been attempted as a matrix for the production of CNT-reinforced composites, due to its relatively high hardness (15–22 GPa), good oxidation resistance and chemical stability [129], but its low fracture toughness has prevented their usage as structural materials [130]. Toughness of ceramics can be improved by adding some reinforcement particles such as whiskers [131] and fibres [132] (or nanotubes [133]) to form composites. The main toughening mechanisms of fibre-reinforced composites are mainly attributed to the deflection at the fibre-matrix interface, crack bridging and fibres pull-out (Fig. 2. 17). When a crack is formed, the reinforcement bridges it in its wake and pull-out does frictional work. These mechanisms can effectively stop the crack from further growth across the whole sample.

Weak fibre matrix interfacial bonding makes the fibre pull-out mechanism easier to occur, as strong bonding facilitates crack propagation straight through the fibres which eventually leads to low fracture toughness [134].

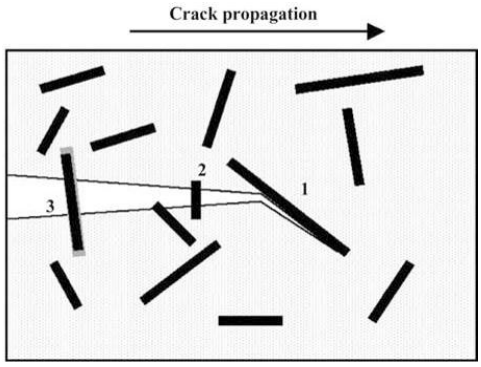

Fig. 2. 17. Schematic of the reinforcement toughening: (1) crack deflection, (2) crack bridging and (3) fibre pull-out [135].

In CNT-reinforced composites, it is proposed that uncoiling and stretching of CNTs play the most significant role in enhancing the toughness [136]. During crack propagation, uncoiling CNTs in the wake are stretched and act as bridges, stopping further propagation (Fig. 2. 18). In the case of facing to larger forces, pull-out mechanism can act as another process to prevent further growth of cracks (Fig. 2. 19), all resulting in tougher composite.

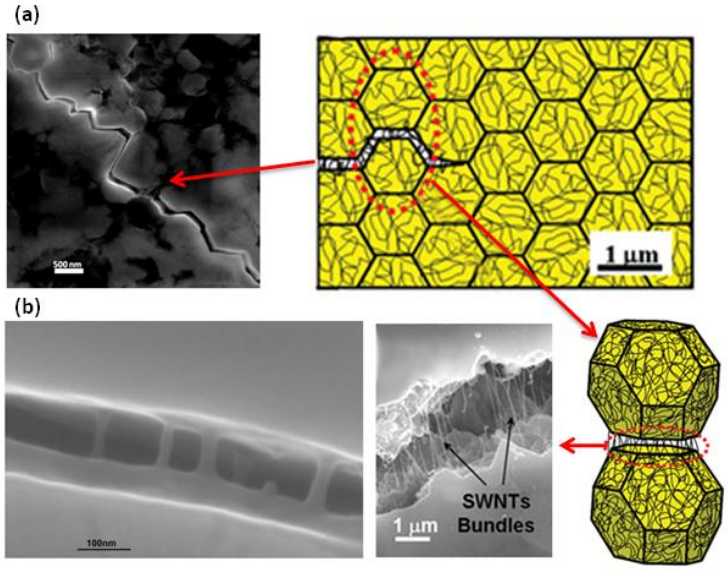

Fig. 2. 18. Schematic and actual SEM images of crack propagation (a) and the bridging mechanism (b) [24, 137, 138].

It is claimed by Kothari et al. [137] that the hollow concentric graphitic structure of CNTs can result in much longer pull-out length in contrast with the solid carbon nanofibres, due to the easy sliding behaviour of the concentric CNT as a result of weak Van der Waals forces between its layers (Fig. 2. 19). The strengthening of such composites is significantly dependant on the effective load transfer from the matrix to nanotubes during the mechanical loading. Homogenous dispersion of CNTs in the ceramic matrix and strong enough nanotube-matrix bonding are also vital in order to have a composite with improved mechanical strength and toughness [130].

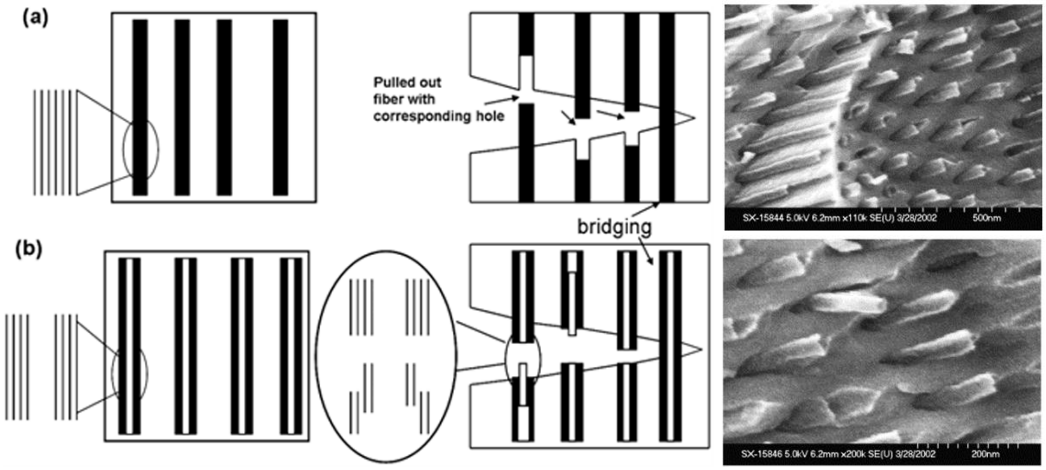

Fig. 2. 19. Schematic and SEM images of the pull-out mechanism in carbon fibres (a), and CNTs (b) reinforced composites [137, 139].

To summarise, using CNTs as nanofillers with their high aspect ratio, superior mechanical strength and flexibility, and also excellent thermal and electrical conductivity, can potentially produce new functional materials by improving the intrinsic drawbacks of ceramics. They can offer a composite with outstanding toughness, as well as improved thermal and electrical properties. It has been shown that the electrical conductivity of alumina-CNT composites can reach up to twelve orders of magnitude higher in contrast with their monolithic counterpart. Also, recent studies have shown that the thermal conductivity of such nanocomposites shows anisotropic behaviour which makes them promising as thermal barrier layer in microelectronic and microwave devices, solid fuel cells and chemical sensors [130, 140]. All these reports,

emphasising on the importance of ceramic matrix nanocomposites and their applications, are the driving force behind the current work.

Fabrication:

Despite the fact that CNTs possess remarkable mechanical properties, their reinforcing effect in ceramic matrices is far below the expectations as the results of inhomogeneous dispersion due to their tendency to agglomerate, inadequate densification of composites and also poor wetting behaviour between CNTs and the matrix [130]. During mechanical deformation, individual CNTs within the cluster may slide against each other causing a drop in the load transfer efficiency. These clusters of CNTs also have negative effect on the composite toughness as they may minimize the crack bridging and pull-out effect significantly.

Such difficulties in producing good quality ceramic matrix composites using CNTs as reinforcement are raised from specific fabrication processes [130]. To date, most CNT-reinforced ceramic nanocomposites have been fabricated by *ex-situ* mixing the ceramic powders with the pre-produced CNTs, followed by a secondary process like hot-pressing [2, 117], or spark plasma sintering (SPS) etc. [26, 141] for densification (Fig. 2. 20). For such procedures, synergy between the matrix and CNTs is generally poor and potential damage to CNTs remains an important issue, as both have negative effects on the resulting properties, especially on the mechanical properties [12]. These methods also need lengthy treatments at high temperature to densify the compacts, and such high temperature environments may oxidize CNTs, resulting in poor properties of final products [130]. The high cost of CNTs is another major issue of such procedures which restricts them for large scale applications [32]. These two methods will be introduced briefly due to their intense usage in producing alumina/CNT composites.

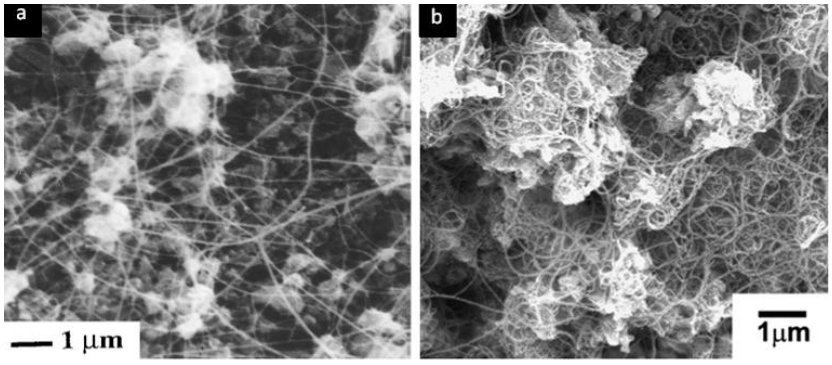

Fig. 2. 20. SEM images of nanocomposites fabricated from powder processing. (a) by SPS process [26]; (b) by hot-pressed method [2]

i. Hot Pressing

Hot pressing is a common process for powder metallurgy that uses high-pressure and low-strain-rate for the fabrication of a powder or powder compact at a temperature high enough to induce sintering process (Fig. 2. 21). For most alumina/CNT composites, CNTs are fabricated separately and by mechanically mixing them with micro and nano powder of alumina or under sonication to prevent agglomeration, composite powders will be formed which will be followed by a secondary process (hot-pressing in this case) to produce the desired composite [20]. This approach will mostly result in poor dispersion of CNTs within the matrix. Recently, there has been a growing interest in *in-situ* production of CNTs on ceramic powder using mixture of alumina and transition metal/metal-oxide catalyst particles followed by CVD process. The produced powder containing CNTs and ceramic powder will then be subjected to hot pressing for the composites. The advantage of this process is direct incorporation of CNTs with the alumina matrix during the procedure [130].

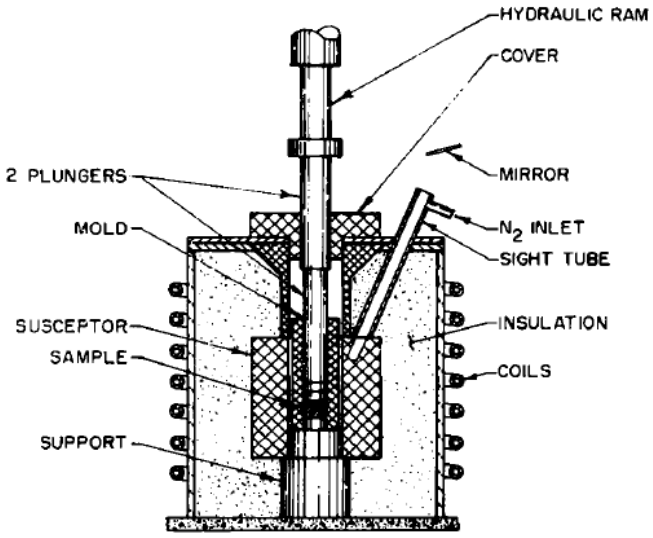

Fig. 2. 21. Schematic of a hot pressing furnace [142].

However, hot pressing occur in high temperature (~1500 ˚C) damaging the CNTs and leading to the formation of disordered graphene sheets at grain boundary junctions (Fig. 2. 22).

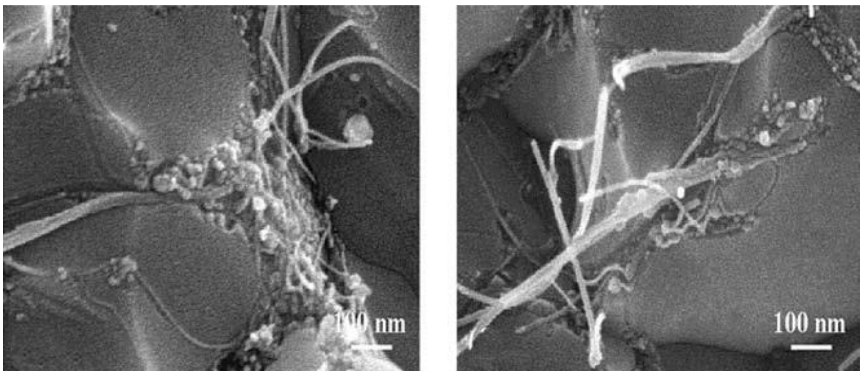

Fig. 2. 22. SEM images of the production of amorphous carbons at grain boundary junctions of a composite as the result of high temperature involved in hot-pressing process [116].

High temperature extrusion is another possible way to consolidate the *in situ* composite powders as CNTs can stand high shear stresses. The extruded composite has higher densification (~90%) compared to hot pressed composites. It has been shown that CNTs prevent the ceramic grains from further growth and promote super-plastic behaviour during extrusion which leads CNTs to align preferentially along the extrusion direction (Fig. 2. 23) [143].

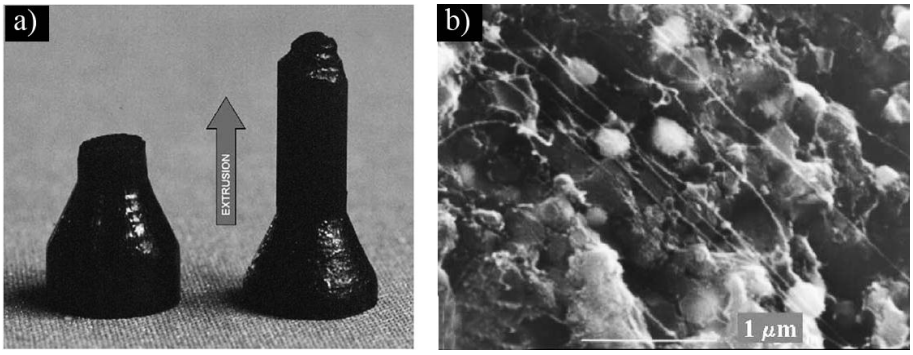

Fig. 2. 23. (a) Photograph of composite created by extrusion during the early stage (left hand) and final (right hand) stage of the process, and (b) alignment of CNTs along the extrusion direction [143].

ii. Spark plasma sintering (SPS)

SPS is a novel method to fabricate compact of ceramics and powdered metals at lower temperature (~1200 ˚C in the case of ceramic/CNT composites) and shorter reaction time compared to other conventional methods. Similar to hot-pressing method, precursors are loaded in a die and an uniaxial pressure is applied during the sintering but instead of using an external heating source, a pulsed direct current passes through the die that is electrically conductive and, if applicable, also through the sample. The die works as a heating source and the specimen is heated from both inside and outside (Fig. 2. 24). In this process, the heat transfer from the die to the sample is very efficient. Consequently, the key factors of this method are the possibility of sintering fully dense samples using very fast heating rates and very short reaction time (minutes). The inventors of SPS claimed that the pulses generated spark discharges and even plasma between the powder particles, therefore spark plasma sintering gets its name [144].

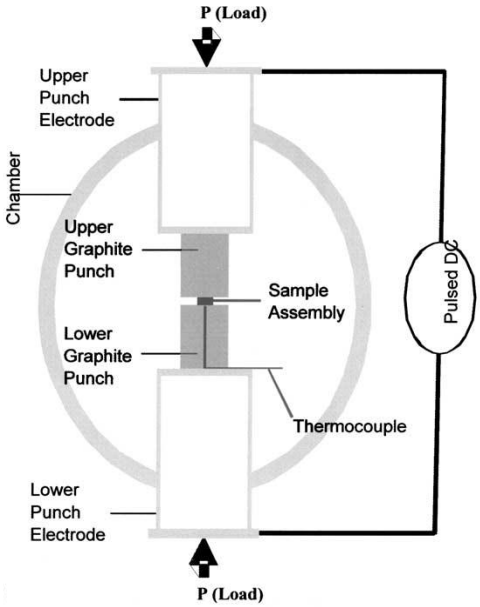

Fig. 2. 24. Schematic of a SPS apparatus [145]

Zhan et al. have reported the successful fabrication of composite by blending and ball milling SWCNTs with alumina nanopowders followed by SPS at 1150˚C for 2-3 minutes, and they have achieved a full density of 100%. The grain size of the composite was also observed to be considerably smaller than that of pure alumina. Therefore, CNTs can effectively retard the grain growth of alumina during spark plasma sintering (Table. 2. 2) [24].

Table. 2. 2. SPS conditions and the resultant properties on alumina/SWNT composite [24].

Materials	SPS conditions	Relative density (%)	Grain size (nm)	Hardness (GPa)	Fracture toughness ($MPa\,m^{1/2}$)
Al_2O_3	1150 °C, 3 min	100	349	20.3	3.3
Al_2O_3/5.7 vol% SWNT	1150 °C, 3 min	100	~200	20.0	7.9
Al_2O_3/10 vol% SWNT	1150 °C, 3 min	100	~200	16.1	9.7
Al_2O_3/10 vol% SWNT	1150 °C, 2 min	95.2	156	9.30	8.1
Al_2O_3/10 vol% SWNT	1100 °C, 3 min	85.8	150	4.40	6.4

Peigney et al. have claimed that the best combination of microstructure and mechanical properties can be obtained by using hetero-coagulation and SPS at lower temperature [2]. Poyato et al. have shown that sintering the colloidally dispersed composite powders at high temperatures (1550 ˚C) converted CNTs to disordered graphite, diamond and carbon-onions (Fig. 2. 25). This showed the temperature sensitivity of this approach and

explained why a balance between these parameters should be identified to avoid CNTs degradation [146].

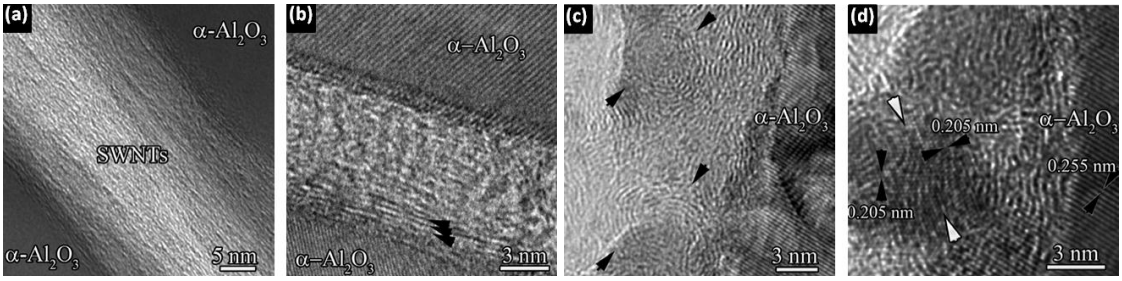

Fig. 2. 25. High resolution TEM micrograph of SWCNT/alumina composite showing (a) aligned SWCNT bundle, (b) disordered graphite and some SWCNTs (arrows), (c) carbon nano-onions (arrows), and (d) diamond nanocrystals [146].

In summary, powder processing of nanocomposites mostly involves different stages which make the fabrication expensive and time consuming. The high processing temperatures, potential damage to CNTs, and long processing time for powder preparation and sintering are the main technical barriers. Parameters such as pressure, temperature and atmosphere are very sensitive and a close monitor of these parameters are required for desirable composite properties [12].

2. 7. 4. Porous ceramic/CNT composite

In-situ synthesizing composites, i.e., by direct growth of CNTs inside pores of engineering ceramics offers the potential to avoid many of the drawbacks arising from *ex-situ* processing, in addition to the advantages of offering short reaction times at lower cost [139, 147]. The open pore substrates are appropriate places for the *in-situ* growth of CNTs and, depending on the level of porosity and degree of filling of these pores, multi-functional engineering ceramics can be resulted. By embedding catalyst particles inside very tiny pores, made by patterning process, followed by CVD, highly ordered CNTs can grow inside to form the composite, as shown in Fig. 2. 26 [139, 148]. Proper substrates are mostly mesoporous silica [28], silicon [29], or anodic aluminium oxide (AAO) membrane [30], and the deposition of carbon occurs on the internal pore surface of the matrix, copying the simple channel structures [31]. This technique features a simultaneous carbon deposition rather than a continuous nanotube growth; therefore the

shape and morphology of CNTs are restricted by the parent pore size and structures which are generally limited to µm to mm in thickness for the composites. These AAO templated deposition leads to a thin layer of composites, suitable for applications such as field emitters [149], nanocapacitors [150], and scanning probes [151]. Innovations to overcome the size limitations are required for this technique.

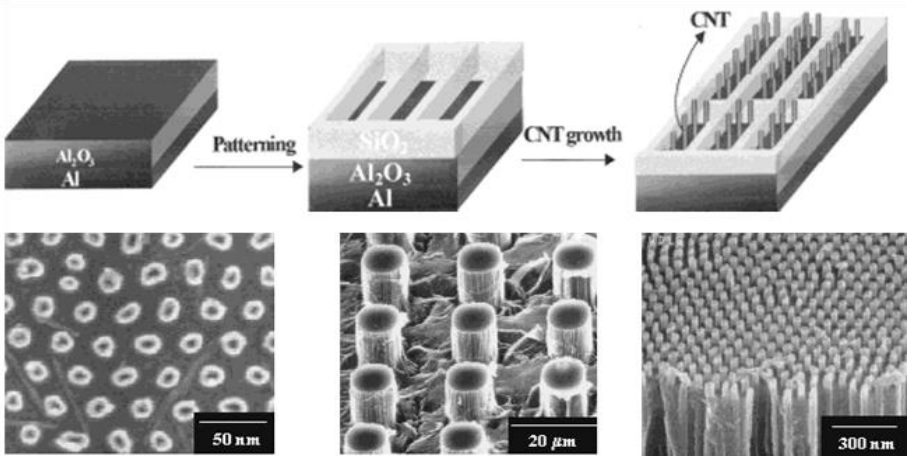

Fig. 2. 26. Schematic of the fabrication method for highly ordered CNTs in ceramics [148].

2. 7. 5. Polymer/ceramic composite

Cellular ceramics consists of different arrangements of space-filling polygons (cells), and can be classified into two broad groups of honeycombs and foams. In honeycomb, the cells form a two-dimensional array; whilst foams are made of three-dimensional arrays of hollow polygons [152]. Ceramic foams can be considered as linked networks of irregularly shaped open (or partly open) or closed (or partly closed) cell polyhedrons with a low fractional density. These porous network materials have a high number of interconnected pores [153, 154], resulting in high specific area, low density, high thermal resistance [155], low thermal conductivity and high flow and fluids permeability [156, 157]. As a result, these materials are promising for a wide range of applications, such as catalyst supports [158], filters for hot gases [159] and molten metals [42].

Polymer-ceramic composites are a rare class of functional materials. The high hardness, stiffness and wear resistance of ceramics combined with the excellent elasticity of polymer can be an advantage in commercial applications, but is limited by

the poor mechanical properties of ceramics [38-40]. This type of composites has a higher initial compressive strength and sustains larger deformations, in comparison to porous ceramics. Therefore, they may absorb energy more efficiently than both components separately, which makes them desirable for lightweight shielding or protective panels against impact loads.

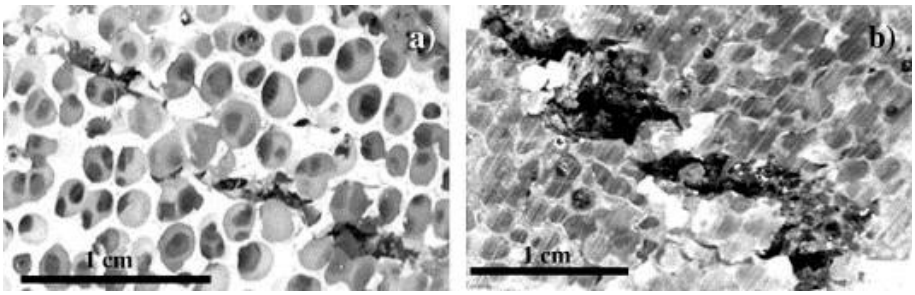

Fig. 2. 27. Optical images of a) $SiO_2.ZrO_2$/polymer, and b) SiC/polymer composite material [42].

- **Mechanical properties:**

Using cellular ceramic (SiC and $SiO_2.ZrO_2$) and epoxy vinyl-ester resin to produce ceramic foam-polymer composite material, Gomez et. al [42] have reported a 50 to 200 times improvement in the initial compression strength of the composites, due to the high stored elastic energy resulted from the incorporation of the polymeric material to the structure. Based on their results, infiltration of polymeric material to the ceramic structure improves the elastic behaviour via awarding a physical joint among the reinforcement and ceramic matrix. They proposed two dominating factors that determine the behaviour of the composite: the interface and wettability. If the polymer does not completely fill the matrix pores, the remaining voids will act as a stress concentration point, reducing the compression strength. If the adherence at the interface is not strong enough, the material will tear, again leading to strength reduction.

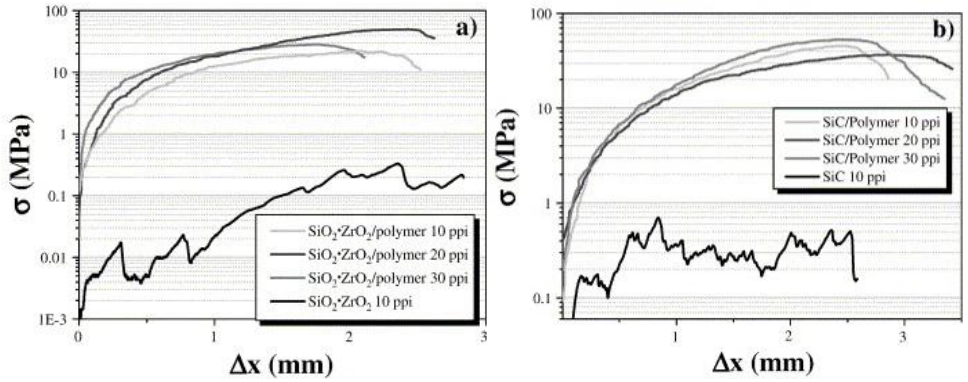

Fig. 2. 28. Compression stresses of a) SiO_2.ZrO_2/polymer and b) SiC/polymer [42].

Wear test evaluation is based on the composite weight loss against wear distance. In a general ball-disc testing, these composites show an abrasive wear. The wear behaviour in small sliding distances is owing to selectively taking materials which forms a protective film on the ball surface. When a critical distance is reached, a blade effect occurs and the take-off particles are joined up to accelerate the wear process [42].

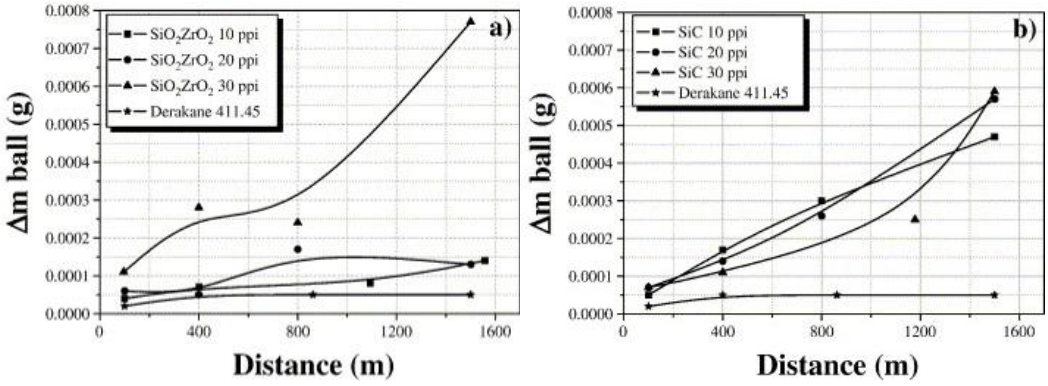

Fig. 2. 29. Variation in weight loss of ball as a function of sliding distance for a) SiO_2.ZrO_2/polymer and b) SiC/polymer [42].

It is also possible to infiltrate the porous ceramics with thermoplastic materials. Boczkowska et al. [40, 41, 160, 161] have published several reports studying the properties of ceramics infiltrated by urea-urethane elastomers. Their composite presents high compression strength along with the ability to sustain large deformation. This is because the elastomer exhibits the rubber elasticity and deforms after the ceramic lost its cohesion (Fig. 2. 30) [41].

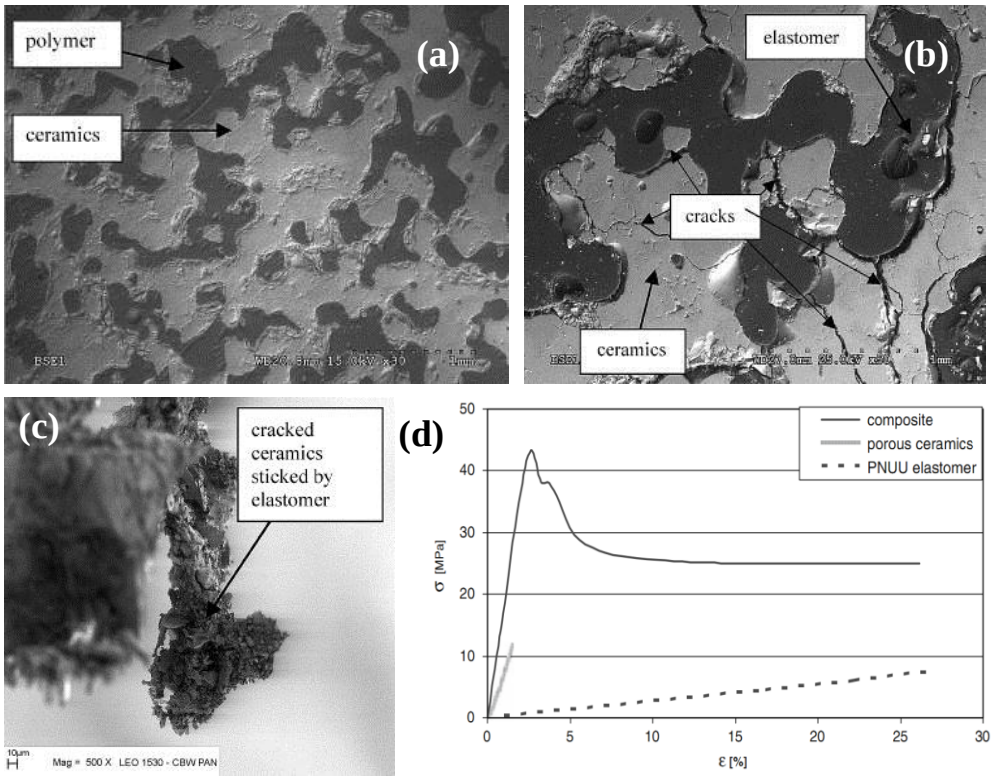

Fig. 2. 30. (a) Microstructure of the ceramic-elastomer composite, (b) crack propagation in composite after compression test, (c) cracked ceramic matrix stuck by the elastomer [41], and (d) stress-strain graph of porous ceramic, elastomer and ceramic-elastomer composite [40].

Although during compression test, micro-cracks occur in their composite (Fig. 2. 30b), the composite maintain cohesion (Fig. 2. 30c) and dissipate mechanical energy [40]. This energy absorbing capacity under compressive conditions is comparable to some aluminium foams [162], and other energy absorbing composite structures [163, 164]. The high compression strength of composite is the result of crack energy dispersion by the elastomer which deflects cracks propagation through the ceramics.

Moreover, it is important to add that the elastomer-ceramic composites display electrical and chemical properties of the ceramic matrix, which makes them useful for a host of sensor and actuator applications, such as piezoelectric polymer-ceramic composites for strain monitoring and hydrostatic sonar sensors [160, 165].

Addition of CNTs into such composites as a reinforcement can potentially lead to further improvement in their properties. Currently, there are no reports available for

such functional material (polymer-ceramic-CNT) to be mentioned here, and this will be a research subject of this thesis.

2. 8. CNT nanofiltration properties

Pollution crisis caused by human activities counts as a major problem all around the world, especially in industrial regions and metropolises. The pollutions into the air and water represent a threat to human health and the surrounding natural resources, affecting the lives of millions of people. Inhaling polluted air, particles in the air enter the body. While micronized particles can be captured by nostril hairs, submicron and nano-sized particles can reach the lungs and subsequently remain in the alveoli and cause respiratory problems [166].

Clean water (free of toxic chemicals and pathogens) plays a vital role in human health, and is a critical feedstock for a variety of industries including pharmaceuticals and food [167]. Difficulties in removing organic (such as bacteria and viruses) and inorganic (such as heavy metal ions) contaminations from water have challenged researchers to meet the rising demands for clean water. Waste waters from many industries including metallurgical, mining and battery manufacturing industries etc. contain one or more toxic heavy metal ions. As these contaminations are non-degradable they can accumulate in living tissues. There has been increasing concern and more stringent regulation standards pertaining to their discharge and removal from aquatic environment [168].

Table. 2. 3. Physical properties of carbonaceous nanomaterials and their related environmental applications [45].

		Environmental Applications						
		Pollution Prevention	Sorbents	Composite Filters	Energy Storage	Antimicrobial Agents	Aligned CNT Membranes	Sensors
Physical Properties	Size		X	X		X	X	X
	Shape					X	X	
	Surface Area	X	X	X	X			
	Molecular Specificity		X		X			X
	Hydrophobicity		X	X		X	X	
	Electrical Conductivity				X			X
	Optical Activity		X					
	Thermal Conductivity	X			X			
Bulk Properties		X						
Individual Properties		X						

Innovations and advances in nanotechnology and nanomaterials have the ability to address many of the above issues. Among these, carbonaceous nanomaterials in both individual and bulk configurations have already opened their way towards many environmental applications (Table. 2. 3). In particular, CNTs have shown great absorbing properties due to their high aspect ratio and large specific surface area. This makes them promising for applications in absorption, filtration and separation industries in both gaseous and aqueous systems [9, 10, 36, 169].

2. 8. 1. Air particulate filtration

Heating, ventilating and air conditioning (HVAC) air filters are intended for air purification work in dark, damp and ambient temperature conditions provide ideal conditions for bacterial and fungal attacks. The situation becomes worse when these micro-organisms adhere to the accumulated dust on the filter and consume the accumulated dust as food and proliferate. As a result, there will be an unpredictable deterioration of quality of air and the production of bad odours. Using CNTs with their antibacterial property, a nanofilter with improved mechanical properties and efficiency could be produced. Such nanofibrous filtering media can be used where high-performance air purification is required like in hospitals, healthcare facilities, research labs, electronic component manufacturers, military and government agencies, food, pharmaceutical and biotechnology companies [170].

The contaminants during air filtration are complex mixtures of particles and most of them are usually smaller than 1000 µm in diameter. Fibrous filters are usually fabricated using fibres of diameters about a few dozen micrometres containing 80–90% porosity. Such structure allows for a high efficiency removal of submicrometre and micrometre particles with a relatively low resistance to the air flow. However, there is a critical particle size that a filter does not filtered out as efficiently as other particles, which is called the most penetrating particle size (MPPS). The fibrous filter efficiency achieves a minimum for this particle size which is usually between 0.1 and 0.5 µm [170]. The minimum efficiency shown in Fig. 2. 31 is contributed to the filtration efficiency of MMPS [171]. Theoretical predictions and preliminary investigations of Podgórski et al. have indicated that significant increase of the filter efficiency for the MPPS can be achieved by only a slight rise of the pressure drop using the nanometre fibres to produce the fibrous filters [172].

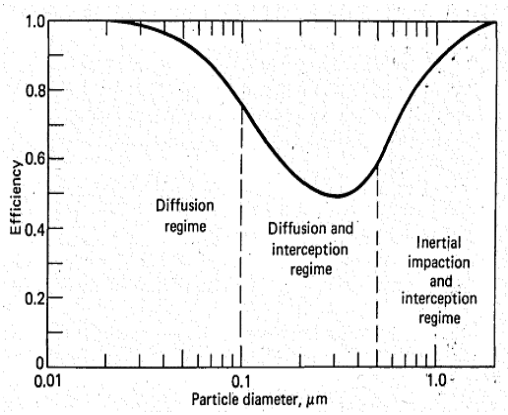

Fig. 2. 31. Collection efficiency of the molecular capture mechanism as a function of particle size. The minimum efficiency is contributed to the MPPS [173].

Halonen et al. [8] fabricated a three-dimensional CNT scaffold particulate filter using micromachined Si/SiO_2 template. They reported an efficiency of better than 99% for particles 0.3 µm using ambient air for testing, and believed that the very high efficiency was attributed to the high density packing of CNTs. The configuration of their filters is shown in Fig. 2. 32.

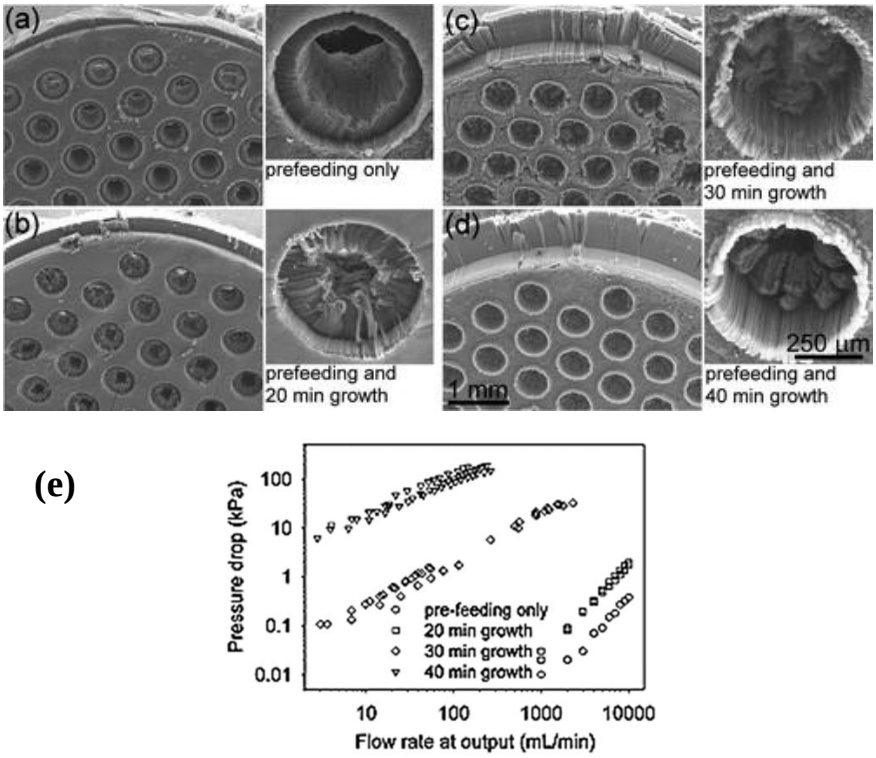

Fig. 2. 32 SEM images of various CNT membranes grown on microstructured and oxidized Si chips: synthesis times of (a) 0, (b) 20, (c) 30, and (d) 40 min. (e) Pressure drop *vs* flow rate of nanotube membranes. Samples with longer growth time show decreased permeability due to the tortuous CNT films and closed up macroscopic holes [8].

Park and Lee [174] first grew CNTs (20 to 50 nm diameter using CVD method) on micron-sized stainless steel fibres, then evaluated their air particulate removal performance using sodium chloride (NaCl) as the test particles. They improved the efficiency from 75% up to 98% by the fabrication of web-like CNTs on their fibres. Similar results have also been reported by Park's group using glass fibre [175].

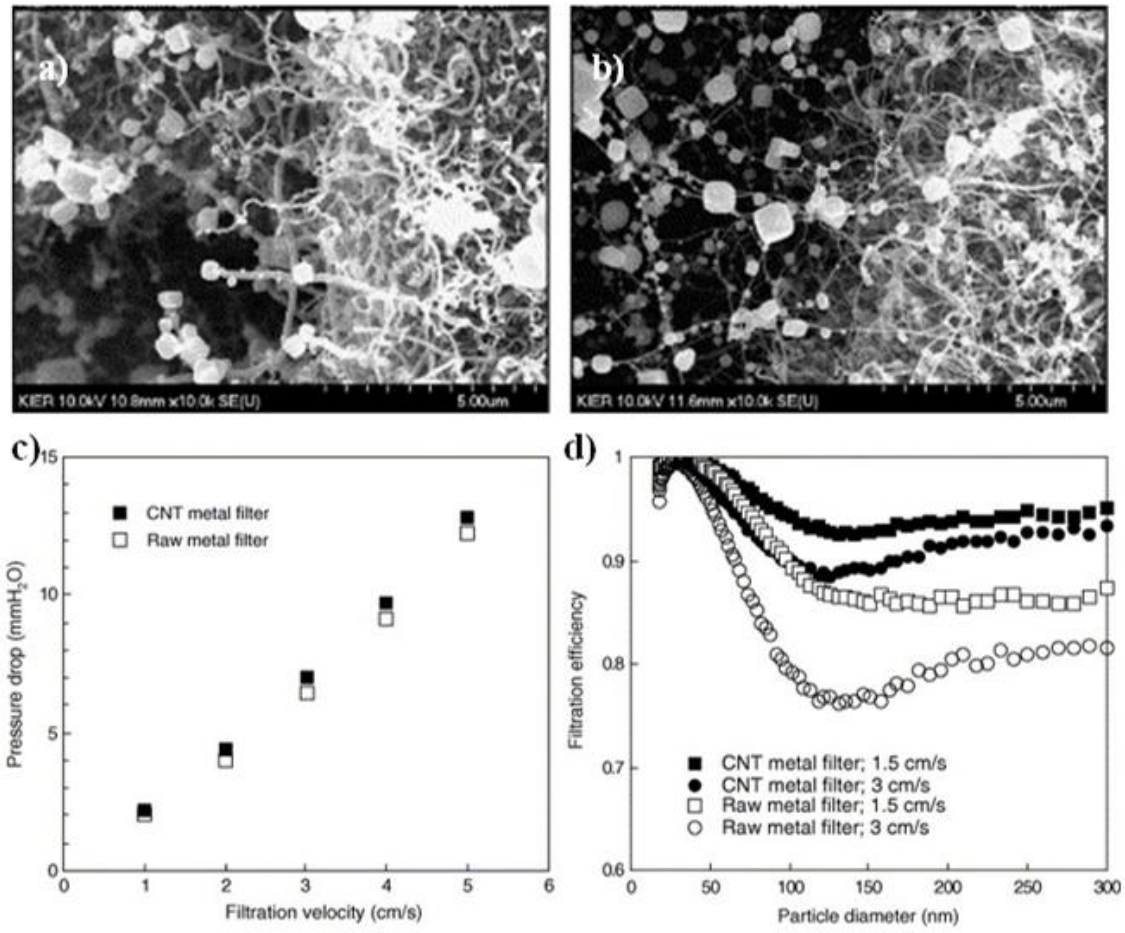

Fig. 2. 33. (a and b) SEM images of NaCl particles collected onto the filter [174]. Performance comparison of the raw metal filter and the metal-CNT-filter. (a) Pressure drop is not significantly changed by the direct growth of CNTs. (b) Filtration efficiency increases by the CNT growth [36].

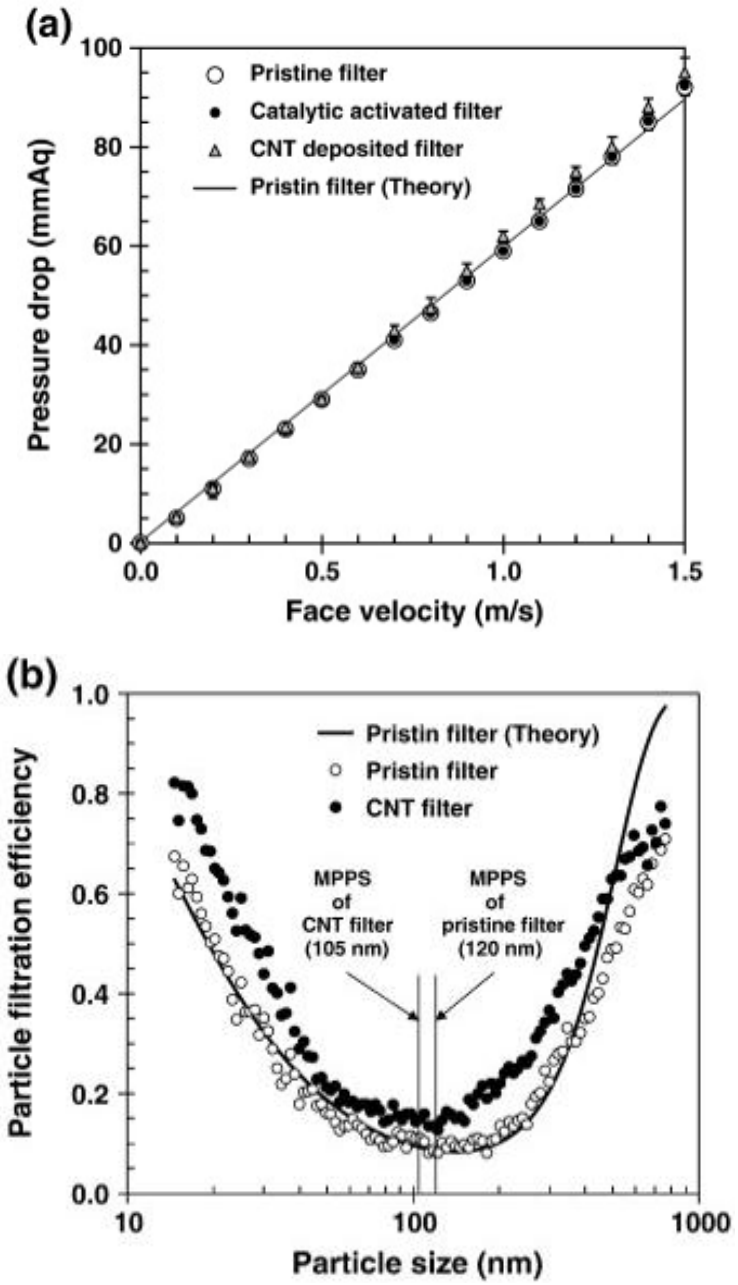

Fig. 2. 34. (a) Pressure drops, (b) particle filtration efficiencies for glass fibre-CNT filter [175].

2. 8. 2. Biological contamination filtration

Biological contaminants form a large portion of the drinking water contaminants, both in terms of number and probability of occurrence in the treatment plant. High efficiency filtration of such contaminations has been achieved using membranes in polymer, ceramic or metal forms [176]. Polymer membranes are fragile and less durable, and they need to have submicron nominal pore sizes for micro and nanofiltration [176]. In conventional membrane filters used in water filtration, strong

bacterial adsorption on the membrane surface affects their physical properties and hinders their reusability. It is suggested that using CNTs in membranes can be an effective way of making a practical hybrid filter with exceptional robustness for reuse. Limited practical studies have demonstrated the use of CNTs for this purpose. The high efficiency of CNTs in filtering micro-organisms from aquatic systems can be explained by their high surface areas and large aspect ratios. The agglomeration of highly densely packed CNTs forms microporous and mesoporous networks with the right pore sizes to immobilize contaminants via physisorption [32]. In addition, the microbial cytotoxicity of CNTs also plays a partial role in their filtration performance [10]. The high thermal stability of CNTs is another factor which allows for higher operating temperatures (~400 ºC), compared to the conventional polymer membrane filters (~52 ºC) [9]. A simple ultrasonication and autoclaving (~121 °C for 30 min) was found to be enough for cleaning these filters for reuse [9].

Brady-Estevez et al. deposited CNTs on a microporous ceramic filter (5 µm pore size) in order to immobilize them and increase the filter permeability. They demonstrated their filters for the removal of viral and bacterial pathogens, with extremely high efficiencies [10].

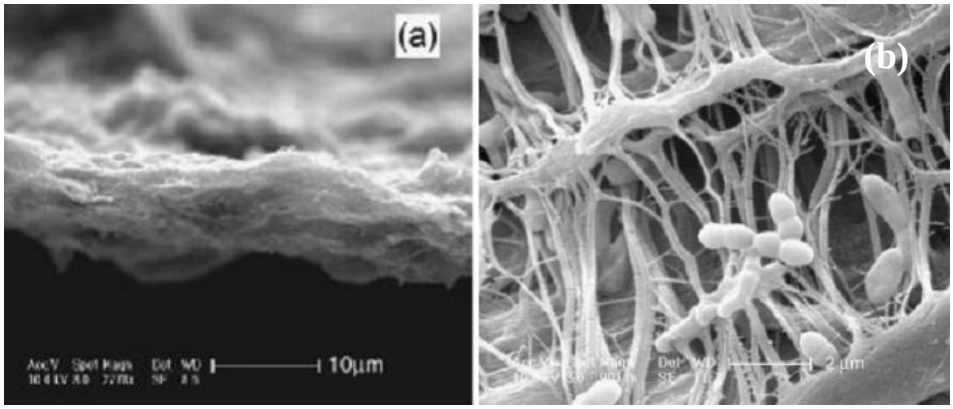

Fig. 2. 35. SEM images of a) the cross-section of SWCNT layer and b) E. coli cells on the base membrane [10]

Srivatava et al. have produced a cylindrical membrane filter with aligned CNTs (Fig. 2. 36) for the removal of hydrocarbons from petroleum wastes, and for as the

removal of viruses and bacteria from water. Their filter was fabricated by pyrolosis of pre-sprayed benzene and ferrocene into a tube quartz mould at 900 ˚C [9].

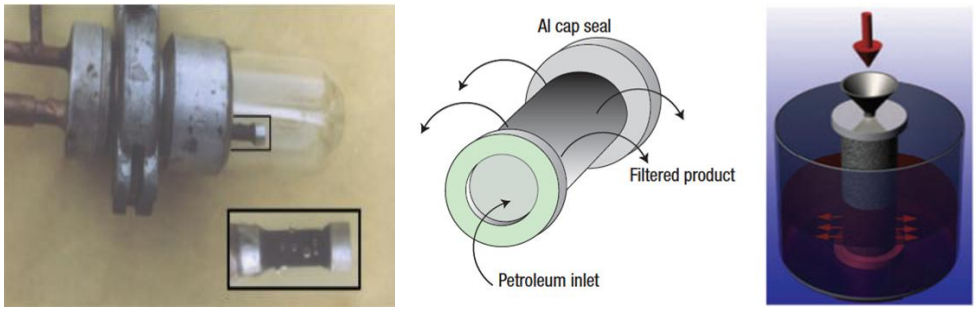

Fig. 2. 36. Cylindrical membrane filter made by aligned CNTs for removing hydrocarbons from petroleum wastes and bacteria and virus separation from water [9].

Akasaka and Watari showed that SWCNTs and thin MWCNTs (~30 nm) which are moderately flexible can be easily wound around the curved surface of Streptococcus mutans (Fig. 2. 37) and be used as a tool for elimination of oral pathogens at nano-level [177]. There are other similar reports using CNTs for filtering bacteria and viruses (Fig. 2. 38) using several steps. First the CNTs were dispersed in a solution contain the bio-contaminants, followed by shaking the suspension for a long enough time to allow the adsorption to complete, then the CNTs were removed using a paper filter or a suitable membrane.

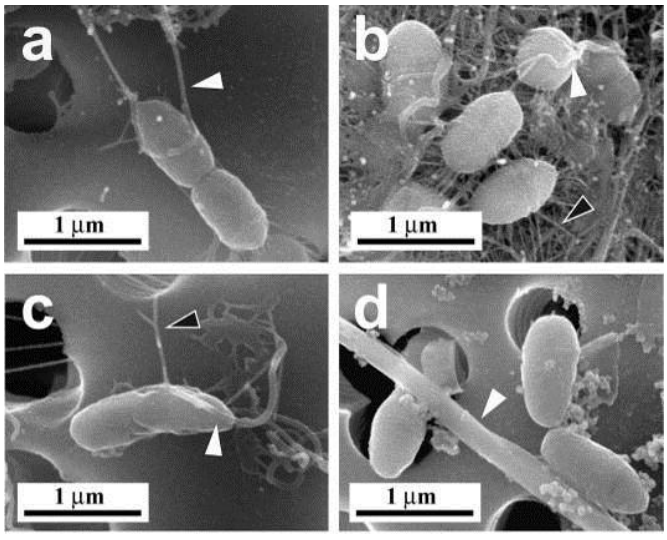

Fig. 2. 37. SEM images of bundles of SWCNTs wound around *S. mutans* (a); the bacteria adhered to the meshwork comprising bundles of SWCNTs (b); 30-MWCNTs wound around bacteria (c); 200-MWCNTs adhered but did not wind (d); The white arrows indicate CNTs. The black arrows indicate fibrous substances produced by bacteria [177].

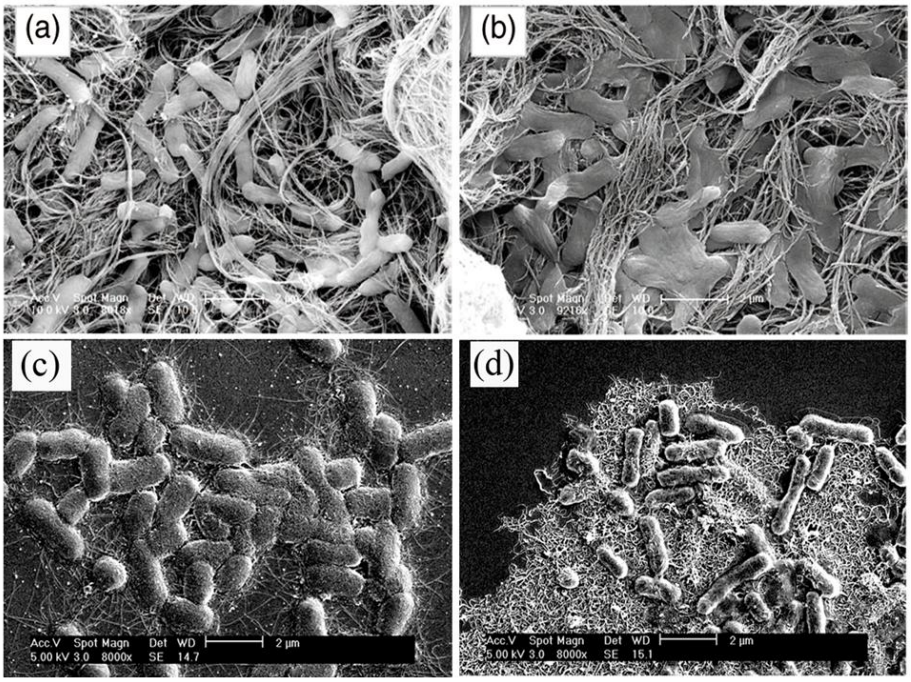

Fig. 2. 38. SEM images of E. coil cells exposed to MWCNTs (a) and SWCNTs (b) [178] and also Salmonella cells exposed to acid treated (-COOH) SWCNTs (c) MWCNTS(d) [179].

2. 8. 3. Heavy metal ions adsorption

The pollution of water resources due to the indiscriminate disposal of metal ions has been causing worldwide concern. In this regard, CNTs have been the subject of many studies which have tried to remove such contaminations from wastewater. Examples include the removal of Cu, Pb, Cd [180], Zn, Mn, Co [33], Ni [181], Cr [182], Hg [183] and U [184] ions.

Sorption mechanism of heavy metals by CNTs is more a chemisorption process rather than physisorption as the chemical interaction between the metal ions and the surface functional groups of CNTs (formed during oxidation) is the dominating mechanism compared to electrostatic attraction and sorption–precipitation [185]. Consequently, the chemical and thermal treatments during functionalization procedure have leading effect on the capability of CNTs for metal ions removal, and their adsorption behaviour is mainly determined by the nature and concentration of the surface functional groups. Table. 2. 4 summarizes the adsorption capacity of different functionalized CNTs synthesized with different carbon sources and catalysts.

Table. 2. 4. Maximum sorption capacities of divalent metal ions with CNTs [185]

Metal ions	Sorbents	STA	STB	q_m	ref.
Ni^{2+}	SWCNTs	0.54	0.23	9.22	[181]
	SWCNTs (NaOCl)	4.42	0.35	47.85	
	MWCNTs	0.44	0.19	7.53	
	MWCNTs (NaOCl)	3.06	0.31	38.46	
Pb^{2+}	CNTs (HNO_3)				[180]
	Xylene–Fe	1.63		14.8	
	Benzene–Fe	1.65		11.2	
	Propylene–Ni	4.04		59.8	
	Methane–Ni	4.31		82.6	
Zn^{2+}	SWCNTs			11.23	[186]
	SWCNTs (NaOCl)			43.66	
	MWCNTs			10.21	
	MWCNTs (NaOCl)			32.68	
Cd^{2+}	As-grown CNTs			1.1	[187]
	CNTs (H_2O_2)	2.52		2.6	
	CNTs ($KMnO_4$)	3.36		11	
	CNTs (HNO_3)	4.04		5.1	

STA = surface total acidity (mmol/g), STB = surface total basicity (mmol/g), q_m = maximum sorption capacity (mg/g).

Different terms and aspects of heavy metal ions adsorption over CNT are well studied and reports have well-covered effective parameters on it. For example, increasing sorption temperature results in a significant rise in the sorption capacity which shows that it is an endothermic reaction [188, 189]. It is obvious that increasing mass of CNTs results in higher adsorption percentage of metals due to availability of more sorption sites. However, this increase is limited up to a certain value [190].

It is shown by Li et al. [188] that the sorption capacity of Pb^{2+} onto CNTs will increase quickly with contact time and then slowly reaches equilibrium. It is apparent that the equilibrium would be reached faster at lower heavy metal concentrations as at such low concentrations the sorption site adsorbed the available metal ions more rapidly [190, 191].

Waste waters from many industries such as metallurgical, chemical and battery manufacturing industries contain more than one toxic heavy metal ions. Thus, running test in competitive condition is more close to the real world situations. Li et al. [34] studied the individual and competitive sorption of Pb^{2+}, Cu^{2+} and Cd^{2+} ions onto HNO_3 oxidized CNTs. The sorption capacities of CNTs for the three metal ions are in the order of Pb(II) > Cu(II) > Cd(II) and the competitive sorption of metal ions also follows the same order. These results do not confirm the affinity order of Cu(II) > Pb(II) > Co(II) found by Stafiej and Pyrzynska as the result of different synthesising method and functionalization processes (Table. 2. 4) [33].

Finally, in order to justify the high initial cost of nanofilters and introduce them as a practical solution for challenges in wastewater treatment, it is important to show their reusability. Liang et al. [192] claimed that the Cd^{2+}, Mn^{2+} and Ni^{2+} ions could be effectively desorbed from the MWCNTs by a 1.0 mol/L HNO_3 solution and the performance was stable up to 50 adsorption–elution cycles without obvious decrease in the recoveries for the studied ions. Chen and Wang [193] found that the Ni^{2+} desorption can ultimately reach 93% at pH < 2.0. Li et al. [188] showed that desorption of the Pb^{2+} increased with decreasing pH of the regeneration solution and reached 100% Pb^{2+} desorption from CNTs using HCl or HNO_3 solutions at a pH of 2.0.

In all these reports, metal ions removal has been performed by soaking loose CNTs into solutions for several hours before being collected using a filter paper, which is slow, time consuming and less controllable [34, 189, 194]. Thus, the immediate technological challenge is how to convert the proven excellent adsorption behaviour of

loose CNT powder into a cost effective and viable filter for specific applications which is another concern of the current work.

2. 8. 4. Other CNT filtration applications

There are also many other reports revealing the successful use of CNTs in filtering applications. Some of them will be briefly introduced here.

Gui et al. have successfully synthesised a sponge with CNTs which can clearly reflect the great adsorption property of this carbon cluster [195]. They fabricated a sponge-like bulk material of self-assembled, interconnected carbon nanotube skeletons with a porosity of >99% and a density close to the lightest aerogels. Their sponge shows high structural flexibility and robustness and also wettability to organics. As they have claimed, their sponge has the ability to be deformed into any shapes elastically and compressed to large-strains repeatedly in air or liquid without collapse (Fig. 2. 39).

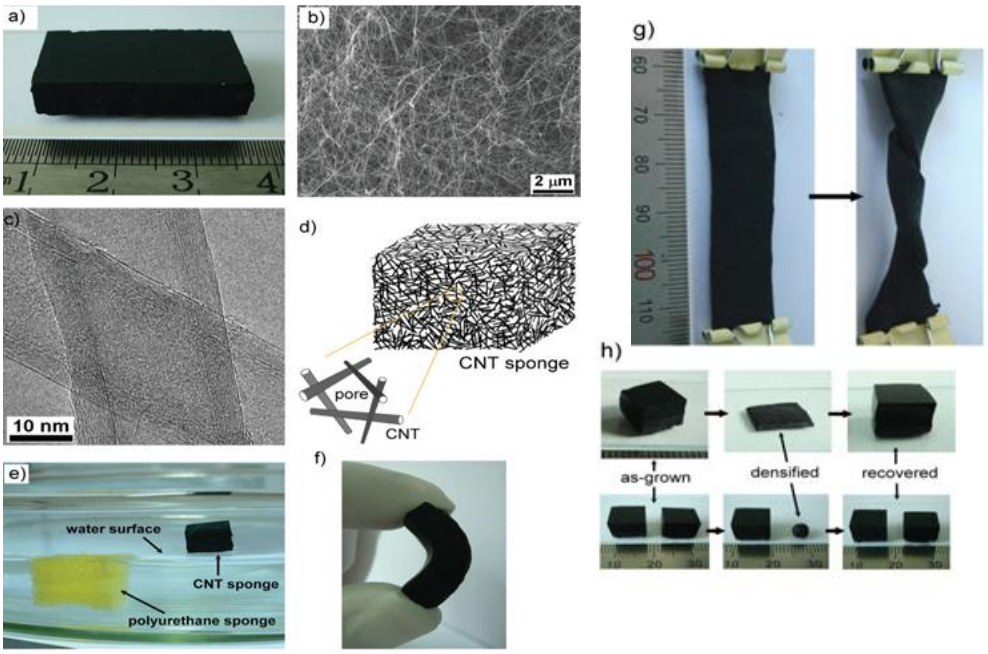

Fig. 2. 39. (a) A monolithic sponge with a size of 4 cm× 3 cm× 0.8 cm, (b) a cross-sectional SEM image of the sponge, (c) TEM image of CNT shows their thin and god quality, (d) illustration of sponge and its open pores, (e) comparison between polyurethane and CNT sponges in which the CNT sponge floating on the top while the polyurethane sponge has sunk after adsorbing water, (f & g) flexibility of the sponge is shown after bending and twisting three round turns without breaking, and (h) densification of the cubic shape sponge into a small pellet and its full recovery to first shape after adsorbing ethanol [195].

This sponge absorbs a wide range of solvents and oil with outstanding selectivity, recyclability, and adsorption capacities up to 180 times of their own weight. It is claimed that one small densified pellet floating on water surface can rapidly eliminate a spreading oil film with an area of up to 800 times that of the sponge showing the promising potential environmental application of CNTs such as water remediation and large-area spill clean-up (Fig. 2. 40) [195].

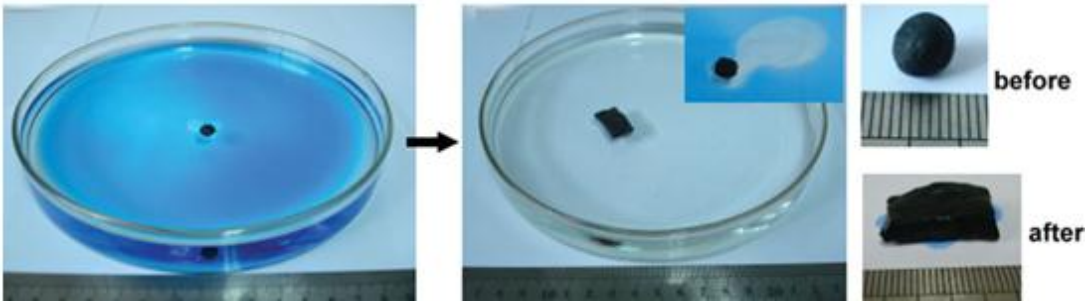

Fig. 2. 40. Large area oil clean-up demonstration. A diesel oil film with an area of 227 cm^2 and 2 grams in total weight spreading on water and the densified sponge (pellet shape) placed in the centre (left panel). The cleaned water surface after complete oil removal process is shown in the middle. The images on right hand side illustrate the change in volume and shape of sponge after adsorption form a 6 mm diameter spherical pellet to a rectangular monolith (2 cm× 1.4 cm× 0.6 cm) [195].

Lee and Baik have also fabricated a nanotube membrane filter with ability to separate diesel and water layers, surfactant-stabilized emulsions, and also phase separation of the high viscosity lubricating oil and water emulsions (Fig. 2. 41). They fabricated their filter on stainless steel mesh using sandwich-like catalyst layer of iron deposited on the mesh using an electron beam evaporator followed by a CVD process [196].

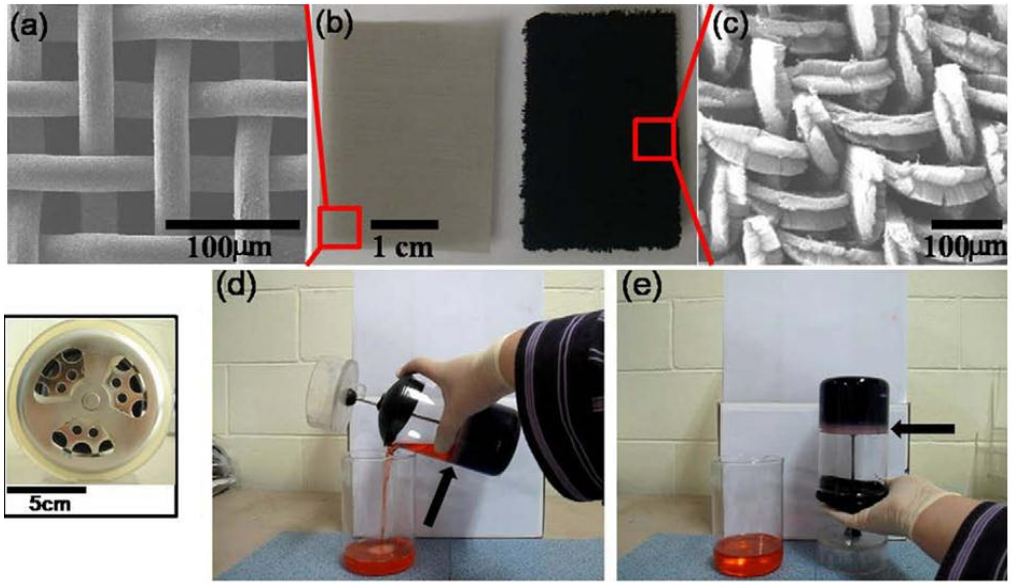

Fig. 2. 41. SEM and optical images of a stainless steel mesh before and after the synthesis of nanotubes (a, b and c), and separation of diesel from water using the membrane (d and e) [196].

Chen et al. have shown that the adsorption capability of oxidized CNTs (O-CNTs) for nicotine and tar from mainstream smoke (MS) is very high and by adding about 20-30 mg of them into the filter tips of cigarettes, it can prevent entrance of these harmful materials into the human body [197].

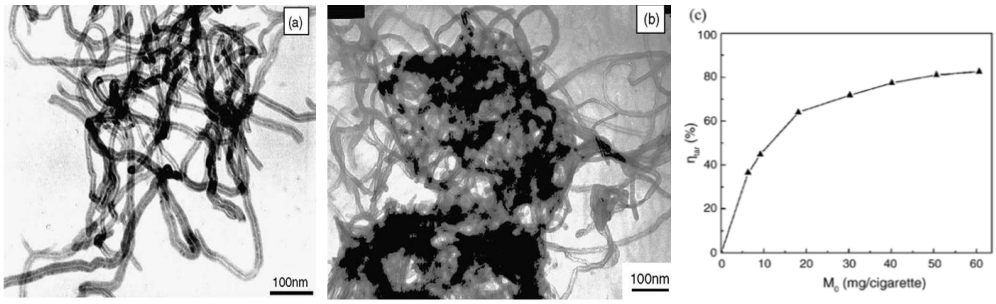

Fig. 2. 42. TEM images of O-CNTs before (a) and after (b) adsorption of tar in the MS, and (c) the removal efficiency of tar (η_{tar}) as a function of O-CNTs mass (M_o) [197].

2. 9. Toxicity of CNTs

Nanomaterials are part of an industrial revolution to develop lightweight but strong materials for a variety of purposes. CNTs are an important member of this class of materials. CNTs are very light and could become airborne and potentially reach the lungs. Lam et al. [198] have exposed mice to SWCNTs in order to study the effect of these nanomaterials. Their results show that high doses of CNTs are toxic if they reach

the lungs. They claimed that mice exposed to low dose (0.1 mg per mouse) of CNT (containing Ni and Y) showed no overt clinical signs. However, 5 of the 9 mice treated with high dose (0.5 mg) of CNT died. All deaths occurred 4 to 7 days after instillation of the CNT. Fig. 2. 43 shows photograph of lungs of mice before and after exposure to CNTs.

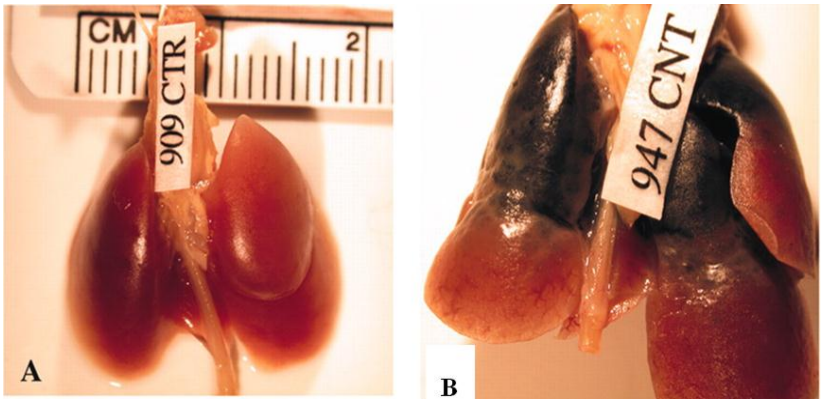

Fig. 2. 43. Lungs from mice instilled with 0.5 mg of a test material per mouse. (A) Serum control. (B) CNT. The portions of the lung receiving CNT have an abnormal appearance [198].

CNTs can penetrate into bacteria, damage the cytoderm and prevent the growth (Fig. 2. 44a) [199]. Animal models have shown that CNTs induce inflammation, oxidative damage and granuloma by different direct exposure ways [200]. There is also a concern about their indirect entrance into the food chain and endangering the downstream lives as well (Fig. 2. 44b) [201]. However, as it was mentioned, low amount of CNTs are nearly nontoxic [32, 201] and considering their capability in removing contaminants with much higher toxicity (such as lead [33], mercury [183] and uranium [184]), one can still justify their usage as an environmental solution.

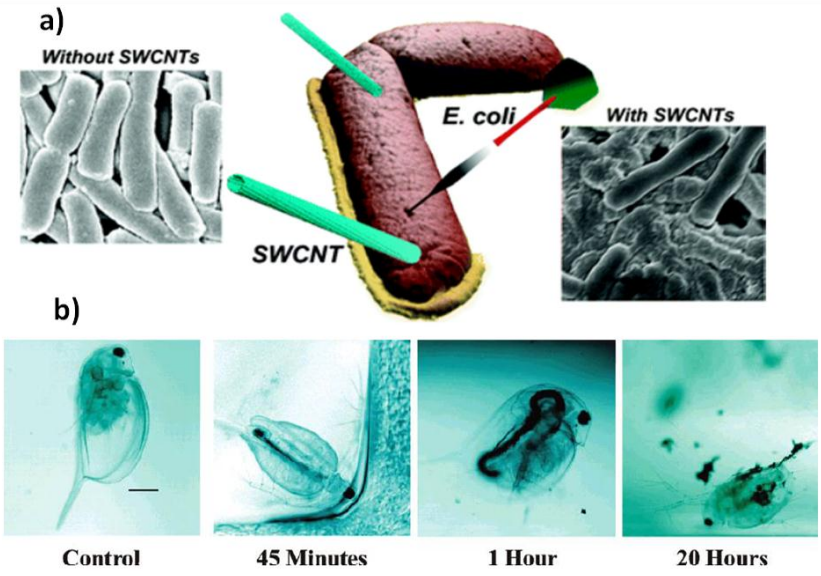

Fig. 2. 44. (a) Penetration of CNTs in bacteria has inhibited their growth [199], and (b) harmful effect of CNTs on *Daphnia magna* (large numbers of tubes filling the gut track at 45 min and 1 h) [202].

2. 10. Summary

In this chapter, the overall characteristics, the synthesising methods, the outstanding properties, and the potential applications of CNTs and relevant composites are described in details. In particular, attention was focused on the role of CNTs in reinforcing composites and on novel filtration applications. Based on the literature survey, the research work in this thesis was aimed to produce ceramic base composites with CNTs as nanofillers, considering both filtration and mechanical properties in an industrial scale. Details concerning the fabrication, mechanical properties and filtration efficiency of the composite will be documented in the following chapters.

The main objectives of this thesis can be summarized as follows:

- Fabrication of ceramic-CNT composites
- Fabrication of polymer-ceramic-CNT composites
- Measuring mechanical properties of the produced composites
- Evaluation of the filtration efficiency of ceramic-CNT composites in the removal of different sources of contaminations

Chapter 3: Experimental methodology

3. 1. Introduction

The experimental procedures used for the fabrication and characterisation of the functional materials presented in this thesis will be discussed in this chapter. This includes information such as chemicals and materials, techniques, synthesis procedures, sample preparations for tests and test parameters.

First section concerns the in-situ CNT fabrication inside different ceramic matrixes (porous ceramic and ceramic foam). The next part explains the infiltration of the prepared low density ceramic (or ceramic foam) composites with two sets of polymers (thermoset: epoxy resin and thermoplastic: Polyamide 12). These sections provide a generic experimental information about the synthesising procedures including the equipment and chemical precursors used. Then, the filtration and mechanical properties of the prepared ceramic-CNT composites will be evaluated. Detailed technical information related to each specific experiment will be further explained in the relevant chapters.

3. 2. In-situ fabrication of high density ceramic-CNT composite

3.2.1. Materials

Porous alumina, with a porosity of 76% and an average pore size of 100-150 µm (supplied by Dyson Technologies) was used as the matrix, to support the CNT growth (Fig. 3.1).

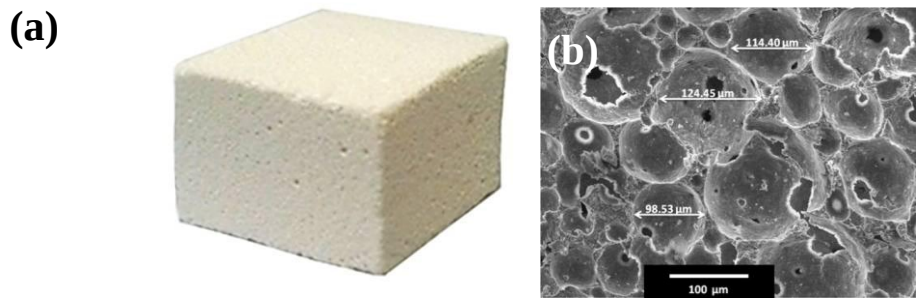

Fig. 3.1. (a) Photograph and (b) SEM image of an alumina brick (10×10×15 mm) used as the substrate for CNT growth.

A wide range of carbon sources and catalysts were used in order to find the best match suitable for the in-situ growth of CNTs inside the porous alumina. List of these materials are shown in Table. 3. 1. These materials are listed in Table. 3. 1. They were all purchased from Sigma-Aldrich, UK.

Table. 3. 1. List of catalysts and carbon sources tested for the in-situ growth of CNTs inside porous alumina in order to find out the most effective matches for nanocomposite fabrication.

Catalyst	**Carbon source**
Ferrocene	Ferrocene
Co nanoparticles	pitch
$Co(NO_3)_2$	styrene
$Ni(NO_3)_2$	camphor

Physical properties of most important carbon sources which were extensively studied in this experimental work are listed in Table. 3. 2.

Table. 3. 2. Physical properties of ferrocene, styrene and camphor [203]

	Ferrocene	**Styrene**	**Camphor**
Chemical formula	$C_{10}H_{10}Fe$	C_8H_8	$C_{10}H_{16}O$
Molecular structure	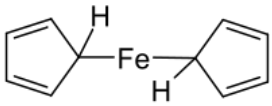	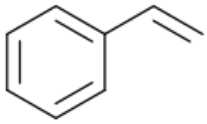	
Molar mass	186.03g/mol	104.15 g/mol	152.23 g/mol
Appearance	light orange powder	colourless oily liquid	White, translucent crystals
Density	1.490 g/cm^{3}at 25 °C	0.906 g/cm³at 25 °C	0.992 g/cm^3 at 25 °C
Melting point	172 °C	-30 °C	175 °C
Boiling point	249 °C	145 °C	204 °C
Solubility	Insoluble in water, soluble in most organic solvents	Insoluble in water	1.2 g dm^{-3} in water, ~2500 g dm^{-3} in acetone

3. 2. 2. Sample preparation

A wide range of temperatures (from 700 up to 1200 ˚C) were examined in accordance with each of carbon sources and catalysts. Carbon sources were introduced into the reaction chamber in two methods: injected into the furnace following conventional CVD process, and also placed inside the porous ceramic as solid carbon source (in the case of camphor) or very viscous source (in the case of pitch). Catalysts were used as both metal powders suspended in solution and also metal salts soluble in water and acetone. Eventually, use of camphor ($C_{10}H_{16}O$, 96%, Sigma-Aldrich) as the

carbon source, and nickel (II) nitrate hexahydrate crystals ($Ni(NO_3)_2 \cdot 6H_2O$, Sigma-Aldrich) as the catalyst lead to the best results.

Since both the catalyst and precursor are soluble in acetone, a solution of both materials was simply prepared. After repeatedly dipping the alumina bricks (10×10×15 mm) in the solution and then evaporating the acetone under a fume cupboard, a sample containing the carbon source and catalyst was obtained, which could be handled and processed easily. The alumina samples were then put into a quartz working tube in a pre-heated horizontal tube furnace at 850 °C under H_2 (Fig. 3. 2). After 3 minutes exposure time, the furnace was turned off and cooled down to room temperature under flowing Ar.

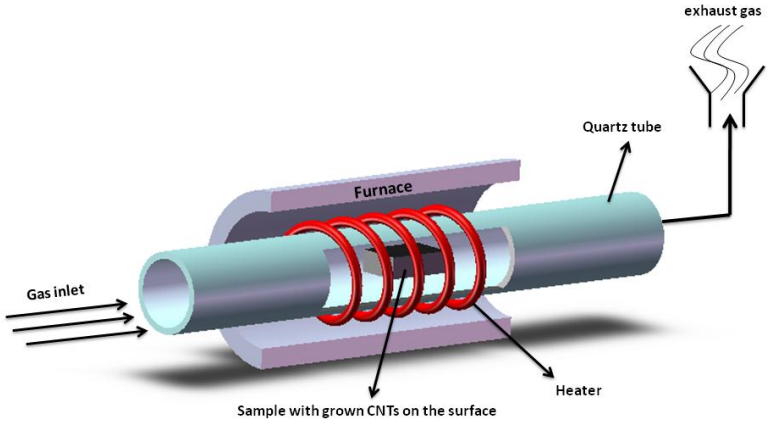

Fig. 3. 2. Schematic of the CVD set-up for the synthesis process

3. 3. In-situ fabrication of low density ceramic-CNT composite

3. 3. 1. Materials

In order to fabricate low density ceramic-CNT composite, camphor and styrene as the carbon source and ferrocene and nickel nitrate as catalyst were extensively used and effects of different growth conditions utilizing them were studied. Similar to previous experiment, ultimately, camphor ($C_{10}H_{16}O$, 96%, Sigma-Aldrich) was used as carbon source and nickel (II) nitrate hexahydrate crystals ($Ni(NO_3)_2 \cdot 6H_2O$, Sigma-Aldrich) as the catalyst. Porous filter ceramics of two different pore sizes (300 and 500 μm, purchased from Dynamic-Ceramic Ltd) with chemical composition of 81% Al_2O_3, 14% SiO_2, 2.5% K_2O and Na_2O and 2.5% other minute oxides (TiO_2,Fe_2O_3, MgO, CaO

and Cr_2O_3) were used as the matrix to support the CNT growth. A photograph and an SEM image of the ceramic are shown in Fig. 3.3.

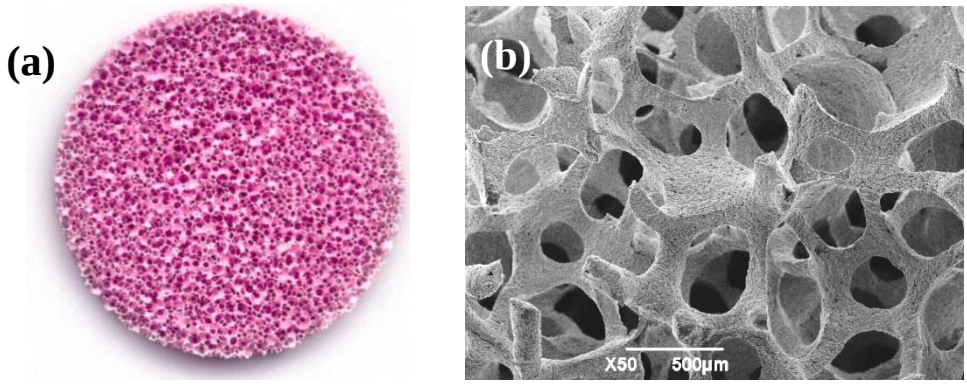

Fig. 3.3. (a) Photograph (disc o.d. 27× 10 mm) and (b) SEM image of ceramic used as the substrate for CNT growth.

3. 3. 2. Sample preparation

This time carbon sources were only precisely injected into the furnace but catalysts were both injected during experiment and placed on ceramic foam prior to the experiment. A wide range of temperatures (from 600 to 1100˚C) and carbon source injection rates (from 0.4 to 5 ml/h) were examined along with different hydrogen flow rates (from 0.1 l/min to 0.7 l/min). These experiments were carried out for different durations from 1 hour up to 6 hours. Effect of the addition of various amounts of ferrocene (from 0.2 wt.% to 2 wt.%) and nickel nitrate in the carbon source solution for possible increasing the CNT yield were also studied. The optimum combined condition for the CNT growth on a ceramic foam was eventually found to be at a H_2 flow rate of 0.30 l/min and carbon source injection rate of 0.8 ml/h and at 780˚C. Fig. 3. 4 presents an illustration of the CVD set-up used in this experiment for the in-situ fabrication of CNTs on a fitted ceramic foam inside quartz tube.

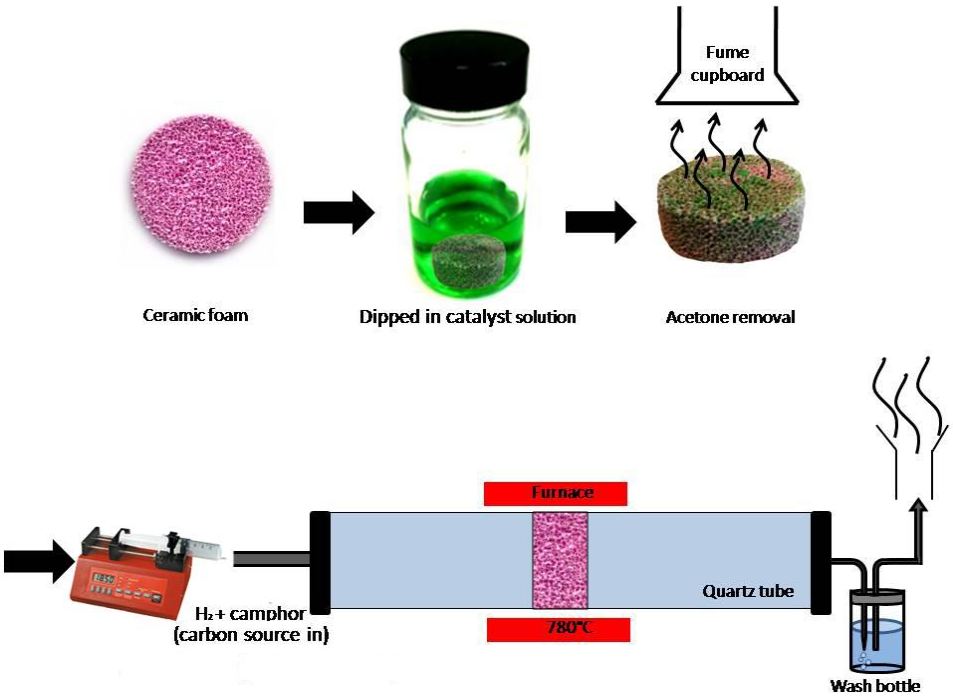

Fig. 3. 4. A schematic of the sample preparation and experimental set-up for the in-situ fabrication of CNTs on a fitted ceramic foam inside quartz tube.

In order to fabricate the ceramic-CNT composite, first, 1 wt. % $Ni(NO_3)_2 \cdot 6H_2O$ was solved in acetone to form a solution, and porous ceramics (o.d. 27 × 10 mm) were dipped in the solution in order to introduce the catalyst onto the surface of the pores. After the evaporation of the acetone under a fume cupboard, the ceramic matrix containing $Ni(NO_3)_2 \cdot 6H_2O$ was then placed in a quartz working tube (i.d. 27 mm) in a horizontal tube furnace. Second, after air was flushed out of the quartz tube using Ar, H_2 was introduced into the furnace at a flow rate of 0.3 L/min. Third, after 30 min reduction heating at 780ºC, a camphor acetone solution (40 vol. %) as the carbon source was injected using a syringe pump into the reaction quartz tube, at a rate of 0.8 ml/h and continued for 90 min. Finally, the furnace was cooled down to the room temperature, to obtain the composite filter.

For samples later used in filtration experiments, i.e. 300 and 500 µm pore sized samples, two sets of functionalized techniques were used to prepare the CNT filter samples:

1. Oxidized at 400 ˚C in air for 2 h. Ceramic-CNT composites were placed inside a quartz tube in furnace at 400˚C while compressed air was used as carrier gas at 0.1 L/min rate.
2. Functionalized in preheated nitric acid solution (70%) at 100˚C for 30 min. Nitric acid was poured in a beaker and placed on a hot plate. Hot plate temperature was adjusted in a way that nitric acid temperature inside baker to be 100˚C (nitric acid boiling point: 120.5˚C). A baker contain cold water was also placed on top of acid dish. Fig. 3. 5 schematically shows the set-up for the functionalization of CNTs.

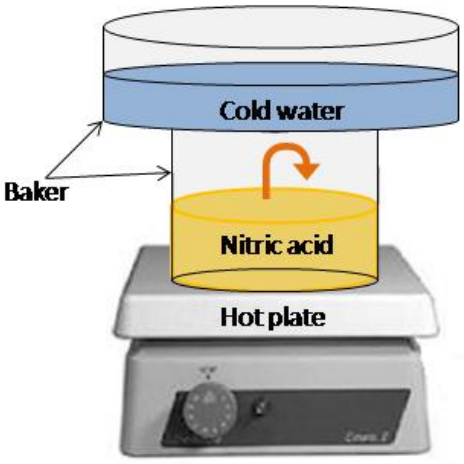

Fig. 3. 5. A schematic of the acid functionalization process of the ceramic-CNT filters

3. 4. Filter tests preparation

Three types of filter assessment were carried out: removal of model bio cells, heavy metal ions and airborne particulates.

- The model yeast *Saccharomyces cerevisiae*, BY4741 [204], was grown to mid exponential phase in YEPD complete media (1% Yeast extract, 2% Peptone, 2% Glucose). Cells were harvested by centrifugation and re-suspended in phosphate buffered saline at a concentration of 1×10^7 cells/ml. After filtration, number of cells in the flow through was determined by haemocytometer counts.
- Analytical grade chloride of iron, copper, cobalt, manganese and zinc (Sigma-Aldrich) were used to prepare stock solution of heavy metal ions

with 1000 mg/l concentration of each of the four metals, which were further diluted to the required concentration before use. The concentrations of metal ions were evaluated by an inductively coupled plasma mass spectrometry (ICP-MS), on a machine of an Agilent 7700x series.

Liquid filtration experiments were carried out by placing the nanocomposite filter in a centrifuge tube and injecting the yeast or heavy metal ions solutions onto it at specific injection rates (Fig. 3.6). Effect of different filter lengths and injection rates were later investigated.

Fig. 3.6. Experimental set-up for yeast and heavy metal filtration.

- Particulate filtration from air: A Lighthouse portable airborne laser particle counter (SOLAIR 3100) was used to record an ambient air passing through the filter, monitoring the concentration of particles ranging from 0.3-10 µm in outlet gas. The placed filter on its inlet was carefully wrapped with thin plastic layer in order to make sure air sucked just from the top surface (Fig. 3.7). Number of air particles counted in the laboratory before filtration is shown in Table. 3. 3.

Fig. 3.7. Lighthouse portable airborne laser particle counter (SOLAIR 3100) with filter placed on its inlet.

Table. 3. 3. Number of air particles before filtration

Particle size	0.3 µm	0.5 µm	1 µm	5 µm	10 µm
air	25,387,145	1,652,726	372,852.2	10,453.1	6,639.2

3. 5. Polymer-ceramic composite reinforced with CNT

By infiltrating the composite filter (with 500 µm pore size) prepared in the previous section with two different types of polymer (one thermoset and one thermoplastic), a new class of functional material was produced. The infiltration processes are described below.

3. 5. 1. Epoxy resin-ceramic-CNT composite

The starting material for this procedure is the same porous ceramic-CNT composites produced earlier. In order to successfully infiltrate the samples with polymer, it is important to functionalize the nanotubes grown on the ceramic substrate at first. The acid functionalization process that was used earlier (Fig. 3. 5) was again utilized for this purpose. An epoxy resin, bisphenol-A diglycidyl ether (DGEBA), epoxide equivalent weight 172-176, (Sigma-Aldrich) was used for the infiltration to make the composite. DGEBA was mixed with a 10 wt.% polyethylene oxide (PEO) (average molar weight M_v=100000, Sigma-Aldrich) as modifier at 80˚C. Then, the curing agent (4,4′-

diaminodiphenylmethane (DDM), Sigma-Aldrich) was added in a stoichiometric amine-epoxy ratio with continuous stirring at 80˚C until a homogeneous blend was achieved. Then, it was tried to infiltrate the polymer into the ceramic. At first, a silica mould was used to do the infiltration (Fig. 3. 8).

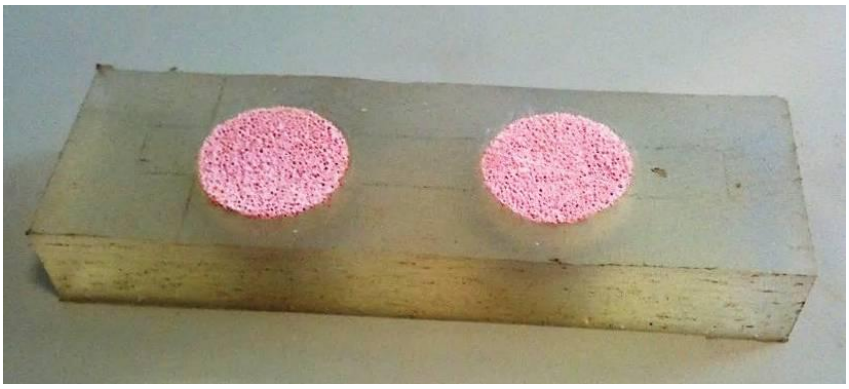

Fig. 3. 8. Silica mould made for infiltration of epoxy resin into the ceramic matrix.

Then, another mould was designed which could cover the disadvantages of the silica mould and improve the degree of filling. This mould requires an extra part which could provide additional amount of polymer for sample to be gradually fed into the substrate during infiltration; unlike the silica mould that could not provide this amount of resin. The extra required polymer placed in part of mould called bank (Fig. 3. 9b part III). It is when ceramic substrate placed in part II, and part I provides a passage way for air to leave the mould. At this stage, the mould was left in a vacuum chamber upside down for a day to remove the air imprisoned inside the sample. After vacuum process, mechanical force caused by turning the screw, applies the pressure to the remaining of polymer in the bank to flow through the ceramic and removes the remained cavities inside the substrate and improves the degree of filling. And finally, sample was cured in oven at 140˚C for 3 hours.

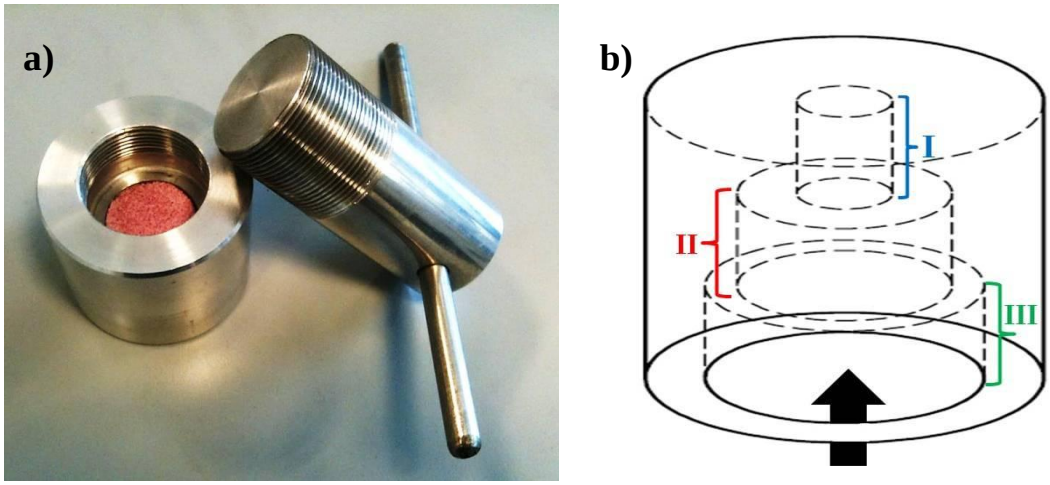

Fig. 3. 9. Photograph of the aluminium mould used for the infiltration of polymer inside ceramic matrix (a); and schematic of mould showing three parts of mould: part I: the passage way for air to be sucked out in vacuum chamber, part II: where ceramic located inside the mould, and part III: the bank for required amount of polymer which will be injected after 24 h vacuuming by turning the screw.

Samples were taken out of mould using a hydraulic press by pushing a bar from top of the alumina mould (Fig. 3. 9, part I). Plain ceramics have also been infiltrated with the polymer using the same procedure, for comparison purposes. Fig. 3. 10 shows the final samples after infiltration. The pink sample is epoxy resin-ceramic sample and the black one is epoxy resin-ceramic-CNT composite. The long yellow part belongs to part I of Fig. 3. 9 that was the passage way for air molecules to leave the mould; and the extra polymers at the bottom of the samples are the additional epoxy resins provided in the back of mould (Fig. 3. 9, part III) which have been shaped by the screw. These parts are very thin and shell like and could be easily broken and removed from the samples.

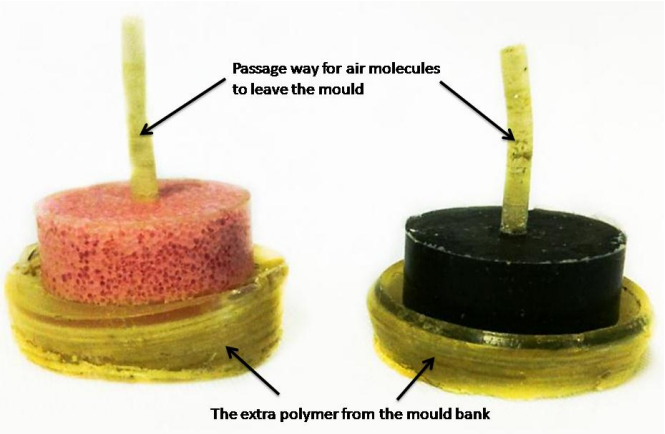

Fig. 3. 10. Optical images of samples after infiltration with epoxy resin.

Before any experiments, samples were carefully polished with different grit papers (80, 120, 240, 600 and 1200) in order to remove the excessive polymer from the surface and to create a uniform flat surface containing polymer, ceramics and CNTs for a reliable result (Fig. 3. 11).

Fig. 3. 11. Photograph of samples after polishing without (left) and with (right) CNTs.

3. 5. 2. Polyamide-ceramic-CNT composite

Polyamide-12 (PA) powders were used as the polymer for infiltration. First, the ceramic-CNT composite was placed inside the mould (Fig. 3. 9) and enough amount of PA-12 was poured on top of it. Shaking the sample allows some powders to penetrate into the sample and pass through it. Then, the mould was put inside a preheated furnace at 200ºC (PA-12 melting point is 178ºC) to melt the polymer. This time the mould placed face down in the oven in order to let the molten nylon flow down due to the gravity and start filling the pores of substrate. Finally, when the mould is still hot and PA-12 is in liquid form, a hydraulic press on the mould was applied to force the nylon slowly injected into the ceramic foam. Then, similar to the epoxy resin samples, specimens were taken out of mould using a bar inserted into the top part of the mould. The final samples are presented in Fig. 3. 12a. Before mechanical testing, samples were carefully polished with different grit papers (from 80 to 1200) as shown in Fig. 3. 12b.

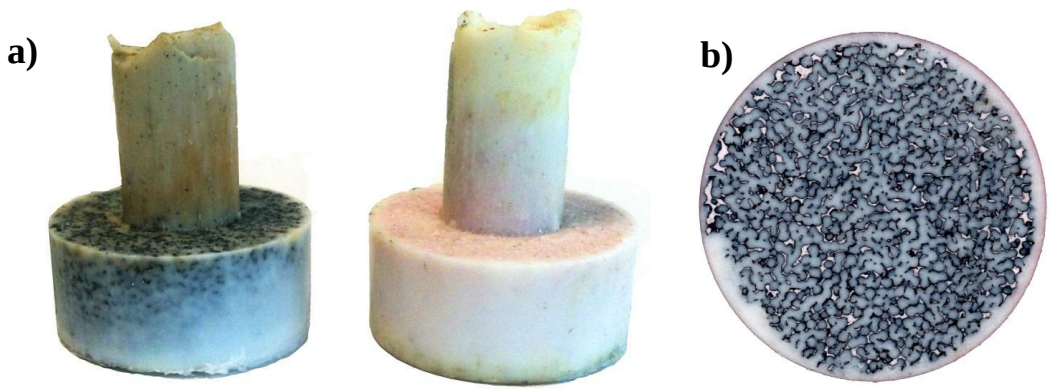

Fig. 3. 12. Photograph of samples after (a) injection of PA 12, and (b) polishing.

3.6. Structural characterization

Different sets of experiments were performed in order to investigate the physical, thermal and mechanical properties of each sample. In this section, basic information about each test and theoretical background will be presented.

3. 6. 1. Scanning electron microscopy

The scanning electron microscope (SEM) is a powerful instrument for imaging surface and subsurface microstructure. In a standard SEM, a stream of electron produced by an electron gun (which usually consists of a tungsten or LaB_6 filament) will be directed towards the sample, using a positive electrical potential. The accelerating voltage is usually between 1 and 30 kV. Two or more condenser lenses are utilized to minimize the stream when the objective lens focuses the electron probe onto the sample. As a result, a thin and focused monochromatic beam with diameter range of 2 to 10 nm will be produced to scan across the surface of sample. The principle of a how the electrons were produced and how they reach the sample surface is illustrated in Fig. 3. 13a. Electrons from the electron source either scatter elastically resulting in back scattered electrons (BSE) or interact with the sample and produce X-rays and new electrons which are called secondary electron (SE). An appropriate detector monitors these electrons or signals and by using modern computer programmes, it provides topographic information of surface of the specimen (Fig. 3. 13b). SE is the most useful signal because of the high signal level combined with high lateral and depth resolution.

BSE offers atomic number contrast that can be used to differentiate phases that contain elements with considerably different atomic numbers [205].

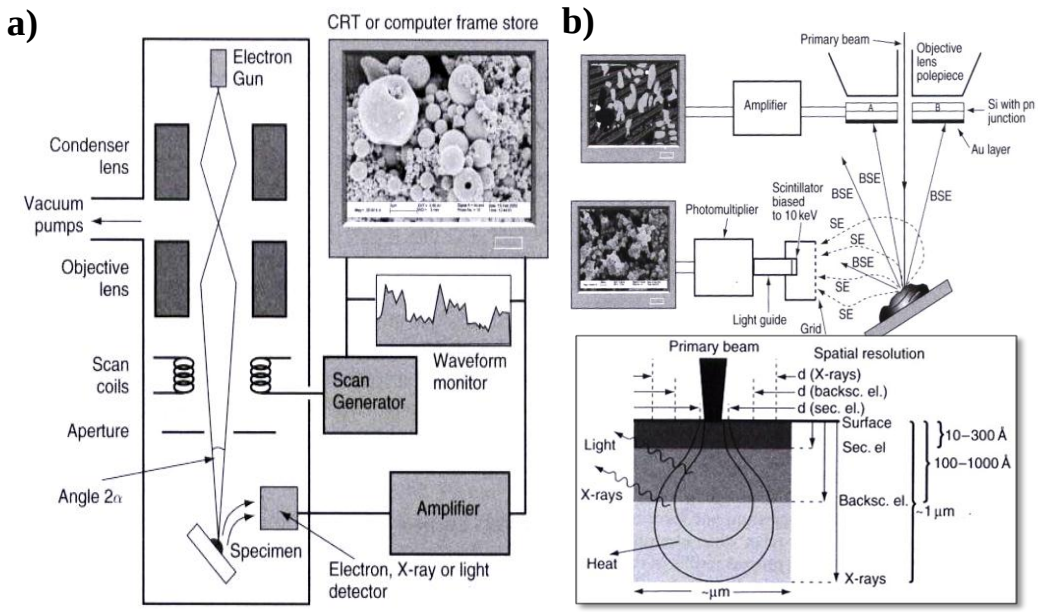

Fig. 3. 13. (a) Schematic of SEM. (b) Schematic diagram of SE and BSE generation by primary beam and their collection by the detector to produce the SEM image [205].

Prior to SEM observation, samples were carefully cut at the mid-plane along their length, using a low speed electric saw. After that, using acetone and compressed air, possible contaminants were removed from the surface of specimen. As CNTs are conductive materials, there was not any charging effect during SEM and consequently, samples were not coated with Au.

3. 6. 2. Transmission Electron Microscopy

Transmission electron microscope (TEM) is an important and powerful tool for imaging the internal microstructure of ultrathin samples. The electron gun is mostly thermionic tungsten or LaB_6, however field emission guns (FEGs) are becoming more common. Compared to SEM, TEM uses considerably higher accelerating voltage in the range between 100 to 400 kV. This high voltage will increase imaging resolution by decreasing electron wavelength. It will also increase the penetration of electrons through the sample, which will allow one to study thicker samples. The samples must be no more than a few hundred nm thick and they are usually in the form of an ultrathin disc.

A schematic of the layout of an analytical TEM is shown in Fig. 3. 14. As shown in Fig. 3.9, two or more condenser lenses demagnify the electron beam to typically 1 μm in diameter. The first condenser lens (C_1) controls the spot size when the second one (C_2) controls the size and coverage of the probe at the sample [205].

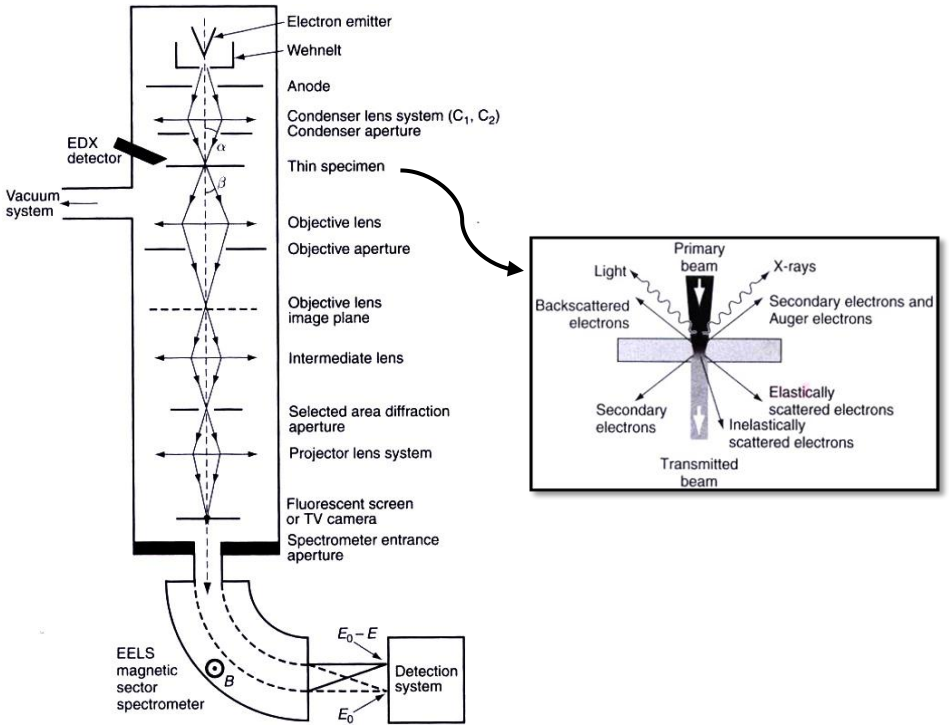

Fig. 3. 14. Schematic illustration of TEM[205]

For TEM sample preparation, the CNT-containing composite was first milled into powder in a mortar, and the powders were then sonicated in acetone before transferring the suspension onto a holey carbon copper grid with a pipette.

3. 6. 3. EDX

Bombardment of high energy electrons on the inner-most electron shell of an atom will result in escape of high energy electrons and as the result, an escape vacancy will be generated. When a single outer electron drops into the inner shell hole, X-ray will be emitted. Energy dispersive x-ray spectroscopy will measure the energy of the emitted X-ray. Due to the well-defined nature of the different atomic energy levels, the elemental composition of the specimen can be easily understood by measuring either

the energies or wavelengths of the X-rays emitted from the sample at the particular position of the electron probe [205, 206].

3. 6. 4. XRD

X-ray powder diffraction (XRD) technique provides an insight into the crystallography of materials. When X-rays hit the surface of crystalline material, they make constructive interference after reflection. The relationship between the incident and reflected X-rays is defined by Bragg's formula:

$$n\lambda = 2d\sin\theta \qquad \textbf{Eq. 3. 1}$$

where λ is the wavelength of the x-rays, d is the inter-lattice spacing, θ is the incident angle and n is an integer [205].

Pre-polished solid samples and finely milled powdered samples were used for XRD. Analysis was performed at 2θ step rotation of 0.02° with a dwell time of 5 sec at room temperature.

3. 6. 5. µCT scan

CT is a non-destructive X-ray inspection technique that makes high-resolution 3D maps of specimens. After reconstruction, the sample can be viewed from any 3D angle, sliced in any direction and accurately measured. This enables detailed analysis of the internal structure of a wide range of components and allows one to detect and measure internal voids and also verify complex internal structures. The µCT was performed using an *X-tekBenchTop 160Xi CT* scanning system in which the sample is X-rayed from a range of angles over 360 degrees. Then, the CT reconstruction engine utilises these X-ray images to calculate the density at all points within the volume to create a 3D model of the specimen [207].

The µ-CT scan does not require any specific sample preparation process and as prepared samples (for all the samples) were scanned in order to obtain the required data.

3. 6. 6. Density

In this study, the densities of samples were obtained using Archimedes principal, which states that the apparent weight of an object immersed in a liquid decreases by an amount equal to the weight of the volume of the liquid that it displaces:

$$D = \frac{W_{air}}{W_{air} - W_{liquid}} \qquad \text{Eq. 3. 2}$$

Where D is the bulk density, W_{air} is the weight of the sample in air and W_{liquid} is the weight of sample in liquid. Distilled water was used as the liquid and an analytical balance with an accuracy of ± 0.01 mg was utilized during the density measurements.

The polished samples as presented in Fig. 3. 11 and Fig. 3. 12b were used for this test. Each test has been repeated for five times for each sample in order to obtain a reliable result.

3. 6. 7. Thermal investigations

Thermal gravity analysis (TGA) involves the determination of the change in weight of the sample in relation to the change in temperature. The TGA was carried out by using a SDTQ600 (TA Instruments, USA). During thermal testing, samples were weighed, using an in-built balance, and heated in air and Ar atmosphere up to 1000°C at a heating rate of 20°C/min. The acquired thermal data was analysed by using the Universal Analysis 2000 computer software provided by TA Instruments, USA.

This test requires very small amount of materials. Therefore, tiny part of each sample was broken (1 to 30 mg) and placed inside the alumina pan. Depend on the required atmosphere, air or Ar were used with 100 ml/min rate. At first, tests were started with an isothermal step at 30°C for 15 min and then, tests were carried out at 20°C/min ramp up to the required temperature.

3. 7. Mechanical property evaluation

Mechanical properties of the composites were determined by performing the compression, hardness and impact tests.

The compression tests were performed using a Lloyds Instruments EZ20 machine, under a preload of 100 N and at a loading rate of 2 mm/min. The test samples were precisely cut using an automatic electric saw (dimensions, sample shape?), to provide flat surfaces required for the test. Then, before the test, their exact area was calculated using ImageJ software. After the test, some photos were taken from samples in order to study the deformation. Up to 16 tests were performed for each of the epoxy resin samples and up to 5 tests for each of the nylon ones.

Impact test was performed using an Instron Dynatup 9250HV at Bristol University. As the diameter of samples was too small to fit into a standard sample holder, therefore a special stainless steel holder, as shown in Fig. 3. 15, was designed to hold the sample.

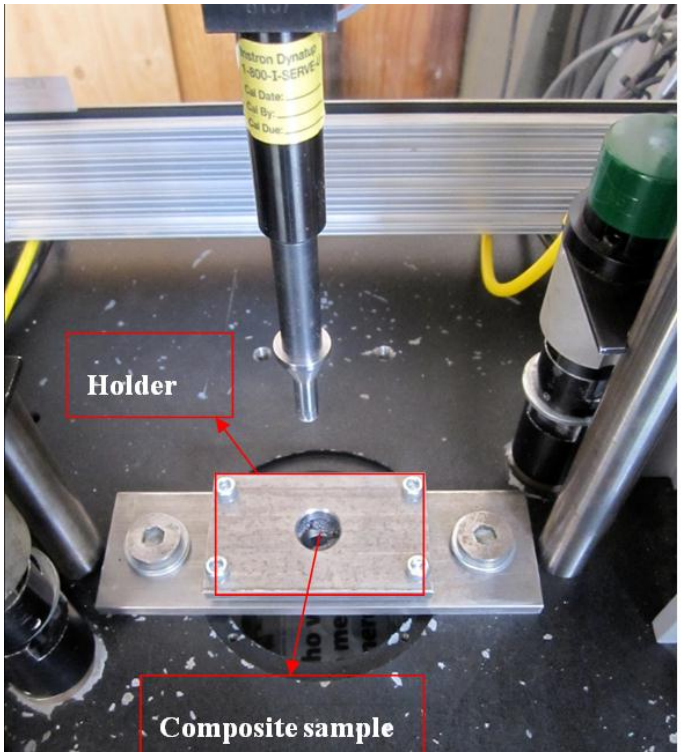

Fig. 3. 15. Photograph of the Instron Dynatup 9250HV test machine used for the impact tests. A special sample holder with the test specimen was fixed between the two plates.

Fig. 3.16.The specially designed mould for increasing the diameter of the composite samples (located in the middle of the holes) by adding an extra epoxy resin ring around the central composites.

In order to increase the margin of sample under the holder, another mould was designed to fix epoxy resin ring around the samples and increase their effective diameter for the test (Fig. 3.16). Consequently, the initial diameter of samples (27 mm) was increased to 40 mm by simply addition of epoxy resin to the surrounding of discs (Fig. 3. 17) where they were placed in the middle of the mould and cured in the furnace. Then, samples were carefully polished by grit papers similar to the previous sample preparation steps for compression test. Impact test was done based on a constant energy of 5J. The absorbed energy and maximum load were evaluated for each sample. For pure epoxy resin and its composites, 5 to 7 samples were tested for each one in order to obtain a reliable result. However for nylon samples, only 2 specimens were available for each experiment.

Fig. 3. 17. Optical image of PA12-ceramic-CNT composite after increasing its diameter by the addition of epoxy resin for impact test.

Finally, the hardness of all samples was evaluated by using a Rockwell hardness machine, using HRH (60 kgf, 1/8 in. ball), as HRH can provide reliable results via its larger ball which will involve a larger area underneath the sample. This allows all the three regions (polymer, ceramic and CNTs) to be involved in the test. The 60 Kgf also has been chosen based on the indicator size on samples. More details and discussions about the tests and their results will be provided in the next chapters. For each set of experiment, after polishing sample surfaces (again similar to compression test sample preparation), based on the consistency of the results, 8 to 20 hardness data were recorded.

3. 8. Summary

The generic experimental methodology and methods used for this research were briefly introduced in this chapter. These include:

- Fabrication process of different samples used in this thesis
- Materials and methods involve in sample synthesis
- Experimental setups
- Basic information about tests and how they were performed
- Sample preparation for each test
- Number of tests and samples for each experiment

Detailed technical information related to each specific experiment will be further explained in the relevant chapters.

Chapter 4: Ceramic/CNT composite

4.1. In-situ fabrication of high density ceramic/CNT composite

4. 1. 1. Introduction

Synthesizing composites by in-situ, direct growth of CNTs inside pores of porous ceramics or ceramic foams with open porosity, offers the advantages of short reaction times and low cost, which allow the porous composites to be used in different fields compared to the fully densified ceramic/CNT composites. So far, the use of mesoporous silica [28], silicon [29], or anodic aluminium oxide (AAO) membrane as the matrices [30] has been widely studied. These substrates could provide the desirable configurations for the production of ceramic/CNT composites. By direct deposition of highly ordered CNTs using CVD process, carbon atoms can accumulate and grow on the internal pore surface, copying the original structural features such as channels (Fig. 4.1) [31]. This technique features a simultaneous carbon deposition rather than a continuous nanotube growth, therefore the resulting shape and morphology of CNTs were restricted largely by the pore structure of the starting AAO membranes, thus the resulting composites are generally limited to μm to mm in thickness, leading to a thin layer of composites which are suitable for specific applications such as in field emitters [149], supercapacitors [150], and scanning probes [151].

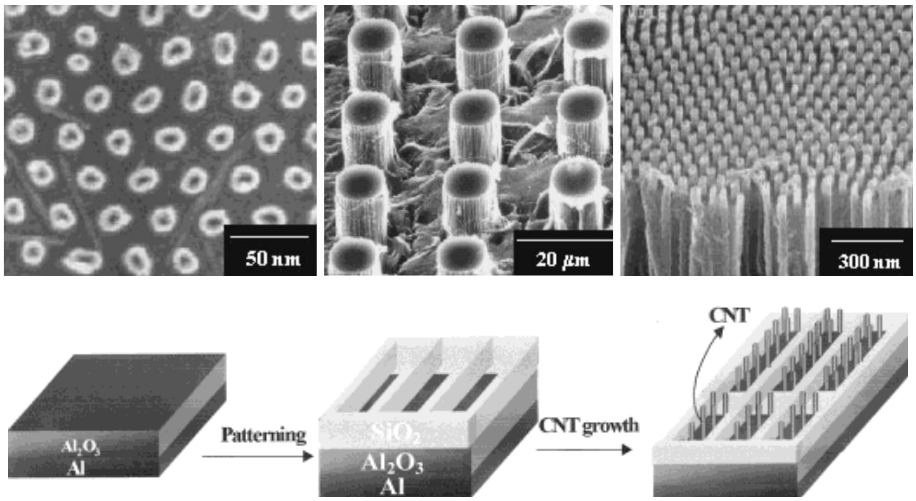

Fig. 4.1. Schematic fabrication method of producing highly ordered CNTs inside AAO [148]

For large and randomly interconnected ceramic foams, the fabrication of composites with CNTs embedded in all directions remains a technical challenge, as for ceramics with such small pore sizes, penetration of carbon atoms into the pores will be restricted by barriers (both ceramic and grown CNTs) which limit the uniformity and depth of the CNT growth [148]. By combining the excellent mechanical properties and large surface areas, such composites are highly desirable for applications in devices for gas absorption, water filtration and purification [32-35], hydrocarbon separation [9], and pollutant air filters [36]. All these properties offer diverse opportunities for the development of fundamentally new CNT-containing advanced composites. This Chapter will demonstrate our effort towards this goal. Two main types of commercial ceramic foams with different densities were used in this study for different purposes of application. The synthesised ceramic/CNT composites were later tested for evaluating the degree of improvement in their properties.

4. 1. 2. Effect of carbon source and catalyst

First, an appropriate catalyst and carbon source based on the prerequisite of the experimental conditions should be chosen. Then, after trial and error testing of a wide range of materials, we aim to find the optimal combinations of catalyst and carbon sources for the composite growth, which will be introduced and discussed in this section. A list of different catalysts and carbon sources used in this experiment is summarised in Table. 4. 1.

Table. 4. 1. A summary of catalysts and carbon sources utilised in this study

Catalyst	**Carbon source**
Ferrocene	Ferrocene
Co nanoparticles	pitch
$Co(NO_3)_2$	styrene
$Ni(NO_3)_2$	camphor

4. 1. 2. 1. Catalyst selection

Due to the small pore size of the ceramic substrate used, a uniform distribution of solid catalyst particles at all sections of the substrate sample was hard to achieve. With

the assistance of ultrasonic probe, the specimen immersed in a cobalt particle and acetone suspension was treated for 30 minutes, in order to allow the catalyst particles to penetrate through the substrate. Subsequent SEM analyses proved that the cobalt particles were agglomerated mainly on the sample surface, rather than penetrating inside (Fig. 4.2). Using surfactants to keep the catalyst particles suspended in the solution was also attempted, again same results were observed during SEM study. Consequently, it seemed that using metal catalyst powders directly was not a feasible approach for achieving uniform catalyst deposition in the matrix, as the tiny pores of the ceramic prevented them from penetrating and particles remained blocked on the outer surface.

a)

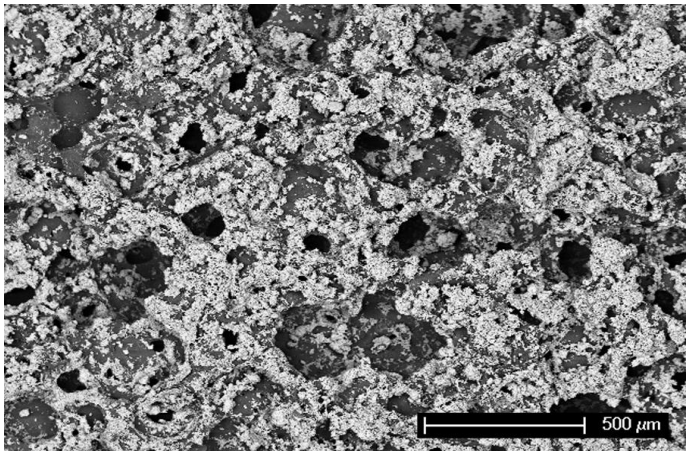

b)

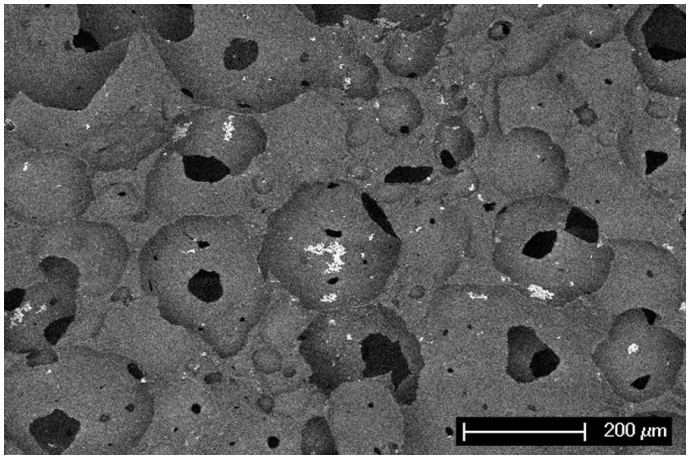

Fig. 4.2. SEM images of: (a) surface, and (b) centre of a sample, revealing the non-uniform distribution of the catalyst particle at various sections of a ceramic matrix.

This inhomogeneous distribution of catalyst particles resulted in a non-uniform growth of CNTs across the sample. A large amount of big sized catalyst particles as shown in Fig. 4.2a resulted in the poor quality of CNTs, even the growth of carbon

fibres; whilst a low amount of catalyst particles with agglomerated particles in some parts (Fig. 4.2b) led to a partial growth of CNTs at some parts, with no growth at other regions, as shown in SEM images in Fig. 4. 3.

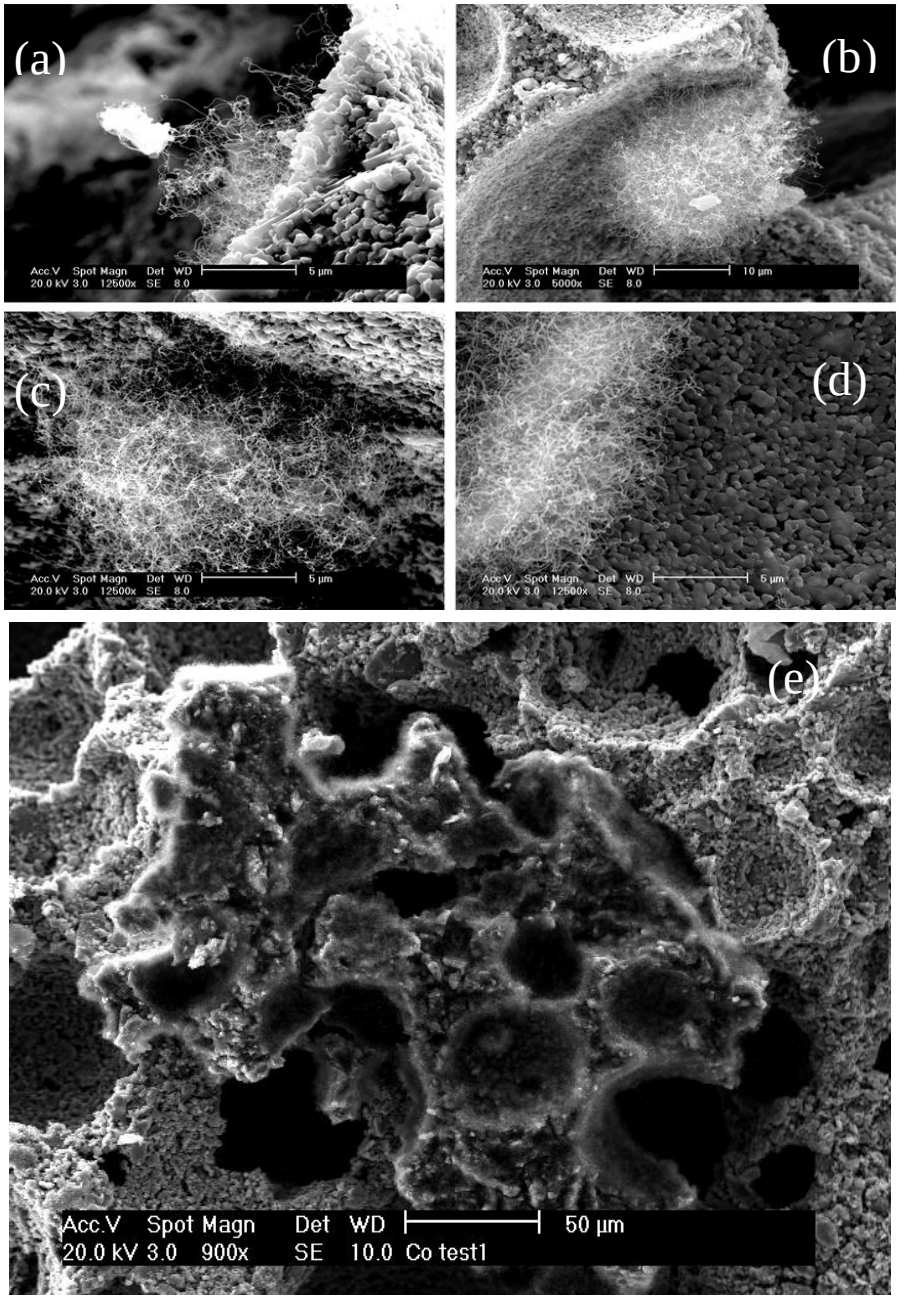

Fig. 4. 3. SEM images showing the agglomoration of catalyst particles in one place which resulted in a reginal growth of CNTs across the sample.

To improve the uniformity of catalyst particles, it was decided to take advantage of metal nitrate salts which are soluble in both water and acetone. In this process, the ceramic samples were first dipped inside the solution of $Fe(NO_3)_2$, $Ni(NO_3)_2$ and $Co(NO_3)_2$ in acetone for several times, then the acetone was allowed to evaporate from

the samples under fume cupboard. The dried sample was heated in a tube furnace under H_2 atmosphere (0.05 l/min) to thermally decompose the metal nitrates to form metal catalytic particles that were required for the CNT growth. As shown in the SEM images in Fig. 4. 4, the resulting catalyst particles were indeed distributed uniformly, without agglomerations.

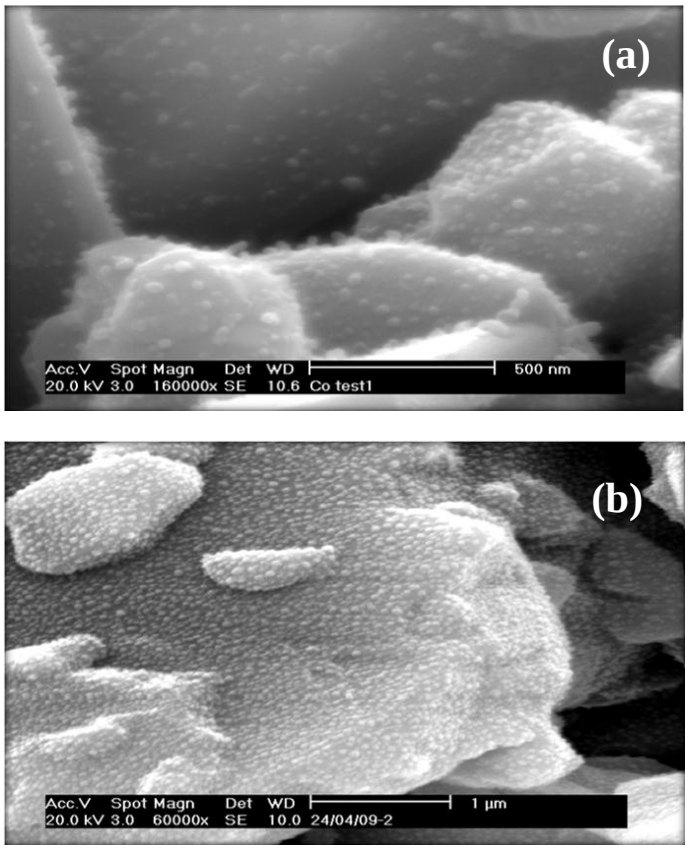

Fig. 4. 4. SEM images show the uniform distributions of catalyst particles inside the ceramic matrices at high (a) and low (b) magnifications

Achieving uniform distribution of catalyst particles on all the surfaces of ceramic foam is an important prerequisite for the fabrication of high quality composites. After this, it is required to provide sufficient amounts of appropriate carbon sources for the catalyst particles to initiate the CNT growth.

4. 1. 2. 2. Carbon source selection

In the case of carbon source selection, different precursors of various conventional and unconventional types were considered. At first, as it is more typical for a CVD process, it was tried to use carbon sources which could be continuously

injected into the furnace. In this regard, ferrocene and styrene were chosen as the carbon source to be injected into the furnace. However, they did not show any promising results as it appears that carbon atoms could only penetrate up to several hundred micrometres inside the foam and could not cover the whole surface areas of the ceramic. To overcome this superficial growth problem, other carbon sources that could be placed inside the sample and initiate the growth within the internal pores of ceramic were investigated. Such precursors should consist of large and long chains of carbon molecules, possessing relatively high melting and boiling point which allows the decomposed carbon species/atoms to remain inside the pores for a longer period of time during the CNT growth at high temperature. This strategy will hopefully initiate the CNT growth across the entire matrix, both the inner and the outer surface.

Table. 4. 2.Physical properties of ferrocene and styrene [203]

	Ferrocene	**Styrene**
Chemical formula	$C_{10}H_{10}Fe$	C_8H_8
Molecular structure	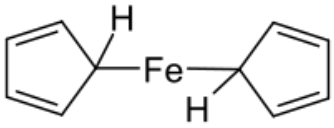	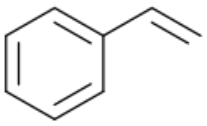
Molar mass	186.03g/mol	104.15 g/mol
Appearance	light orange powder	colourless oily liquid
Density	1.490 g/cm^{3}at 25 °C	0.906 g/cm³at 25 °C
Melting point	172 °C	-30 °C
Boiling point	249 °C	145 °C
Solubility	Insoluble in water, soluble in most organic solvents	Insoluble in water

Tar pitch was the first chemical used in this study. First, nickel nitrate was placed inside the sample using dip-coating technique as described earlier, to become the

catalyst material. Second, the pitch was warmed up to reduce its viscosity and allowed it to fill into the ceramic pores. Third, the specimen was placed inside a preheated furnace under H_2 atmosphere (at a flow rate of 0.2 l/min). A wide range of temperatures (from 700 up to 1200 ˚C) were examined in order to overcome the oily nature of the pitch which covered the entire ceramic (Fig. 4. 5a). The results showed that we were successful in providing sufficient amount of carbon source for all sections of sample; however these carbon atoms could not be formed in the shape of nanotubes.

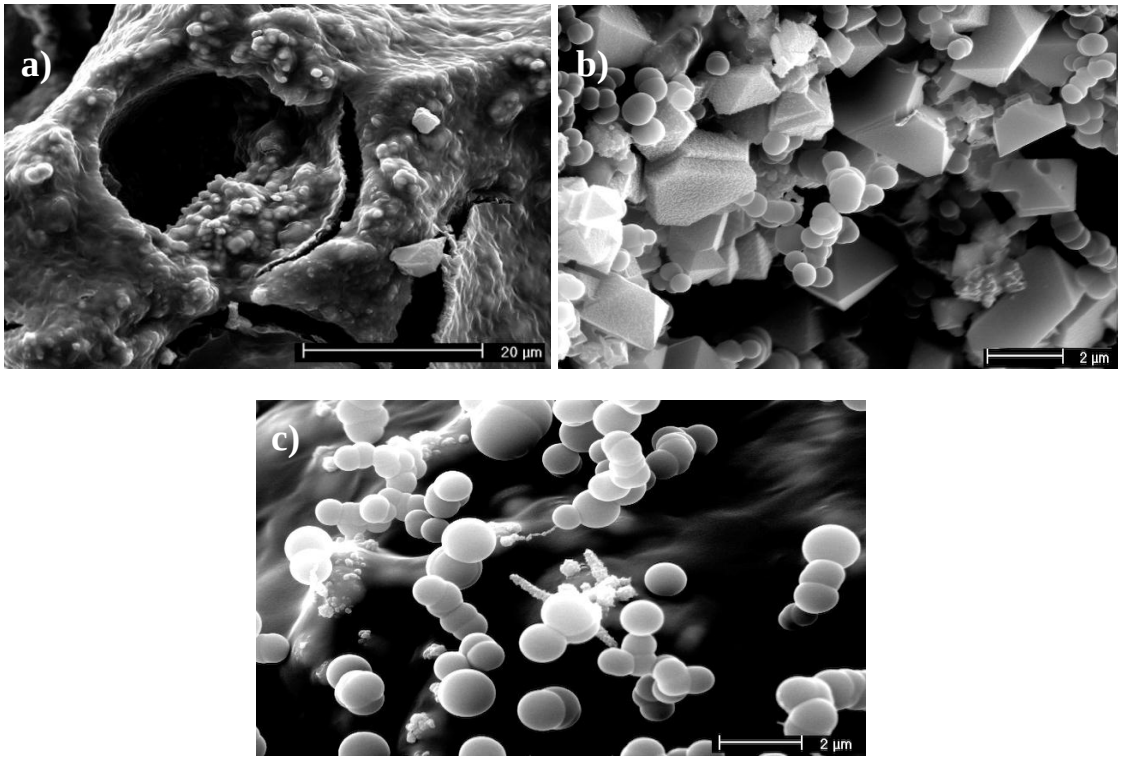

Fig. 4. 5. SEM images: (a) The oily surface of the sample owing to the tar pitch, (b) different carbon materials produced, and (c) sphere carbon being the dominant products.

SEM images showed that a wide range of carbon materials was produced (Fig. 4. 5b). This is owing to the contaminants contained in the tar pitch, and these contaminations severely affected the quality of the final product. After a few trials, it was found that it was extremely difficult to control the materials growth, however in most cases spherical carbon was the major product in our experiments (Fig. 4. 5c).

So far, it can be concluded that:

- Use of ferrocene and styrene as carbon source resulted in a limited growth of CNTs only on the surface of the ceramic foam, with low penetration depth.
- Use of viscous tar pitch placed inside sample, it is possible to provide sufficient amounts of carbon source for all sections of the bulk ceramic sample, but the carbon failed to convert into CNTs.

Camphor ($C_{10}H_{16}O$) was chosen as another possible carbon source which could also be placed inside the sample via solution, or be used directly as a solid source. Camphor has been successfully used for the fabrication of C60 [208] and CNTs [209]. Camphor is an environment-friendly and waxy white crystalline solid with very strong and pleasant odour. It can be extracted from the latex of cinnamomumcamphora tree of lauracea family, and is an abundant material in Asian countries [210]. Compared with other widely used conventional chemical precursors, camphor is a green, cheap, carbon-rich, hydrogen-rich and oxygen-present source. Physical properties of camphor are summarized in Table. 4. 3.

Table. 4. 3. Physical property of camphor [203]

Chemical formula	$C_{10}H_{16}O$
Molecular structure	
Molar mass	152.23 g/mol
Appearance	White, translucent crystals
Density	0.992 g/cm^3 at 25 °C
Melting point	175 °C
Boiling point	204 °C
Solubility in water	1.2 g dm^{-3}
Solubility in acetone	~2500 g dm^{-3}

Since both the catalyst and the camphor precursor are soluble in acetone, a solution consisting of both materials was simply prepared (Fig. 4. 6). After repeatedly dipping the alumina bricks (10×10×15 mm) in the solution as described earlier, a sample containing both the carbon source and catalyst was obtained, which could be handled and processed easily. The experimental parameters for camphor were similar to those of the tar pitch test.

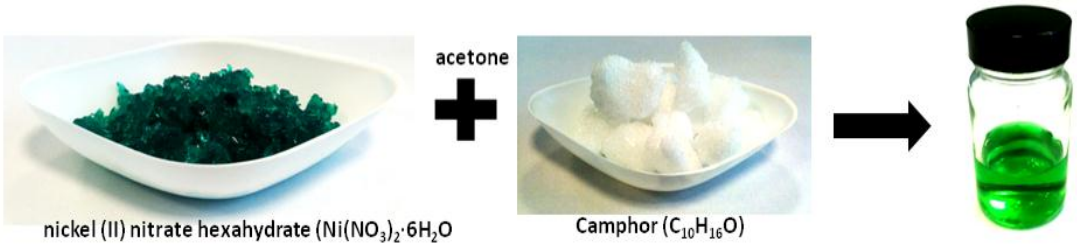

Fig. 4. 6. A photograph of the acetone solution containing nickel nitrite and camphor

SEM images of sample showed the successful growth of CNTs with high quantity and quality on the surface of the ceramic foam (Fig. 4. 7). However, in order to investigate the quality and coverage of CNTs in all sections of samples, the samples were cut open at the mid-plane along their length, as shown in Fig. 4. 8a. Then, they were examined at three typically representative locations as marked in Fig. 4. 8b: the centre (A), the 1/4 position (B) and near the surface (C), to demonstrate the effectiveness of the CNT growth in different sections. SEM images contributed to points A, B and C showed the successful growth of nanotubes at all sections of sample (Fig. 4. 9). These SEM images along with detailed results and discussions are presented in the next section.

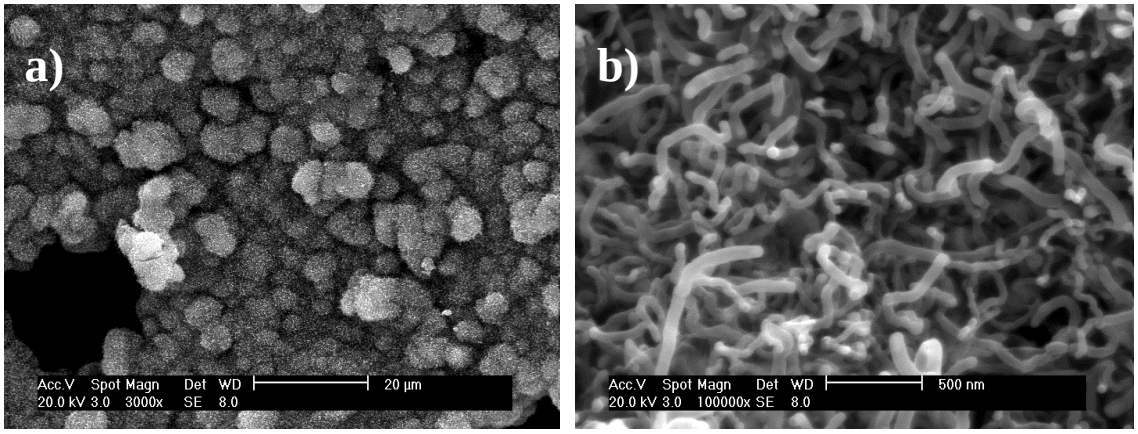

Fig. 4. 7. SEM images of the surface of a sample synthesised using camphor as the carbon source and nickel nitrate as the catalyst at low (a) and high (b) magnifications.

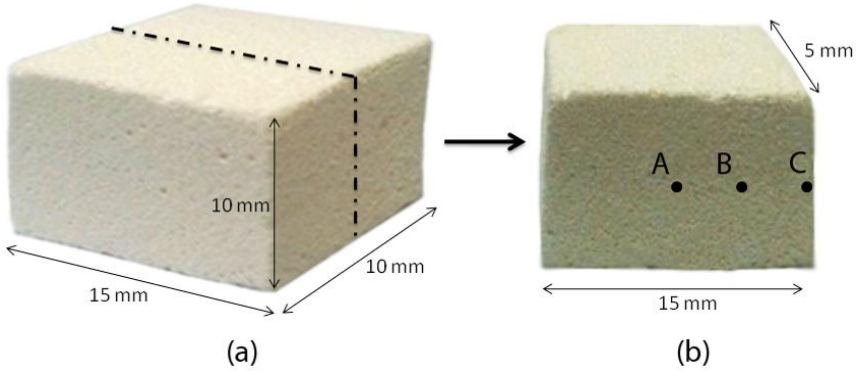

Fig. 4. 8. (a) The alumina brick dimensions. The broken line illustrates where the sample was sectioned for SEM investigation. (b) Showing the locations (A, B and C) examined after CNT growth.

To conclude, after using different carbon sources in various phases, camphor (used as solid source) showed the most promising results with good quality of CNTs grown at all sections of the ceramic foam. Thus, our next focus will be on camphor as the carbon source and nickel nitrate as catalyst in this thesis.

4. 1. 3. Yield and quality of nanocomposite

Prior to and after the growth, the alumina brick samples were weighed using a precision balance, to estimate the CNT yield. A 13% weight increase in samples after optimizing the synthesis parameter has been recorded, which is the gross yield in the sample including both the CNTs and the catalyst involved as a whole. Therefore, if the higher theoretical density of 1.8 g/cm^3 of multi-walled CNTs is taken from literature

[6], it is estimated that the introduction of CNTs accounts for about 7% volume in the composite, *i. e.* about 7% pores within the alumina have been occupied by CNTs.

As mentioned earlier, in order to investigate the quality and the coverage of CNTs in all sections of the samples, SEM characterisation was performed for three locations of A, B and C as shown in Fig. 4. 8b, as a function of distance from surface. In Fig. 4. 9e and f, it is clear that there are more CNTs near the surface, and that the quantity of CNTs decreases towards the centre. In the central section (Fig. 4. 9a and b), the CNTs appear to be shorter in length and fewer in quantity, as opposed to Fig. 4. 9e and f. Overall, the CNTs seem to be fine and uniform, with little evidence of amorphous carbon particles on the surface or within the matrix, indicating the high quality of the resulting CNTs.

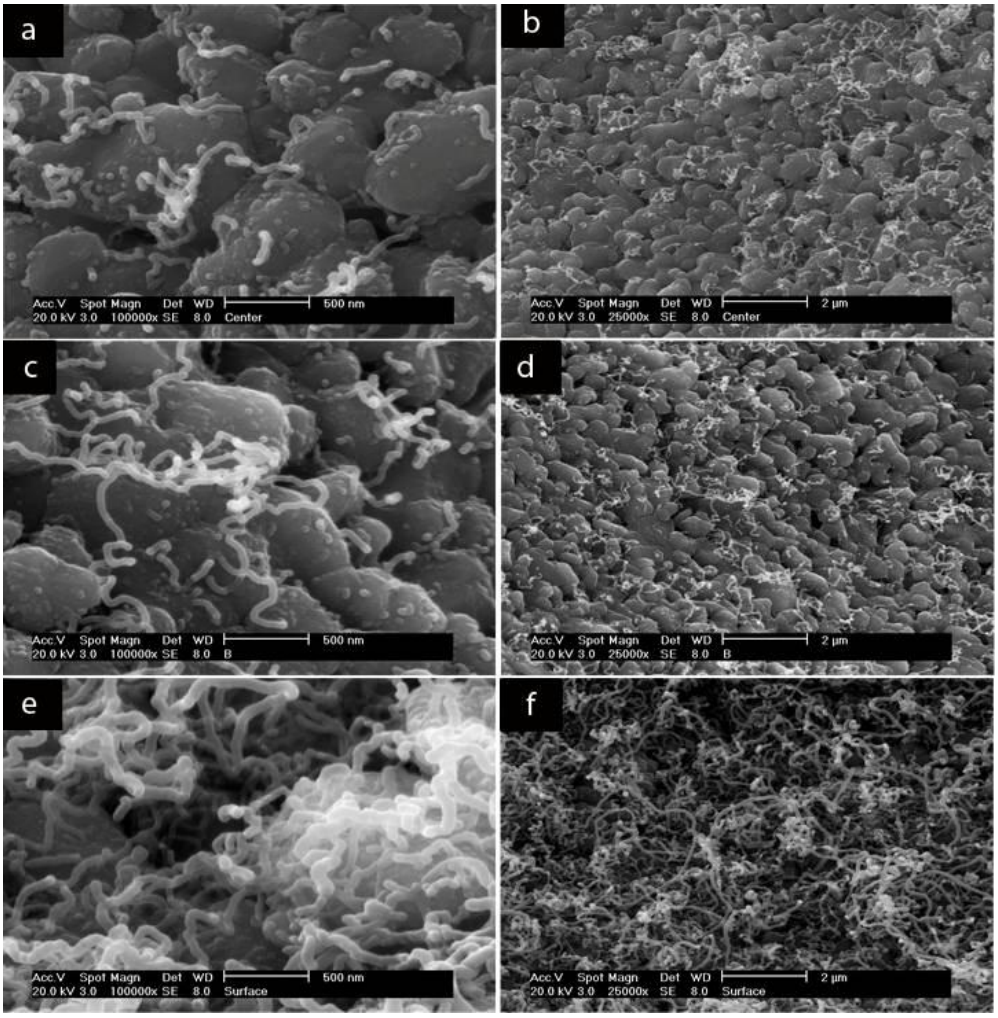

Fig. 4. 9. SEM images of CNTs grown inside the ceramic matrix, taken from centre (a, b), ¼ thickness position (c, d), and near the surface of the sample (e, f).

The bi-cyclic cage-structure of camphor has a significant effect on the efficient CNT growth, as the hexagonal and pentagonal carbon rings of camphor may re-arrange into CNTs with no needs of breaking into atomic carbon. Whilst the abundant hydrogen in camphor facilitated the growth by reducing the catalyst particles, the oxygen atom present in the camphor molecule would help oxidize the potentially formed amorphous carbon in-situ. Consequently, every atom of camphor has a constructive role to play in the CNT growth [211].

Achieving sufficient quantities of CNTs to fill the high levels of porosity present in these samples is difficult by using this process; however the process has the capacity to deposit CNTs on the internal surfaces across the entire matrix, whilst retaining the porous features of the alumina brick.

The number of the resulting CNTs varies through the cross sections, which emphasizes the significant challenge for the uniform synthesis of CNT across much larger bulk samples, as opposed to very thin CNT/membrane composites [151]. In some cases, agglomeration of the catalyst must have occurred (circled in Fig. 4. 10a), leading to clumps of CNT (circled in Fig. 4. 10b). Nevertheless, this strategy is expected to avoid the limitations of existing CVD process, to some extent, in which gas or liquid vapour has been widely used as the carbon supply [11]. In those processes, the initial CNT growth will block the passage of the carrier gases and carbon sources from the outer section of the matrix inward, thus limiting the depth of CNT growth from just micrometer to millimetres [148]. By adopting the methods used in this study, the solid precursor introduced directly inside the sample, upon decomposition, has promoted the on-site growth of CNTs across the outer and inner sections of the sample.

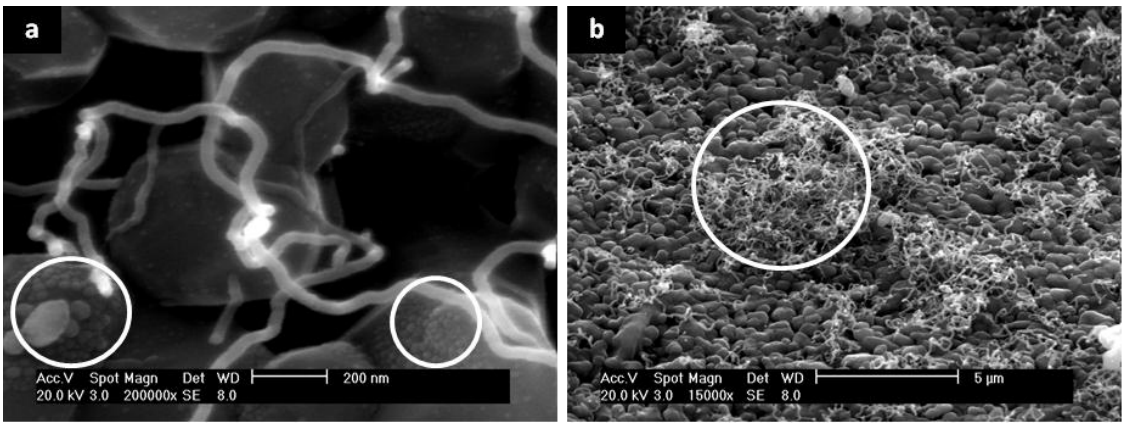

Fig. 4. 10. SEM images. Agglomerations of the catalyst particles circled in (a), leading to the formation of clumps of CNT in matrix circled in (b).

TEM results (Fig. 4. 11a) reveal that the resulting nanomaterials are indeed hollow, being CNTs rather than solid carbon nanofibres, with average diameters of 30-70 nm and lengths up to several micrometres. Fig. 4. 11b shows a bamboo texture for a CNT which happens when a limited number of graphitic layers are oriented perpendicular to the nanotube axis, thus forming compartments [19]. The circled part in Fig. 4b shows a small carbon cluster attached to the nanotube.

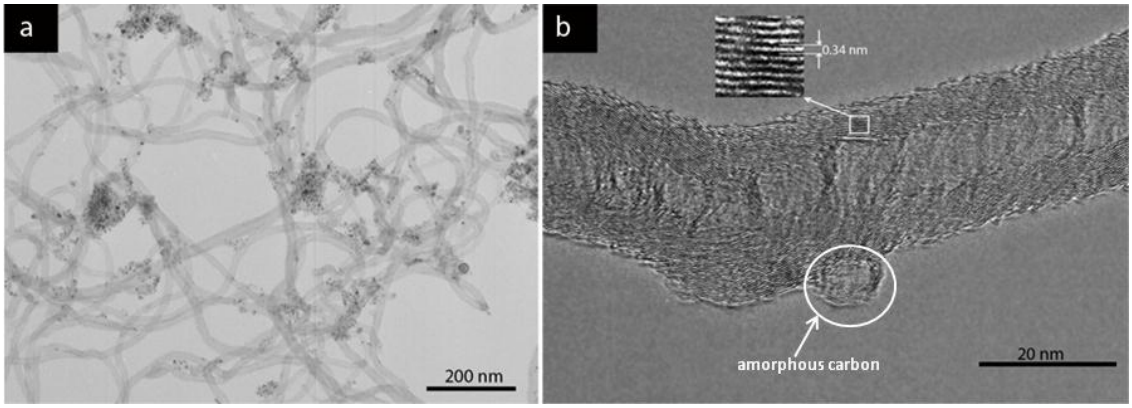

Fig. 4. 11. TEM images of CNTs collected from the composite sample. (a) The hollow structural feature of the nanotubes is visible, and the high contrast black dots are the catalyst particles, and (b) showing the atomic inter-layer distance is 0.34 nm and an attached carbon particle, circled.

4. 1. 4. Growth mechanism

By dipping the alumina bricks in the catalytic solution ($Ni(NO_3)_2$ and acetone), the formation of catalyst nucleation sites on the internal surface of the matrix was achieved which acted as the required localized catalyst for the CNT growth [212, 213], as shown in Fig. 4. 4. The widespread dispersion of catalyst particles, along with a sufficient source of carbon, would be expected to result in uniform on-site growth of CNTs on the surface of the alumina cavities. Although the sublimed camphor continues to leave the sample through the internal pore channels, given the rapid heating rate, there is sufficient carbon available after conversion of the nitrate to Ni for sustained growth of CNTs. The higher carbon concentration at the surface clearly leads to increased CNT formation in these areas, leading to CNT densities that are only uniform in each equivalent distance section. In order to understand the growth mechanism, SEM investigation was performed at very high magnefications. Fig. 4. 12c shows an extrusion or root growth of CNT from the catalyst particles attached to the alumina surface, and the tips of these resulting CNTs are generally catalyst-free (Fig. 4. 12d). For CNTs to work effectively as a functional phase within the matrix, a strong interface connection or binding strength to the matrix is important, to prevent CNTs from floating or falling out during service, such as in filter applications. Of the two main mechanisms of CNT growth on a substrate, namely root growth and tip growth [68, 71, 72, 214], improved adhesion of the nanotubes to the matrix is expected under the condition of root growth, as was observed under the current experimental conditions.

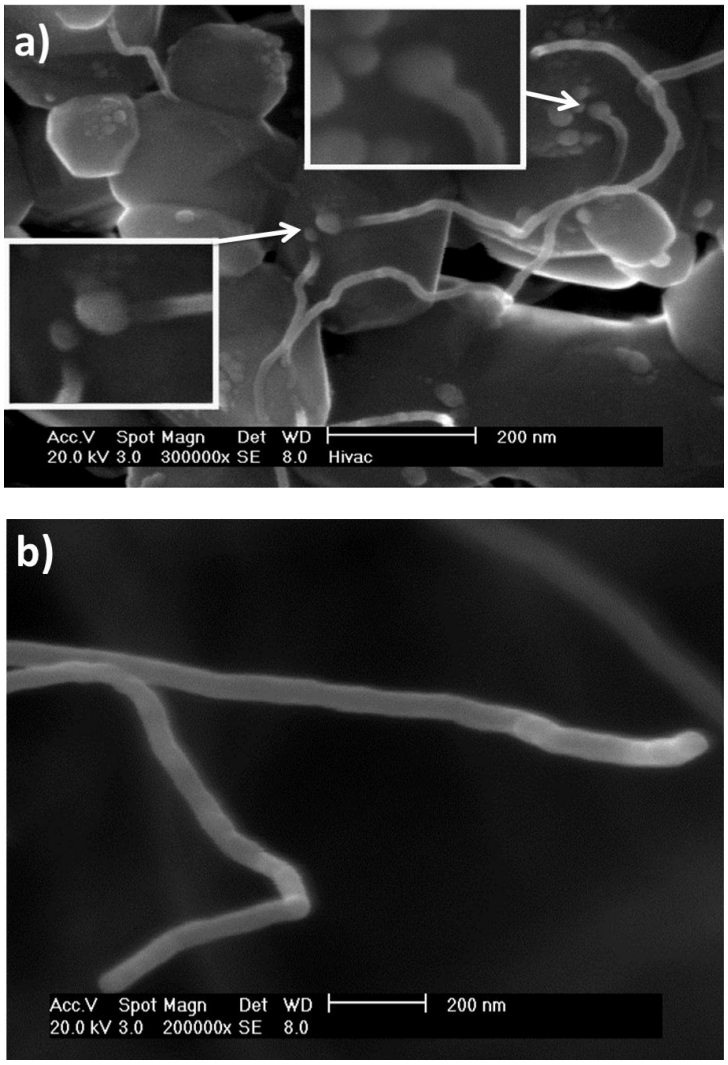

Fig. 4. 12. SEM images: (a) evidence of the 'root' growth of CNTs, and (b) CNTs with catalyst-free tips.

The formation of a viable nucleation site from the catalyst source occurs in a number of stages. At around 400 °C, the nickel nitrate thermally decomposes to form a stable oxide (NiO) which can be further reduced, in a hydrogen atmosphere, yielding metallic nickel nanoparticles across the entire pore surfaces, according to the following steps [215]:

$$Ni(NO_3)_2{\cdot}6H_2O \rightarrow Ni(NO_3)_2{\cdot}4H_2O \rightarrow Ni(NO_3)_2.2H_2O \rightarrow Ni(NO_3)(OH)_{1.5}O_{0.25}{\cdot}H_2O \rightarrow Ni_2O_3 \rightarrow NiO \xrightarrow{H_2} Ni$$

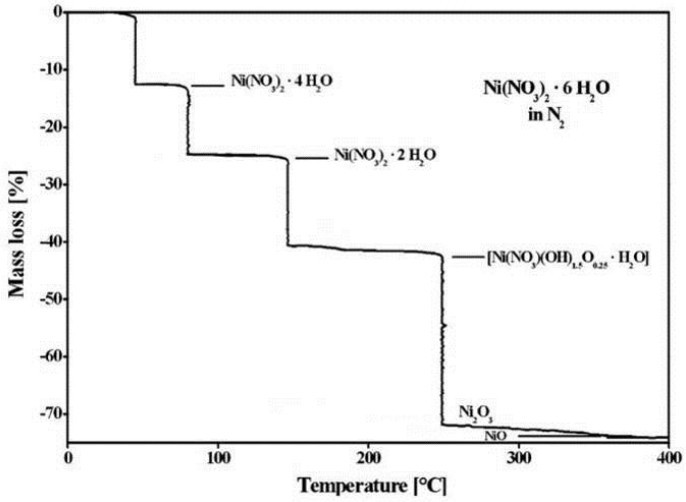

Fig. 4. 13. Thermal decomposition of nickel (II) nitrate hexahydrate [215]

Our TGA results (Fig. 4. 14) confirmed that decomposition of catalyst particles would be completed at 325˚C in Ar and the catalyst would lose 75% of its weight when NiO was formed.

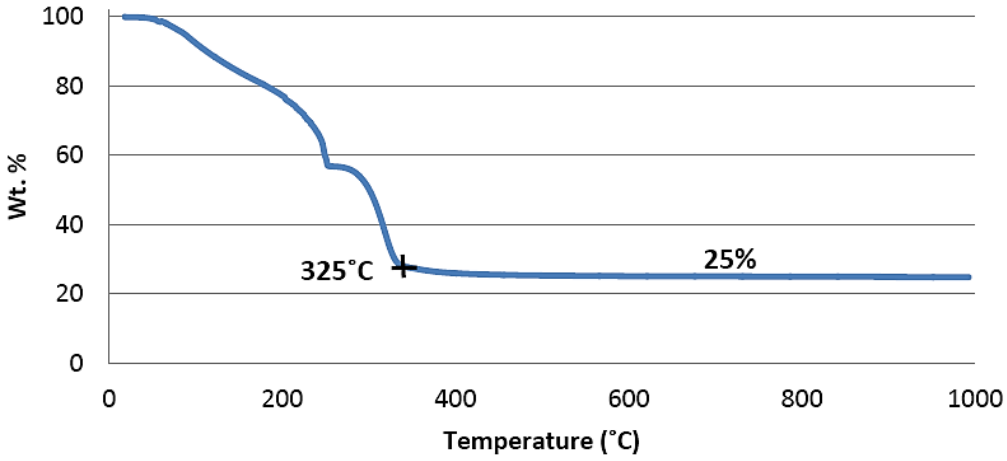

Fig. 4. 14. TGA result of catalyst particle under Ar atmosphere which indicates that the catalyst decomposition finalised at 325˚C with a total weight loss of 75%.

To account for the root growth, interaction between Ni nanoparticles and the alumina substrate should be considered. Indeed, at elevated temperature the interaction took place in an extremely short period of time, after the localized temperature reached a critical point. It is very difficult to determine how this process would actually affect the CNT growth, as whether such interactions occur before, during, or after the CNT growth. During the experiments, samples were introduced into the pre-heated working tube at a temperature high enough for all the three processes (activating catalyst,

sublimating camphor and growing CNTs) to happen simultaneously, which makes it difficult to clearly define these process steps. Examination of the nickel-aluminium-oxygen phase diagram (Fig. 4. 15) at the processing temperature [216, 217] indicates that nickel and α-alumina could form a solid solution [23], rather than the $NiAl_2O_4$ spinel phase, which does not form under strongly reducing conditions such as in a hydrogen atmosphere [218, 219]. The red line in Fig. 4. 15b, shows the stability limit of spinel. When the oxygen activity is under this line, nickel and α-alumina can form a solid solution. The dissolution of nickel atoms into the alumina will result in strong adhesion, making the root growth of CNTs possible. Further experimental evidence is still required to clarify the exact interfacial structures promoting the root growth.

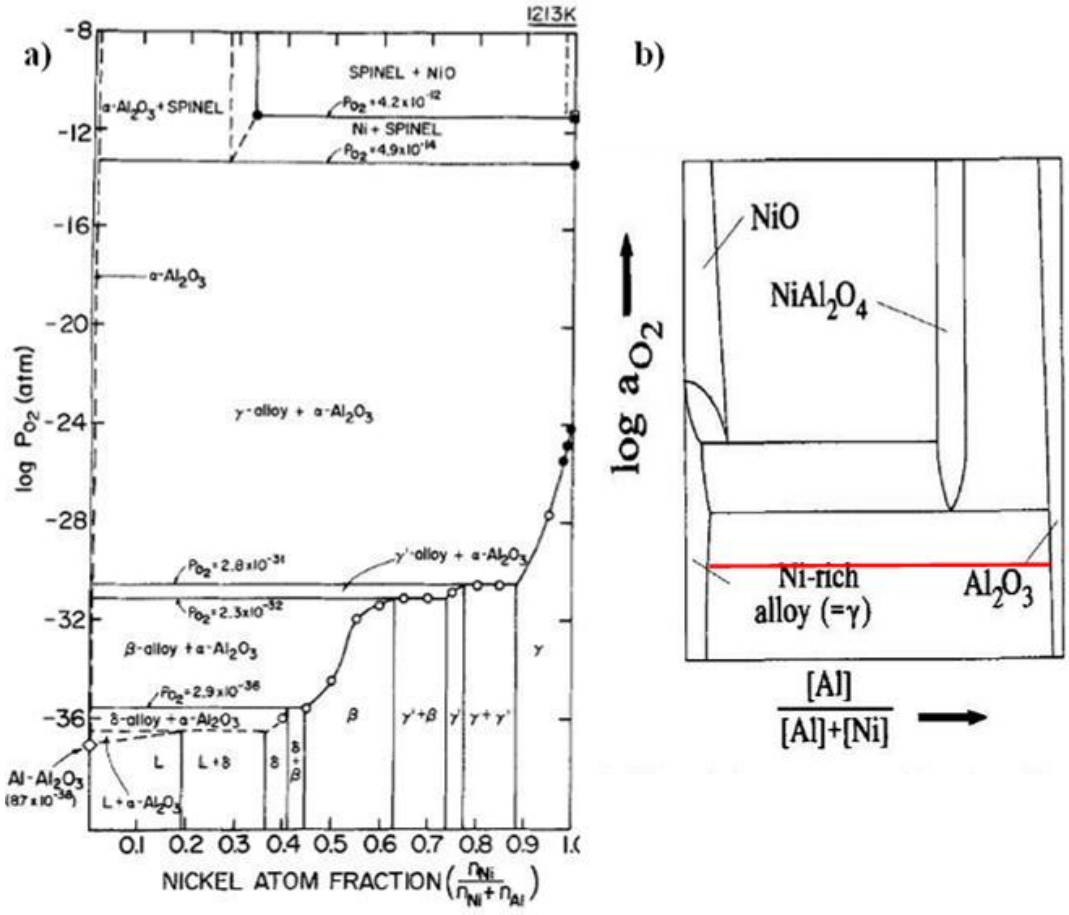

Fig. 4. 15. Nickel-aluminium-oxygen phase diagram at constant temperatures [216, 217].

The hydrogen atmosphere under which the pyrolysis was conducted can explain the fine quality of the CNT, however it would be uneasy for hydrogen to reach the growing CNTs deep inside the alumina pores. It is believed that the formation of small

amounts of amorphous carbon inside the matrix may be due to the existence of oxygen in the camphor which readily oxidized the amorphous carbon *in-situ*, as described by Kumar and Ando [209]. They also found that the amount of catalyst required when using camphor was lower, by a factor of 10, compared to other carbon sources, which makes the final CNT composites less contaminated with metal particles [209]. In fact, the metal catalyst particles, shown as dark and high contrast dots in Fig. 4. 11a, are in relatively low abundance in the CNTs.

4. 2. Low density Ceramic/CNT composite

4. 2. 1. Introduction

In previous section, fabrication of high density ceramic/CNT composite was described. Those high density ceramics have got their own specific applications as mentioned earlier. At the meantime, low density ceramics or ceramic foams are also widely used in applications such as burner enhancers, soot filters for diesel engine exhausts, catalyst supports, and biomedical devices [220-222]. Ceramic foams are linked networks of irregularly shaped open (or partly open) or closed (or partly closed) cell polyhedrons with a low fractional density. Closed-cell foams are composed of polyhedral like cells connected via solid faces, i.e., with no interconnectivity between them, whereas open-cell structures have solid edges and open faces, with fluid flow possible from one cell to another [222]. Fig. 4. 16 shows the open-cell structure with three components: struts, that are made of solid ceramic material; cells, that are approximately spherical voids enclosed by struts; and finally windows, which are openings connecting the cells with each other. These open structures are sponge-like creating an interconnecting porosity in the range of 75%-90% or even higher. The large number of interconnected pores in these materials results in high specific areas and low density, in addition to their high thermal resistance, low thermal conductivity and high flow and fluid permeability [157]. This low resistance to fluid flow is favourable for direct growth of CNTs on ceramic foams using conventional CVD process. However, considerable turbulences will be generated by the tortuous flow paths that count as a

challenge for fabrication of such ceramic/CNT composite. It is expected that the deposition of CNTs on ceramic foams can considerably enhance their filtration performance.

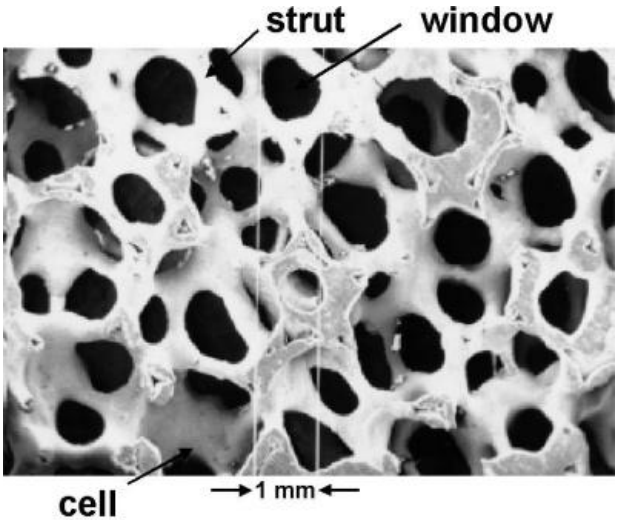

Fig. 4. 16. Open-cell ceramic foam composed of three parts of strut, cell, and window [222].

In this section, we demonstrated the experimental procedures for the construction of such low density ceramic/CNT composite, by a direct growth of CNTs in ceramic foams. The performance of the fabricated composites will be assessed in the next chapter.

4. 2. 2. Ceramic/CNT composite synthesis parameters

Malgas et al. [223] have studied the effect of different parameters on the CNT growth using camphor (carbon source) and ferrocene (catalyst) in a CVD process. They claimed that the reaction temperature, carbon source/catalyst mixture ratio and carrier gas flow rate had the most dominating effect on the nanotube growth. The importance of these factors will be addressed in this work as well. Table. 4. 4 summarizes the key differences in ceramic/CNT composite fabrication processes using high and low density ceramics.

Table. 4. 4. Key differences between the fabrication processes of high and low density ceramic/CNT composites.

	High density ceramic	**Low density ceramic**
Ceramic pore size	100-150 µm	300 & 500 µm
Catalyst	$Ni(NO_3)_2$, saturated solution in acetone	$Ni(NO_3)_2$, 1 wt.% solution in acetone
Carbon source	Camphor (solid form)	Camphor (40 vol.% in acetone solution, injection rate of 0.8 cc/h)
Temperature	850˚C	780˚C
Total reaction time	3 min	2 h

4. 2. 2. 1. Effect of carbon source and catalyst

Based on the previous sections, the same catalyst and carbon source were chosen for the direct growth of CNTs on current ceramic foams. Unlike the previous part in which solid camphor was used as the carbon source, a camphor-acetone solution was used in this experiment in order to achieve a precise control over the continuous feeding of carbon source into the reaction chamber via controlling the solution injection rates. This is due to the considerably higher gas permeability of the ceramic foam used in this experiment.

As was discussed before, the distribution and size of the catalyst particles are critical issues in the growth mechanism of CNTs, as a finer catalyst will result in a higher yield and higher quality of the synthesised CNTs [224]. At first, nickel nitrate crystals were solve in water for deposition of catalyst on ceramic foam. But after dipping the sample in the catalyst solution, the water removal from the sample prior to the experiment is a time consuming process. Further, SEM images revealed that to deposit catalyst particles in small size and well distributed forms is a difficult task by

using water solution, as the nickel nitrate crystals tend to agglomerate and form bigger clusters (Fig. 4. 17). Consequently, it was decided to prepare the catalyst solution in acetone. It is easy to dissolve the catalyst crystals in acetone and one can easily remove the acetone from the sample under the fume cupboard, leaving a uniform deposition of catalyst on the surface of the ceramic.

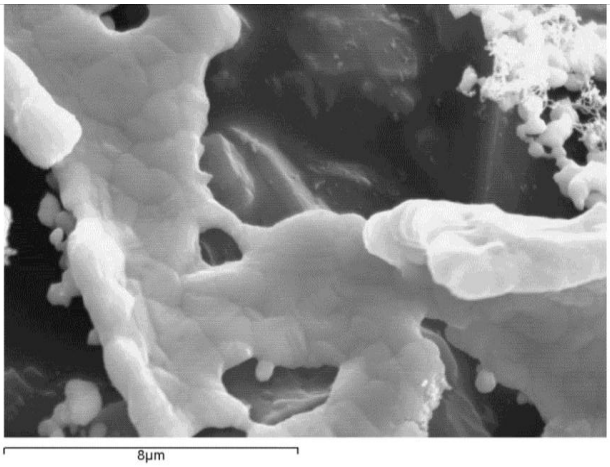

Fig. 4. 17. SEM image of big catalyst clusters formed on the ceramic. The slow process of water removal gives enough time for the nickel nitrate particles to agglomerate, especially at the bottom of the sample due to gravity.

For samples that the catalyst was prepared in acetone solution, better quality and quantity of CNTs than those prepared in water are observed during SEM investigations; however the quality of samples still did not meet our expectations. Further investigations by SEM using BSE showed a high amount of accumulated catalyst particles in the samples (Fig. 4. 18). Thus, the concentration of nickel nitrate in the catalyst solution was gradually reduced down to 1wt. % and the SEM images showed significant improvements in the CNT quality of the samples.

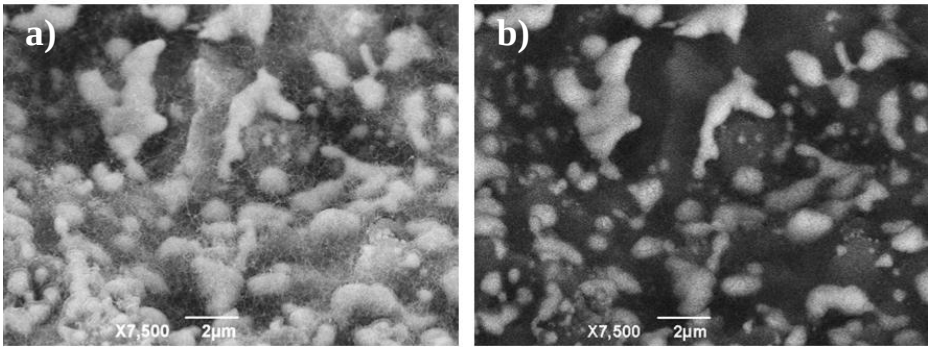

Fig. 4. 18. (a) SEM images of sample using SE shows the growth of CNTs near some big particles, (b) SEM BSE image of the same place proves the big particles to be $Ni(NO_3)_2$.

The ceramic foam used as substrates has very rough surface. SEM image in Fig. 4. 19a shows the rough surface of a ceramic foam, after having been embedded in the catalyst solution and thermally decomposed the catalyst particles at 780˚C under H_2 atmosphere for 30 min. The tiny catalyst particles (1wt. % solution) cannot be detected in Fig. 4. 19a. Circled parts in Fig. 4. 19b shows high magnification SEM image of squared part in Fig. 4. 19a, which reveal the catalyst size and distribution on ceramic substrate.

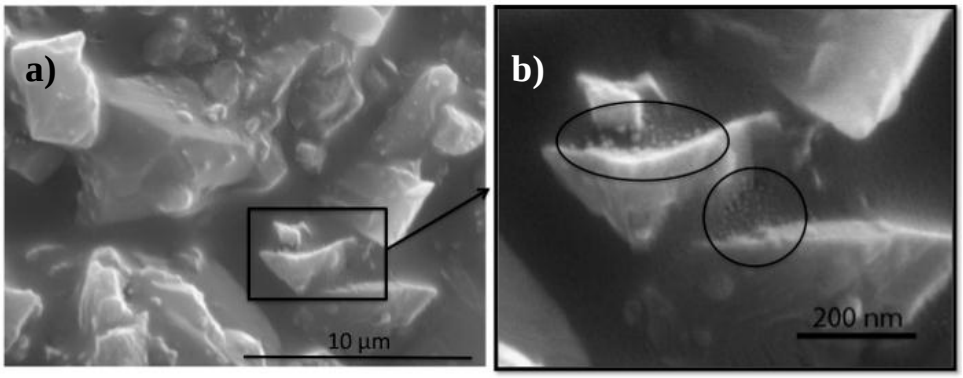

Fig. 4. 19. (a) SEM images of the rough surface of a ceramic foam after heat treatment in a furnace at 780˚C(b) Tiny catalyst particles are shown in the inset at higher magnefication.

The effectiveness of using styrene as a carbon source was also tested by injecting it into the furnace using ceramic foam coated with nickel nitrate as catalyst. Different injection rates and temperatures were tested to find an optimum set of conditions for the CNT growth. SEM images revealed that for most of the experiments used styrene, the growth of CNTs was not uniform and did not cover all surface of the sample, and that those parts with grown CNTs showed a very poor quality of nanotubes with more micro-sized fibres rather than nanotubes (Fig. 4. 20). Fig. 4. 20a shows the growth of thick CNTs and carbon fibres on the surfaces of a ceramic foam, whilst plenty of amorphous carbon was found at inner sections of the foam, as presented in Fig. 4. 20b. By changing the carbon injection rates and using different temperatures (up to 1000˚C), there was no obvious improvement for the quality of the samples using styrene as the carbon source.

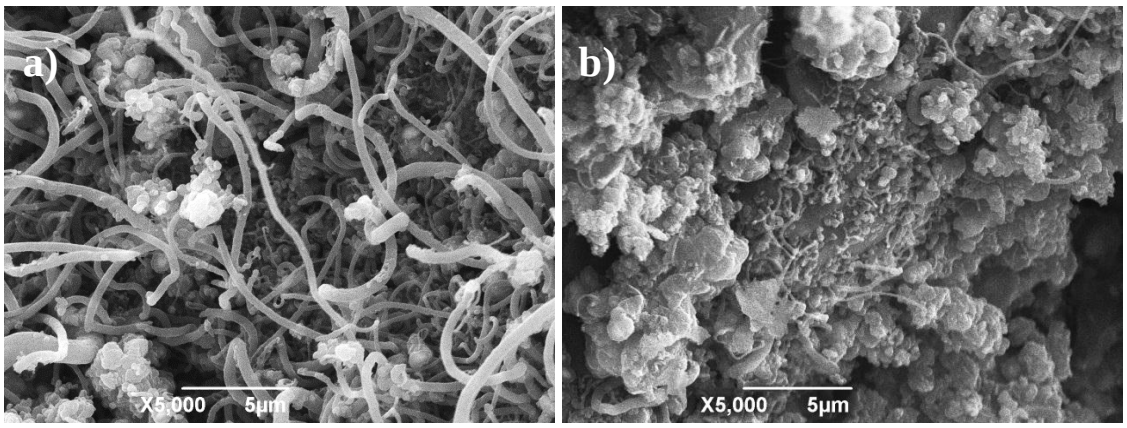

Fig. 4. 20. Poor quality of samples were observed using styrene as carbon source.(a) Thick CNTs and CNFs grown on the surface of a ceramic foam; and (b) massive amounts of amorphous carbons were detected at inner layers of ceramic foam.

As it was mentioned earlier, Malgas et al. [223] have reported that carrier gas flow rates (N_2 in their case) is an important factor with dominating effect on the nanotube growth. They showed that higher nitrogen carrier gas flow rates led to CNTs with a higher degree of graphitization. Their data indicate that more defects (carbonaceous particles) are presented when the nitrogen flow rates are high. Our experimental conditions are different from theirs, therefore we cannot compare our result directly with their data. In our experiment, the ceramic matrix and working quartz tube in the furnace have the same diameters (27 mm). If we consider the gas flow through the porous ceramic foam, a pressure drop will be caused by the foam. Therefore, unlike Malgas et al. results [223], a low speed of carrier gas could cause the lack of enough carbon atoms at the back face of the ceramic, whilst a very high speed of gas would blow away the carbon atoms very quickly before they have enough time to interact with the catalyst and initiate the growth, resulting in the poor quality of products. Fig. 4. 21 shows samples prepared at a low carrier gas speed (0.1 l/min), with surface facing the gas inlet side exhibiting a high quality of CNTs whilst the other face being covered with amorphous carbon. A high amount of carbon atoms might also count for the defects by dropping the quality of final sample, leading to the formation of amorphous carbon (Fig. 4. 22a) or carbon fibres (arrowed in Fig. 4. 22b). A low amount of carbon atoms will also leave the back of the ceramic without enough required sources

for the growth (similar result as presented in Fig. 4. 21). Therefore, finding the right balance between the injection rates of the carbon source and the speeds of the H_2 carrier gas is important for the successful growth of CNTs on the foam ceramic substrate. Based on this concept, a wide range of injection rates (from 0.4 to 5 ml/h) was examined along with different hydrogen flow rates (from 0.1 l/min to 0.7 l/min). These experiments were carried out for different durations from 1 hour up to 6 hours. The optimum combined condition for CNT growth on a ceramic foam, based on SEM investigations, has found to be at a H_2 flow rate of 0.30 l/min and carbon source injection rate of 0.8 ml/h. This setting results in uniform growth of carbon nanotubes all over the ceramic discs.

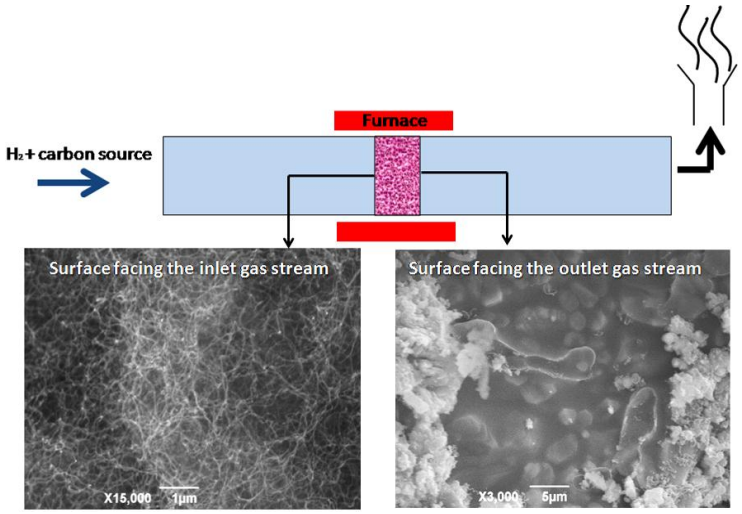

Fig. 4. 21. Illustration of quality of sample at two surfaces faced to inlet (left) and outlet (right) of furnace revealing dominating effect of carrier gas speed on quality of sample.

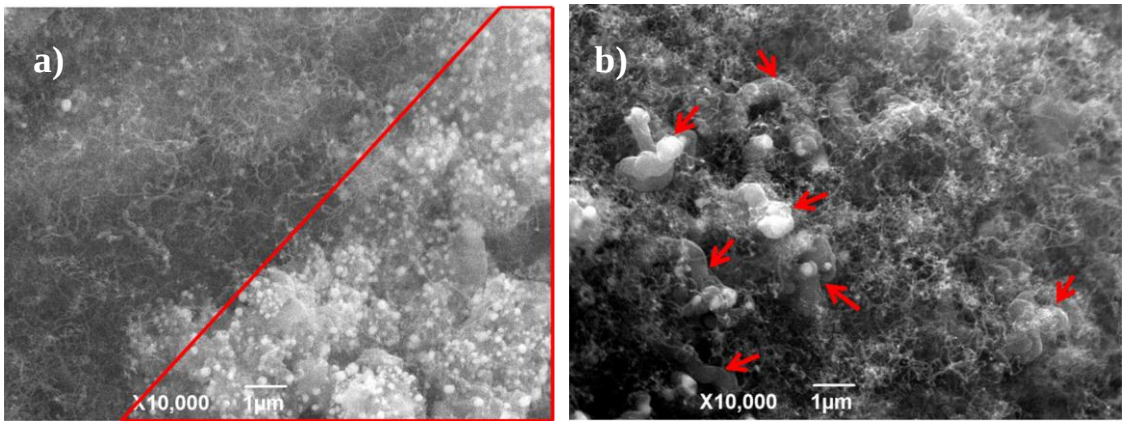

Fig. 4. 22. Fabrication of amorphous carbon (a) and CNFs (arrowed in b) beside CNTs dropping quality of composite as result of high injection rate of carbon source into the furnace.

4. 2. 2. 2. Effect of temperature on CNT growth

The CVD temperature plays a significant role in the CNT growth and this effect varies under different experimental conditions. For example, using camphor as the carbon source and Fe-Co-zeolite system as the catalyst, Kumar and Ando have claimed that for a fixed metal concentration, raising the reaction temperature increases the yield of CNTs and their diameter distribution [225]. They have shown that by optimising the catalyst concentration in their system, MWCNT and SWCNT can be selectively grown as a function of temperature [211]. They have also shown that camphor does not decompose below 500˚C. At 550˚C, they managed to grow CNTs of very short-length. Increasing the temperature from 650˚C up to 750˚C, they produced high quality CNTs. After 750˚C, they obtained low quality CNTs with drastically increased diameters. At 850˚C and above, SWCNTs started to grow. At 900 ˚C, they were able to prepare large bundles of SWCNTs. They concluded that 650 and 900˚C are the optimum temperature for making MWCNTs and SWCNTs, respectively. As another example, after testing a wide range of temperatures (600-1050˚C), Li et al. have reported that the appropriate temperature for fabricating pure CNTs with large yields is between 750 and 850˚C. They have revealed that CNTs cannot grow at either low (600˚C) or high (1050˚C) temperatures [226]. Consequently, it was important for us to find the optimum temperature for our experimental condition.

We found out that it was possible to grow CNTs on ceramic substrate under our experimental conditions, at temperatures ranging between 700 and 850˚C. However, at 700˚C, the grow depth of good quality CNTs is limited to several millimetres from the surface facing the inlet of furnace. At this temperature, the quality of CNTs drops dramatically at centre of ceramic foam toward the back face of sample as shown in Fig. 4. 23. Similar results were also obtained at 850˚C.

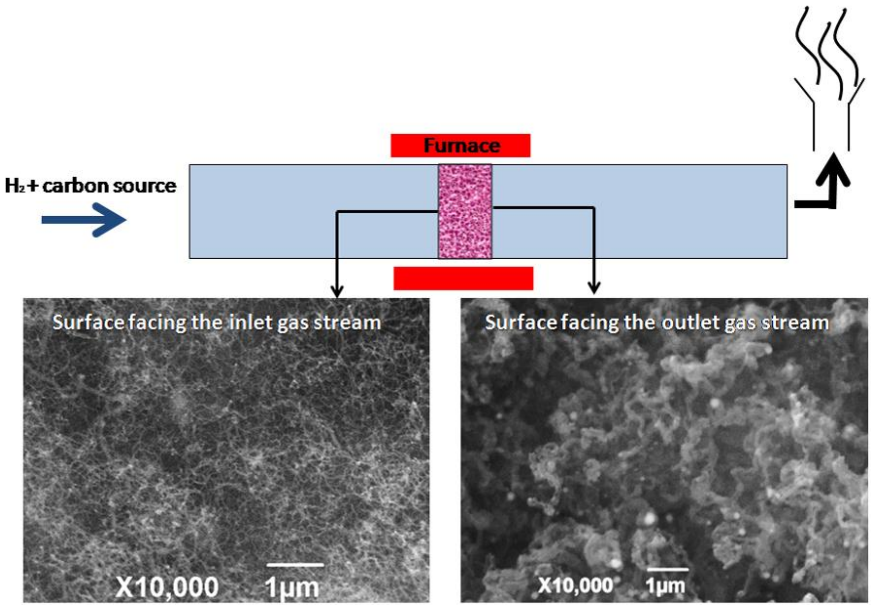

Fig. 4. 23. SEM images showing the quality of CNTs on surfaces facing the inlet (left) and outlet (right) stream of furnace. Sample was produced at 725˚.

At temperatures >850˚C and <700˚C, the amount of amorphous carbons observed in SEM investigations increased dramatically when almost no CNTs could be gradually detected anymore (Fig. 4. 24).

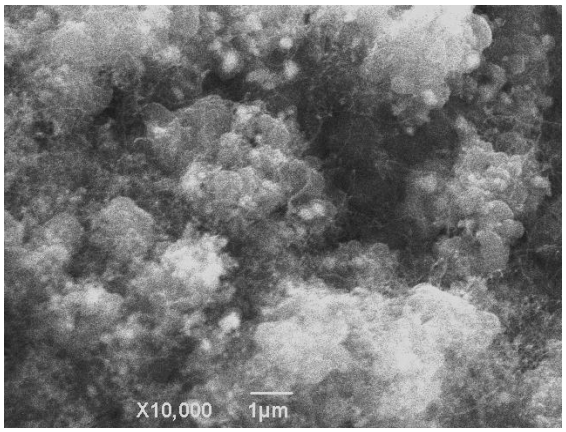

Fig. 4. 24. SEM image of a sample prepared at 850˚C showing the CNTs covered by a large amount of amorphous carbon, taken from the surface facing the front gas inlet side of the sample.

In order to investigate the possibility of producing SWCNTs on our ceramic substrate, similar experiments were carried out at higher temperatures. However, at those temperatures (up to 1100˚C) we were unable to detect any CNTs. Thus, considering our experimental condition and furnace limitation, we found there was no SWCNT growth under these conditions.

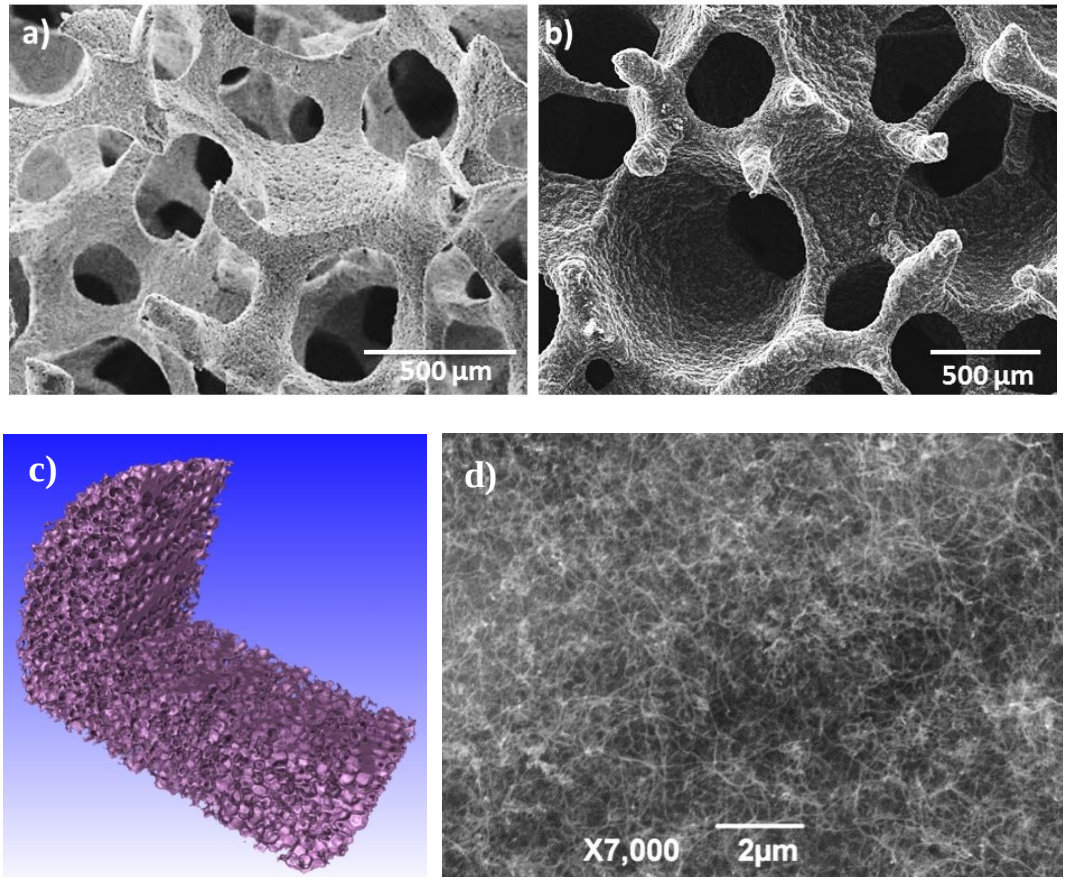

Fig. 4. 25. a, Low magnification SEM images of a porous ceramic matrix before the CNT growth; b, Low magnification SEM image of the ceramic/CNTs composite; c, a µ-CT scan 3D image of a ceramic substrate showing the interconectivity feature of the foam; and d, SEM image of CNTs grown on ceramic foam produced at 780˚C.

To conclude, under our experimental circumstances, good quality CNTs have been successfully synthesised at temperatures ranging from 750 to 800˚C, and based on the quality (from SEM results), 780˚C was chosen as the optimum temperature for further synthesis work. The physical change in ceramic appearance after CNT deposition can be seen in Fig. 4. 25a and b where the densely deposited CNTs layers located in the inner wall of the ceramic matrix. µCT-scan of ceramic/CNT composite in Fig. 4. 25c shows the interconnectivity of pores across the substrate which allows for the uniform catalyst deposition and CNT growth in all sections of matrix; however, it cannot detect CNTs on substrate due to resolution limitation. Fig. 4. 25d shows the high quality CNTs produced at 780˚C where CNTs were uniform at all sections of the sample (at both faces).

4. 2. 3. Yield of CNTs

The functional properties of composite containing CNTs are dominated by the CNT quantity [227]. As a result, scientists try to further improve properties of such materials by further increasing the yield of CNTs. However, there are technical challenges on increasing the content of CNTs for different applications, as CNTs tend to agglomerate in composites. In this context, it was tried to increase the yield of CNTs by gradually increasing the reaction time up to 6 h, but still similar weight increase was observed in all the experiments. Another alternative way to increase the yield is providing continuous supply of carbon source and catalyst during the synthesis process. In order to supply the required catalyst, in two different sets of experiment, ferrocene and nickel nitrate were added to the carbon source solution.

Similar to Kumar and Ando's [209] experimental conditions, ferrocene was introduced into to the camphor solution (carbon source). Unlike their work where they used solid mixture, we added ferrocene (different wt. %) to the camphor acetone solution (40 vol. %). The ferrocene in the carbon source solution will be decomposed simultaneously with the carbon source, leaving the decomposed iron atoms to form the catalytic particles to promote the CNT growth [223]. In fact, these Fe particles floating at the reaction quartz tube are so active that they promote the growth of CNTs everywhere, leading to the formation of a thick layer of CNTs deposited in the quartz working tube prior to reaching the ceramic sample. Fig. 4. 26 show this thick layer of CNT nanoforest removed from the quartz tube at low and high magnifications. Kumar and Ando also reported the fabrication of a large amount of CNTs deposited on the inner wall of their quartz tube using a camphor-ferrocene mixture [209]. In our case, this phenomenon actually reduced the yield of CNTs in the composite, as most of the carbon were accumulated and grew on this layer rather than grew inside the ceramic pores.

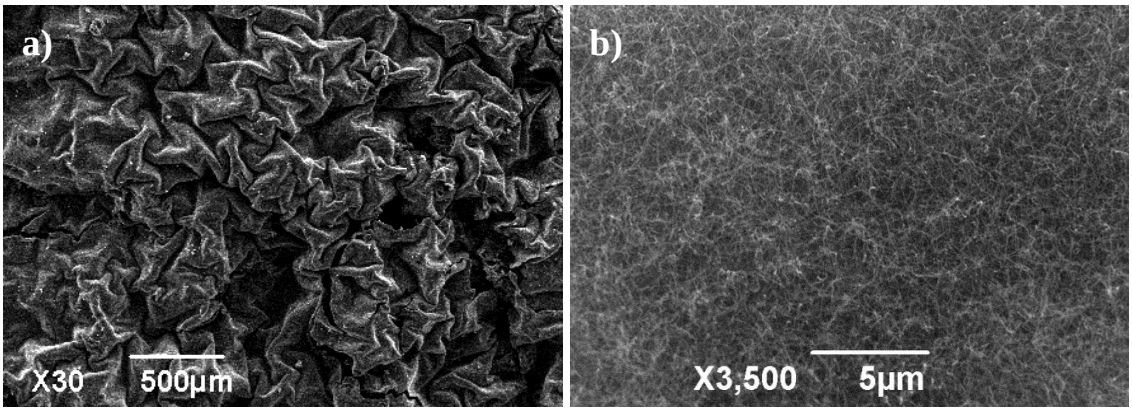

Fig. 4. 26. A thick layer of CNT collected from the quartz working tube when using ferrocene mixed with carbon source at low (a) and high (b) magnefications.

Further, by increasing the flow rate of the hydrogen carrier gas from 0.1 to 0.7 l/min, in order to force the decomposed iron nanoparticles from the ferrocene to penetrate through the ceramic foam, rather than depositing on the outer surface of the foam or on the inner surface of the quartz tube, this problem appeared to be partially solved. However, the introduction of iron nanoparticles during the growth has resulted in an excessive amount of iron particles sitting on top of the resulting CNTs, which acted as contaminant and dropped the quality of the final product. Fig. 4. 27 shows these iron particles (bright particles) stuck among CNTs. By gradually reducing the amounts of ferrocene in the solution (from 2 wt.% to 0.2 wt.%), we tried to solve this problem. However, after all of the mentioned variations, still similar weight increase was reported for the final sample, indicating the ineffectiveness of this procedure in increasing the yield of CNTs.

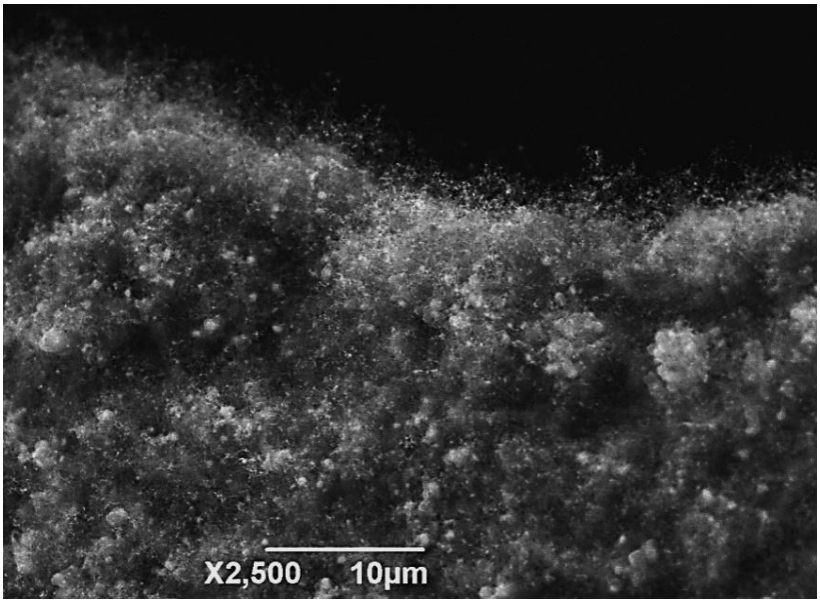

Fig. 4. 27. Iron nanoparticles (bright particles) stuck among CNTs as the result of addition of ferrocene.

As another approach to increase the yield of CNTs, $Ni(NO_3)_2$ was added to the camphor-acetone solution, to avoid the problem of excessive amounts of iron produced by ferrocene. The resulting sample showed a 3.8 % weight increase. However, further SEM investigation proved that there were large amounts of metal particles (Fig. 4. 28c & d) among the good quality CNTs (Fig. 4. 28a and b) in the sample. Besides contaminating the sample, these metal particles made our estimation on the yield unreliable. It was tried to calculate the amount of CNTs by subtracting the weight of blank ceramic foam and 75% of the weight increase (based on TGA results presented in Fig. 4. 29b after catalyst deposition) from the weight of the final sample. This calculation strategy cannot estimate the additional weight of these extra metal particles, as they are much heavier than CNTs. Therefore the resulting yield is unreliable neither. After several experiments, it seems to us that the yield of CNTs could not be improved simply by the addition of catalyst to the carbon source.

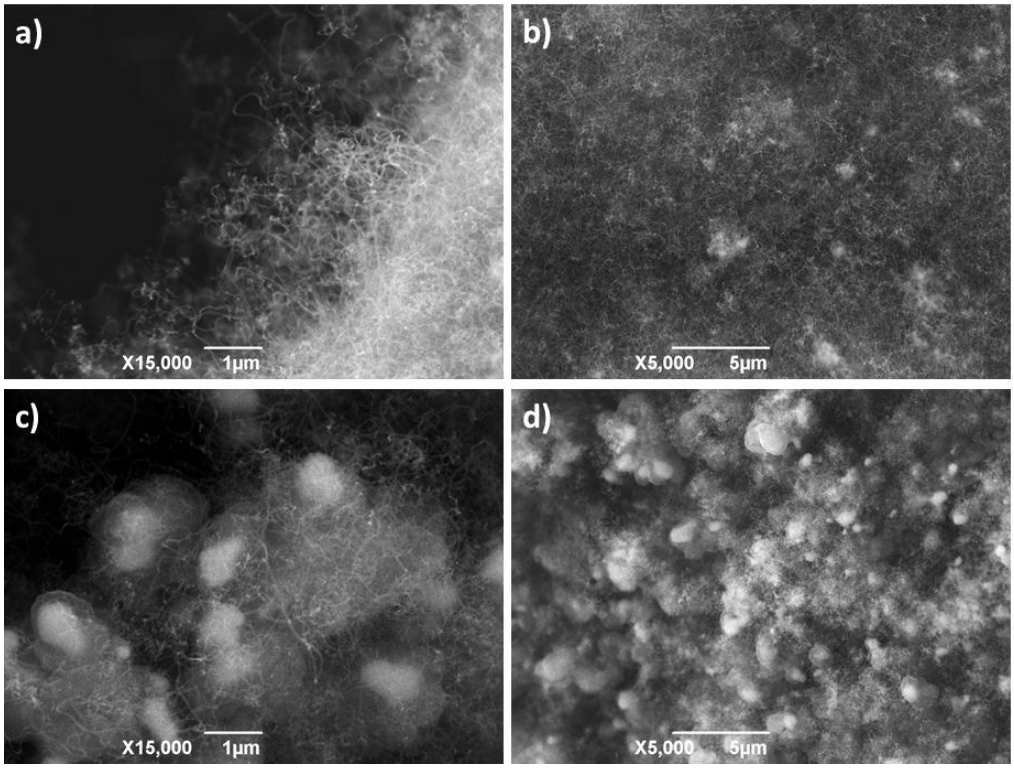

Fig. 4. 28. SEM images show addition of nickel nitrate to the camphor-acetone solution result in deposition of nickel particles inside the sample affecting its quality at high (a, c) and low (b, d) magnifications.

Table. 4. 5 summarises the weight of samples at different stages of experiment.

Table. 4. 5. Weight of samples at different stages suggesting the yield of CNTs

no.	M_e	M_c	M_f	M_{cat}	M_{CNT}	*Experimental condition*
1	4.4295	4.4457	4.4840	0.0122	0.0423	normal procedure*
2	3.3695	3.3869	3.4273	0.0130	0.0448	normal procedure
3	3.0085	3.0231	3.0717	0.0109	0.0522	normal procedure
4	4.1116	4.1241	4.1069	0.0094	0.0433	normal procedure
5	3.6183	3.6318	3.6812	0.0101	0.0528	increase reaction time to 6 h
6	4.0554	4.0722	4.1069	0.0126	0.0389	addition of 2 wt.% ferrocene, H_2 rate of 0.3 l/min
7	2.4716	2.4868	2.5478	0.0114	0.0648	addition of 2 wt.% ferrocene, H_2 rate of 0.7 l/min
8	3.7071	3.7263	3.7736	0.0144	0.0521	addition of 0.2 wt.% ferrocene
9	2.5444	2.5622	2.6411	0.0133	0.0833	addition of $Ni(NO_3)_2$

M_e: weight of blank ceramic (g)

M_c: weight of ceramic after being dipped in the catalyst solution and having removed the acetone (g)

M_f: weight of ceramic/CNT composite (g)

$M_{cat}=0.75\times(M_c - M_e)$ (g)

$M_{CNT}=M_f - M_{cat} - M_e$ (g)

* normal procedure means the final settings which were used for ceramic/CNT composite fabrication as described in chapter 3.

Finally, a multi-stage growth was developed in order to improve the CNT yield. In this process, after the first CNT growth experiment was finished and the sample was cooled down to room temperature, the entire resulting composite was again dipped in the same catalyst solution. After the removal of the acetone, the first stage composite was then put back into the furnace for the second stage of CNT growth, i.e. another 30 min in hydrogen atmosphere (0.3 l/min) for reducing the catalyst nanoparticles at 400˚C. Based on TGA results of the composite in Ar, presented in Fig. 4. 29a, the onset weight loss of CNTs in argon is at 630˚C and the thermal decomposition of $Ni(NO_3)_2$ (Fig. 4. 29b) in Ar finishes at 325˚C , 400˚C was chosen for the catalyst activation at this stage to avoid any damage to the pre-grown CNTs. Then, after increasing the temperature to 780˚C, the carbon source (camphor acetone solution 40 vol. %) was injected into the furnace at a rate of 0.8 cc/h for 1.5 h using hydrogen as the carrier gas (0.3 ml/h). This process also could not meet the expectation for increasing the carbon nanotubes yield as it is shown in Fig. 4. 31.

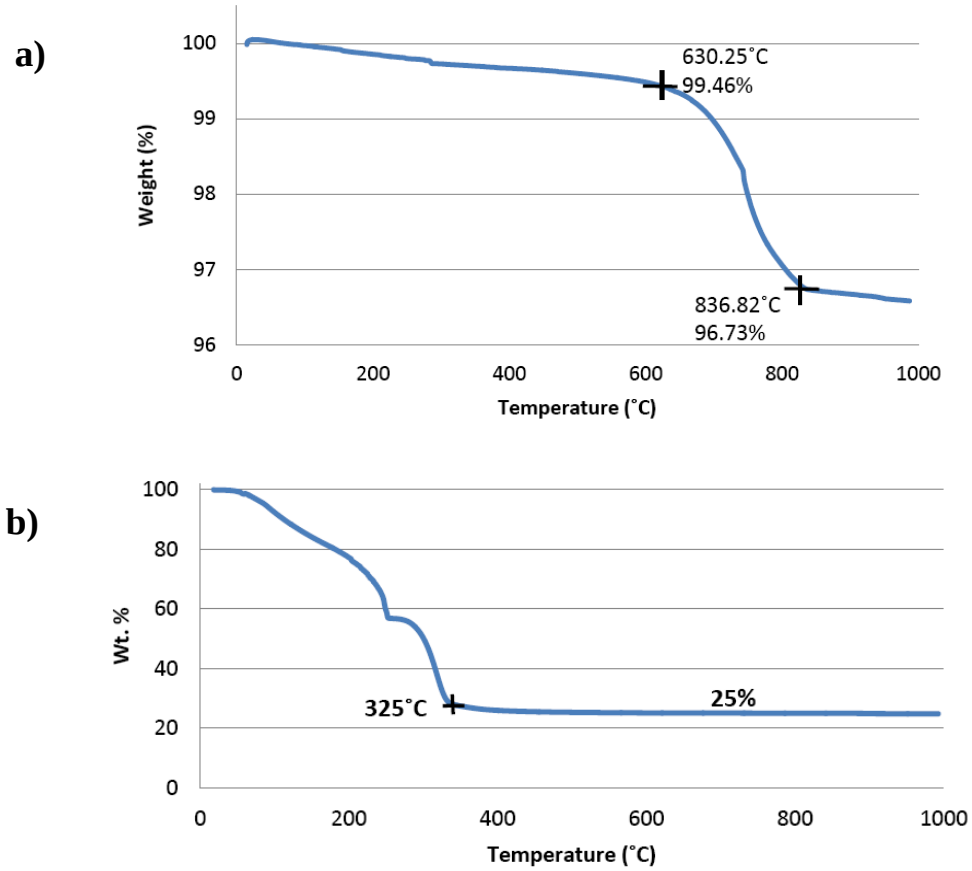

Fig. 4. 29. TGA results show the thermal stability (up to 630˚C in argon) of CNTs grown on ceramic matrix (a), and decomposition temperature of nickel nitrate in argon, (b).

TGA result presented in Fig. 4. 29a also indicates the total yield of CNTs is 2.7 wt. %. This value increases up to 3.1 wt. % (Fig. 4. 30) for other samples. These different yields could partly be a result of the removal of CNTs during sample preparation for TGA investigation or unavoidable changes in synthesising parameters such as the amount of deposited catalyst on sample.

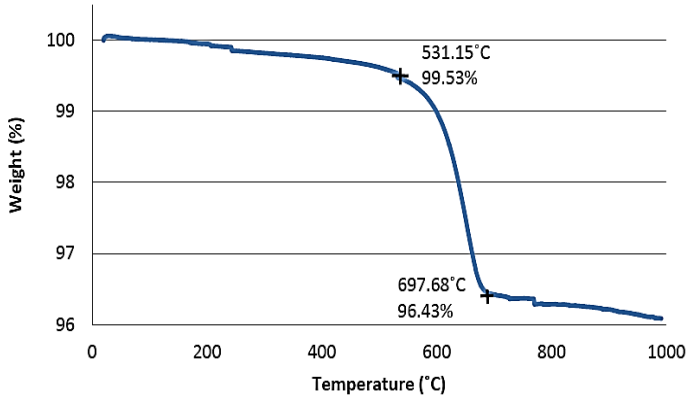

Fig. 4. 30. TGA of ceramic/CNT composite conducted in air that shows yield of 3.1 wt. % for CNT growth.

Fig. 4. 31 shows SEM images of samples prepared during multistage process at different magnifications, where existence of plenty amount of amorphous carbon is visible.

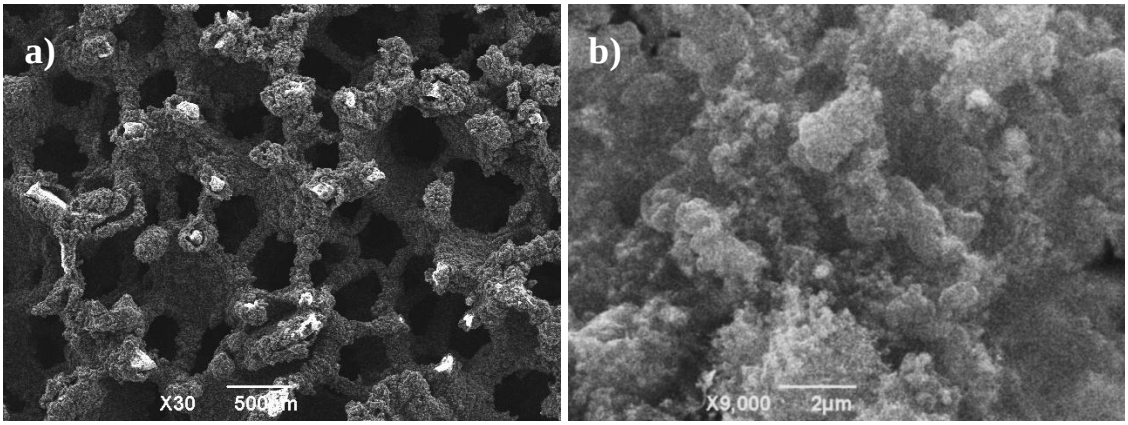

Fig. 4. 31. SEM images of samples produced during the multi-stage process for increasing the yield of CNTs. It is clear that the sample surface is covered with amorphous carbon and the pre-produced CNTs have been destroyed.

To conclude, three different approaches for increasing the yield of CNT on ceramic substrate were tested, and the limited improvements achieved are inconclusive. Further study and approaches may be required in the future.

4. 2. 4. CNT characterization

After finalising the experimental conditions and finding the best settings for CNT growth on ceramic foams (as described in chapter 3), SEM images were taken from sample. Fig. 4. 32 shows the surface of the sample faced to the outlet of gas stream, at two different magnifications. It shows the high quality and quantity of the CNTs covering the ceramic foam surfaces. It is clear now that moving from front face toward backside face of the sample, the quality of CNTs drops (referring to Fig. 4. 21 and Fig. 4. 23).

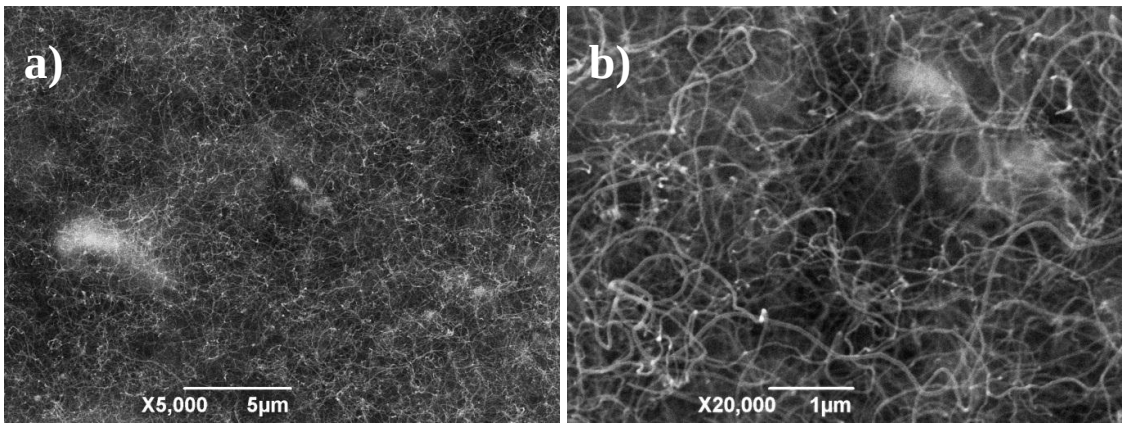

Fig. 4. 32. SEM images of the sample after synthesising large amount of CNTs at low (a) and high (b) magnifications.

TEM results have also confirmed the quality of CNTs being high. One CNT with a Ni particle as the catalyst at a tip of a nanotube is shown in Fig. 4. 33.

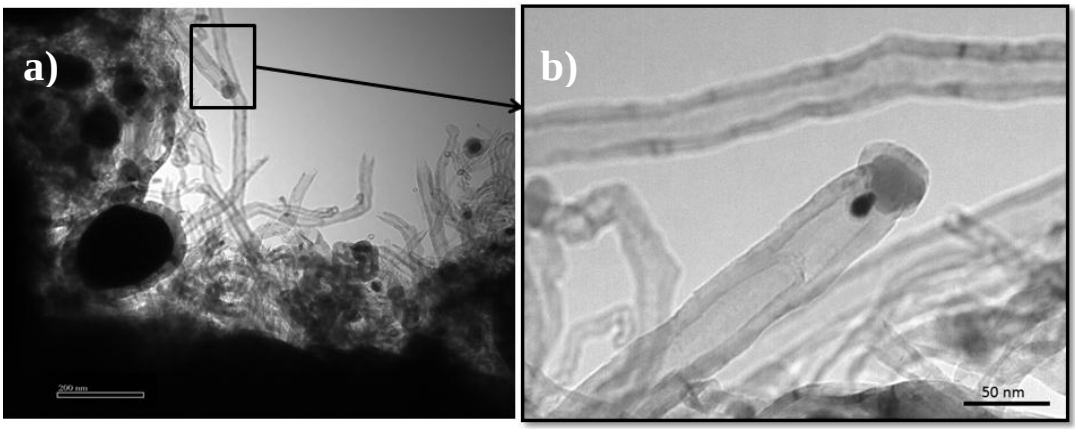

Fig. 4. 33. (a) TEM image of CNTs showing the structure feature of the produced nanotubes; and (b), a higher magnefication TEM image of the zoomed part in (a) which shows one catalyst particle attached to the tip of a CNT.

Understating the exact growth mechanism of CNTs in this approach seems very difficult and complicated as we have also observed CNTs with open ends (Fig. 4. 33a), CNTs with catalyst detached to its end (tip growth) (Fig. 4. 33b), CNTs attached to the substrate without any catalyst particle at the tip suggesting root growth mechanism (Fig. 4. 34a), and also catalyst at both ends (Fig. 4. 34b). We believe that for CNTs with open ends might be the result of falling off catalyst particles during grinding process for TEM sample preparation. Thus, we cannot clearly define one growth mechanism for present growth. However, tip growth is believed to be the main growth mechanism.

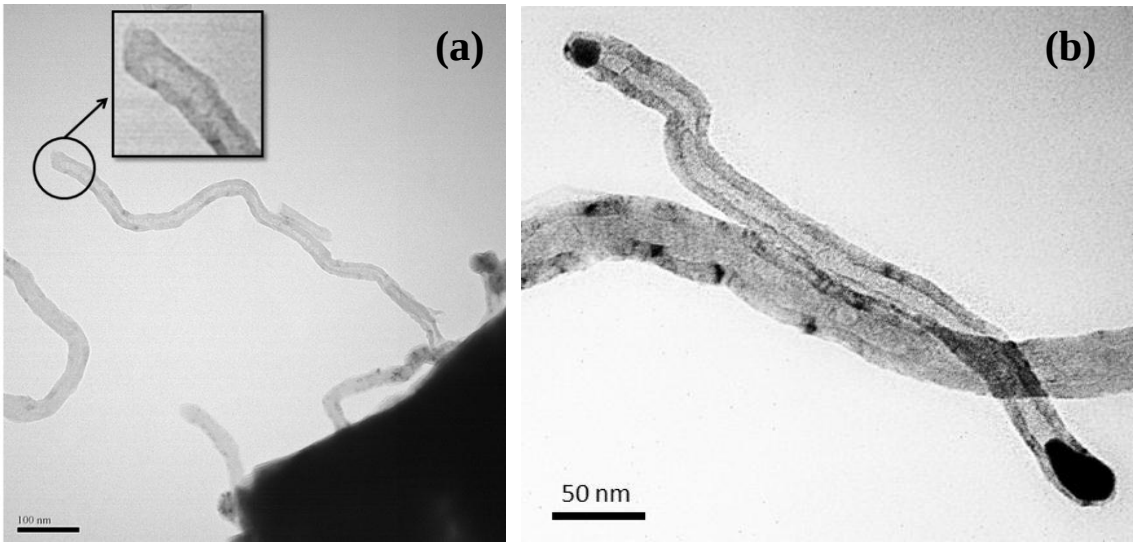

Fig. 4. 34. TEM images of CNT (a) free of catalyst at tip, and (b) catalyst particles encapsulated at both ends.

As seen in Fig. 4. 33 and Fig. 4. 34, the resulting nanomaterials are indeed hollow, being CNTs rather than solid carbon nanofibres, with average diameters of 40 nm and lengths up to several micrometres (Fig. 4. 35).

Fig. 4. 35. TEM image shows the length of a CNT.

4. 3. Conclusion

Large scale in-situ growth of CNTs inside ceramic matrixes possesses technical challenges. Intensive researches for direct on-site growth of CNTs inside such porous alumina (100-150 µm pore size) and ceramic foam (300 and 500 µm pore sizes) matrixes were carried out.

For porous ceramic substrate with 100-150 µm pore sizes:

- The effects of different catalysts and carbon sources on the fabrication process were studied
- Uniform coating of catalyst (nickel nitrate) on all surfaces of ceramic substrate was achieved by using catalyst solution rather than use of metal powders
- Use of tar-pitch as carbon source resulted in mostly fabrication of sphere carbon
- Camphor was used as carbon source which counts as a green regenerative and cheap source
- High melting and boiling point of camphor along with its solubility in acetone and its solid form were the most important technical parameters of this carbon source
- A novel unconventional method was introduced for the first time
- Process involves introducing both catalyst and carbon source inside the ceramic matrix and initiating the growth from inside
- The resulting MWCNTs have average diameters of 30–70 nm and lengths of up to several micrometers
- SEM and TEM investigations suggest tip growth as the growth mechanism
- The reaction time is considerably short (3 min)
- Process results in uniform distribution of CNTs at all section of ceramic matrix as function of distance from surface
- A 13% weight increase in samples after optimizing the synthesis parameter has been achieved. This weight increase includes the weight of both CNTs and catalyst particles.

- Such an easy fabrication process at low reaction time is favourable for mass production at industrial scale

For ceramic foam with 300 and 500 µm pore sizes, different method was introduced:

- As the ceramic foam has high gas permeability, carbon source was injected into the furnace (conventional CVD process)
- Catalyst solution concentration had a dominating effect on CNT growth. This effect was carefully studied and 1 wt. % concentration of nickel nitrate in acetone solution founded to be the optimum condition
- Temperature was introduced as another important factor which plays an important role in quality of CNTs. A wide range of temperatures (from 600 to 1100˚C) were tested and detailed results were presented. 780˚C was eventually chosen as reaction temperature
- Injection rate and carrier gas flow rate (H_2) were named as other controlling parameters which their effects were clearly discussed as well. 0.3 L/min and 0.8 cc/h were used for H_2 flow and carbon source injection rates, respectively.
- SEM and TEM investigations suggest again tip growth as growth mechanism with average diameter of 40 nm and lengths up to several micrometres
- TGA results revealed a 3 wt. % of CNTs can be yielded
- It was tried to increase the yield of CNTs by addition of ferrocene and nickel nitrate to the carbon source solution and also by developing a multi-stage process. Limited improvements achieved are inconclusive. Further study and approaches may be required in the future.

Chapter 5: Ceramic-Polymer composite reinforced with CNTs

5. 1. Introduction

Exploring the marvellous properties of CNTs has opened up its way in many scientific researches toward engineering applications. There are many attempts to use ceramics as a matrix for the synthesis of nanocomposites, availing their chemical inertness, high stiffness and thermal stability with relatively low density as discussed in previous chapter. There has been also an increasing interest in the studies of polymer-CNT nanocomposites, due to the unique combination of the promising properties and versatility of construction of multifunctional structures of each component [228]. Practically, almost all polymers can be processed to make nanocomposites [229]. Many polymers, such as epoxy [230], polycarbonate [231], polyamide [232-234], polyimide [235], polystyrene [236], and polypropylene [237], have been used to prepare polymer-CNT nanocomposites. However, infiltration of polymers into porous ceramics is a relatively new idea, which counts as a novel class of functional materials with a great potential for industrial applications. The high hardness, stiffness and wear resistance of ceramic, combined with the elasticity properties of polymers, can be an advantage in many commercial applications which are now limited by the poor mechanical properties of ceramics [38-40]. This type of composite materials has higher initial compressive strengths in comparison to porous ceramics, and could sustain larger deformations. Therefore, such composites could absorb energy more efficiently than both their constituent components separately, making them a desirable material as lightweight shielding or panels for protecting objects and structures against impact loads [41, 42].

We believe that the addition of CNTs to this new class of functional materials may further significantly improve their properties. This represents the first effort to fabricate such polymer-ceramic composite reinforced with CNTs.

5. 2. Epoxy resin-ceramic-CNT composite

Recently, miscible thermosetting polymer blends have received growing attention for special applications [238]. Epoxy resins are unique among the thermoset resins due to several factors [239]:

- Minimum pressure is needed for the fabrication of products normally used for thermosetting resins;
- Cure shrinkage is low, hence low residual stress in the cured product;
- Use of a wide range of temperatures by judicious selection of curing agents permits good control over the degree of cross linking;
- Availability of the resin ranging from low viscous liquid to tack-free solids.

High mechanical strength, low creep, strong anticorrosion and good electrical properties are among other advantages of epoxy resins. Consequently, they are widely used in structural adhesives, composite materials and surface coatings. Meanwhile, these materials also have a main shortcoming of low toughness and suffer from brittle behaviour due to their high cross linking density, therefore are prone to fracture [239]. Addition of CNTs might help to overcome this limitation and improve their composite toughness.

The most important curing agent for epoxy resins is the diglycidyl ether of bisphenol A (DGEBA). The choice of curing agents depends on the required physical and chemical properties, processing methods and curing conditions [240]. Different hardeners can be used as curing agent. Triethelentetramine (TETA) and 4,4′-diaminodiphenylmethane (DDM) are the most important curing agents. However, studies have shown that the DGEBA/DDM system exhibits better mechanical properties (Young's modulus, tensile strength, hardness, flexural strength, and compression strength) than the DGEBA/TETA system [240, 241]. It has also been shown that the addition of polyethylene oxide (PEO) to the epoxy resin can improve its mechanical properties[238]. Table. 5. 1 shows the mechanical properties and fracture toughness of DGEBA/DDM/PEO blends for

different PEO contents and cure temperatures for comparison purposes [238]. Clearly, the best improvements in mechanical properties have been obtained at 10 wt. % PEO addition and cured at 140°C. This is why the DGEBA/DDM/PEO system has been chosen for this experimental work.

Table. 5. 1. Mechanical properties and fracture toughness of DGEBA/DDM/PEO blends for all PEO contents and cure temperatures [238]

	$T_{cure} = 80°C$		$T_{cure} = 140°C$	
PEO (wt%)	E (MPa)	σ (MPa)	E (MPa)	σ (MPa)
0	2330 ± 25	94, 4 ± 1.01	2425 ± 45	94, 5 ± 1.79
10	2615 ± 20	103, 9 ± 1.23	2530 ± 45	98, 3 ± 1.48
20	2540 ± 30	95, 2 ± 1.73	2500 ± 35	91, 6 ± 1.3
30	1560 ± 45	53, 6 ± 1.14	1210 ± 60	42, 2 ± 1.84

Fig. 5.1 schematically shows the molecular structure of the DDM and DGEBA.

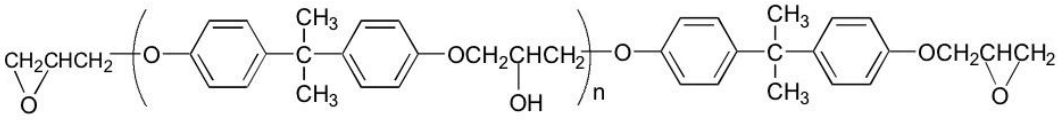

Diglycidyl ether of bisphenol A (DGEBA)

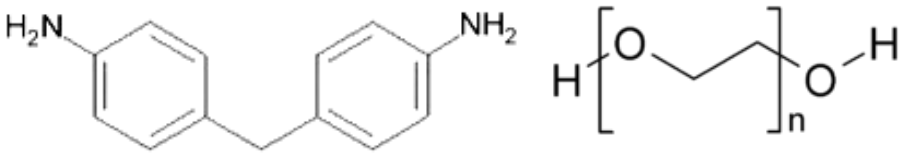

4,4′-diaminodiphenylmethane (DDM) Polyethylene oxide (PEO)

Fig. 5.1. Schematic illustration of the molecular structure of DGEBA, DDM and PEO [240, 241]

5. 2. 1. Sample preparation

The starting material for this part of work is acid functionalized ceramic-CNT nanocomposite with 500 µm pore size, prepared in previous section. Samples were infiltrated by DGEBA/DDM/PEO system. In order to produce the epoxy resin blend, the DGEBA was first mixed with a 10 wt.% PEO as a modifier at 80˚C. Then, the

curing agent DDM was added in a stoichiometric amine-epoxy ratio with continuous stirring at 80˚C until a homogeneous blend was achieved. The polymer is ready for infiltration at this step. In order to reach satisfactory level of filling, several approaches were tested such as using a silicone mould (Fig. 3. 8), as easy removal of samples from mould without damaging is an important factor.

Due to the large porosity of ceramic substrate, and the large amount of air introduced into the epoxy resin during mixing chemical process, the sample was put in a vacuum chamber to remove the air. During this process, a large amount of resin was forced out of the mould, therefore more polymer was required. The silicone mould could not satisfy this requirement.

A special aluminium mould was then designed as shown in Fig. 3. 9, with the capacity to provide extra polymer for the moulding process (Fig. 3. 9b part III). When the ceramic substrate placed in part II, and part I provides a passage way for air to leave the mould, enough polymer remains inside the mould to completely fill the samples. The mould designed for the infiltration of epoxy resin into the ceramic is shown schematically in Fig. 3. 9b. The mechanical force caused by turning the screw applies the pressure to overcome the viscosity and drives the polymer flowing through the cavities, improving the degree of filling. It is obvious that the removal of cavities will have a significant effect on the final mechanical property of the sample, as they can act as stress concentration points and cause failure under stress.

μ-CT scan confirmed that the degree of filling was more than 95% for different samples. Lower degree of filling particularly happened in samples with CNTs which may be attributed to the poor wettability of CNTs with epoxy resin. Fig. 5. 2 shows the plain ceramic, epoxy resin-ceramic, and epoxy resin-ceramic-CNT composites, after polishing.

Fig. 5. 2. Photograph of a plain ceramic matrix (left) before and after polymer infiltration (middle), and the ceramic-CNT-epoxy resin composite (right).

Two composite samples were then cut in half, and their cross sections are shown in Fig. 5. 3. From these cross sections, it can be seen that a high degree of filling has been achieved. It can also reveal that CNTs have grown in all the interconnected pores of the ceramic substrate, and the shear stress caused during injection resin seemed do not remove the CNTs from the internal pore surfaces and they remained intact. It is however some CNTs have indeed been removed from some parts of ceramic (bright arrowed parts in Fig. 5. 3b) during the polishing and cutting procedure.

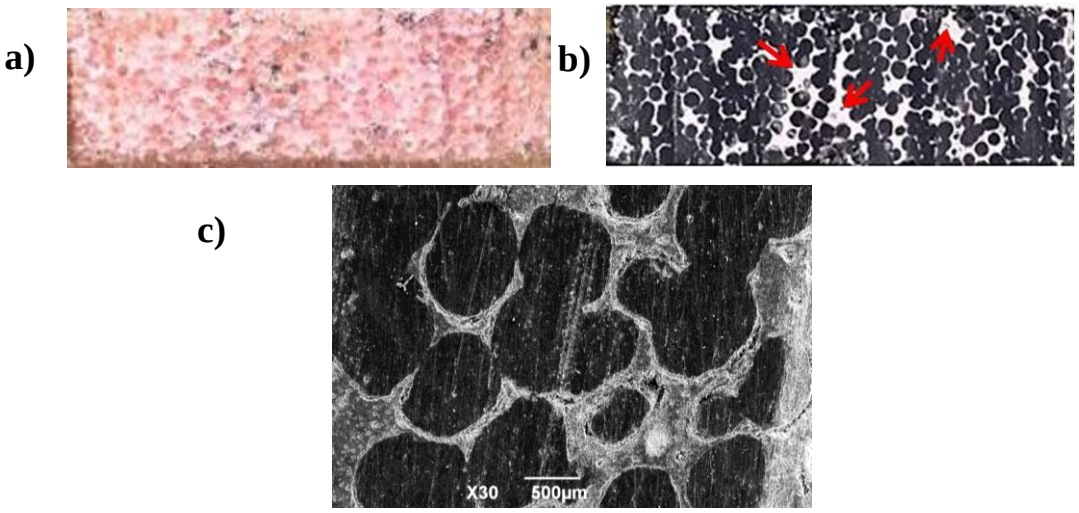

Fig. 5. 3. Optical images of the cross-section of the epoxy resin-ceramic composite (a), and epoxy resin-ceramic-CNT composite (b). Low magnification SEM image of the composite containing CNTs (c).

After the samples were further cured inside the aluminium mould for 3 hours at 130˚C, a TGA investigation in air showed that the cured epoxy resin was stable up to 350˚C (Fig. 5. 4). This result is an indication of the top range of temperatures the composite could be used, as both ceramic and CNT are much more thermally stable.

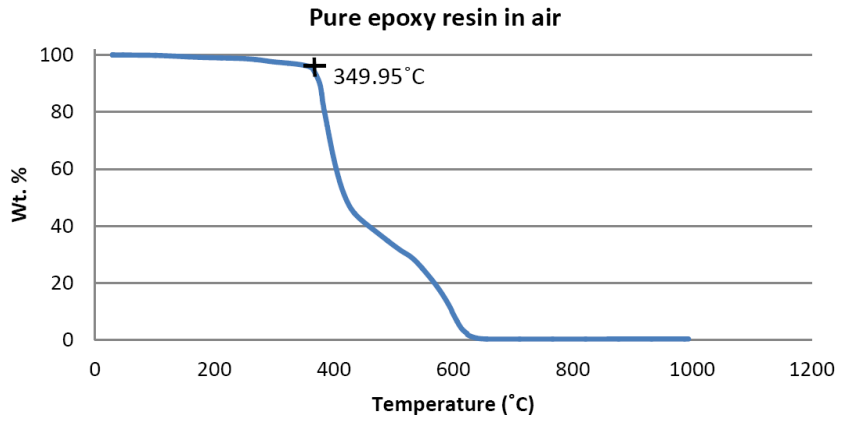

Fig. 5. 4. TGA result for pure epoxy resin in air which suggests its stability up to 350˚C in air

In order to show how CNTs have been embedded inside the epoxy resin and to make sure they have survived the infiltration process, not being removed from the internal walls of ceramic, SEM investigation was performed. To observe CNT clearly, it was necessary to remove part of the ceramic, which allows for looking into the cracks and interfaces between the ceramic and resin. For this purpose, the composite was broken into small pieces (Fig. 5. 5a). Scanning the cracks and sample interfaces, we successfully observed the CNTs (Fig. 5. 5). The pits arrowed in Fig. 5. 5d are believed to arise from small cavities.

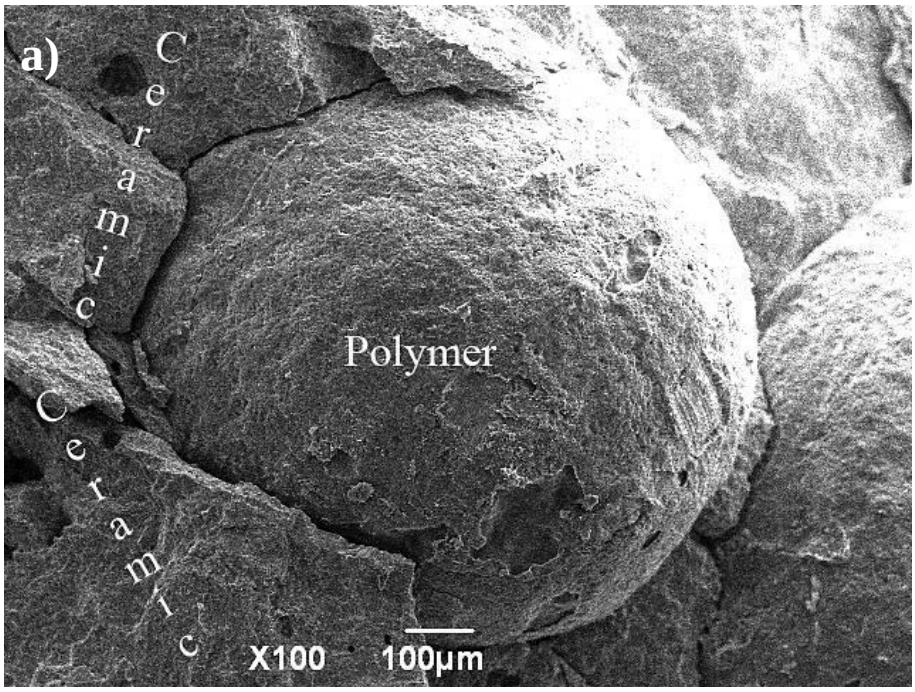

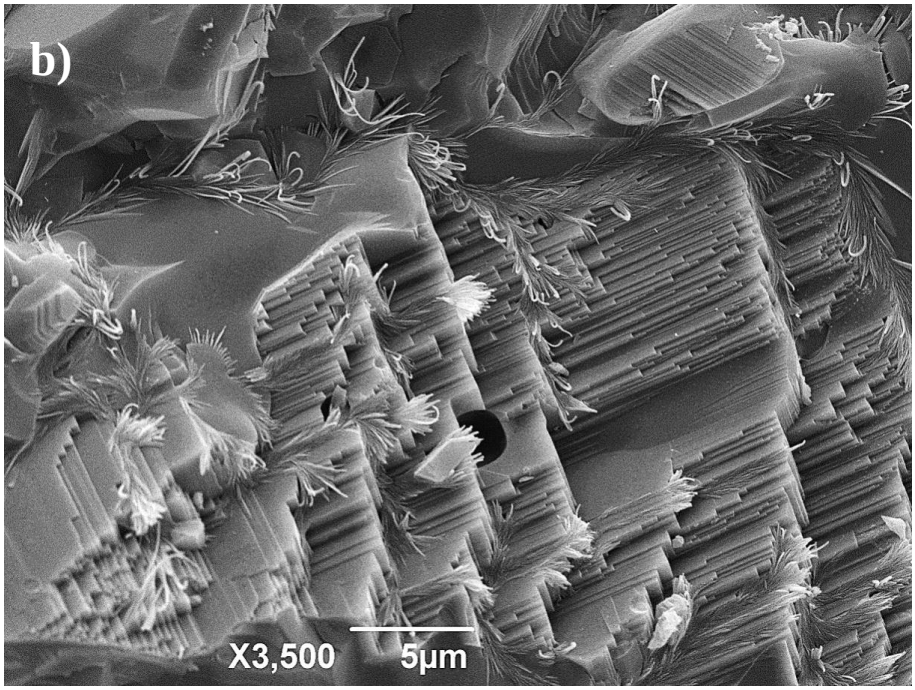
b)
X3,500
5µm

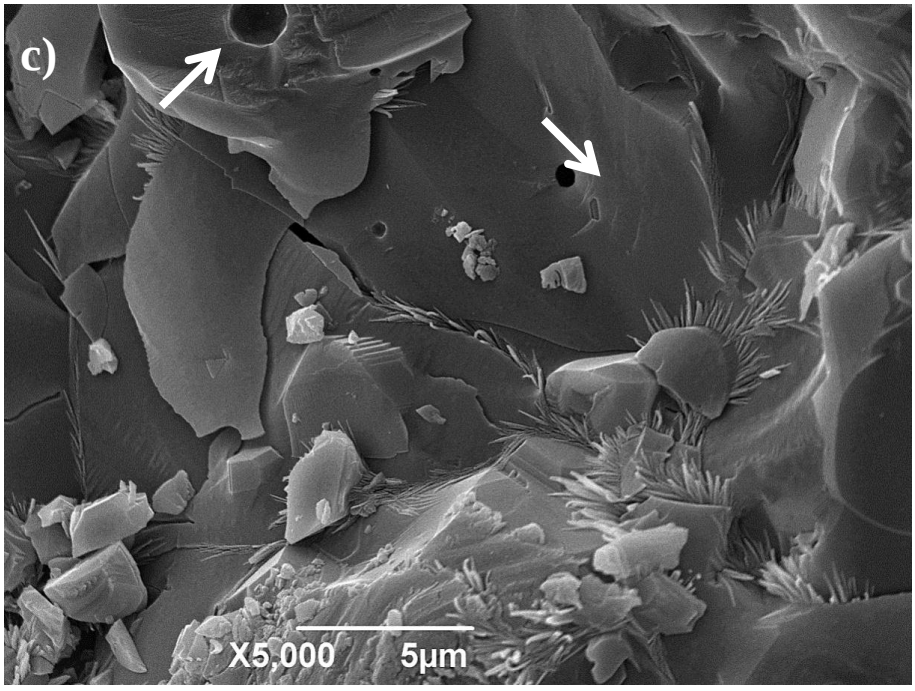
c)
X5,000
5µm

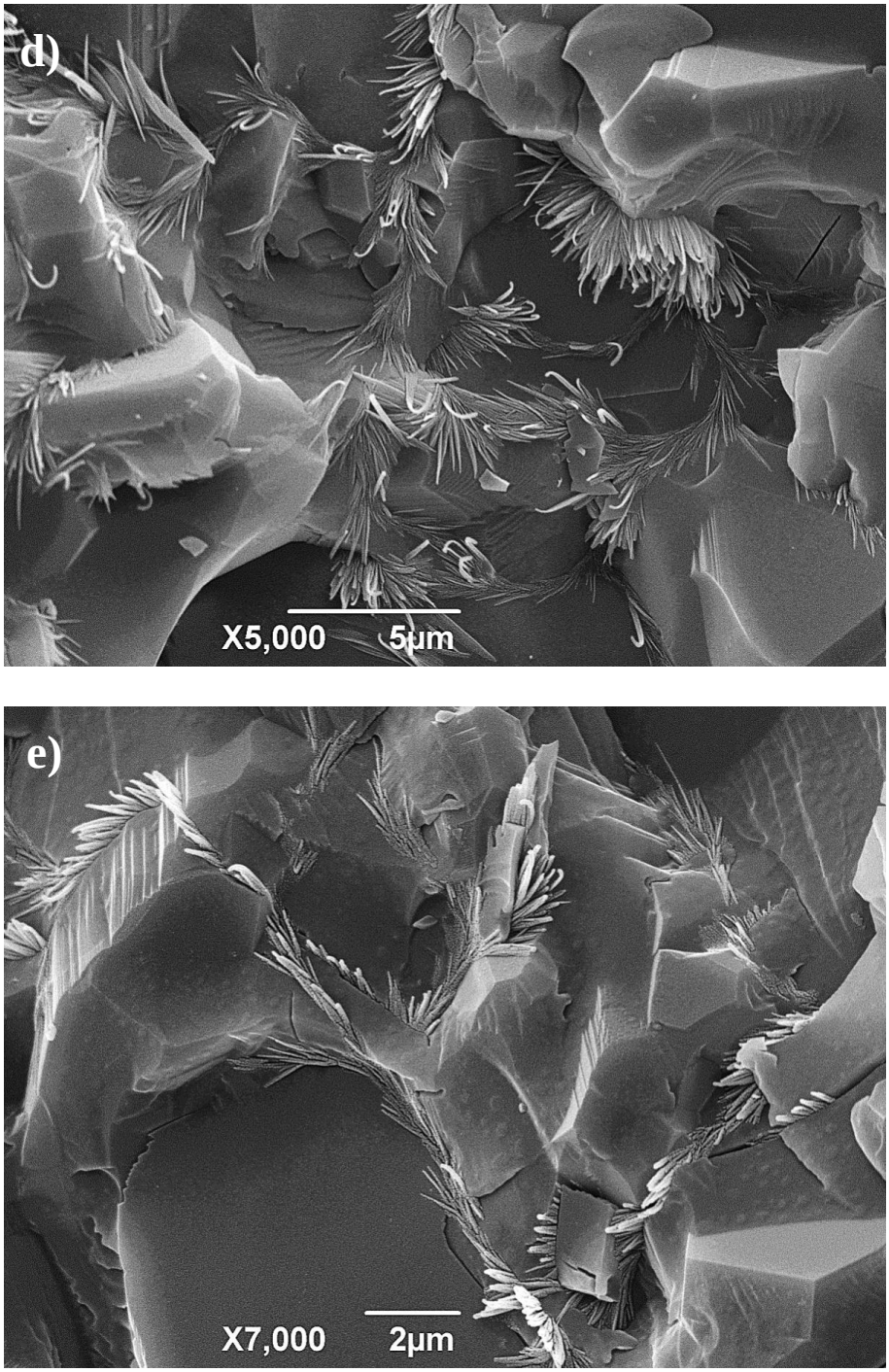

Fig. 5. 5. SEM images of CNTs embedded inside the epoxy resin at different magnifications.

SEM images in Fig. 5. 5 revealed that CNTs have been distributed evenly in all over the composite. This shows that we have managed to overcome one of the most difficult challenges in fabrication of polymer-CNT composite which is agglomeration of CNTs inside the matrix as it was well explained in literature review in chapter 2. Here, CNTs look straightened and thicker compared to their condition before epoxy resin

infiltration. This can be explained by considering the long vacuum time along with the shear stress applied during the infiltration process which has straightened the nanotubes. Large van der Waals forces can attach CNTs together; when these forces combine with the shear stress of epoxy resin infiltration, CNTs stick to each other and form thicker fibres after they were entangled with epoxy resin as can be seen in SEM images.

Using Archimedes principle, we obtained the densities of the samples and the results are presented in Fig. 5. 6. The error bar in the figure is the result of different density of ceramic substrates supplied by Dynamic-Ceramic Ltd.

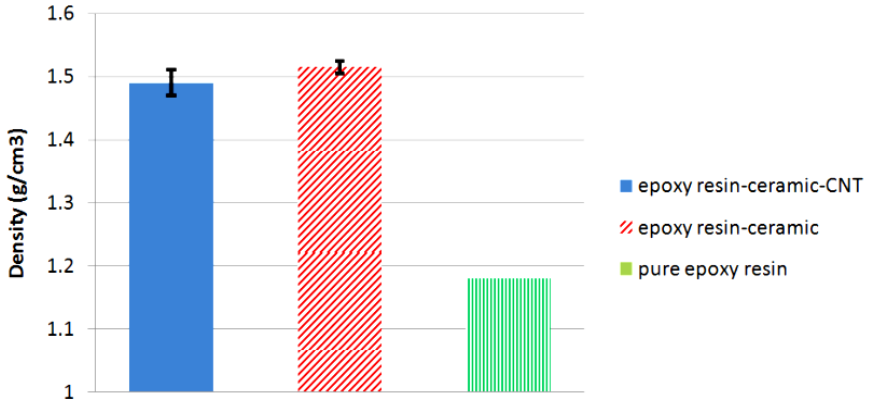

Fig. 5. 6. Densities of pure epoxy resin, polymer-ceramic and polymer-ceramic CNT composites obtained by Archimedes principal.

5. 3. Polyamide 12-ceramic-CNT composite

Polyamides (PA) have also been used widely for the fabrication of composites [232-234, 242]. Polyamides were the first studied and commercially used matrices of polymer nanocomposites [243].For processing PA 12, there are several grades of PA (PA6, PA11, PA12, and PA66). The mechanical properties of PA12 are generally good and all the molten-state methods are usable for this processing: extrusion, injection, compression, blow moulding, thermoforming, machining for high hardness grades and also welding [244]. Some of these properties are [229, 244, 245]:

- More flexible than PA6 and PA66,
- Adapted to extreme climates,

- Less sensitive to water and moisture
- Better behaviour at low temperatures
- Good stress cracking resistance
- Low density
- High abrasion resistance
- High elongations at break but much limited strains at yield
- PA12 fibres represent excellent strength/toughness balance
- Generally good chemical resistance

It also has some shortcomings, such as:

- Expensive
- Lower modulus and hardness compared to the other grades
- Larger shrinkage and coefficient of thermal expansion
- Weak fire resistance, easy to burn to generate flames

Overall, PAs possess very interesting properties for various industrial applications [229, 244]. Therefore, it is chosen in this thesis to fill the ceramic-CNT composite.

5. 3. 1. Sample preparation

The same aluminium mould (Fig. 3. 9) was used to infiltrate the polyamide 12 into the ceramic substrate. PA12 were in solid powder form. The bank of the mould was first filled with the PA powder. After shaken it is put into an oven (200°C) to allow for the powder/molten penetrating into the porous ceramic and pass through. This facilitates the wettability of the substrate with PA12. Unlike the epoxy resin, injecting the PA12 into the porous ceramic requires much higher pressure. Furthermore, the injection should take place very quickly before the PA drops temperature which increases its viscosity and potentially damage the substrate. The high injection pressure was supplied using a hydraulic press.

µ-CT scan was used to evaluate the degree of filling, and to investigate any possible damages to the ceramic substrate. Fig. 5. 7 shows the µ-CT scan image of a

damaged substrate. This broken sample had a similar appearance to other ones and could only be detected by using µ-CT scan.

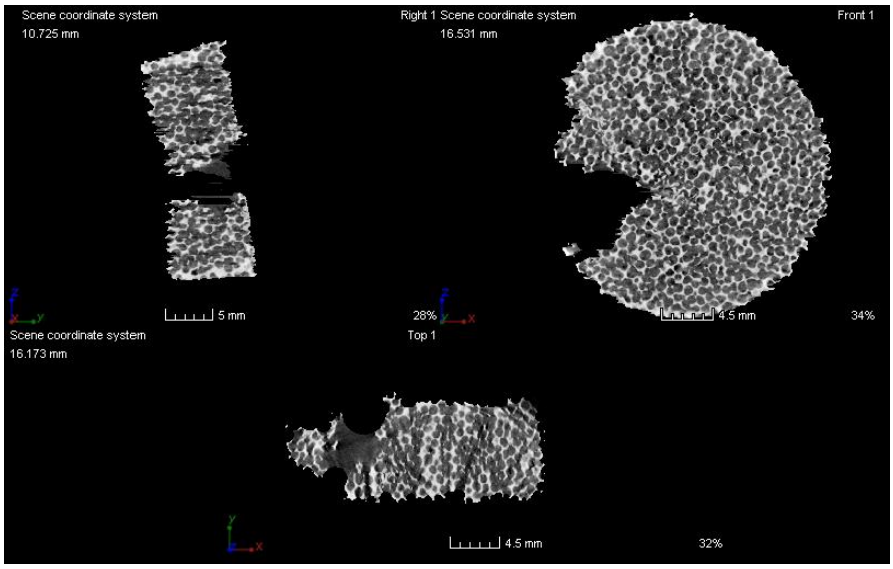

Fig. 5. 7. µ-CT scan image of a broken ceramic substrate as the result of high injection pressure.

Further µ-CT scan results have confirmed that it is possible to successfully infiltrate PA12 into the ceramic substrate with up to 99.85% degree of filling (Fig. 5. 8).

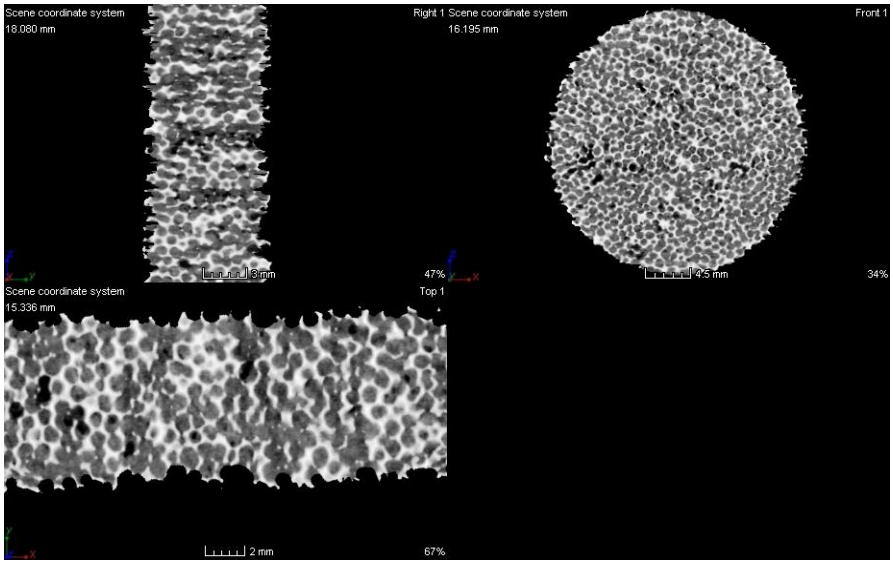

Fig. 5. 8. µ-CT scan proved the successful infiltration of PA12 into the porous ceramic substrate with more than 99% degree of filling.

Polished surface of one sample is shown in Fig. 5. 9. The black curve lines are CNTs surrounding the ceramic pores. Interconnectivity of pores is detectable here. Grey parts are PA12 and brighter white parts are contributed to the ceramic substrate.

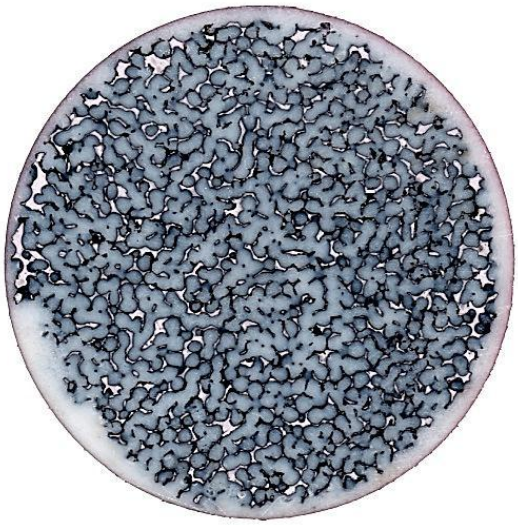

Fig. 5. 9. Photograph of the polished surface of a polyamide-ceramic-CNT composite. Black curves, grey parts and white bright parts are contributed to the CNT, PA12 and ceramic, respectively. The interconnectivity feature of the pores is also visible in this photo.

Similar to the epoxy resin-ceramic-CNT composite, the SEM investigation was performed on purposely fractured composite surface in order to identify the CNTs inside the composite (Fig. 5. 10).

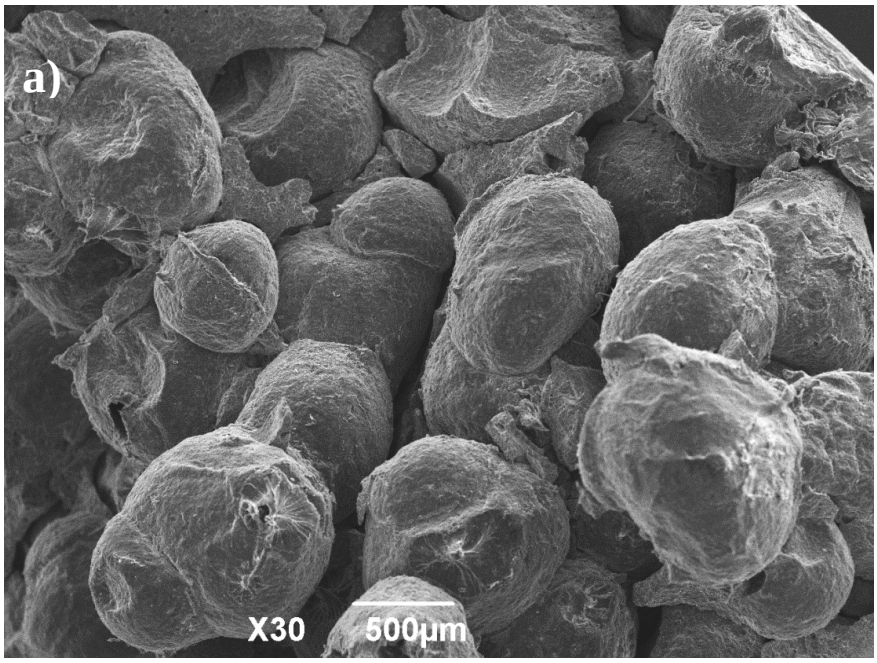

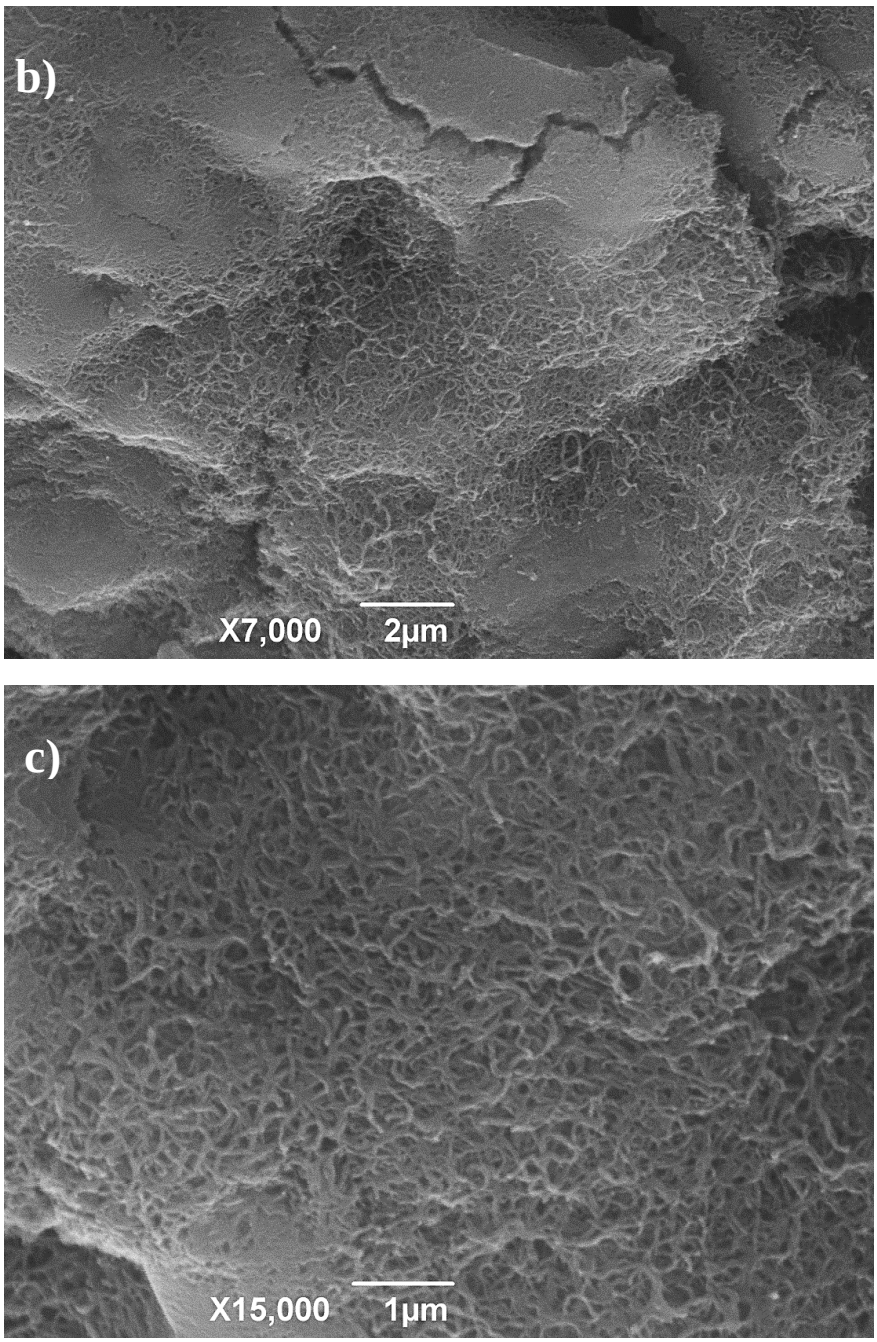

Fig. 5. 10. SEM images of CNTs embedded inside PA12 at different magnifications.

As can be seen in Fig. 5. 10, the shear stress applied during the infiltration did not induce further improvements in nanomaterial alignment. This result implies that these nanotubes orient rather easily under shear flows, but have significant in-built curvature from their synthesis, which cannot be straightened [245]. However, in epoxy resin-ceramic-CNT composite, separated and mostly straightened CNTs were visualized (Fig. 5. 5). A possible explanation for this different appearance of CNTs inside these two polymers (PA12 and epoxy resin), can be the long vacuum time (24 h) used for epoxy

resin composite preparation. This high level of vacuum for such a long time can steadily apply the required force for straightening of nanotubes when the epoxy resin gradually entangles them. During this process, some of the aligned CNTs will attach to each other and form thicker strings. And CNTs remained in that position after epoxy resin cured. When in PA12 composite, the injection force by its own is not strong enough to induce further improvements in nanomaterial alignment and apply the similar effect as vacuuming. Also, the PA12 infiltration is relatively happening at shorter time and it solidifies very quickly at room temperature which cannot provide the required force and time for straitening the CNTs. Wettability of CNTs is another dominating factor. A tailored functionalization of CNTs can lead to the formation of covalent bonds between CNTs and the polymeric matrix, resulting in a strengthened interface and an improved wettability of the CNTs [246]. Wettability by its own is greatly dependant on the viscosity of the polymers [247]. This dominating factor (viscosity) can also explain the different envisaged shapes of CNTs in our thermoset and thermoplastic polymers. A high viscosity matrix will cause poor wetting/ interpenetration [247]. Epoxy resin has considerably lower viscosity compared to the PA12. This low viscosity increases it wetting with CNT when nanotubes can also move easier and straightened by lower force compared to the condition in the viscous molten PA12. Good wetting between aligned CNTs and epoxy resin has been previously confirmed which indicated strong interfacial adhesion [121, 248].

Finally, the density of composite material and PA12 were also studied using the Archimedes principle and results are presented in Fig. 5. 11. As mentioned earlier, the ceramic substrates have different densities, therefore the error bar in Fig. 5. 11 are relatively large.

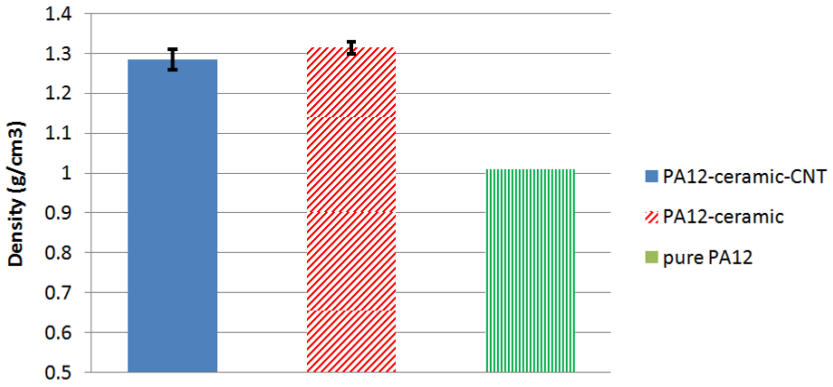

Fig. 5. 11. Densities of PA12, PA12-ceramic and PA12-ceramic CNT composites obtained by Archimedes principal.

5. 4. Conclusion

After having successfully fabricated ceramic-CNT composite, we further extended our research into a novel class of functional material, by infiltration of these composites with two types of polymer: a thermoset epoxy resin and a thermoplastic PA12.The infiltration processes were developed and a high degree of filling of these multiple component composites has been achieved (confirmed by µ-CT scan). Results also indicate that infiltration has not damaged the ceramic truss while CNTs have been distributed uniformly inside the matrix.

Chapter 6: Filtration properties of low density ceramic/CNT composite

6. 1. Introduction

Pollution has been one of the major modern problems confronted by mankind today which represents a sever threat to surrounding natural resources and to our health. The threat of pollutants and contaminants arises from different sources, including submicron and nanosized particles in polluted air, which will reach the lungs and subsequently remain in the alveoli and cause respiratory problems [166], or heavy ions, toxic chemicals and pathogens in contaminated water, which will cause severe damage to our daily life as well as to a variety of industries including pharmaceuticals and food [167]. In particular, toxic heavy metal ions in wastewater from industries such as metallurgical, mining and battery manufacturing could accumulate in living tissues and lead to irritation and cancerous concerns. Stringent standards are now in place to regulate their discharge to and removal from aquatic environment [34]. New technologies are in constant demand for the reduction and completely removal of these harmful contaminants, in order to improve the quality of life.

Nanofibres and nanotubes have emerged as a promising filtration material, and increased research interests have focused on their application for water and air purification. In particular, CNTs, owing to their high surface areas and large aspect ratios, have received special attentions for their excellent capabilities as a nanosorbent for filtering organic, inorganic and other contaminants from water [32]. Either embedded in membranes or supported on other structural media such as metal or ceramic truss, CNTs have been explored for the construction of new filters. CNTs deposited on a microporous membrane can be highly efficient in the removal of viral and bacterial pathogens [10, 249]. Although CNTs have been widely considered promising in the removal of heavy metal ions from wastewater, it is hard to find a practical one for industrial application.

A densely packed CNTs network containing various pore sizes from micropores to mesopores can immobilize pollutants either in air or in aqueous via physisorption [32]. However, the high pressure drop across the network and the high fabrication costs [8, 175] restricted their applications in air filters. For heavy metal ions adsorption over CNTs, chemical interaction involving valence (bond) forces through sharing or exchanging electrons is known to be the dominating mechanism (chemisorption) [194]; in addition, the microbial cytotoxicity of CNTs could also play a role in improving the filter performance [10]. However, the immediate technological challenge is how to convert the proven excellent adsorption behaviour of a loose CNT powder into a cost effective and practical filter for specific applications via proper treatment, akin to the breakthrough made in CNT oil filter [37].

In this chapter, the filtration performance of the ceramic/CNT composite will be assessed for the removal of bioorganic and inorganic contaminants from water, and of particulates from air. The model yeast Saccharomyces cerevisiae, BY4741 [204], was used as bioorganic model; and different heavy metal ions solution in water including Fe^{2+}, Cu^{2+}, Mn^{2+}, Zn^{2+} and Co^{2+} were used as inorganic contamination. The solution containing these contaminants were later simply passed through the ceramic/CNT composite filter fabricated in chapter 4 using a syringe pump. For air particulate filtration, number of particles ranging from 0.3-10 µm in ambient air before and after placing the ceramic/CNT filter on inlet of a Lighthouse portable airborne laser particle counter (SOLAIR 3100) as was discussed in chapter 3 were recorded to evaluate air filtration efficiency. These results, representing a big leap towards practical application, may open new opportunities for CNT engineering.

6. 2. Wettability and functionalization of filter

Although the Al_2O_3 used in this work is very absorbent, it can be seen clearly in Fig. 6. 1 that the CNT-coated filter is hydrophobic which originates from the hydrophobic characteristics of as-prepared CNTs [250]. Functionalization of the CNTs to modify

their surface behaviour is therefore an important step for the filter to be utilized in water systems, where improved wettability is desired for many practical applications [32]. It is possible to modify sidewalls or ends of CNTs with covalent or non-covalent attachments that provide better surface contact with adsorbents [251]. However, this type of surface treatment involves chemical solvents or acid and will usually lead to localized CNT densification and bundle formation on the ceramic surfaces (both external and internal) during the drying process, which could reduce the effective contact surface areas of the filter and result in reduced functionality for some applications. An alternative air oxidation process (at 400 ˚C) was also used to modify the CNTs in the filter. Compared with the wet chemistry method, this allows maintaining the original orientation and distribution of the CNTs on the surface of the filter cavities without being disturbed which is important for some applications such as air particulate filtration.

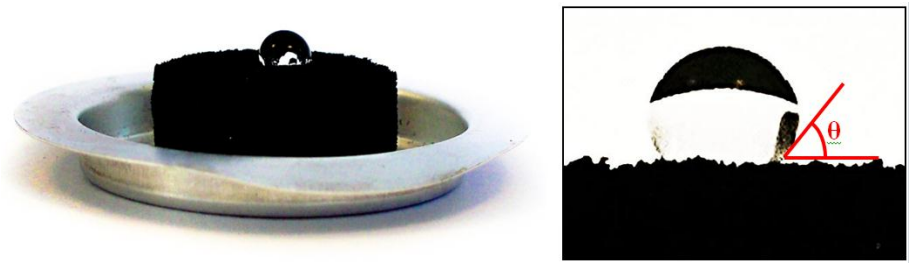

Fig. 6. 1. An illustration of the surface hydrophobic behaviour of filter with as-CNTs

6. 3. Yeast filtration

Liquid filtration experiments were carried out by placing the composite filter in a centrifuge tube and injecting the yeast solution onto it at specific injection rates using a syringe pump. Filtration was done by using a 300 µm pore-sized CNT filter (CNT-300) when later a 500 µm pore-sized CNT filter (CNT-500) was used as well in order to study the effect of pore size in yeast filtration efficiency.

After the filtration of yeast, the filter was carefully cut open to expose the internal structures. Followed by drying the samples in an oven at 100ºC for several hours, the dry composite samples were further investigated by SEM. Due to the high conductivity

of CNTs which formed a continuous network within the open channelled substrate, the samples exhibited good conductivity. Thus, all SEM investigations were performed without any coating. As samples contain large amount of water after filtration, to obtain high quality images of fresh yeast cells in the filter using a standard SEM is not feasible. Therefore drying in oven was unavoidable. Thus, for demonstration purpose, several droplets of yeast solution were placed on a filter which would quickly satisfy the requirement for SEM observation, to present the fresh appearance of cells blocked by the CNTs (Fig. 6. 2).

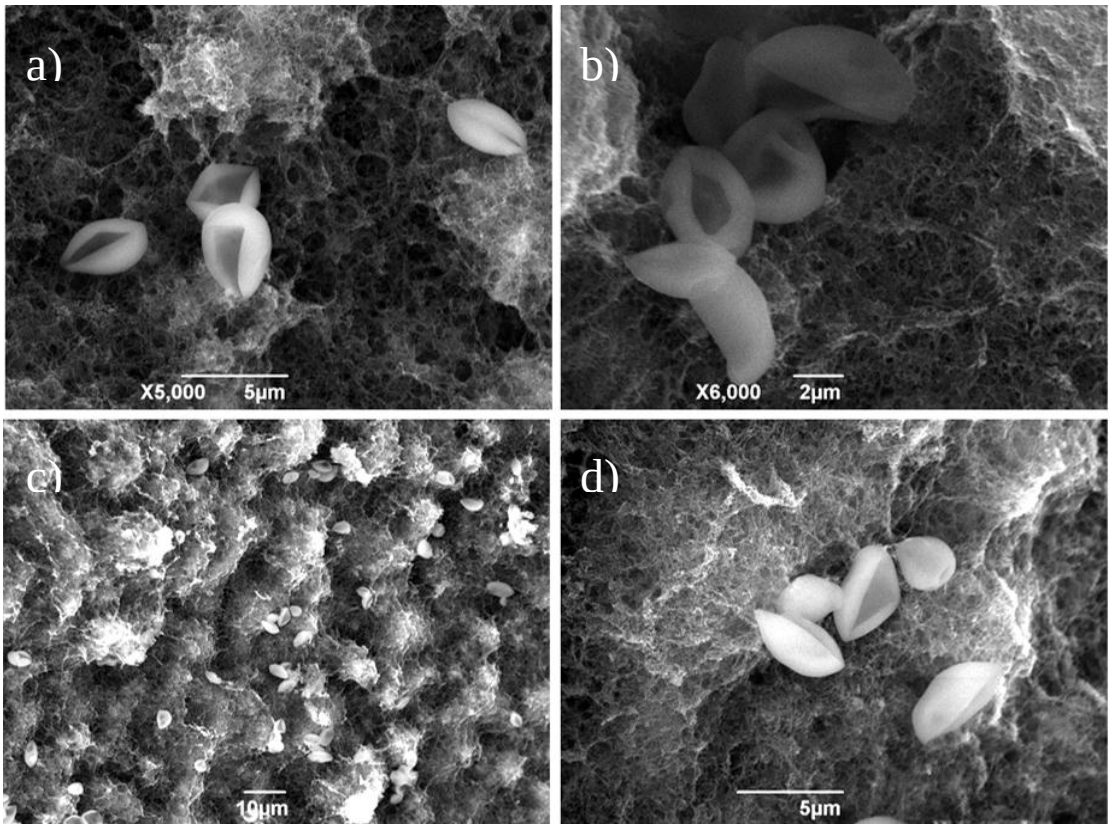

Fig. 6. 2. SEM images of fresh yeast cells placed on CNT nanofilter at different magnifications.

Fig. 6. 3 shows the filtered large yeast cells (large bright particles) attached to the CNT surfaces after the filter was dried in oven. At higher magnification, it is found that a yeast cell was wounded by the tangled CNTs. It is believed that the exposed long and tangled CNTs on the internal filter cavity surfaces would physically 'capture' and immobilize the yeast cells, whilst allow water passing through (Fig. 6. 3d). The pit arrowed in Fig. 6. 3a is believed to arise from a fallen off yeast cell after the filter was

cut open. The overall size of these pits must have been increased during the drying out process owing to shrinkage of both CNT networks and the cells.

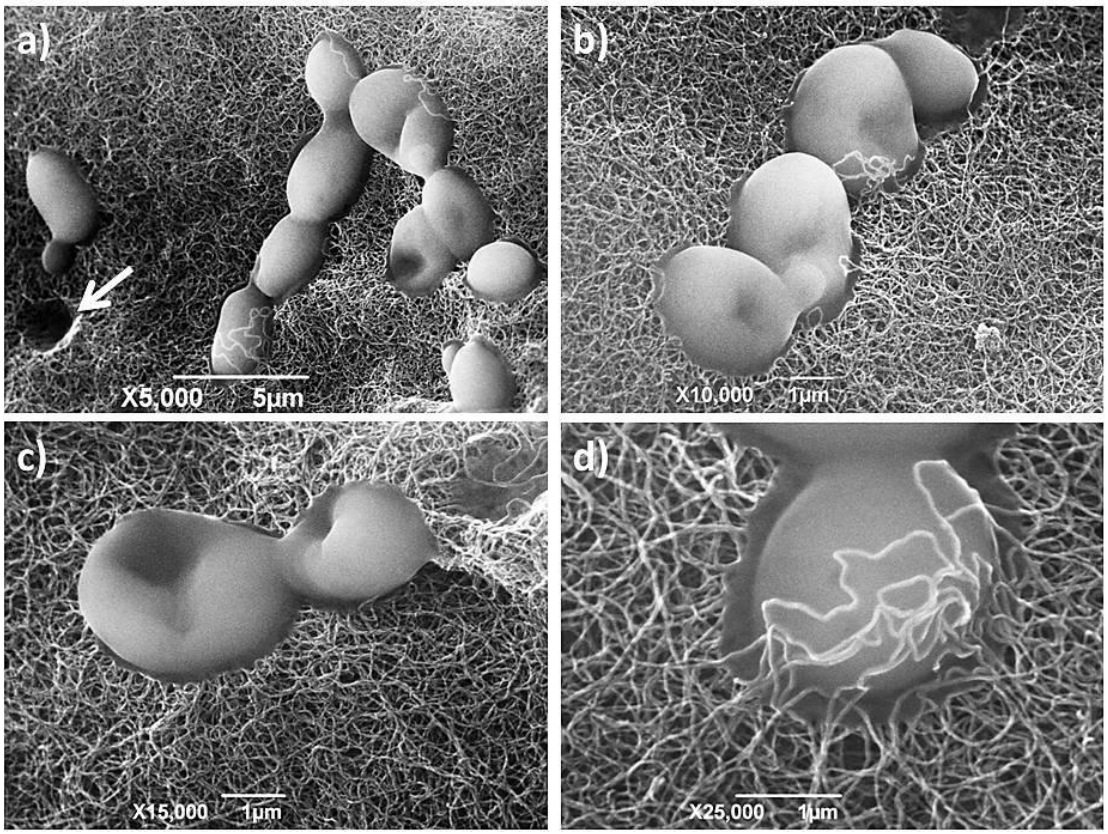

Fig. 6. 3. SEM images of the filtered yeast cells by CNTs at different magnifications. The tangled CNTs are closely connected with the yeast cells and have immobilised them.

Both the filter length and stock solution flow rates have showed strong influence on the overall filtration efficiency, and the results are summarised in Fig. 6. 4. 50 mm and 70 mm long filters both reached a maximum efficiency of 98% at a flow rate of 20 ml/h. A further reduced flow rate of 10 ml/h was also tested, and the results exhibited no further improvement, with the efficiency remaining at 98%. Parallel experiments using the plain porous Al_2O_3 discs without CNTs were also performed on a 20 mm long filter at a 20 ml/h flow rate, and merely achieved an efficiency of <5%, possibly due to physical blockage, against a 68% efficiency obtained using 20 mm long CNT filter at similar flow rate. These results have clearly proved that CNTs played the decisive role in the filter. At lower liquid flow rate, longer interaction time between CNTs and the yeast cells will become possible; and the longer filters offer more barriers on the cells'

pathway, resulting in improved efficiency. However, by further reducing of the flow rate, the maximum efficiency of 98% was achieved and we could not further improve the efficiency. For low injection rate (20 ml/h), the results were very consistence with less than 0.5% fluctuation however for higher speeds (40 and 80 ml/h), the experimental error increased to 1% and 2.3%, respectively. Fig. 6. 4 present the maximum efficiency obtained in the experiments. For each case, based on the consistency of the results, experiment was repeated 3 to 5 times.

a)

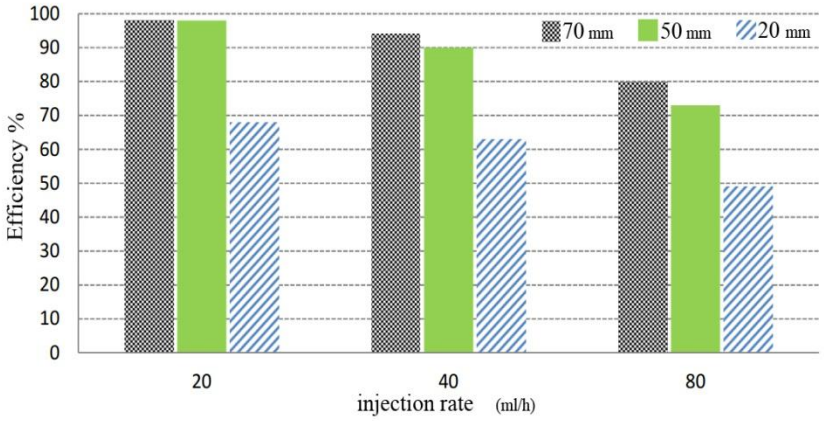

b)

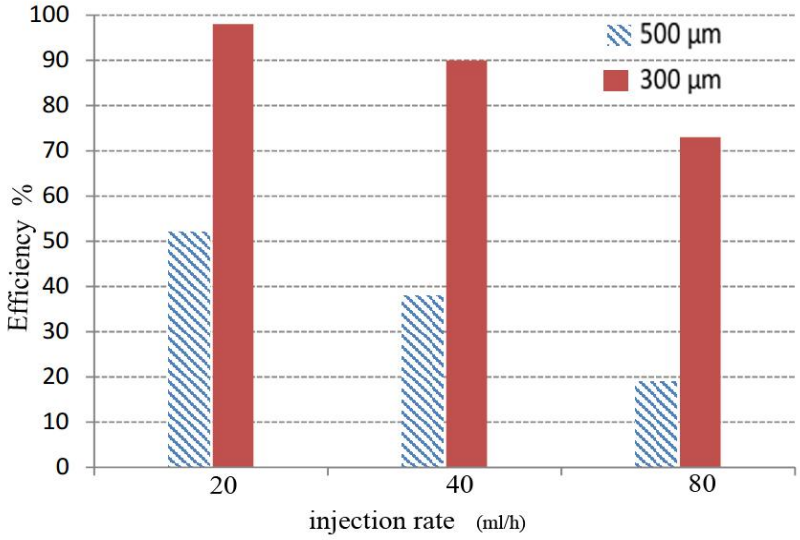

c)

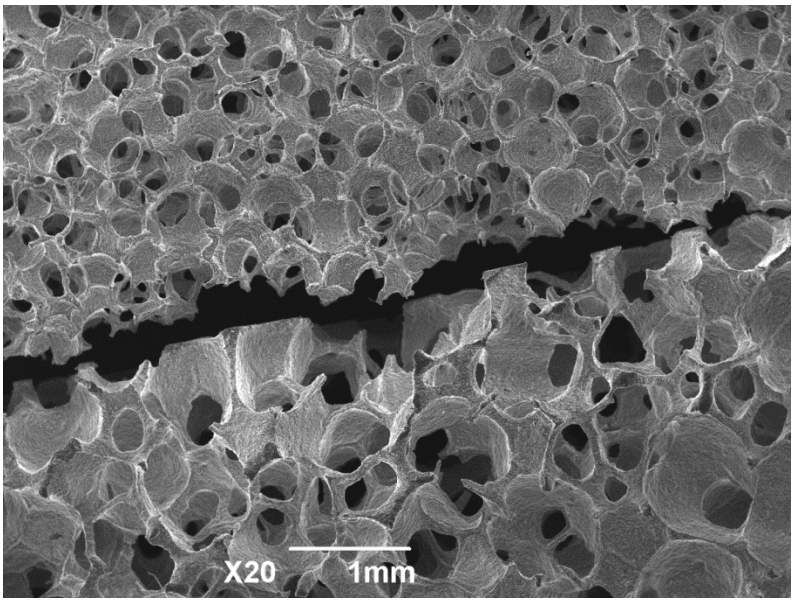

Fig. 6. 4. Composite filter efficiency for yeast cells and the role of CNTs in the filtration. a, Composite filter efficiency for yeast as a function of filter length and injection rate; b, Composite filter efficiency for yeast as a function of injection rate and filter pore sizes; and c, SEM image of two ceramic substrates with 300 µm (on top) and 500 µm (on bottom) pore sizes.

To verify the influence of initial pore sizes, we conducted experiments using filters of different pore sizes but with identical 50 mm filter length, and the result is shown in Fig. 6. 4b. Higher efficiencies for the 300 µm pore-sized CNT filters across varied flow rates are obvious, compared to that of the 500 µm pore-sized filters. The finer pore-sized matrix has indeed helped to achieve higher efficiency. However, this poses a challenge for uniform CNT growth inside the much finer pores as was discussed earlier in chapter 4. It is suggested that following that strategy, it is possible to fabricate filters with smaller pore sizes and further improve the efficiency of filtration. With the assistant of the substrate supplier (Dynamic-Ceramic Ltd), we have tried to further reduce the pore size of the ceramic foam. However, this was technically challenging and caused lots of defects in the ceramic substrate, such as different densities of the samples or hollow defective samples as shown in Fig. 6. 5.

Fig. 6. 5. Hollow ceramic foam produced by the supplier.

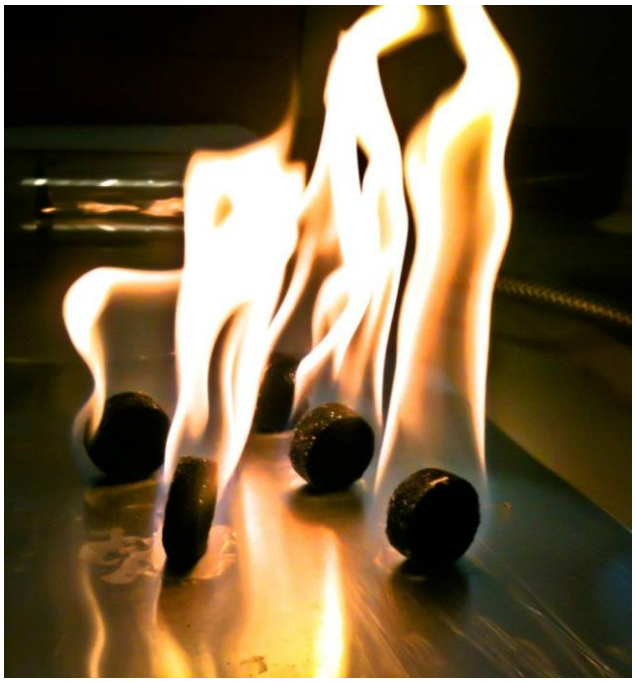

Fig. 6. 6. Several filters burning after filtration of yeasts by adding acetone, representing a method for the filter regeneration.

Compared with membranes that are used for micro and nanofiltration, the current composite filters have clear advantages, such as being robust and durable, and in particular reusable. The reusability feature of the current filters is demonstrated in Fig. 6. 6. Due to the high thermal stability and resistance of both the matrix and CNTs, the bio-contaminants inside the filter can simply be burnt off without damaging the CNTs, because of the lower burn off temperature for yeast, leaving the filter functionality almost intact.

CNTs are reported to have high thermal stability. However, this stability varies for different CNTs with different structures. Our TGA investigation of the pristine CNTs grown under identical experimental conditions used for filter production has showed that the onset weight loss occurred at temperature over 530˚C in air (a), which

proves the weight loss of the filter in Fig. 6. 7b is contributed totally to CNTs. Thus, it is believed that the bio-contamination removal process by burning the dirt out will not damage the CNTs. This is further confirmed by SEM and TEM studies, as shown in Fig. 6. 8.

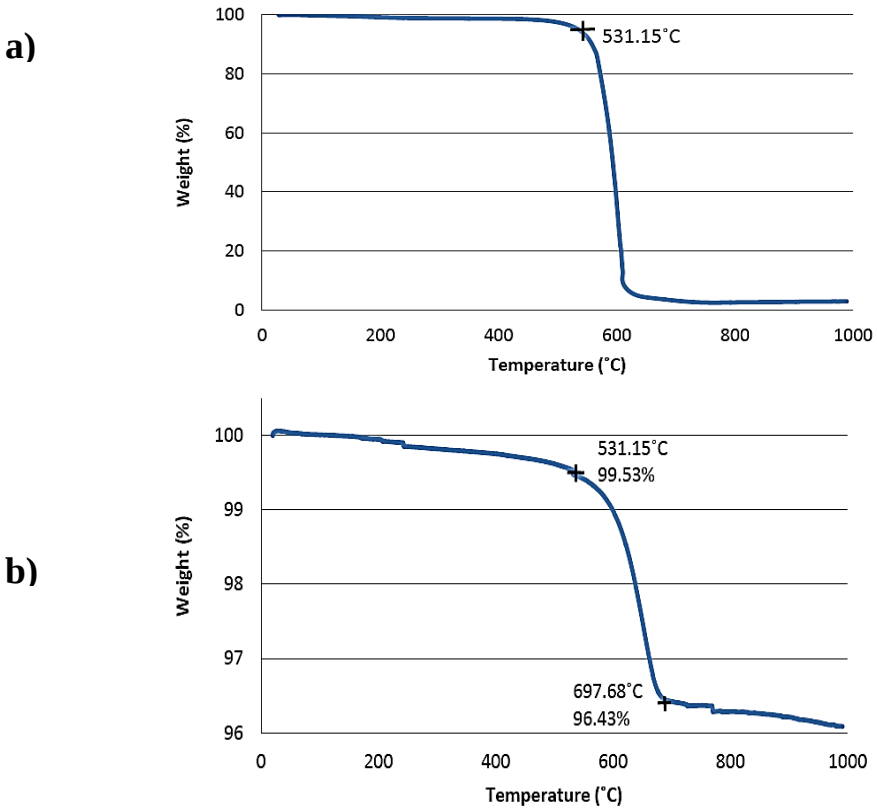

Fig. 6. 7. TGA results show the high thermal stability (up to 530˚C in air) of CNTs grown on ceramic matrix (a), showing an unchanged onset weigh loss temperature after burning, and the total weight loss owing to CNT content, (b).

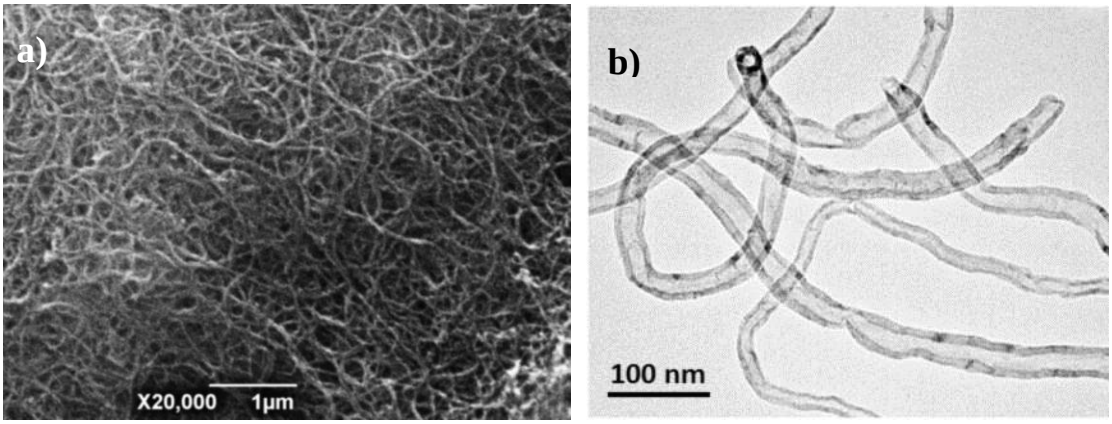

Fig. 6. 8. SEM (a) and TEM (b) images of CNTs after burning the filter, showing their morphologies identical to pristine CNTs.

Fig. 6. 9 compares the results obtained for a 50 mm long filter with 300 µm pore size with 20 ml/h injection rate after being reused for three times, suggesting the excellent reusability of filters. This result has verified that the burning recycled filters have showed negligible differences in filtration efficiency, suggesting a promising robust and reusable feature for the present CNTs/ceramics composite filters.

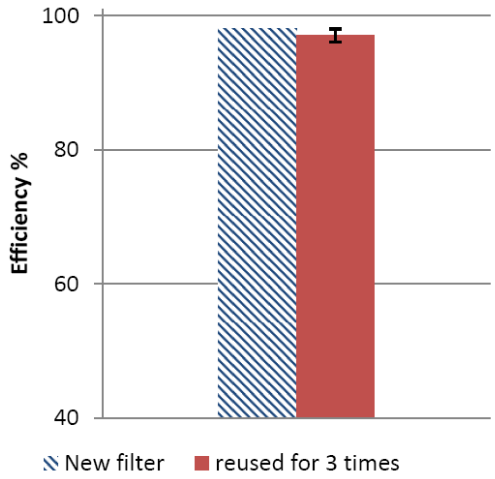

Fig. 6. 9. Filters maintained their high removal efficiency after three burning cycles.

6. 4. Air filtration

Heating, ventilating and air conditioning (HVAC) air filters are intended for air purification working in conditions of dark, damp and ambient temperature which provide ideal environment for bacterial, mould and fungal attacks. The situation becomes worse when these micro-organisms adhere to the accumulated dust on the filter and consume the accumulated dust as food and proliferate. As a result, there will be an unpredictable deterioration of the quality of air and production of bad odour [170]. By using CNTs with their antibacterial property [10], it is possible to address this issue with added features of improved mechanical properties and efficiency. A Lighthouse portable airborne laser particle counter (SOLAIR 3100) was used to record an ambient air passing through the filter, monitoring the concentration of particles ranging from 0.3-10 µm in outlet gas. Filter was placed on the inlet of particle counter (Fig. 6. 10) and carefully wrapped with thin plastic layer in order to make sure air sucked just from the top surface. This allows the whole length of filter be effective in filtration process.

Table. 6. 1 presents number of air particles before filtration. Composite filters of two different pore sizes, 300 µm and 500 µm, and various length combinations were tested in this study.

Table. 6. 1. Number of air particles before filtration

Particle size	0.3 µm	0.5 µm	1 µm	5 µm	10 µm
air	25,387,145	1,652,726	372,852.2	10,453.1	6,639.2

Fig. 6. 10. Lighthouse portable airborne laser particle counter (SOLAIR 3100) with filter placed on its inlet.

Fig. 6. 11 displays the resulting particulates filtration efficiencies in air for different pore sized samples (300 and 500 µm) with and without CNTs. Filter efficiency was calculated by counting the differences between the amount of contaminant concentrations in the media before and after the filtration. The results show that with the incorporation of CNTs, the filtration efficiencies have increased dramatically against the plain ceramics, particularly for particles with smaller sizes of 0.3 and 0.5 µm. The 100 mm long composite filters can stop nearly 90% and 95% of such particles, compared with 28% and 60% respectively, which are tripled and doubled.

This blockage influence can be explained by considering the Brownian diffusion mechanism. Longer filters result in decreased gas flow velocity, which allows particles

to have more time interacting with the exposed CNTs on the pore surface. A nose hair effect is believed to be the main mechanism for blocking these finer particulates. In this regard, in consistence with the results reported by Guan and Yao [252], the amount of CNTs will be the dominating factor on the efficiency, compared to ceramic pore size, as demonstrated in Fig. 6. 11b. In Fig. 6. 11b, the initial efficiency of 300 µm pore sized plain ceramic is higher than that of CNT-500 µm pore sized filter for a short 10 mm filter, for 0.5 µm particles, but increasing the filter length which allows more nanotubes to be involved, gradually raised the composite efficiencies. For 100 mm long filters, the CNT-500 µm filter has reached 85% compared with 60% for the 300 µm pore sized plain ceramic filter. Interestingly, a 10 mm long CNT-300 µm or a 20 mm long CNT-500 µm is enough to capture all the particles ≥5 µm, which is equivalent to a 80 mm long 300 µm pore sized or a 100 mm long 500 µm pore sized plain ceramic, i.e. 8 and 5 times more efficient separately. For such big particles, inertia impaction and interception counts as the filtration mechanism [253].

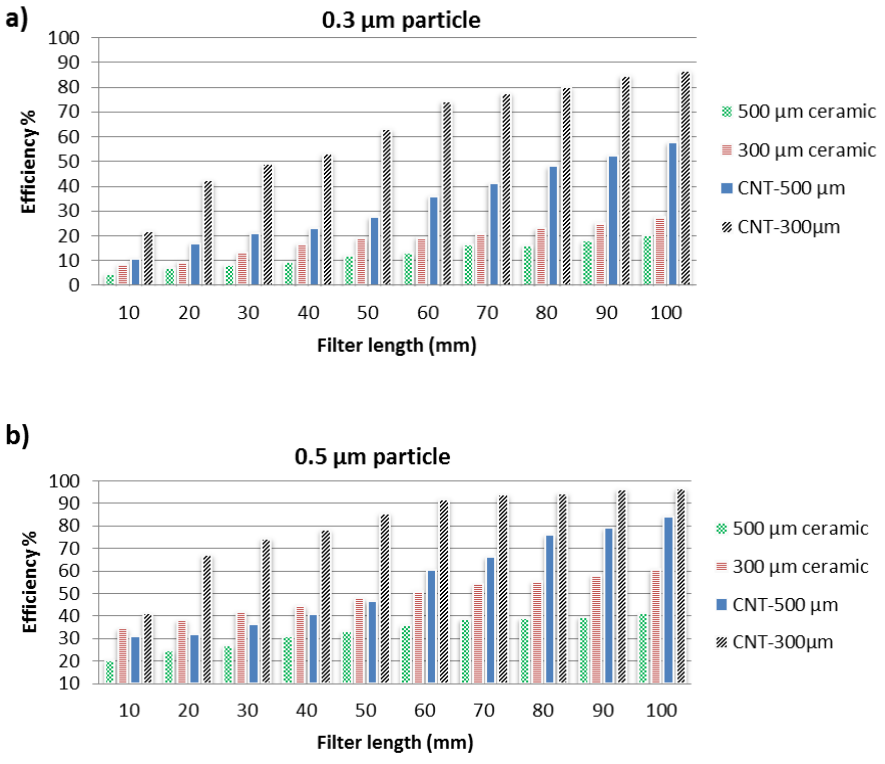

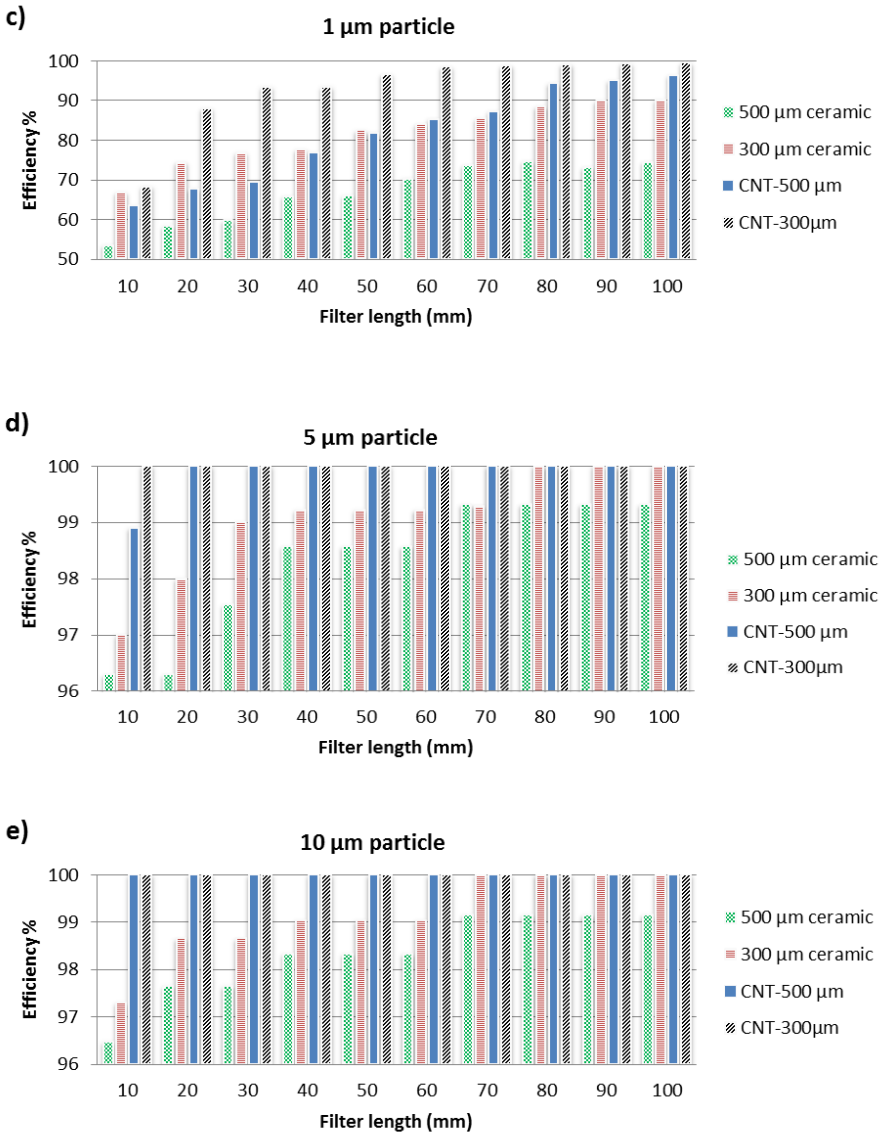

Fig. 6. 11. Air particulate filter efficiency as a function of filter length for 0.3 µm (a), 0.5 µm (b), 1 µm (c), 5 µm (d), and 10 µm particles.

Fig. 6. 12 summarises the filter efficiencies for particles < 5 µm. It can be seen that for a 300 mm long composite filter it is possible to capture more than 99.6% of particles (> 0.3 µm) in air. It is noted that after reaching 90% efficiency, further improving of the efficiency to almost 100% requires much more effort. This is explained by comparing Fig. 6. 11a and Fig. 6. 12 for 0.3 µm particles, in which a change of filter length from merely 10 to 20 mm for the CNT-300 µm filter results in a huge efficiency jump, nearly doubled; but from 200 to 300 mm leads only to a 1.2% increase in efficiency.

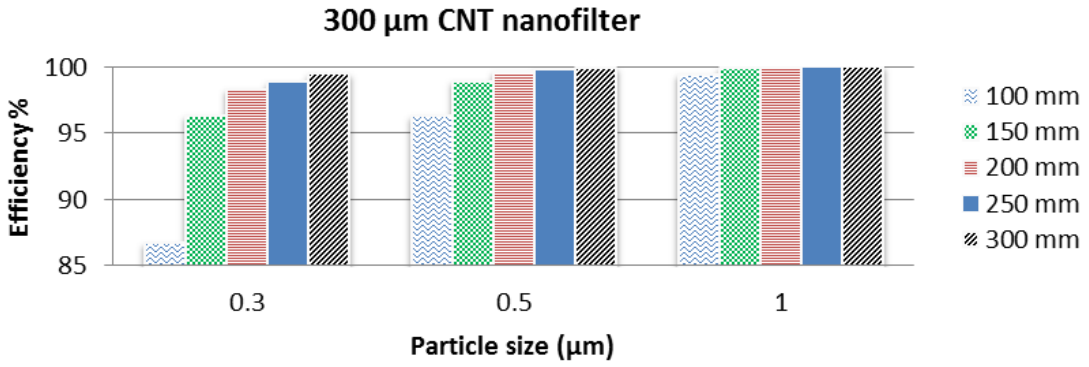

Fig. 6. 12. Filtration efficiency as a function of particle size for CNT-300 filter.

It is also noteworthy that the pristine CNT filters and air-oxidized CNT filters exhibited very similar efficiencies for particular filtration in air, which has indirectly confirmed the filtration mechanism dominantly being a physical interception (Fig. 6. 13).

High efficiency particulate air (HEPA) filters have minimum removal efficiency of 99.97% of particles greater than or equal to 0.3 µm in diameter[170]. This challenging particle size at which the filter has its lowest efficiency is defined as the most penetrating particle size (MPPS), and for smaller particles, efficiency starts to increase again. For this reason, HEPA filters are often tested using this challenge particle of 0.3 µm diameter. This analysis suggests that we could expect higher filtration efficiency for particles < 0.3 µm, which we could not perform at this stage.

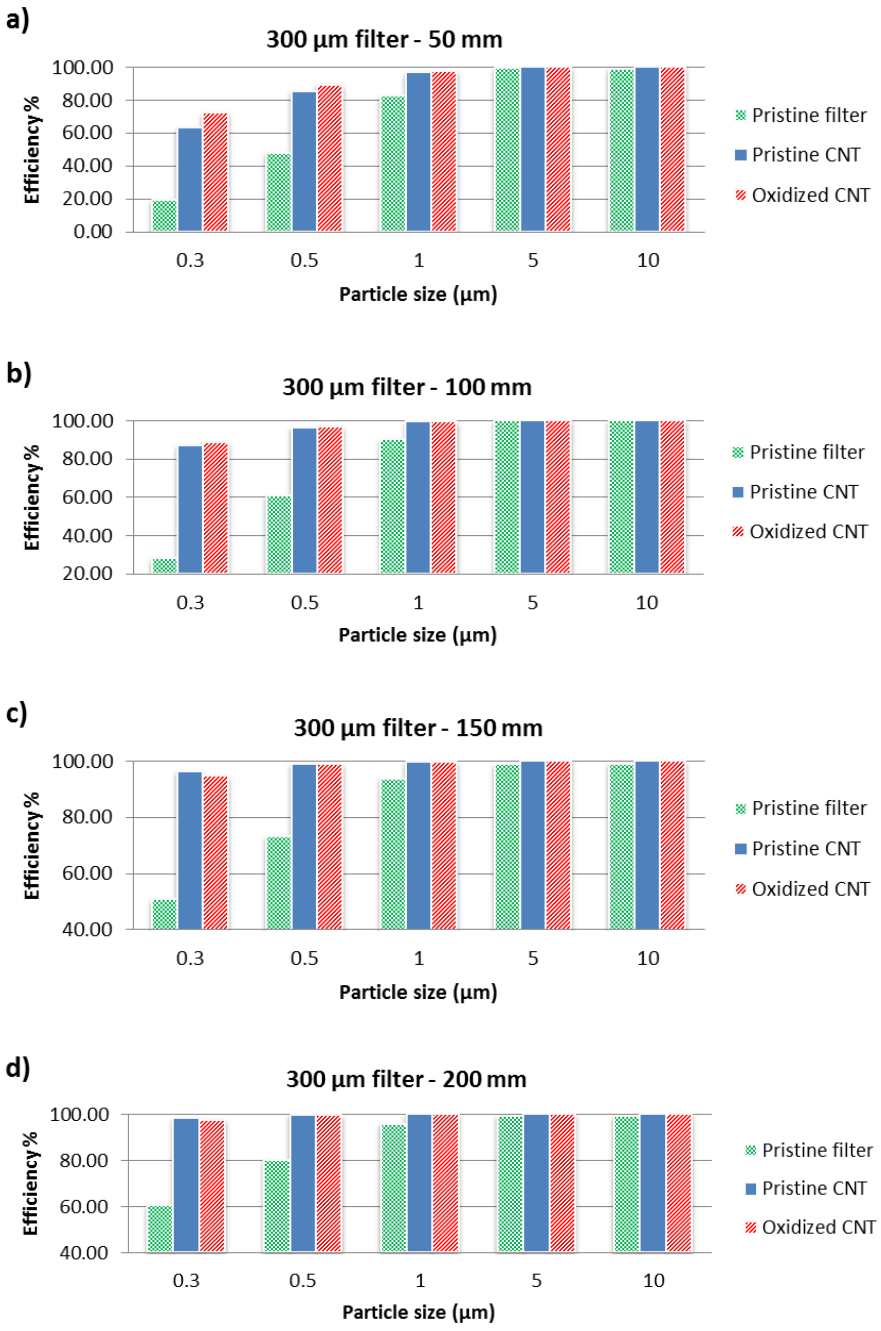

Fig. 6. 13. Pristine CNT and air oxidized CNT filters show similar efficiencies for particulate filtration in air. Figures represent filter efficiency of a pristine filter, pristine CNT-300, and air oxidize CNT-300 for different filter lengths of 50 mm (a), 100 mm (b), 150 mm (c), and 200 mm (d) as a function of particle sizes.

It is important to mention that the number of particles in air varies quickly as the result of any small movement in the workplace which cause turbulences and change the number of particles. Consequently, numbers of particles in work area were evaluated without filters before each test for more reliable comparison. However, the results were

in good consistency particularly for big particles (5 and 10 µm) where efficiency reaches 100% very quickly and the error was found to be negligible.

Pressure drop is an important factor in gas filtration. As shown by the µ-CT scan image in Fig. 6. 14a, the ceramic substrate consists of randomly interconnected channels lay in different directions. This shape of cellular ceramic causes considerable turbulences generated by the tortuous flow paths, resulting in raise in the pressure drop. The pressure drops for a 10 mm thick filter for both ceramic-300 and ceramic-500 are presented in Fig. 6. 14c. This was obtained by measuring the difference of air pressure between the inlet and out let ($\Delta P=P_1-P_2$) of a 25 cm long quartz tube with a filter sealed and placed in its middle as schematically shown in Fig. 6. 14b.

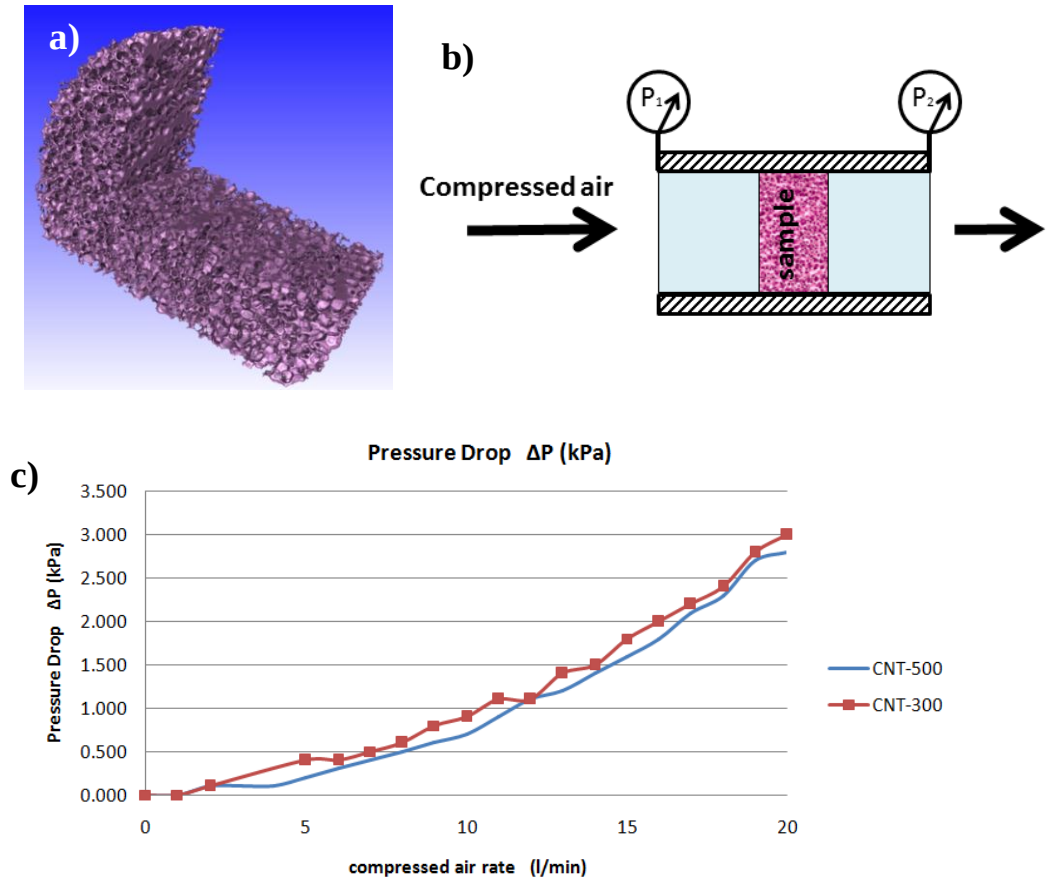

Fig. 6. 14. a, µ-CT scan 3D image of a ceramic substrate showing the interconectivity; b, a schematic illustration of set-up for measuring the pressure drop; and c, the pressure drop of a 10 mm disc as a function of air flow rates.

As could be predicted, the thin coating of CNT on ceramic matrix compared to the big pore sizes (300 to 500 µm) would have negligible effect on the pressure drop for current filters. Therefore, these filters may suit for air filtration applications where air flow rate is low or pressure drop is uncritical. Fig. 6. 15 shows the difference between pressure drop of 500 µm pore sized filter with and without CNT fabrication. This indicates that considering the experimental error, fabrication of CNTs on ceramic foam has negligible effect on these filters pressure drop.

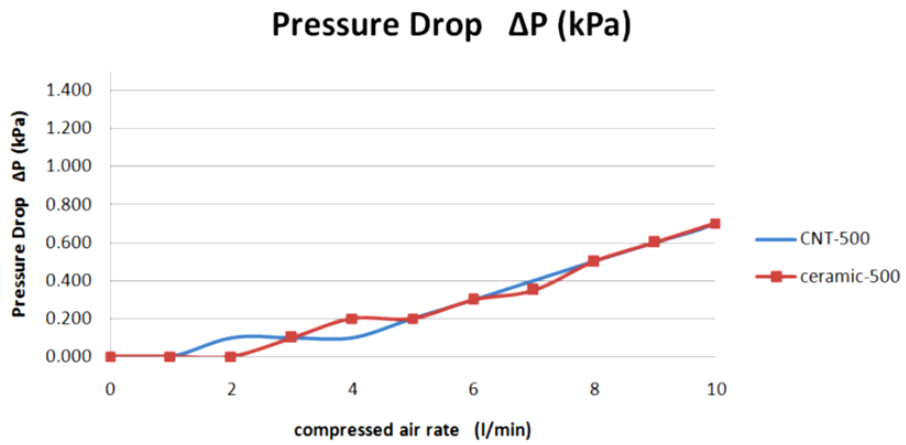

Fig. 6. 15. Comparison between pressure drop of 500 µm pore sized filter with and without CNTs.

However, it is still possible to modify the substrate pore or channel configuration using specifically designed unidirectional ceramic template (Fig. 6. 16). By applying the same CNT composite filter fabrication method one can make highly stable, efficient air particulate filters with lower pressure drop suitable for applications such as diesel particulate filters for engines.

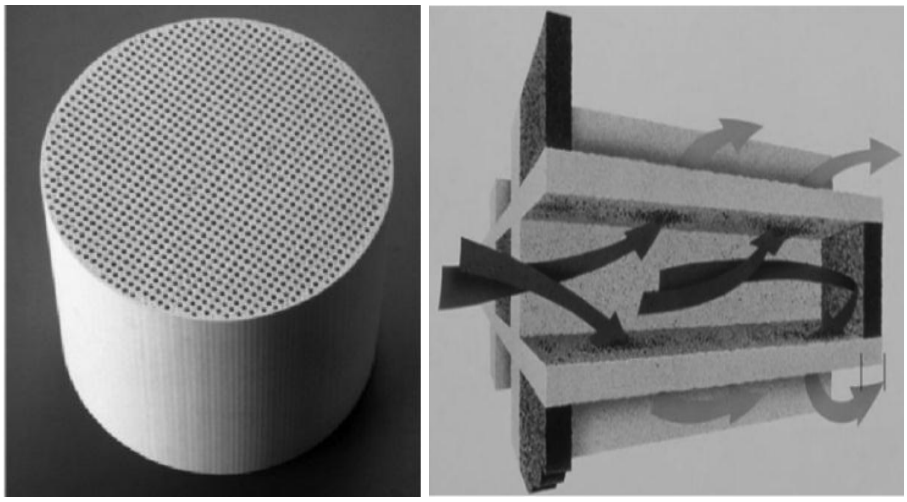

Fig. 6. 16. Diesel particulate filter with parallel channels which reduce the pressure drop in diesel engines [254].

6. 5. Heavy metal ions filtration

Prior to investigating the CNT composite filter in the removal of heavy metal ions from water, the corresponding plain porous ceramics were tested at room temperature in order to rule out their effect, and a negligible adsorption capacity of less than 4% efficiency was recorded for 300 µm pore sized specimen. Therefore, any higher efficiency would be contributed to the presence of CNTs.

As presented in Fig. 6. 17, for a single Cu ion sample (12 mg/l of $CuCl_2$), the initial adsorption efficiency of an air oxidized 20 mm long CNT-300 filter reached 99.99% ± 0.01 in a wide range of solution flow rates from 2 to 30 ml/h, suggesting that almost all the Cu ions were completely removed regardless of flow rates of the adsorption solution, which is extremely promising.

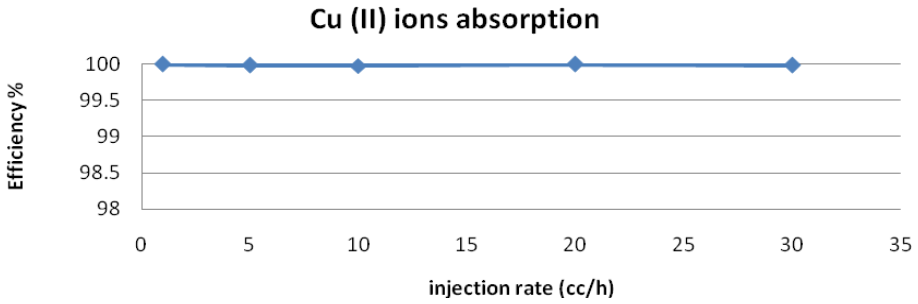

Fig. 6. 17.Single metal (Cu^{2+}) adsorption as a function of injection rates using 20 mm long, 300 µm pore-sized filter.

However in reality, most of the contaminations from water contain mixed heavy metal ions, sometime unknown. Therefore a systematic investigation was carried out to explore their full filtration potentials for mixed metal ions. It is expected that different surface functional groups, which were introduced during the functionalization of ceramic-CNT composite via either acid treatment or air oxidation at 400 °C, will have strong influence on metal ions adsorption. Two differently functionalized CNT filters of 10 mm long were immersed in a beaker containing 30 ml solution of Fe, Cu, Zn and Mn ions (each with a concentration of 5 mg/l) for 10h, expecting them to reach equilibrium. As shown in Fig. 6. 18a, the air oxidized sample adsorbed most of the Fe^{2+} and Cu^{2+}, with only a negligible amount of adsorption for Zn^{2+} and Mn^{2+}, in contrast to the acid functionalized sample which adsorbed ~20% Zn and Mn ions under the same conditions. Interestingly, the total amounts of absorbed ions are almost identical, 40%, just at different portions. In Fig. 6. 18b, the detailed adsorption amounts of individual metals have been shown in mg. It can be seen that each of the filters has adsorbed almost 0.27 mg of heavy metals in total but different functional groups have led to different adsorption portions under this competitive condition.

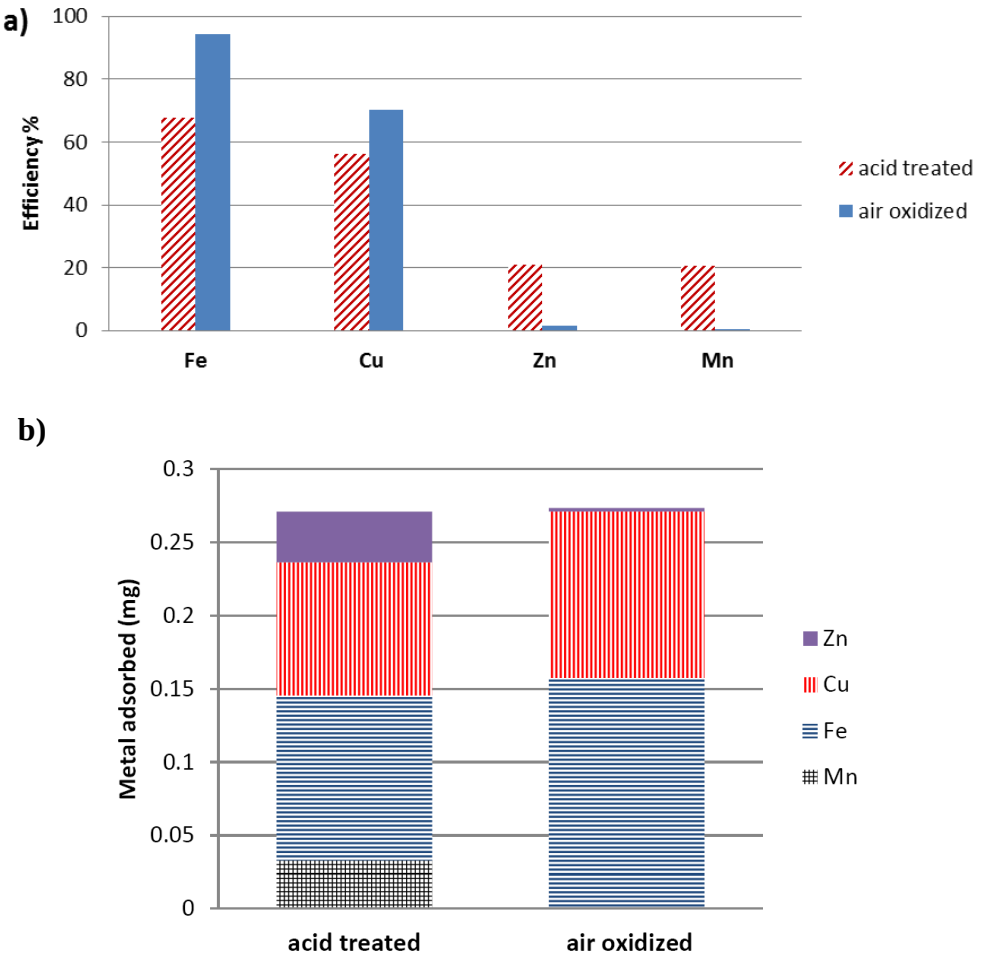

Fig. 6. 18. (a) Adsorption efficiency of 10 mm long functionalized filters for 30 ml of heavy metal solution containing 5 mg/l of each of Fe^{2+}, Cu^{2+}, Mn^{2+}& Zn^{2+}. One filter was oxidized in air and the other was treated in acid. (b) The adsorbed amount of metal ions in mg shows different tendencies for various ions when the total adsorbed amount is almost similar.

This result has confirmed that in mixed ion situation, competitive adsorption mechanism dominates the adsorption process. Fe^{2+} and $Cu^{2+}$with higher electronegativity tend to adsorb and occupy almost all possible adsorption sites on CNT surfaces, therefore exhibited higher adsorption tendency, leaving Zn^{2+} and Mn^{2+} with low or almost no adsorption. This experiment also shows that the acid functionalized CNTs could have provided more active groups than that of the air oxidised sample, and the adsorption tendency must have been varied for different ions. Adsorption capacity of CNTs strongly depends upon their surface total acidity and increases by a rise in the amount of surface total acidity groups (including carboxyl, lactones and phenols) [185].

The chemical and thermal treatments during the functionalization procedure can affect the nature and concentration of the surface functional groups. The surface of untreated CNTs contains a small amount of basic functional groups, in addition to amorphous carbon, carbon black and carbon particles. Gas phase oxidation at 400˚C can introduce functional groups such as hydroxyl and carbonyl surface groups to the surface, whilst liquid acid oxidation can generate carboxylic acid functional groups on the surface of CNTs, as well as cleaning the amorphous carbon from the CNT surfaces. This will facilitate the ion-exchange capability of CNTs, as the introduced functional groups cause a rise in negative charge on CNT surfaces and the oxygen atoms in functional groups donate a single pair of electrons to metal ions, resulting in higher cation exchange capacity [33, 34].

Fig. 6. 19 shows the filter efficiencies versus filter length for Fe^{2+}, Mn^{2+}, Zn^{2+} and Cu^{2+}. All the results presented here are contributed to the acid treated filters at an injection rate of 120 ml/h. As expected, longer filters containing more CNTs resulted in a higher adsorption efficiency, and all reached about 100% for the 50 mm long filters at different injection rates. Fe^{2+} showed a lower adsorption tendency at first, however when more solution passed through the filters, Fe^{2+} adsorption efficiency remained high compared with other ions (Fig. 6. 19b). Fig. 6. 19b also exhibits the saturation point for Mn^{2+} and Zn^{2+}. After passing through over 60 ml solution, the Mn^{2+} and Zn^{2+} adsorption efficiencies quickly dropped to 0%, whilst Fe^{2+} and Cu^{2+} remained relatively high. When more solution was passed through, a very strange negative efficiency was observed for Mn^{2+} and Zn^{2+}, as shown in Fig. 6. 19b. We believe that the filter starts to release the initially adsorbed Mn^{2+} and Zn^{2+}that are replaced by the newly absorbed Cu^{2+} and Fe^{2+} back into the solution, causing such an abnormal concentration which was even higher than the stock solution. This indicates that they are completely lost in the competition with Cu^{2+} and Fe^{2+}. The result also revealed that that in the competition between Fe^{2+} and Cu^{2+}, Fe^{2+}were the winner. By maintaining its high adsorption efficiency, Fe^{2+} forced the Cu^{2+} out.

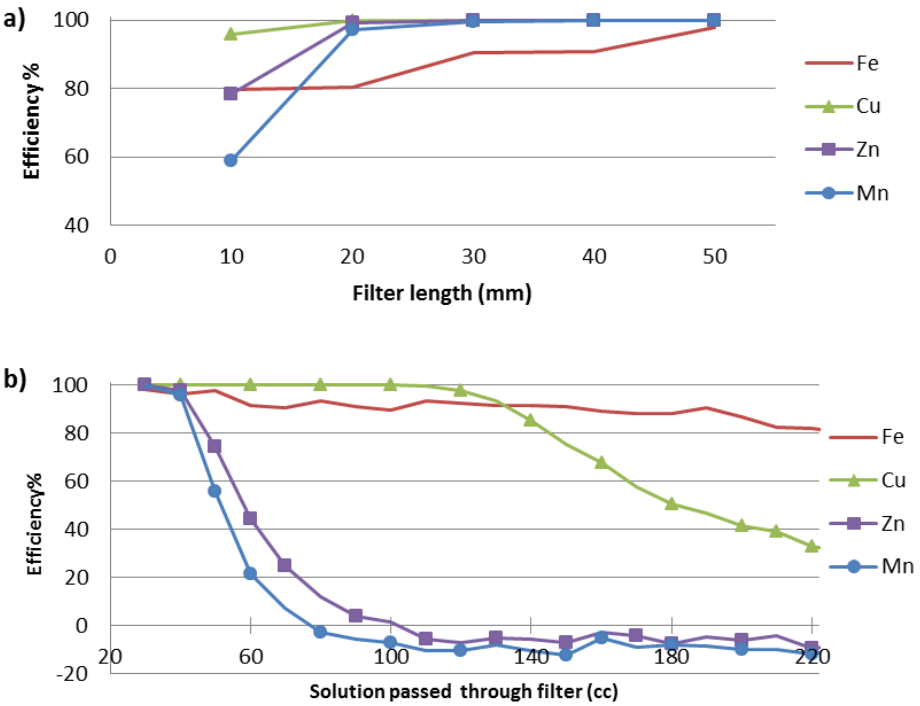

Fig. 6. 19. (a) Adsorption efficiency of filters as a function of their lengths, tested using heavy metal solution containing 5 mg/l of each of Fe^{2+}, Cu^{2+}, Mn^{2+}& Zn^{2+}; and (b) The saturation point of a 50 mm long filter tested using the same solution.

As Fe^{2+} and Cu^{2+} ions have much higher adsorption tendencies compared to Mn^{2+} and Zn^{2+}, they were replaced with Co^{2+} in order to investigate the adsorption efficiency of these heavy metals ions in a less competitive environment, and the result is displayed in Fig. 6. 20. In this case, the filter exhibited similar efficiencies for all three ions, over 95% when passed up to 80 ml of solution, indicating a much higher saturation point in a less competitive environment.

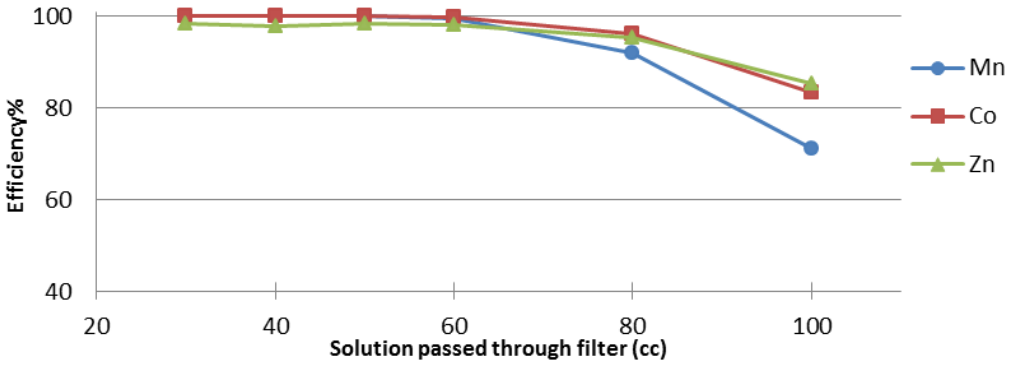

Fig. 6. 20. The saturation point of 50 mm long filters tested using heavy metal ion solution containing 5 mg/l of each of Co^{2+2}, Mn^{2+} and Zn^{2+}.

Furthermore, injection rates from 1 - 500 ml/h were tested, and only a 15% drop in adsorption efficiencies was observed for changing solution flow rate from 120 ml/h to 500 ml/h for the 20 mm long filter tested using heavy metal ion solutions containing 5 mg/l of each of Co^{2+}, Mn^{2+} and Zn^{2+} (Fig. 6. 21), which suggests that the current filters could be used in a faster stream and they can maintain a high efficiency. It is also possible to have the same complete ion removal at higher injection rates by increasing the length of filter. Increasing temperature, further improvement in adsorption efficiency is also possible as was previously shown by Lu et al. for Zn^{2+} [189].

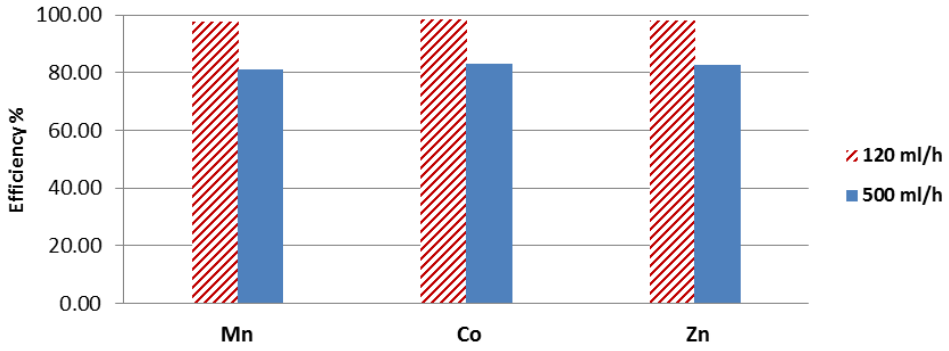

Fig. 6. 21. Filter efficiency for individual metal ions under a competitive condition at different injection rates.

In order to justify the high initial cost of current filters and introduce them as a practical solution for challenges in wastewater treatment, it is important to know their reusability. It has been well-discussed in the literature that it is possible to desorb metal ions from CNTs in acidic solutions (pH<2) without a noticeable drop in their filtration efficiency [185]. Based on these report, we have reused our samples for several times by desorbing the metal ions in an acidic solution (HNO_3), and obtained similar results.

However, it has also been evidenced that during the acidic desorption process small amounts of CNTs were released to the solution. As the toxicity of CNTs by their own is a concern [198], it is important to take this fact into account and a possible secondary protective process (such as placing a membrane in the outlet of filters) to capture the potentially released CNTs should be useful. Comparing with most recent reports that loose CNTs were soaked into solutions for several hours before they were collected using a filter paper, which is slow, time consuming and less controllable [34, 189, 194], we believe that the current composite filters are robust, cheap, highly efficient, versatile and reusable. We hope that these results will be an important step for CNT filters toward applications in industrial scale.

6. 6. Conclusion

After successful synthesising of ceramic-CNT composites, they were used in filtration application for the removal of biological yeast cells and heavy metal ions from water, and for the removal of airborne particulates from air, under diverse experimental parameters. Filters were functionalized in two different methods (acid treatment and air oxidation) and the effects of these various functional groups on filtration properties were studied. Detailed experimental set ups and results were presented in this chapter and most important ones are listed here:

Yeast cells filtration:

- Maximum efficiency of 98% was achieved for yeast cell removal using 70 mm long CNT-300 filter at 20 ml/h injection rate when plain ceramic has negligible filtration efficiency.
- SEM images of yeast cells inside filter revealed that they were captured by the tangled CNT networks. These tangled CNT networks on the surface of the internal filter cavity can physically 'capture' and immobilize the yeast cells whilst allowing water to pass through.
- Yeast cells filtration was shown to be function of filter pore size, injection rate and filter length. Smaller pore, slower injection rate and longer filters increased the filtration efficiency significantly.
- Finally, it was confirmed by TGA, SEM and TEM investigations that it is possible to reuse the filters by burning the contaminants which justify use of CNTs in filtration application.

Air particulates filtration:

- Air particulate filtration is function of filter length (CNT loading) and pore size. CNT loading was shown to be the dominating factor in filtration efficiency.
- Incorporation of CNTs into the porous ceramics dramatically increases their filtration efficiencies and for a 300 mm long CNT-300 efficiency of more than 99.6% was achieved.

- The pristine CNT filters and air-oxidized CNT filters exhibited very similar efficiencies for particular filtration in air, which suggests that the mechanism of filtration is mainly through physical interception.
- Effect of CNTs in air particulate filtration with Brownian diffusion mechanism is more dominating for smaller particles (0.3 μm). And for big particles (5 and 10 μm), inertia impaction and interception counts for the filtration mechanism.

Heavy metal ions filtration:

- A negligible adsorption capacity of less than 4% was recorded with the ceramic filters
- A complete removal (99.99% ± 0.01) of single heavy metal ion (Cu) from water was achieved.
- 10 mm long CNT-300 filters functionalized by acid treatment and air oxidation presented different adsorption tendency for metal ions when the sum total of heavy metal ions absorbed was almost identical between filters at 40%. This result demonstrated that in the presence of mixed ions, their competitive binding to CNTs dominates the adsorption process.
- Finding the saturation point of 50 mm long CNT-300 filter for removal of Fe^{2+}, Mn^{2+}, Zn^{2+} and Cu^{2+} ions, it was revealed that Fe^{2+} and Cu^{2+} have higher adsorption tendencies and when the situation become more competitive, they replace their ions with Mn^{2+}, Zn^{2+} and release them to the solution again. However, in a less competitive environment (Co^{2+}, Mn^{2+} and Zn^{2+} solution), much higher saturation point (with almost similar metal ions adsorption amount) was achieved.
- Filters maintained their high efficiency at higher injection rates. This is a promising result for industrial use of these CNT filters.
- Finally, it was shown that it is possible to desorb the adsorbed heavy metals from CNT filters while maintaining their high efficiency. This justifies the high initial cost of fabricating CNT filters at industrial scale.

Chapter 7: Compression and impact behaviour of polymer-ceramic-CNT composites

7. 1. Introduction

After the successful preparation of composite materials, I will continue to evaluate their mechanical properties. As discussed in the literature review (chapter 2), CNTs alone hold exceptional mechanical properties such as high elastic modulus [81], large elastic strain and fracture strain that are expected to provide extra absorption of energy and increased toughness in composites[53]. Similar conclusions have also been drawn by theoretical studies [11]. However, their composite material properties need to be verified experimentally, as the fabrication processes and application conditions have strong influences on these performances. In this chapter, the mechanical properties of our CNT composites including compression strength, hardness and impact resistance will be studied.

7. 2. Compression strength

7. 2. 1. Epoxy resin-ceramic-CNT composite

Fig. 7.1 presents the results of the compression test for plain ceramic, pure epoxy resin, epoxy resin-ceramic and epoxy resin-ceramic-CNT composites. While the plain ceramic strength is only 5.2 MPa, the epoxy resin-ceramic composite showed a significant increase in its compressive strength with a value of 114.7 MPa. This behaviour has been dominated by the epoxy resin which has a yield point of 115.3 MPa. Epoxy resin-ceramic-CNT composite also showed almost a similar strength of 111.8 MPa. In Fig. 7.1, the compression graph of the plain ceramic has been shifted to the right for better observation. The tress-strain profile shows that the composite deformed in a constant way, even the compression load was over 100 times of that of the plain ceramics, the structure did not collapse.

It is expected that epoxy resin-ceramic-CNT composite should have an equal or higher compressive strength compared to the epoxy resin-ceramic composite. But it

shows a lower level of ultimate stress. This small difference of 2.6% in the strength of the two composites can be explained by considering the experimental errors and also looking at different densities of the ceramic substrates used in these composites as mentioned in chapter 4, Table 4. 5. Up to the yield point, both composites showed a very similar behaviour following the characteristic behaviour of pure epoxy resin. Similar to our results, it has been previously reported that in polymer-CNT composites, at a fundamental level, the carbon nanofillers are not providing the strengthening effect that was hoped for [245].It is considered that the poor intrinsic quality of MWCNTs, and the difficulties of stress transfer, either from matrix to filler, or internally within the nanotube structure, are all contributed to this phenomenon. However, after the yield point, the compression graphs of the two composites start to separate and show different characteristics. At this point, the role of CNTs becomes dominating and they start to be involved in the compression stress more efficiently by transferring stress and sustaining more energy. In the sample reinforced with CNTs, the collapse of ceramic occurred at a very early stage, and then the sample passed its yield point. After further compression, the strong interface between the nanotubes and the polymer matrix could result in further increase in the resistance of sample as a whole. The difference in the appearance of both samples after compression test can be seen in Fig. 7.2, in which the epoxy resin-ceramic composite has totally broken into pieces but the epoxy resin-ceramic-CNT composite has just been pressed. In this regard, that the inter-connected ceramic foam has just played the role of a truss for uniform deposition of CNTs. But when it collapsed, it caused the formation of continuous cracks inside the composite which eventually led to the failure of the sample. The addition of a continuous CNT coating on internal surfaces inside the ceramic foam would have acted as a preserver and kept these broken ceramic pieces together, thus preventing the sample from sudden failure. Therefore, the sample can stand much higher compressive stresses due to the effect of CNTs. This value is even much higher compared with the pure epoxy resin.

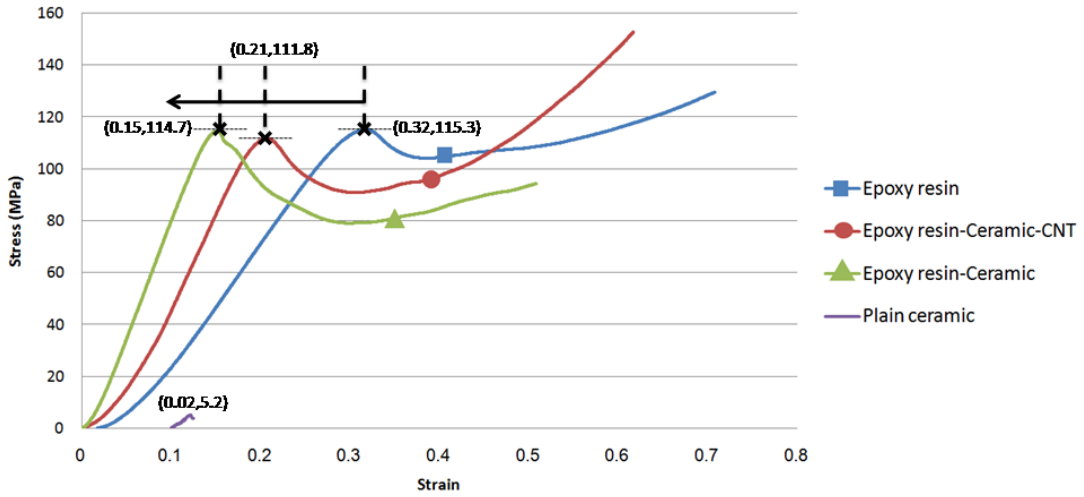

Fig. 7.1. Compression test results of the plain ceramic, pure epoxy resin, epoxy resin-ceramic composite and epoxy resin-ceramic-CNT composite samples. The plain ceramic graph has been slightly shifted to the right for better observation.

Another important factor which should be considered in the compression test of these samples is the strain at the ultimate stress point as it is shown in Fig. 7.1. Although all the three samples (pure epoxy resin, epoxy resin-ceramic, epoxy resin-ceramic-CNT) have almost similar ultimate stress values (115.3, 114.7 and 111.8, respectively), the pure epoxy resin exhibits more elastic deformation (0.32) compared to the other two samples. The addition of ceramic to the epoxy resin causes its earlier failure and the sample passes its elastic region 113.3% sooner compared to the pure epoxy resin (0.15) due to the formation of continuous cracks inside the composite which acted as concentrated stress points and eventually led to the sample failure. The addition of CNTs into the epoxy resin-ceramic composite increases the maximum strain of this composite (0.21) in elastic deformation region. It means that the epoxy resin-ceramic-CNT composite can resist plastic deformation 40% more than the epoxy resin-ceramic composite.

Fig. 7.2. Optical image of the compressed samples where the left one is the epoxy resin-ceramic-CNT composite and the right one is the epoxy resin-ceramic one.

To conclude, despite from high expectations that CNTs should increase the yield point of composites, both composites had similar yield points following the characteristics of pure epoxy resin. However, the effect of CNTs became dominant beyond the yield point. The composites were capable of sustaining compression stresses even higher than that of the pure epoxy resin.

7. 2. 2. Polyamide-ceramic-CNT composite

Fig. 7.3 shows the compression test results of PA12 infiltrated ceramic foam composites, with and without CNTs. A significant improvement in the compression strength of 96.6 MPa for the PA12-ceramic composite containing 0.5 wt. % CNTs has been achieved, compared with 37.3 MPa for the non-CNT-containing sample.

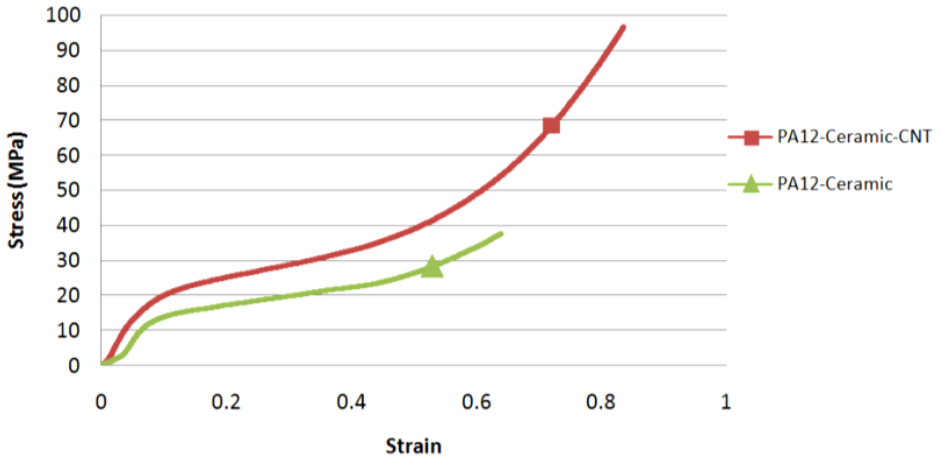

Fig. 7.3. The compression test profiles of PA12-ceramic and PA12-ceramic-CNT composites.

In order to understand the exact behaviour of our composites, it is important to compare the compression behaviour with the plain ceramic and pure PA12 counterparts, and the results are presented in Fig. 7.4. Similar to previous epoxy resin samples, the infiltration of plain ceramic foam with PA12 has improved its strength by 261% (from 5.2 to 18.8 MPa). In order to determine the behaviour of composite, as claimed by Gomez et al. [42], it is required to consider two dominating factors:

1. Ceramic–polymer interface
2. Wettability of polymer.

If the polymer does not fill the pores completely, they will act as a concentrated stress point, decreasing the compression strength. Equally, if the adherence between the ceramic and polymer was not suitable, it would exist as a material tearing, and the strength would also decrease [42]. As a result, the collapse of ceramic foam under compressive stresses will cause an early failure of the sample compared to the pure PA12. But this negative effect will be reduced by the addition of CNTs which can hold the broken ceramic trust parts together, if a strong bonding between the CNTs, PA12 and ceramic is presented. This strong bonding will also result in a higher degree of filling with less stress points, as confirmed in previous chapter by our µ-CT scan investigations. As a result, the composite reinforced with CNTs shows a significant improvement under compressive stress compared to those without CNTs. However, again, this behaviour is affected and governed by the PA12 characterization. Similar to the epoxy resin test results, the CNT-reinforced composite can withstand much higher stresses compared to both the PA12-ceramic composite and the pure PA12 sample. This high compressive strength along with the ability to sustain a large deformation is the result of the elastomer behaviour that shows the rubber elasticity and deforms after the ceramics loosens their cohesion [41]. When CNTs presented, the increase in this cohesion between the ceramic and the PA12 allows the sample to absorb more energy and sustain more deformations.

The compression behaviour of the PA12 samples under the chosen experimental conditions is similar to that of the creep test result. The equation of each sample have been calculated (shown in Fig. 7.4) in order to obtain the inflection point in the graph which allow to define the yield stress point. These equations and their inflection points are as followed:

$Y_1 = 19.032x^6 + 3286.6x^5 - 6392.1x^4 + 4092.5x^3 - 1795.6x^2 + 363.44x - 3.5683$

$$\begin{cases} \mathbf{x_1 = 0.25 \Rightarrow Y_1 = 29.6} \\ x_{2,3} = 0.45 \pm 0.1i \end{cases}$$

$Y_2 = -1809.4 + 5427.5x^5 - 6356.9x^4 + 3958.6x^3 - 1344.4x^2 + 251.54x - 2.0606$

$$\begin{cases} \mathbf{x_1 = 0.26 \Rightarrow Y_2 = 18.8} \\ x_2 = 0.74 \\ x_{3,4} = 0.37 \pm 0.19i \end{cases}$$

$Y_3 = -3936.4x^6 + 11100x^5 - 12322x^4 + 7094.6x^3 - 2181.3x^2 + 367.06x - 1.1351$

$$\begin{cases} \mathbf{x_1 = 0.24 \Rightarrow Y_3 = 26.6} \\ x_2 = 0.83 \\ x_{3,4} = 0.41 \pm 0.14i \end{cases}$$

where Y_1, Y_2 and Y_3 are equations for the pure PA12, PA12-ceramic and PA12-ceramic-CNT composites, respectively.

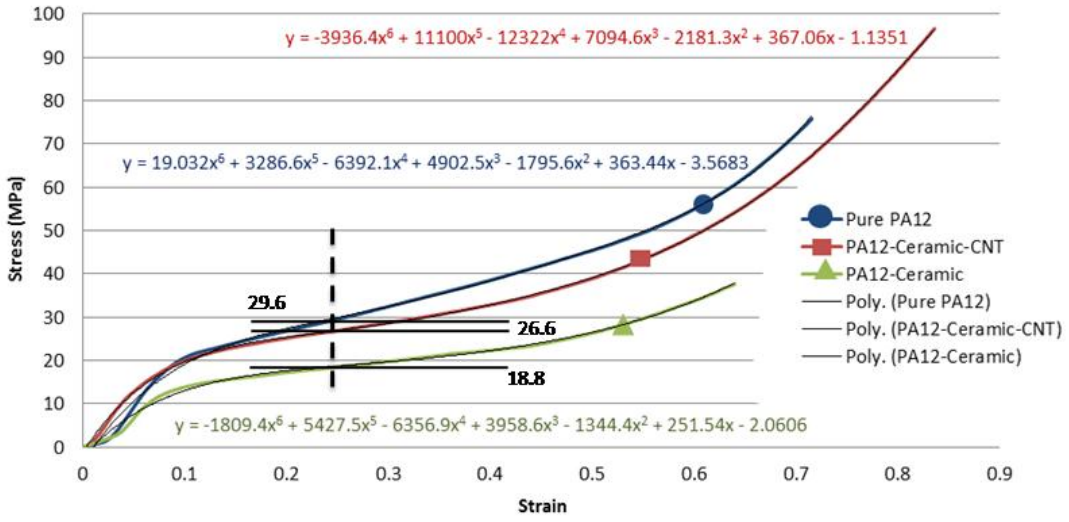

Fig. 7.4.The compression test results of the plain ceramic, pure PA12, PA12-ceramicand PA12-ceramic-CNT composite samples. The plain ceramic graph has been slightly shifted to the right for a clearer view.

Consequently, the addition of ceramics to the pure PA12 decreases its yield stress by 57% (from 29.6 to 18.8 MPa). Furthermore, the addition of CNTs increases the yield stress of PA12-ceramic composites by 41% (from 18.8 to 26.6 MPa), which recovers the property of PA12. The yield stress points for all the samples are almost at the same strain of 0.25.

Based on literature, the pull-out and bridging mechanisms play important roles in strengthening the composite. However, in our PA12 composite, we could not detect CNTs in wakes behaving as a bridge or as the evidence of pull-out mechanism by SEM investigation. The CNTs are oriented rather easily under shear flows, but have significant in-built curvature from their synthesis, which cannot be straightened [245]. As a result, we can detect plenty of coiled CNTs distributed evenly within the PA12matrix, as shown in Fig. 7.5. These coiled CNTs when faced to large stresses, act as a reinforcement phase and improved the mechanical strengths of the composites by stretching.

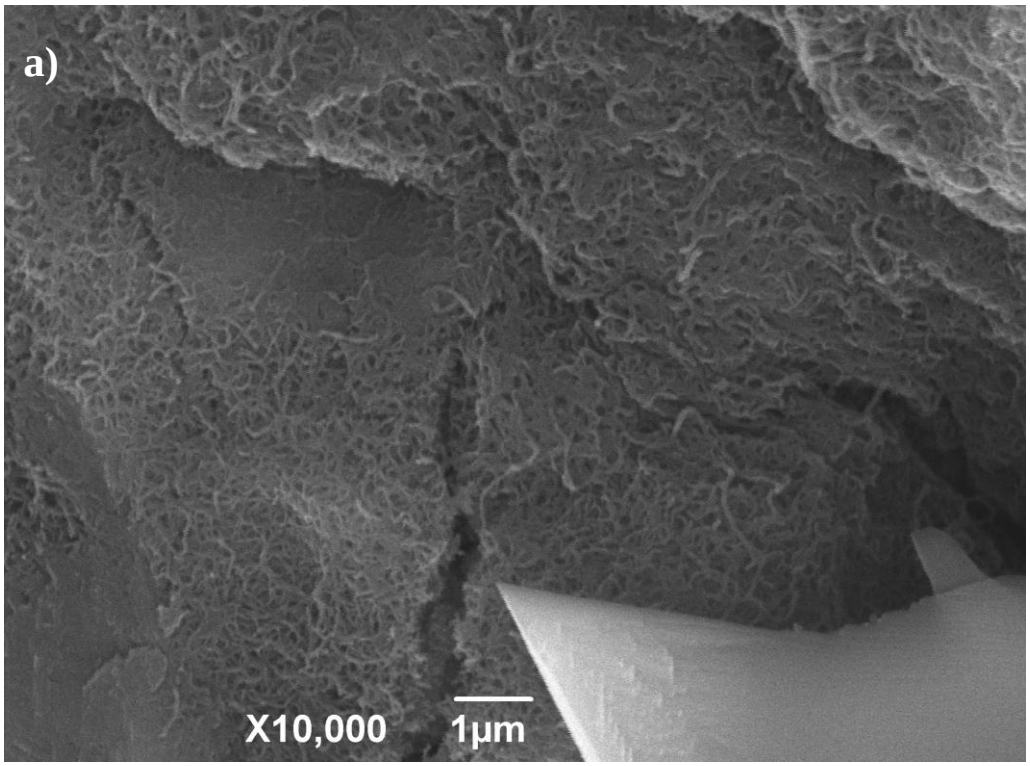
a)
X10,000
1µm

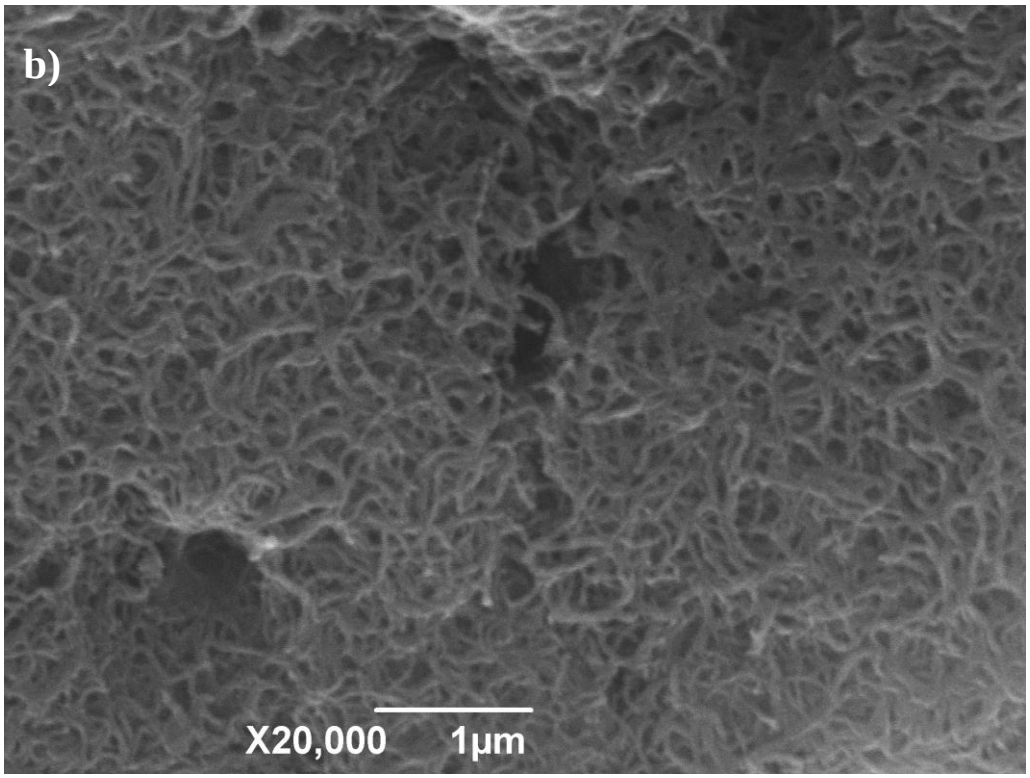
b)
X20,000
1µm

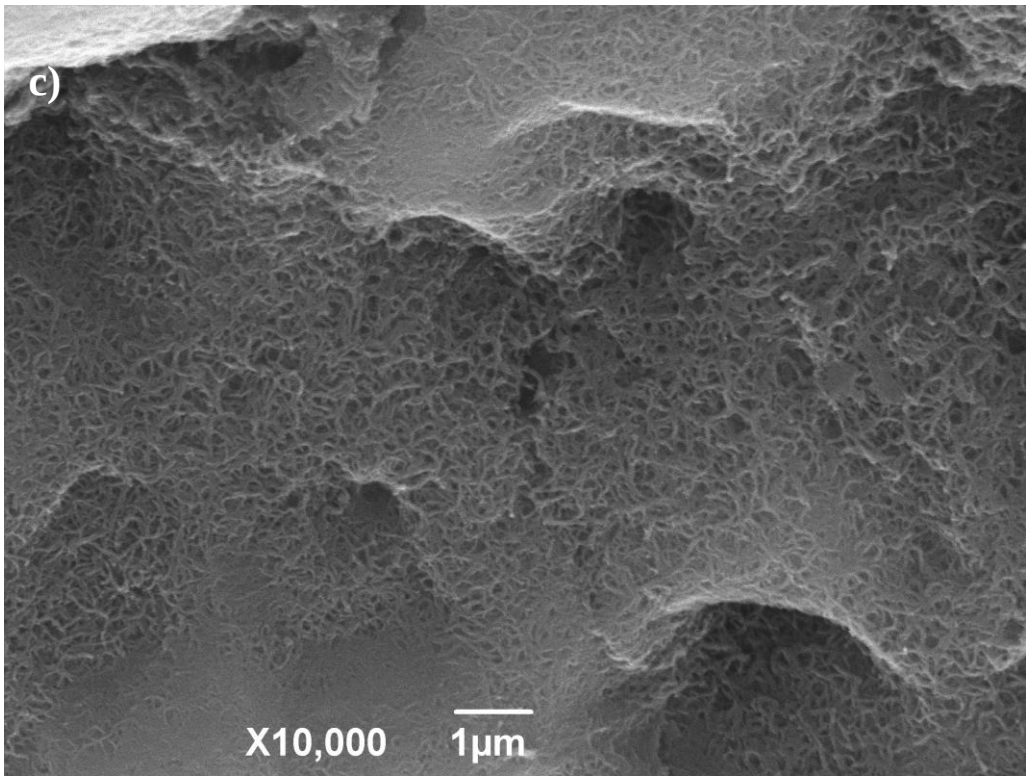

Fig. 7.5. SEM images of PA12-ceramic-CNT composite after the compression test at different magnifications.

7. 3. Hardness

In order to perform the hardness test, it was important to choose a big enough indent ball which could show the overall effect of all the three phases in the composite by applying the load on them. Therefore, a 1/8 inch ball has been chosen as the indent tip. The weight used in the experiment also will affect the results. Heavy weights may crush the ceramic and deform the samples; whilst light weights may hardly make any indention on samples. After a few initial trials, the 60 kgf load was chosen which gave rise to an acceptable indent on the sample. But, the hardness values for each of the composites till showed a wide range of results; the variation depends on the portion of ceramic (hard region), polymer (soft region) and CNTs under the indenter. For example, when the hardness of the epoxy resin was 63 HRH, the hardness of epoxy resin-ceramic was read between 65and 85 HRH and epoxy resin-ceramic-CNT composite ranging from 75 to 135 HRH. These results can clearly show the improvement in the hardness of specimens especially after the addition of CNTs. However, these wide ranges of

results (80% variation) prevent us from introducing a single value as the hardness of our sample for these composites.

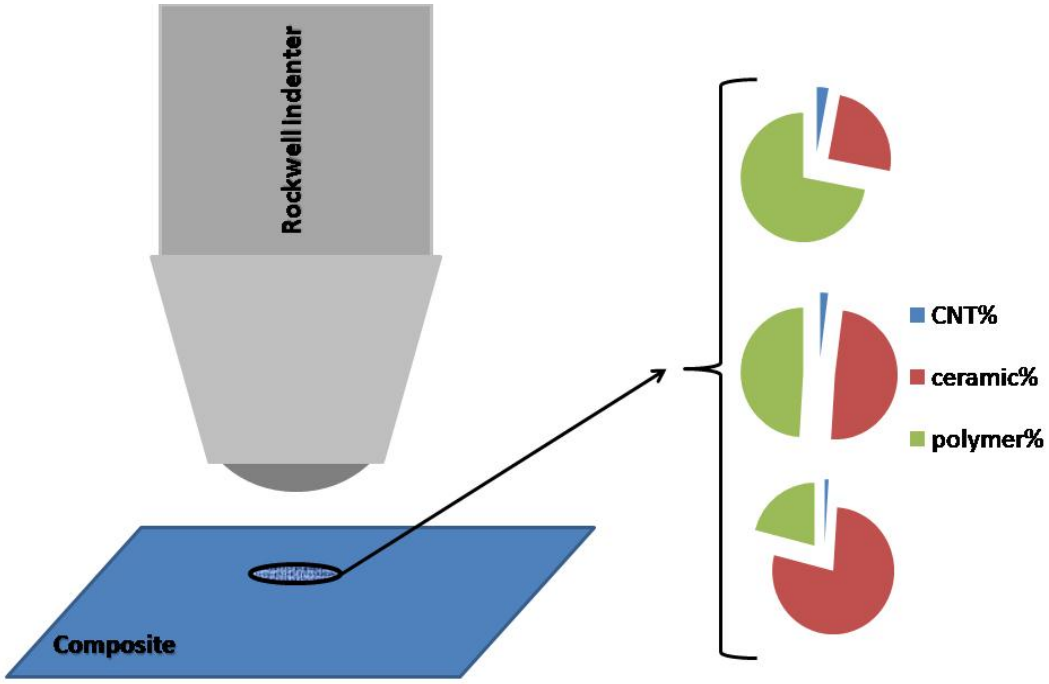

Fig. 7.6. Schematic of hardness test and how its results can be affected by different portions of CNT, polymer and ceramic placed under the indenter.

7. 4. Impact and toughness

In order to investigate the impact resistance of our functional materials, as described in chapter 3, the drop tower tests were performed under constant energy mode (5 J) and the results are presented as followed:

7. 4. 1. Epoxy resin based composite

Epoxy resin is a hard and brittle polymer,[255]and as 70% of our composite consists of this polymer, it is important to study its impact resistance for easy comparison later. Fig. 7.7a illustrates the impact behaviour of the pure epoxy resin. As it can be seen, the sample shows a sharp peak which represents a brittle break. This behaviour is the dominate characteristics of other composites made of resin, as shown in the next two graphs obtained from the composite materials which show almost identical profiles. When the brittle epoxy resin collapse, the whole sample structure will fail. The addition of ceramic to the polymer slightly improves the impact resistance of the

specimens (Table. 7. 1). This improvement became more obvious when CNTs were introduced to the composites. With their high impact resistant capacity [256], which makes the sample more tougher (as discussed in the compression test section), the composites can withstand a higher impact load and absorb more energy. It is clear in Fig. 7.7c that the absorbing peak of epoxy resin-ceramic-CNT composite becomes broader compared with the other two samples.

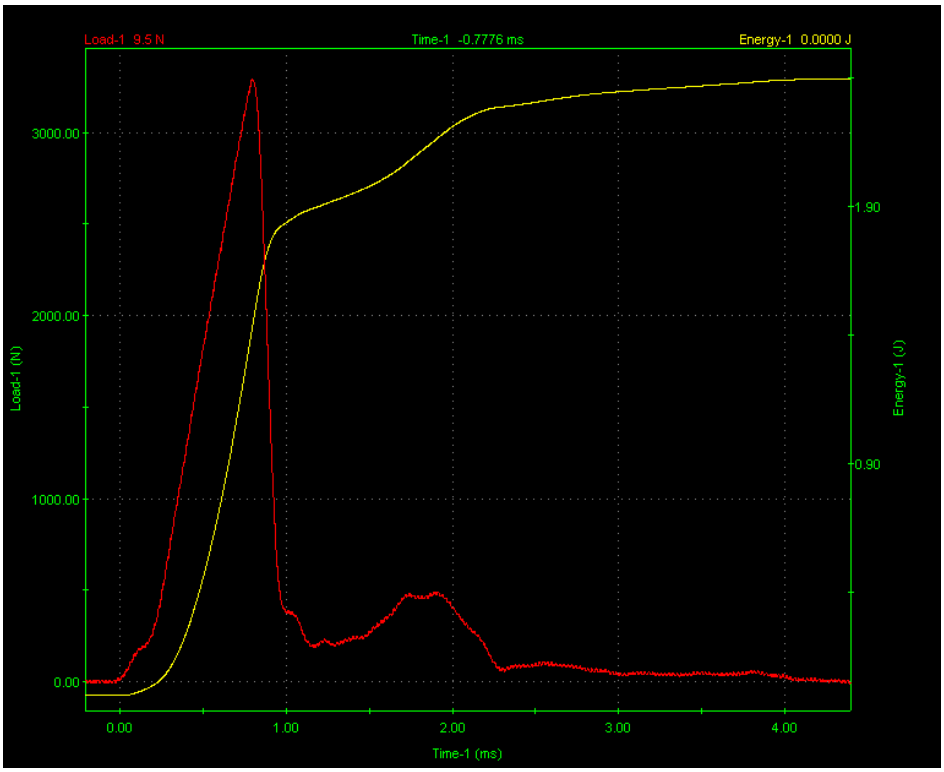

(a)

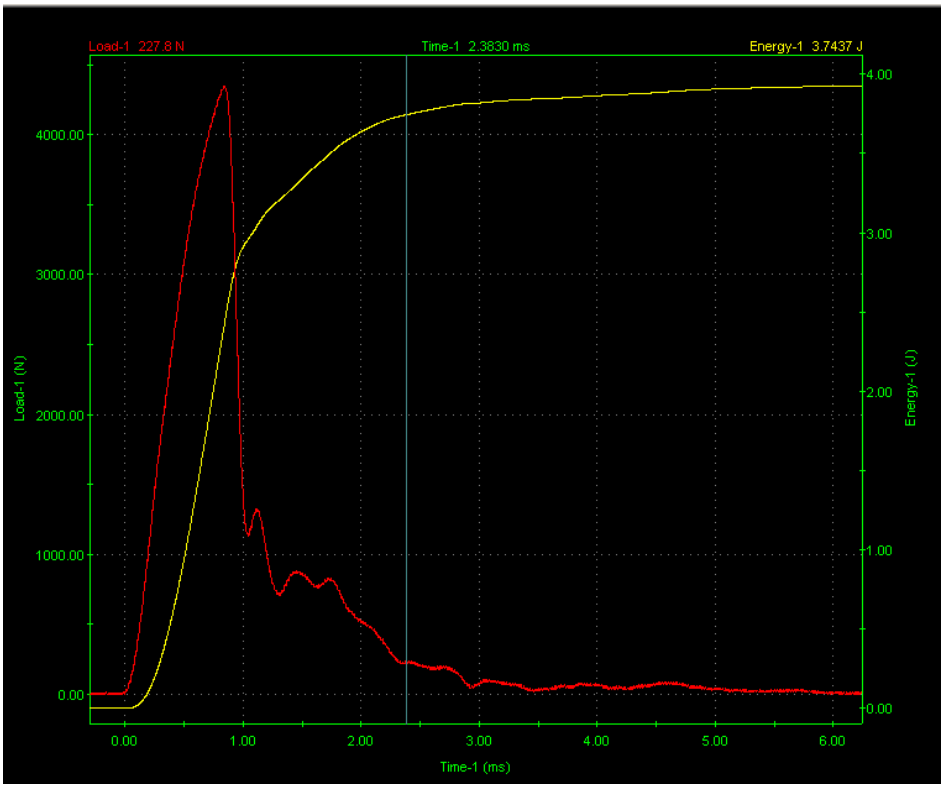

(b)

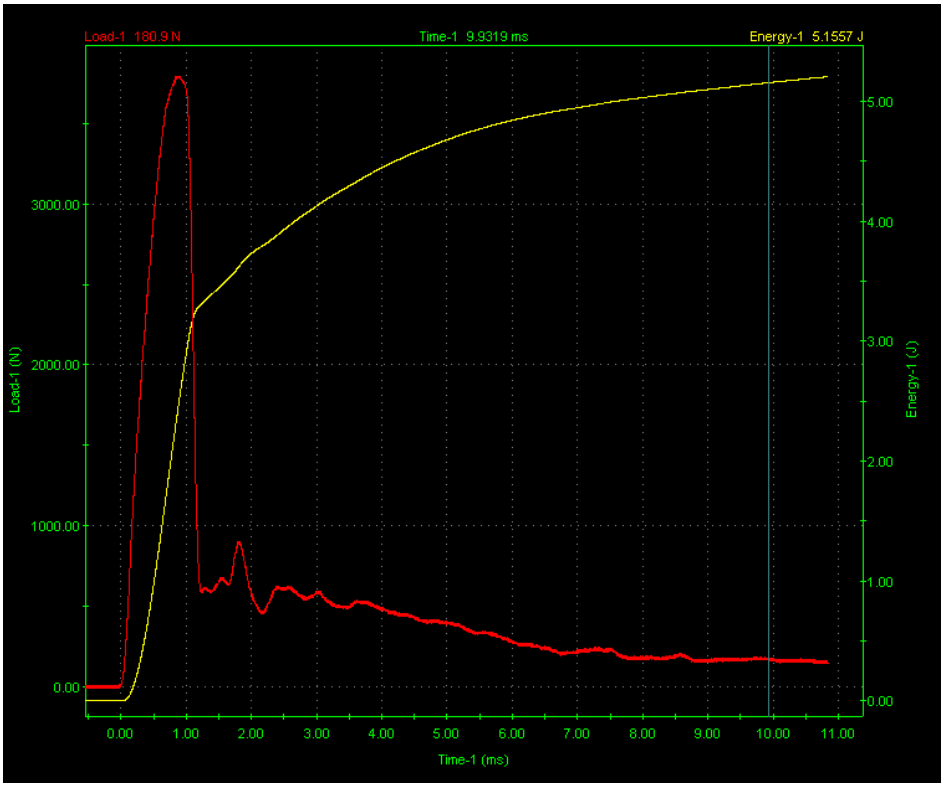

(c)

Fig. 7.7. Impact test profiles of pure epoxy resin (a), epoxy resin-ceramic (b), and epoxy resin-ceramic-CNT (c) composites obtained under constant impact energy of 5 J.

Important data from Fig. 7.7 are summarized in Table. 7. 1 which shows the maximum load, energy to this maximum load and total energy absorbed during the impact test. In total, the epoxy resin-ceramic-CNT composite absorb 117.2% and 32.7% more energy than those of pure epoxy resin and epoxy resin-ceramic composite, respectively. And both composites required a higher load to break compared with the pure epoxy resin.

Fig. 7.8 shows the appearance of the samples after the impact test. It is clear that all the three types of sample have been failed and broken in a similar pattern.

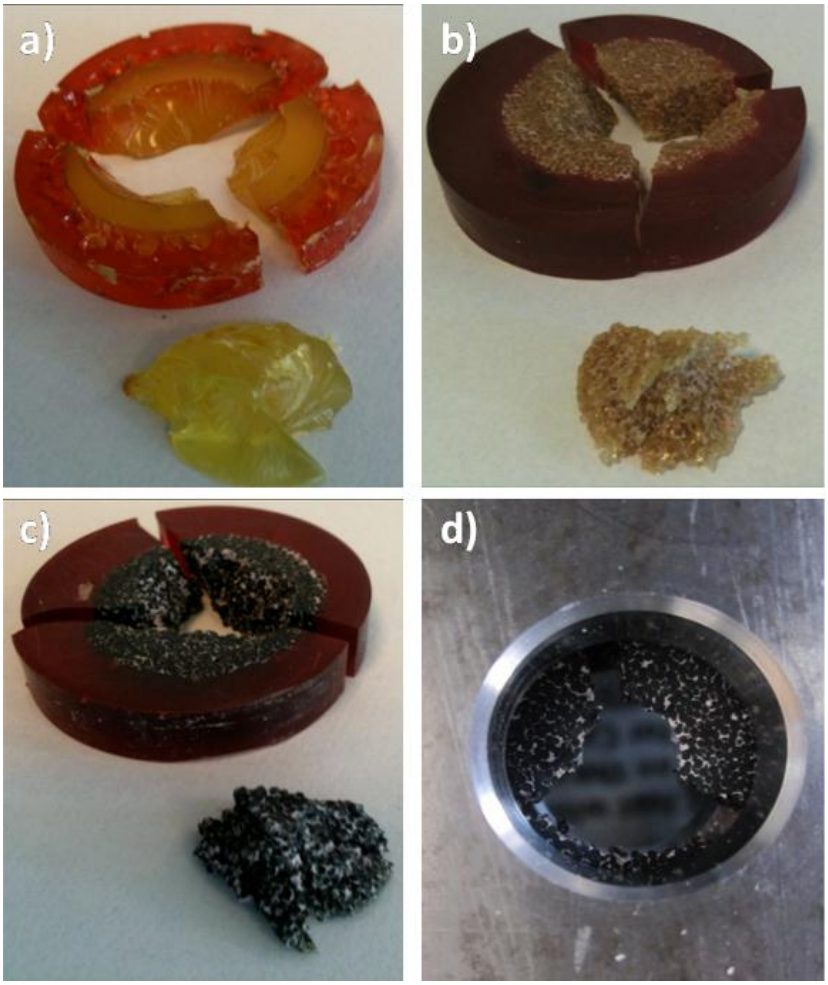

Fig. 7.8. Optical images of different post impact samples. (a) and (b) represent the pure epoxy resin and epoxy resin-ceramic samples, respectively. (c) and (d) represent the epoxy resin-ceramic CNT composites.

Table. 7. 1. Peak load, energy to maximum load and total energy absorbed during impact test are summarized for the pure epoxy resin, epoxy resin-ceramic and epoxy resin-ceramic-CNT composites.

	Pure epoxy resin	**Epoxy resin-ceramic composite**	**Resin-ceramic-CNT composite**
Peak load (N)	3294.6	4351.1	3794.5
Energy to max load (N)	1.4242	2.4076	2.3880
Total energy (J)	2.3968	3.9233	5.2057

SEM investigations of the fracture surfaces revealed the role of CNTs in improving the toughness of composites. The stress-transfer from the matrix to the reinforcements has to be performed via the interface, which can be influenced by a chemical functionalization of the CNT surface. A tailored functionalization can lead to the formation of covalent bonds between CNTs and the polymeric matrix, resulting in a strengthened interface and an improved wettability of the CNTs [246]. It has been shown that even at low nanotube contents, the epoxy resin-CNT composites exhibit a significant increase in fracture toughness, as well as an enhancement of stiffness [246].The red insets in Fig. 7.9a and Fig. 7.9b show the CNTs that are still connected to the polymer at both ends. This represents the bridging mechanism. More energy will be required to pull these CNTs out of the polymer which increases the toughness of sample. Similar situations can be evidenced in Fig. 7.9d and Fig. 7.9e where a plenty of CNT act as bridges connecting polymers at two sides of wakes. Uncoiling CNTs can be seen in Fig. 7.9c in a wake which still can be further stretched and act as a bridge. Fig. 7.9 also shows evidence of pull-out mechanism occurred in our sample. The blue insets in Fig. 7.9a and Fig. 7.9b present nanotubes which have faced to larger forces and pulled out of the polymer by absorbing more energy (increased toughness).

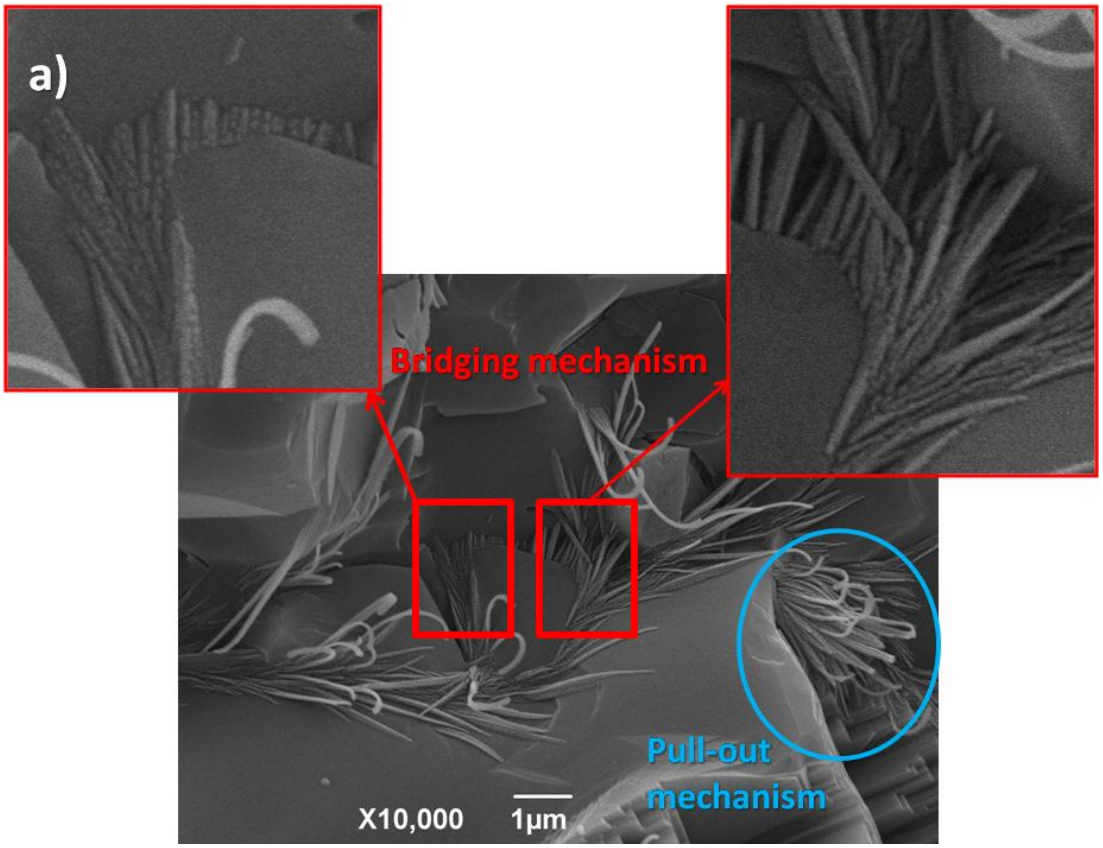
a)
Bridging mechanism
Pull-out
mechanism
X10,000
1µm

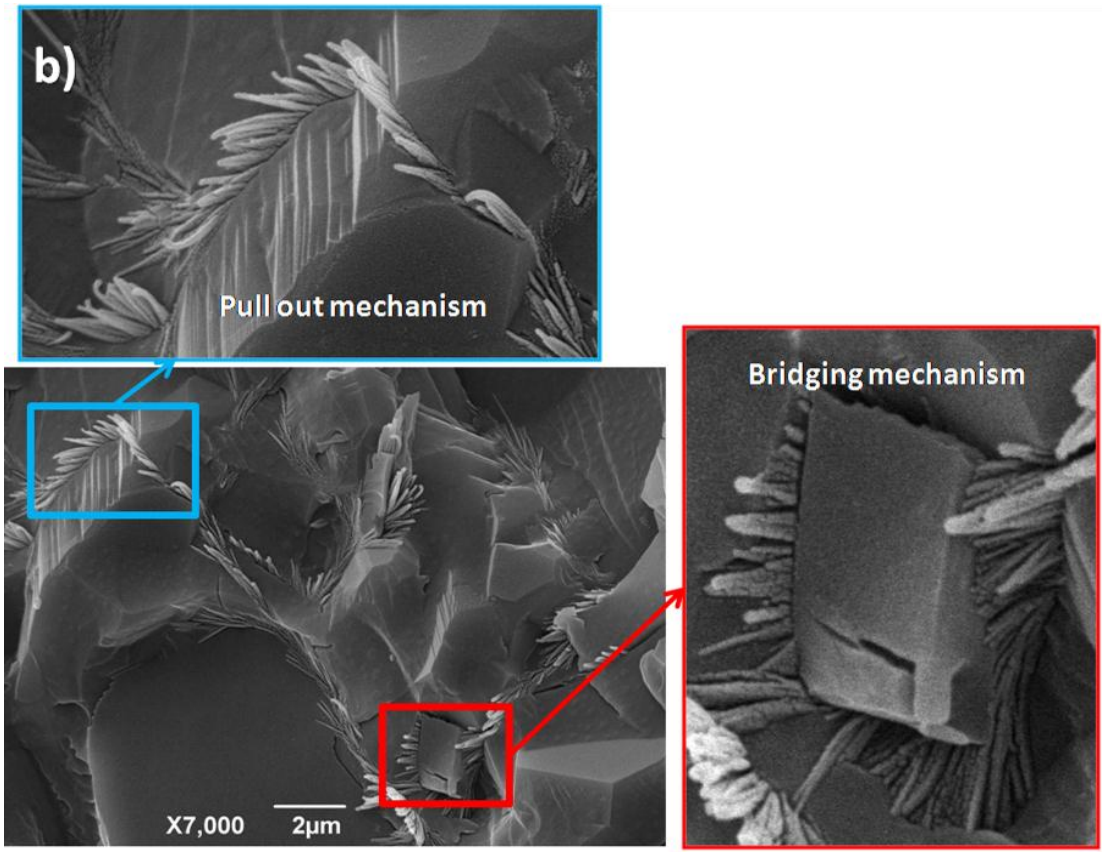
b)
Pull out mechanism
Bridging mechanism
X7,000
2µm

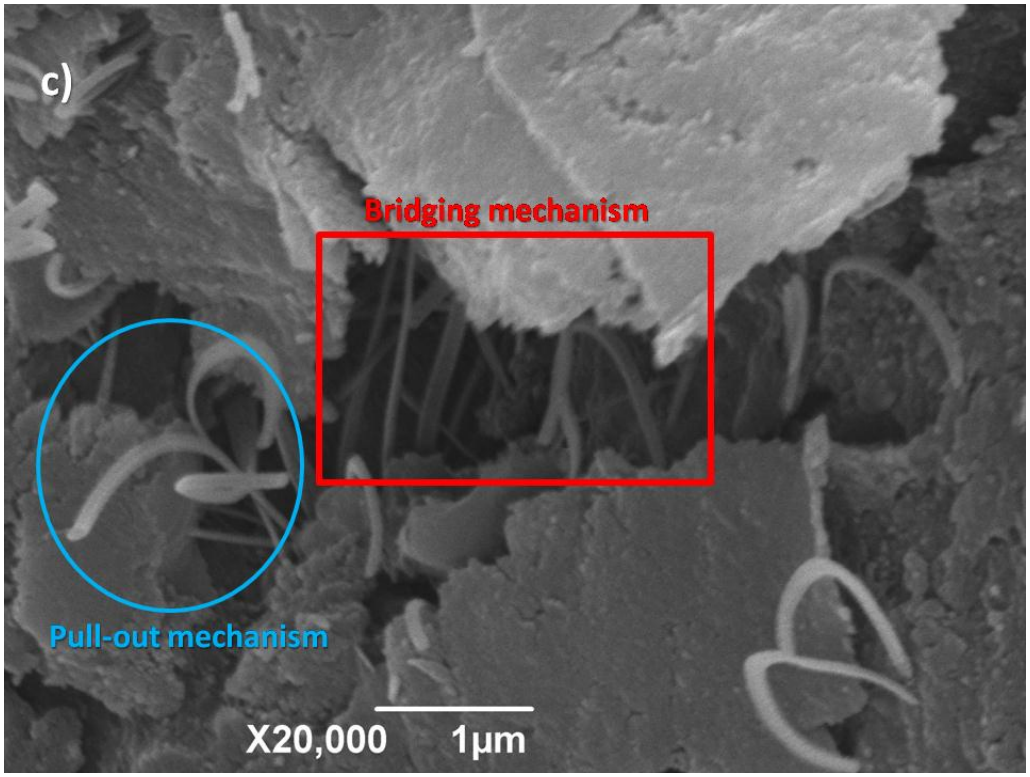
c)
Bridging mechanism
Pull-out mechanism
X20,000
1µm

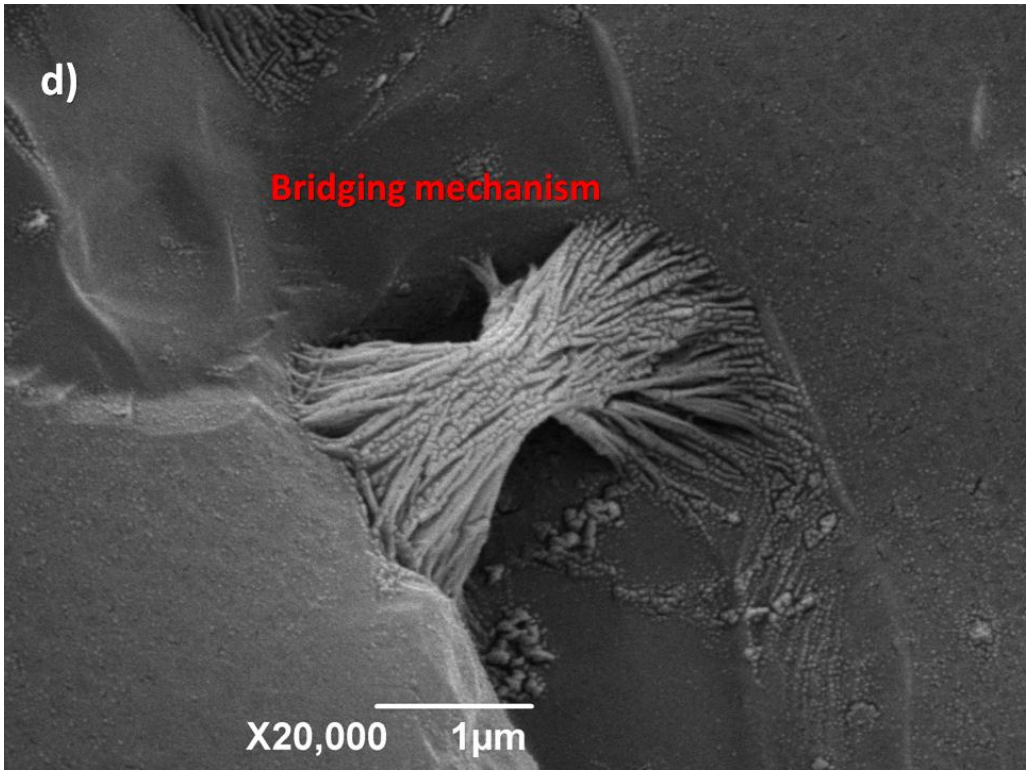
d)
Bridging mechanism
X20,000
1µm

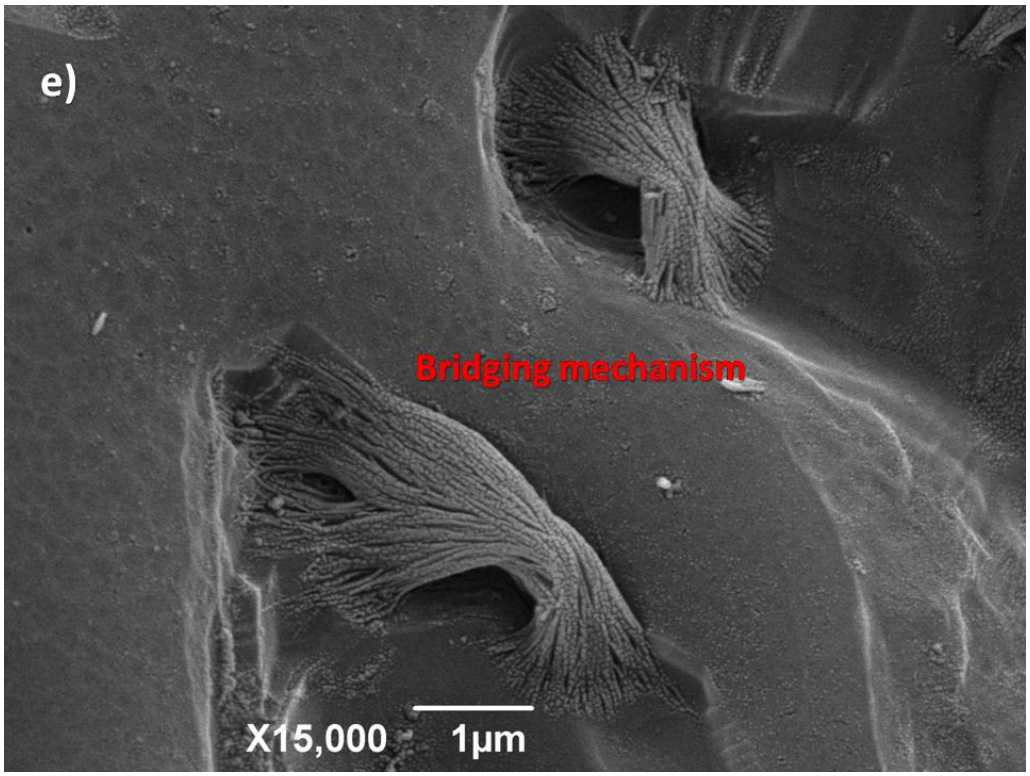

Fig. 7.9. SEM images of a fracture surface of the epoxy resin-ceramic-CNT composite reveal the bridging mode and pull-out mode of CNTs within the composite acted as the toughening mechanism.

As discussed in chapter 2, when a crack is formed, the reinforcement bridges it in its wake and pull-out does the frictional work. These mechanisms can effectively stop the crack from further growth across the whole sample [134]. In CNT-reinforced composites, it is proposed that uncoiling and stretching of CNTs also play an important role in enhancing the toughness [136]. During the crack propagation, CNTs in the wake are stretched and act as extra bridges, stopping the cracks from further propagation. In the case of larger forces, CNTs will be forced out of the resin matrix. This mechanism known as pull-out, which requires a high energy to defeat the strong bonding between CNTs and matrix and will act as another process to prevent further growth of cracks, resulting in a tougher composite [136]. In this regard, homogenous dispersion of CNTs in the ceramic matrix is the most dominating factor which in our case, use of ceramic foam as trust has significantly improved their dispersion.

7. 4. 2. Polyamide based composite

Unlike epoxy resin, PA12 is a tough polymer [257]. Our results for the impact tests of pure PA12 also confirm this fact (Fig. 7.10a). As 70% of composites consist of PA12, the composite toughness is basically dominated by the behaviour of PA12. Consequently, the addition of a ceramic and CNTs at this low fraction (0.5 wt. %) only improved the impact resistance of our composites slightly. They exhibit a similar profile under impact load (constant energy mode of 5 J) (Fig. 7.10b and c).

a)

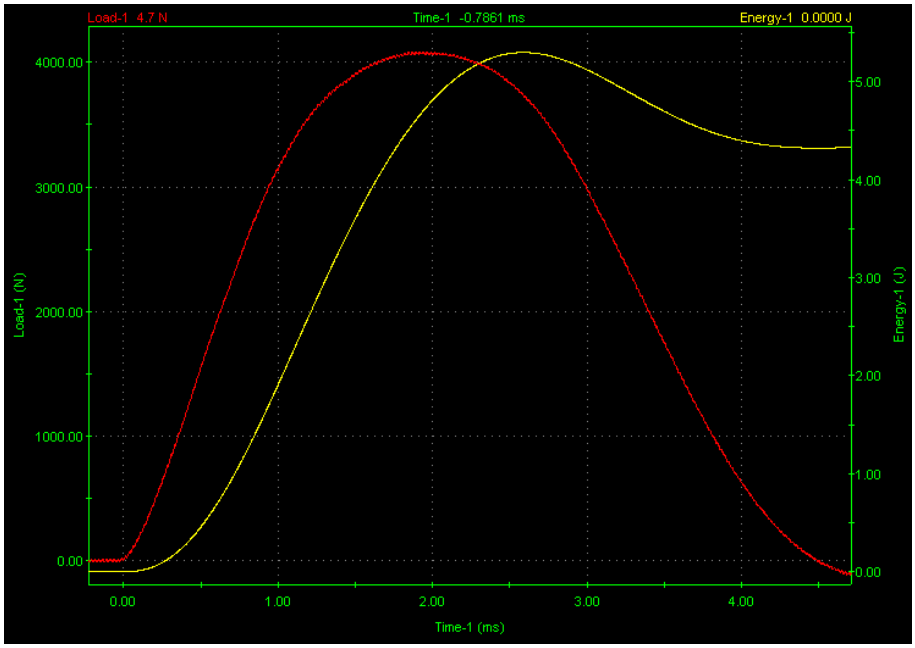

b)

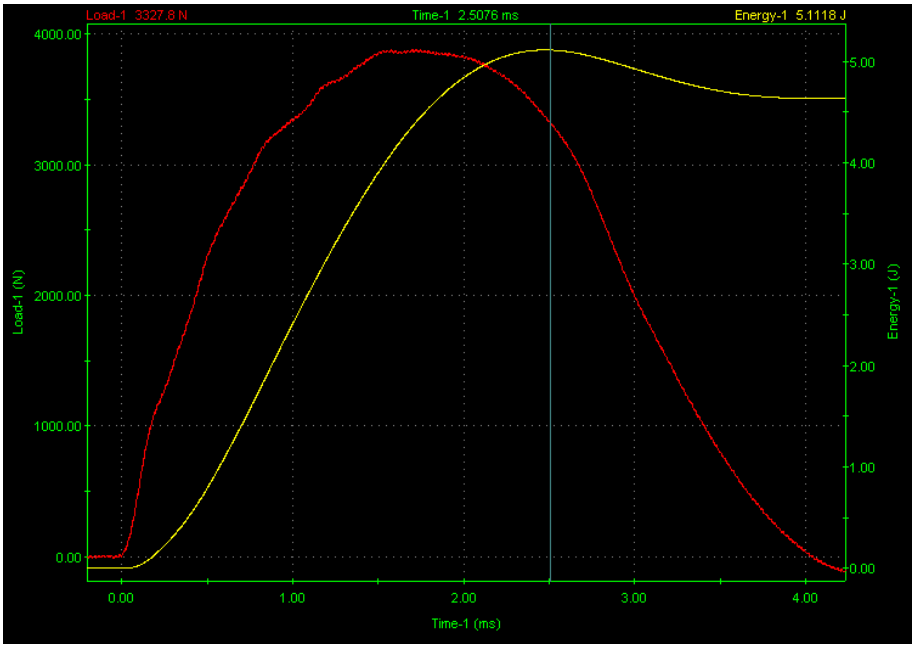

c)

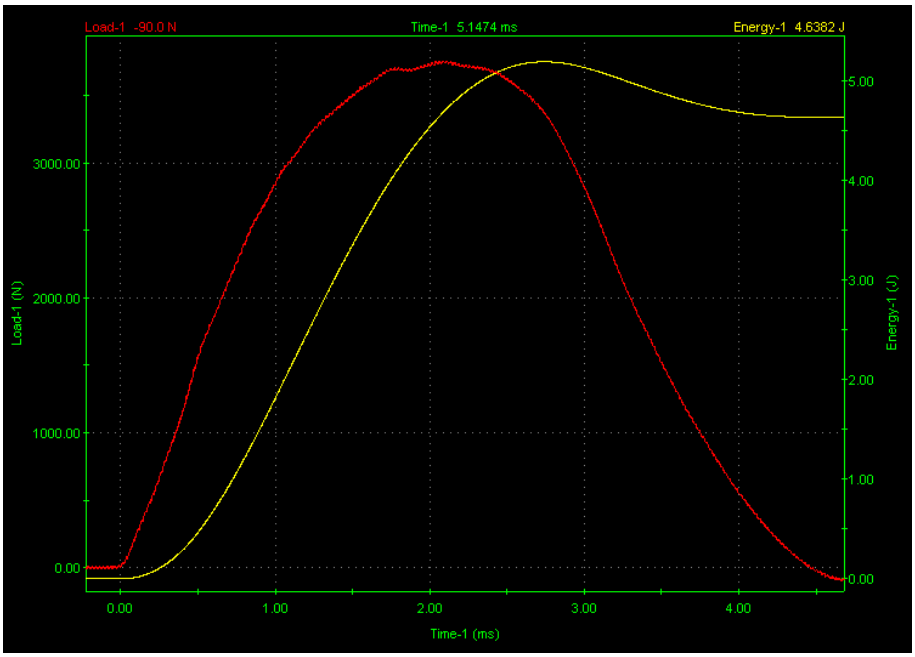

Fig. 7.10. Impact test results of the pure PA12 (a), PA12-ceramic (b), and PA12-ceramic-CNT (c) composites obtained under constant energy of 5 J.

Fig. 7. 11 shows the appearance of the samples after the impact test. It is clear that crack have been formed at the surface of all the three types of sample; however they have not being completely failed facing the impact as it was evidenced in epoxy resin samples (Fig. 7.8). This shows that the PA12 samples are capable of adsorbing higher level of energies compared to epoxy resin ones. The red circles in Fig. 7. 11 shows the cracks and they have been scale up for better observation.

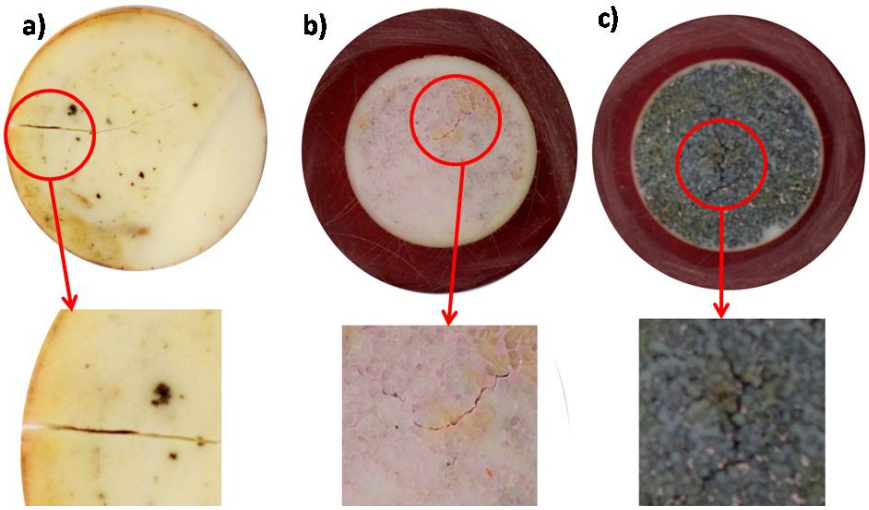

Fig. 7. 11. Optical images of different post impact samples. Pure PA12, PA12-ceramic composite and PA12-ceramic-CNT composites are presented in (a), (b) and (c), respectively. The red circles clearly show the cracks at the surface of samples.

Table. 7. 2 summarizes the maximum load, energy to this maximum load and total energy absorbed during the impact test for pure PA12, PA12-ceramic and PA12-ceramic-CNT composites, which shows all the three types of material having a very similar characteristic, unlike the results for the epoxy resin composites.

Table. 7. 2.Peak load, energy to maximum load and total energy absorbed during impact test are summarized for pure PA12, PA12-ceramic and PA12-ceramic-CNT composites.

	Pure PA12	PA12-ceramic composite	PA12-ceramic-CNT composite
Peak load (N)	4083.4	3882.4	3752.6
Energy to max load (N)	4.6014	4.3976	4.6381
Total energy (J)	4.3209	4.6341	4.6330

To conclude, the addition of CNTs (at such a small volume fraction) can improve the impact resistance of those polymer composites which are brittle by their own, however CNTs cannot improve the compression strength of such composites. On the other hand, the addition of CNTs to tougher/softer composite materials such as polyamides did not have a significant effect on their impact resistance; however it could considerably improve the mechanical strength under compressive stresses.

7. 4. Conclusion

- The addition of 13 wt. % CNT (this weight percent includes catalyst particles) to the porous ceramic (100-150 μm pore sized) increases the compressive strength by 34.4% (compared to the as received ceramic) and 8.3% (compared to the heat treated sample).
- The reinforcement effect of CNTs in the epoxy resin-ceramic-CNT composite in compression test becomes clearer after the yield point where it could deforms 40% more elastically compared to the epoxy resin-ceramic composite as a result of the CNT reinforcement.
- The formation of plenty of cracks in epoxy resin-ceramic composites during compression test completely broke the samples, whilst the addition of CNTs to the composite stopped the crack propagation and the samples did not break into pieces.
- Ceramics added to pure PA12 decreased its yield stress by 57%, and the CNT addition increased the yield stress of PA12-ceramic composites by 41% and recovered the materials properties to some extent.
- The impact toughness of both the epoxy resin and PA12 composites were dictated by the behaviour of their polymers, as they are the main ingredients (70%) of the composites. Epoxy resin-ceramic-CNT composite showed a brittle break characteristic, absorbing 117.2% and 32.7% more energy compared to the pure epoxy resin and epoxy resin-ceramic composite, respectively.
- Bridging and pull-out mechanisms counted for the improved toughness of epoxy resin-CNT composites.

Chapter 8. Summary and conclusions

In summary, it was tried to use the extraordinary properties of CNTs in different applications. This includes the fabrication of new functional materials by addressing their mechanical properties and also producing nanofilters for different sorts of contaminations in various media. For this purpose, new methods were introduced and developed in a way to fit our demands. This work tried to address the current technical challenges on fabrication of ceramic/CNT nanocomposites and improve the uniformity of CNTs distribution inside matrix and preventing their agglomerations which all count as current difficulties for fabrication of such nanocomposites. Based on the technical demands, new methods and devices were developed and introduced for the fabrication of polymer-ceramic-CNT composites for the first time.

After an introduction in **chapter 1**, describing the main idea and motivations behind the demands in this field for fabrication of ceramic/CNT composites and challenges for synthesising of such functional materials, **chapter 2** provides detailed data and information covering all aspects about CNTs, fabrication processes, composites, and applications particularly filters.

In **chapter 3**, the experimental methodology described all the fabrication processes, materials and characterisation techniques used in fabrication and properties evaluation. Detailed data about techniques and instruments involving in experiments were also discussed.

In **chapter 4**, fabrication of ceramic/CNT composites were reported by direct in-situ growth of CNTs inside different ceramic substrates. For high density ceramic (100-150 µm pore sized), the nanocomposite was made by placing camphor as a green carbon source inside the matrix. For ceramic foam (300 and 500 µm pore sized), the composite was produced by injection of acetone-camphor solution in to the reaction chamber. In both processes, similar catalyst (nickel nitrate) was used. It was shown that this catalyst

is capable of improving the uniformity of catalyst particle distribution on ceramic matrix at very small size which directly improved the quality of the final product. This was achieved by introducing the catalyst as a solution rather than solid powders. Furthermore, the effect of different parameters on CNT growth such as catalyst and carbon source, temperature, carrier gas speed and etc. were also intensively studied and described.

In **chapter 5**, the prepared ceramic-CNT composite with 500 µm pore size was used to be infiltrated with two different sets of polymers: one thermoset (epoxy resin) and one thermoplastic (PA12). Based on the different requirements for each polymer, different approaches for infiltration of composites were developed and discussed. It was shown that high degree of filling has been achieved, using µ-CT scan investigations. Furthermore, SEM investigations proved that CNTs have survived the infiltration process and they were still well distributed inside the matrix. This was the first report for fabrication of such a functional material.

In **chapter 6**, the ceramic-CNT nanocomposites were used in filtration application for the removal of bioorganic (yeast cells) and inorganic (heavy metal ions) contaminants from water, and of particulates from air. Dominating effects on filtration properties were clearly discussed and reviewed. This includes effect of pore size, injection rate and functionalization methods. Reusability of filter was addressed as another important factor in this chapter. These results represent a big leap towards practical applications that may open new opportunities for CNT engineering.

In **chapter 7**, the mechanical properties of prepared high density ceramic-CNT, epoxy resin-ceramic-CNT and PA12-ceramic-CNT composites were evaluated and discussed. This includes assessing compression test, hardness and impact test.

In conclusion:

- Fabrication of CNTs in high density ceramic matrix at 850 °C under a H_2-Ar atmosphere using CVD process was introduced. This includes introducing an

unconventional CVD process for the first time by placing the green carbon source (camphor) inside the engineered high density ceramic substrate. The resulting CNTs with average diameters of 30-70 nm and lengths up to several micrometers are dispersed uniformly at each section of the alumina matrix. An improvement in the compression strength of the composites (8.3% and 34.4% compared to the heat treated and as received samples, respectively), has been obtained due to the inclusion of CNTs.

- CNTs were also directly synthesised on ceramic foam (Ø27 mm × 10 mm, 300 and 500 µm pore sized) at 780 °C under a H_2 atmosphere. Similar catalyst and carbon source were used. Uniform CNT (with 3 wt% yield) distribution was achieved at all sections of sample. These ceramic-CNT composites were used as nanofilters and their filtration efficiencies were assessed.

- CNT nanofilters showed very promising results. 98% of the yeast cells were filtered. The filtration efficiency was a function of filter pore size, filter length (CNT loading) and injection rate. SEM images of yeast cells inside filter revealed that they were physically captured by the tangled CNT networks.
- More than 99.6% of the air particles (size ranges from 0.3 to 10 µm) were filtered using 300 mm long CNT filter. CNT loading was shown to be the dominating factor in filtration efficiency compared to the ceramic pore size. Oxidized CNT filter and pristine one showed similar efficiencies suggesting that the mechanism of filtration is mainly through physical interception. Brownian diffusion mechanism was claimed to be the dominating filtration mechanism for smaller particles (0.3 µm) when for big particles (5 and 10 µm), inertia impaction and interception counts for the filtration mechanism.
- A complete removal of heavy metal ions from water was reported particularly for single ion removal tests. In the presence of mixed ions, their competitive binding to CNTs dominates the adsorption process suggesting that sorption

mechanism of heavy metals by CNTs is more a chemisorption process rather than physisorption. Based on this fact, filters in less competitive conditions had higher adsorption efficiencies for all the metal ions in solution when for more competitive conditions, metal ions with higher adsorption tendencies (Fe^{2+} and Cu^{2+}) replaced other ions and released them into the solution. These filters maintained their high efficiency at higher injection rates (500 ml/h) which makes them promising candidates for industrial filtration applications.

- Filters were shown to be capable of being reused while maintaining their high efficiencies. This can justify the high initial cost of producing CNTs.
- Ceramic-CNT composites were then successfully infiltrated with two different sets of polymers (one thermoset: epoxy resin, and one thermoplastic: PA12) fabricating novel polymer-ceramic-CNT functional materials.
- All the samples (pure epoxy resin, epoxy resin-ceramic and epoxy resin-ceramic-CNT) showed similar behaviour under compression test. This behaviour was dominated by the epoxy resin and samples had very close yield stresses. The reinforcing effect of CNTs in the epoxy resin-ceramic-CNT composite under compression test becomes clearer after the yield point. The addition of ceramic to pure epoxy resin caused its failure at a much lower strain. However, the epoxy resin-ceramic-CNT composite deforms 40% more elastically compared to the epoxy resin-ceramic composite as a result of the CNT reinforcement.
- Ceramics added to the pure PA12 decreased its yield stress by 57%, and the CNT addition increased the yield stress of PA12-ceramic composites by 41% and recovered the materials properties to some extent.
- The impact toughness of both the epoxy resin and PA12 composites were dictated by the behaviour of their polymers, as they are the main ingredients (70%) of the composites. Epoxy resin-ceramic-CNT composite showed a brittle break characteristic, absorbing 117.2% and 32.7% more energy compared to the

pure epoxy resin and epoxy resin-ceramic composite, respectively. Bridging and pull-out mechanisms are counted for the improved toughness of epoxy resin-CNT composites.

Chapter 9. Future work

Base on the obtained results, some suggestions for future work are proposed:

In high density ceramic-CNT composite:

- More investigation can be done for increasing the yield of CNTs along with improving the uniformity of nanotube distribution inside the ceramic matrix. It was shown that there were still many catalyst particles remained inside the matrix without any growth that indicates further efforts are needed to find a way to provide more carbon source inside the sample.

- The produced composite can be then subjected to the mechanical test evaluation and also for filtration application for smaller contaminants such as viruses and bacteria where we had faced the maximum efficiency of 98% for yeast cells with 300 µm pore sized nanofilter where this ceramic has 100-150 µm pore sizes.

In low density ceramic-CNT composite:

- Again, increasing the yield of CNTs can still be subject of further studies along with developing a new precise measuring step in order to provide the exact amount of synthesised CNTs inside ceramic foam. These two data will allow one to study the isotherm of heavy metal ions adsorption in filtration application.

- It is required to develop a procedure to monitor the released amount of CNTs following the environmental concerns. This study can be further carried out by designing a special holder (such as polymer membranes) to minimise CNT release into the environment by colleting them from outlet stream.

- It is recommended to follow a similar fabrication approach using a diesel particulate filter as substrate. Based on the promising results obtained from air particulate filtration in this thesis, such filter is expected to have extremely good potential for car engines which can be a great interest for nanotechnology in

everyday use application. Pressure drop of such fabricated filter needs to be also addressed.

In polymer-ceramic-CNT composite:

- The new class of functional nanomaterial introduced in this thesis needs to be subject of further studies. It is required to fabricate bigger samples. This will allow one to evaluate more mechanical properties of them.

- There are still many polymers which can be used to infiltrate the ceramic-CNT composite. This can produce new engineered functional materials with required properties. Thus, intensive investigations can be carried out in this field by addressing more different polymers.

References

[1] Iijima S. Helical microtubules of graphitic carbon. Nature. 1991;354(6348):56-8.

[2] Peigney A, Laurent C, Flahaut E, Rousset A. Carbon nanotubes in novel ceramic matrix nanocomposites. Ceramics International. 2000;26(6):677-83.

[3] Van Lier G, Van Alsenoy C, Van Doren V, Geerlings P. Ab initio study of the elastic properties of single-walled carbon nanotubes and graphene. Chemical Physics Letters. 2000;326(1-2):181-5.

[4] Thostenson ET, Ren Z, Chou T-W. Advances in the science and technology of carbon nanotubes and their composites: a review. Composites Science and Technology. 2001;61(13):1899-912.

[5] Yu MF, Lourie O, Dyer MJ, Moloni K, Kelly TF, Ruoff RS. Strength and Breaking Mechanism of Multiwalled Carbon Nanotubes Under Tensile Load. Science. 2000;287(5453):637-40.

[6] Xie XL, Mai YW, Zhou XP. Dispersion and alignment of carbon nanotubes in polymer matrix: A review. Materials Science and Engineering: R: Reports. 2005;49(4):89-112.

[7] Komarov FF, Mironov AM. Carbon Nanotubes: Present and Future. physics and chemistry of solid state. 2004;5:411-29.

[8] Halonen N, Rautio A, Leino AR, Kyllönen T, Tóth G, Lappalainen J, et al. Three-Dimensional Carbon Nanotube Scaffolds as Particulate Filters and Catalyst Support Membranes. ACS Nano. 2010;4(4):2003-8.

[9] Srivastava A, Srivastava ON, Talapatra S, Vajtai R, Ajayan PM. Carbon nanotube filters. Nat Mater. 2004;3(9):610-4.

[10] Brady-Estévez AS, Kang S, Elimelech M. A Single-Walled-Carbon-Nanotube Filter for Removal of Viral and Bacterial Pathogens. small. 2008;4(4):481-4.

[11] Thostenson ET, Ren Z, Chou TW. Advances in the science and technology of carbon nanotubes and their composites: a review. Composites Science and Technology. 2001;61(13):1899-912.

[12] Curtin WA, Sheldon BW. CNT-reinforced ceramics and metals. Materials Today. 2004;7(11):44-9.

[13] Sung UL, Won SC, Byungyou H. A comparative study of dye-sensitized solar cells added carbon nanotubes to electrolyte and counter electrodes. Solar Energy Materials and Solar Cells.94(4):680-5.

[14] Shaheer Akhtar M, Park JG, Lee HC, Lee SK, Yang OB. Carbon nanotubes-polyethylene oxide composite electrolyte for solid-state dye-sensitized solar cells. Electrochimica Acta.55(7):2418-23.

[15] Jung SM, Jung HY, Suh JS. Horizontally aligned carbon nanotube field emitters fabricated on ITO glass substrates. Carbon. 2008;46(14):1973-7.

[16] Lahiri I, Seelaboyina R, Hwang JY, Banerjee R, Choi W. Enhanced field emission from multi-walled carbon nanotubes grown on pure copper substrate. Carbon.48(5):1531-8.
[17] Xu J, Fisher TS. Enhancement of thermal interface materials with carbon nanotube arrays. International Journal of Heat and Mass Transfer. 2006;49(9-10):1658-66.
[18] Robertson J. Realistic applications of CNTs. Materials Today. 2004;7(10):46-52.
[19] Bhushan B. Handbook of Nanotechnology. 2nd ed. New York: Springer; 2006.
[20] Siegel RW, Chang SK, Ash BJ, Stone J, Ajayan PM, Doremus RW, et al. Mechanical behavior of polymer and ceramic matrix nanocomposites. Scripta Materialia. 2001;44(8-9):2061-4.
[21] Osayande LI, Okenwa IO. Fracture Toughness Enhancement for Alumina Systems: A Review. International Journal of Applied Ceramic Technology. 2008;5(3):313-23.
[22] An JW, Lim DS. Effect of carbon nanotube additions on the microstructure of hot-pressed alumina. Ceramic Processing Research. 2002;3(3):201-4.
[23] Jinpeng F, Daqing Z, Minsheng W, Zening X, Jun S. Preparation and Microstructure of Multi-Wall Carbon Nanotubes-Toughened Al_2O_3 Composite. Journal of the American Ceramic Society. 2006;89(2):750-3.
[24] Zhan GD, Kuntz JD, Wan J, Mukherjee AK. Single-wall carbon nanotubes as attractive toughening agents in alumina-based nanocomposites. Nat Mater. 2003;2(1):38-42.
[25] Ahmad I, Cao H, Chen H, Zhao H, Kennedy A, Zhu YQ. Carbon nanotube toughened aluminium oxide nanocomposite. Journal of the European Ceramic Society. 2009;30(4):865-73.
[26] Kumari L, Zhang T, Du GH, Li WZ, Wang QW, Datye A, et al. Thermal properties of CNT-Alumina nanocomposites. Composites Science and Technology. 2008;68(9):2178-83.
[27] Lyckfeldt O, Ferreira JMF. Processing of porous ceramics by `starch consolidation'. Journal of the European Ceramic Society. 1998;18(2):131-40.
[28] Li WZ, Xie SS, Qian LX, Chang BH, Zou BS, Zhou WY, et al. Large-Scale Synthesis of Aligned Carbon Nanotubes. Science. 1996;274(5293):1701-3.
[29] Fan S, Chapline MG, Franklin NR, Tombler TW, Cassell AM, Dai H. Self-Oriented Regular Arrays of Carbon Nanotubes and Their Field Emission Properties. Science. 1999;283(5401):512-4.
[30] Herold-Schmidt U, Hinsberger R. Abrasive wear resistance of anisotropic two phase Fe-Ni-C steels. Wear. 1987;120(2):151-60.
[31] Sui YC, Acosta DR, González-León JA, Bermúdez A, Feuchtwanger J, Cui BZ, et al. Structure, Thermal Stability, and Deformation of Multibranched Carbon Nanotubes Synthesized by CVD in the AAO Template. The Journal of Physical Chemistry B. 2001;105(8):1523-7.

[32] Upadhyayula VKK, Deng S, Mitchell MC, Smith GB. Application of carbon nanotube technology for removal of contaminants in drinking water: A review. Science of The Total Environment. 2009;408(1):1-13.
[33] Stafiej A, Pyrzynska K. Adsorption of heavy metal ions with carbon nanotubes. Separation and Purification Technology. 2007;58(1):49-52.
[34] Li YH, Ding J, Luan Z, Di Z, Zhu Y, Xu C, et al. Competitive adsorption of Pb2+, Cu2+ and Cd2+ ions from aqueous solutions by multiwalled carbon nanotubes. Carbon. 2003;41(14):2787-92.
[35] Li YH, Zhao YM, Hu WB, Ahmad I, Zhu YQ, Peng XJ, et al. Carbon nanotubes – the promising adsorbent in wastewater treatment. Physics. 2007;61:698–702.
[36] Park SJ, Lee DG. Development of CNT-metal-filters by direct growth of carbon nanotubes. Current Applied Physics. 2006;6(Supplement 1):e182-e6.
[37] Ajayan PM. Nanotubes from Carbon. Chemical Reviews. 1999(99):1787-99.
[38] Kalita SJ, Bose S, Hosick HL, Bandyopadhyay A. Development of controlled porosity polymer-ceramic composite scaffolds via fused deposition modeling. Materials Science and Engineering: C. 2003;23(5):611-20.
[39] Cui C, Baughman RH, Iqbal Z, Kazmar TR, Dahlstrom DK. Improved piezoelectric ceramic/polymer composites for hydrophone applications. Synthetic Metals. 1997;85(1-3):1391-2.
[40] Babski K, Boczkowska A, Kurzydlowski K. Microstructure–properties relationship in ceramic–elastomer composites with 3D connectivity of phases. Journal of Materials Science. 2009;44(6):1456-61.
[41] Konopka K, Boczkowska A, Batorski K, Szafran M, Kurzydlowski KJ. Microstructure and properties of novel ceramic-polymer composites. Materials Letters. 2004;58(30):3857-62.
[42] Gómez de Salazar JM, Barrena MI, Morales G, Matesanz L, Merino N. Compression strength and wear resistance of ceramic foams-polymer composites. Materials Letters. 2006;60(13-14):1687-92.
[43] Kroto HW, Heath JR, O'Brien SC, Curl RF, Smalley RE. C60: Buckminsterfullerene. Nature. 1985(318):162-3.
[44] Novoselov KS, Geim AK, Morozov SV, Jiang D, Zhang Y, Dubonos SV, et al. Electric Field Effect in Atomically Thin Carbon Films. Science. 2004;306(5696):666-9.
[45] Mauter MS, Elimelech M. Environmental applications of carbon-based nanomaterials. Environmental Science and Technology. 2008;42(16):5843-59.
[46] Odom TW, Huang JL, Kim P, Lieber CM. Structure and Electronic Properties of Carbon Nanotubes. Phys Chem. 2000(104):2794-809.
[47] Hamada N, Sawada S-i, Oshiyama A. New one-dimensional conductors: Graphitic microtubules. Physical Review Letters. 1992;68(10):1579-81.
[48] Audier M, Oberlin A, Coulon M, Bonnetain L. Morphology and crystalline order in catalytic carbon. Carbon. 1981(19):217-24.
[49] Rodriguez NM, Chambers A, Baker RT. Catalytic engineering of carbon nanostructures. Langmuir. 1995(11):3862-6.

[50] Saito Y. Nanoparticles and filled nanocapsules. Carbon. 1995;33(7):979-88.
[51] Hariss PJF. Carbon nanotubes and related structures: Cambridge Univ. Press; 1999.
[52] Journet C MW, Bernier P, Loiseau A, de la Chapelle ML, Lefrant S, et al. Large-scale production of single-walled carbon nanotubes by the electric-arc technique. Nature. 1997;388:756–8.
[53] Yahachi S, Keishi N, Kenichiro K, Takehisa M. Carbon nanocapsules and single-layered nanotubes produced with platinum-group metals (Ru, Rh, Pd, Os, Ir, Pt) by arc discharge. Journal of Applied Physics. 1996;80(5):3062-7.
[54] Rinzler AG LJ, Dai H, Nikolaev P, Huffman CB, Rodriguez- Macias FJ et al. Large-scale purification of single-wall carbon nanotubes: Process, product and characterization. Applied Physics. 1998;67(1):29–37.
[55] Zhang Y, Iijima S. Formation of single-wall carbon nanotubes by laser ablation of fullerenes at low temperature. Applied Physics Letters. 1999;75(20):3087-9.
[56] Ren ZF HZ, Xu JW, Wang DZ, Wen JG, Wang JH et al. growth of a single freestanding multiwall carbon nanotube on each nanonickel dot. Applied Physics Letters. 1999;75(8):1086–8.
[57] Ren ZF HZ, Xu JW, Wang JH, Bush P, Siegal MP et al. Synthesis of large arrays of well-aligned carbon nanotubes on glass. Science. 1998;282:1105–7.
[58] Huang ZP XJ, Ren ZF, Wang JH, Siegal MP, Provencio PN. Growth of highly oriented carbon nanotubes by plasmaenhanced hot filament chemical vapor deposition. Applied Physics Letters. 1998;73(26):3845–7.
[59] Guo T, Nikolaev P, Thess A, Colbert DT, Smalley RE. Catalytic growth of single-walled manotubes by laser vaporization. Chemical Physics Letters. 1995;243(1–2):49-54.
[60] Guo T, Nikolaev P, Rinzler AG, Tomanek D, Colbert DT, Smalley RE. Self-Assembly of Tubular Fullerenes. The Journal of Physical Chemistry. 1995;99(27):10694-7.
[61] Rinzler AG, Liu J, Dai H, Nikolaev P, Huffman CB, Rodríguez-Macías FJ, et al. Large-scale purification of single-wall carbon nanotubes: process, product, and characterization. Applied Physics A: Materials Science & Processing. 1998;67(1):29-37.
[62] Wei BQ, Vajtai R, Ajayan PM. Sequence growth of carbon fibers and nanotube networks by CVD process. Carbon. 2003;41(1):185-8.
[63] Tibbetts GG, Devour MG, Rodda EJ. An adsorption-diffusion isotherm and its application to the growth of carbon filaments on iron catalyst particles. Carbon. 1987;25(3):367-75.
[64] Tibbetts GG. Why are carbon filaments tubular? Journal of Crystal Growth. 1984;66(3):632-8.
[65] Du C, Pan N. CVD growth of carbon nanotubes directly on nickel substrate. Materials Letters. 2005;59(13):1678-82.

[66] Dai H. Carbon nanotubes: opportunities and challenges. Surface Science. 2002;500(1-3):218-41.
[67] Derbyshire FJ, Presland AEB, Trimm DL. Graphite formation by the dissolution--precipitation of carbon in cobalt, nickel and iron. Carbon. 1975;13(2):111-3.
[68] Baker RTK. Catalytic growth of carbon filaments. Carbon. 1989;27(3):315-23.
[69] Baker RTK, Harris PS. Formation of Filamentous Carbon in Chemistry and Physics of Carbon. 1978:83.
[70] Sinnott SB, Andrews R, Qian D, Rao AM, Mao Z, Dickey EC, et al. Model of carbon nanotube growth through chemical vapor deposition. Chemical Physics Letters. 1999;315(1-2):25-30.
[71] Deck CP, Vecchio K. Growth mechanism of vapor phase CVD-grown multi-walled carbon nanotubes. Carbon. 2005;43(12):2608-17.
[72] Baker RTK, Barber MA, Harris PS, Feates FS, Waite RJ. Nucleation and growth of carbon deposits from the nickel catalyzed decomposition of acetylene. Journal of Catalysis. 1972;26(1):51-62.
[73] Li C, Zhu H, Suenaga K, Wei J, Wang K, Wu D. Diameter dependent growth mode of carbon nanotubes on nanoporous SiO2 substrates. Materials Letters. 2009;63(15):1366-9.
[74] Ren ZF, Huang ZP, Wang DZ, Wen JG, Xu JW, Wang JH, et al. Growth of a single freestanding multiwall carbon nanotube on each nanonickel dot. Applied Physics Letters. 1999;75(8):1086-8.
[75] Huang ZP, Xu JW, Ren ZF, Wang JH, Siegal MP, Provencio PN. Growth of highly oriented carbon nanotubes by plasma-enhanced hot filament chemical vapor deposition. Applied Physics Letters. 1998;73(26):3845-7.
[76] Bower C, Zhou O, Zhu W, Werder DJ, Jin S. Nucleation and growth of carbon nanotubes by microwave plasma chemical vapor deposition. Applied Physics Letters. 2000;77(17):2767-9.
[77] Okai M, Muneyoshi T, Yaguchi T, Sasaki S. Structure of carbon nanotubes grown by microwave-plasma-enhanced chemical vapor deposition. Applied Physics Letters. 2000;77(21):3468-70.
[78] Ren ZF, Huang ZP, Xu JW, Wang JH, Bush P, Siegal MP, et al. Synthesis of Large Arrays of Well-Aligned Carbon Nanotubes on Glass. Science. 1998;282(5391):1105-7.
[79] Yakobson BI, Brabec CJ, Bernholc J. Nanomechanics of Carbon Tubes: Instabilities beyond Linear Response. Physical Review Letters. 1996;76(14):2511.
[80] Salvetat J-P, Briggs GAD, Bonard J-M, Bacsa RR, Kulik AJ, Stöckli T, et al. Elastic and Shear Moduli of Single-Walled Carbon Nanotube Ropes. Physical Review Letters. 1999;82(5):944.
[81] Wong EW, Sheehan PE, Lieber CM. Nanobeam Mechanics: Elasticity, Strength, and Toughness of Nanorods and Nanotubes. Science. 1997;277(5334):1971-5.

[82] Demczyk BG, Wang YM, Cumings J, Hetman M, Han W, Zettl A, et al. Direct mechanical measurement of the tensile strength and elastic modulus of multiwalled carbon nanotubes. Materials Science and Engineering A. 2002;334(1-2):173-8.
[83] Kuan HC, Ma CCM, Chang WP, Yuen SM, Wu HH, Lee TM. Synthesis, thermal, mechanical and rheological properties of multiwall carbon nanotube/waterborne polyurethane nanocomposite. Composites Science and Technology. 2005;65(11-12):1703-10.
[84] Lide DR. CRC Handbook of Chemistry and Physics. 73 ed: CRC Press; 1993.
[85] Lasjaunias JC. Thermal properties of carbon nanotubes. Comptes Rendus Physique. 2003;4(9):1047-54.
[86] White CT, Todorov TN. Carbon nanotubes as long ballistic conductors. Nature. 1998;393(6682):240-2.
[87] Huxtable ST, Cahill DG, Shenogin S, Xue L, Ozisik R, Barone P, et al. Interfacial heat flow in carbon nanotube suspensions. Nature Materials. 2003;2(11):731-4.
[88] Nan CW, Liu G, Lin Y, Li M. Interface effect on thermal conductivity of carbon nanotube composites. Applied Physics Letters. 2004;85(16):3549-51.
[89] Yang K, Gu M, Guo Y, Pan X, Mu G. Effects of carbon nanotube functionalization on the mechanical and thermal properties of epoxy composites. Carbon. 2009;47(7):1723-37.
[90] Niyogi S, Hamon MA, Hu H, Zhao B, Bhowmik P, Sen R, et al. Chemistry of Single-Walled Carbon Nanotubes. Accounts of Chemical Research. 2002;35(12):1105-13.
[91] Baughman RH, Zakhidov AA, de Heer WA. Carbon Nanotubes-the Route Toward Applications. Science. 2002;297(5582):787-92.
[92] Lee NS, Chung DS, Han IT, Kang JH, Choi YS, Kim HY, et al. Application of carbon nanotubes to field emission displays. Diamond and Related Materials. 2001;10(2):265-70.
[93] Teo KBK, Chhowalla M, Amaratunga GAJ, Milne WI, Pirio G, Legagneux P, et al. Field emission from dense, sparse, and patterned arrays of carbon nanofibers. Applied Physics Letters. 2002;80(11):2011-3.
[94] de Jonge N, Lamy Y, Schoots K, Oosterkamp TH. High brightness electron beam from a multi-walled carbon nanotube. Nature. 2002;420(6914):393-5.
[95] Semet V, Vu Thien B, Vincent P, Guillot D, Teo KBK, Chhowalla M, et al. Field electron emission from individual carbon nanotubes of a vertically aligned array. Applied Physics Letters. 2002;81(2):343-5.
[96] Milne WI, Teo KBK, Amaratunga GAJ, Lacerda R, Legagneux P, Pirio G, et al. Aligned carbon nanotubes/fibers for applications in vacuum microwave devices. Current Applied Physics. 2004;4(5):513-7.
[97] Saito Y, Uemura S. Field emission from carbon nanotubes and its application to electron sources. Carbon. 2000;38(2):169-82.

[98] Sugie H, Tanemura M, Filip V, Iwata K, Takahashi K, Okuyama F. Carbon nanotubes as electron source in an x-ray tube. Applied Physics Letters. 2001;78(17):2578-80.
[99] Yue GZ, Qiu Q, Bo G, Cheng Y, Zhang J, Shimoda H, et al. Generation of continuous and pulsed diagnostic imaging x-ray radiation using a carbon-nanotube-based field-emission cathode. Applied Physics Letters. 2002;81(2):355-7.
[100] Graham AP, Duesberg GS, Seidel R, Liebau M, Unger E, Kreupl F, et al. Towards the integration of carbon nanotubes in microelectronics. Diamond and Related Materials.13(4-8):1296-300.
[101] Martel R, Schmidt T, Shea HR, Hertel T, Ph A. Single- and multi-wall carbon nanotube field-effect transistors. Applied Physics Letters. 1998;73(17):2447-9.
[102] Endo M, Kim YA, Hayashi T, Nishimura K, Matusita T, Miyashita K, et al. Vapor-grown carbon fibers (VGCFs): Basic properties and their battery applications. Carbon. 2001;39(9):1287-97.
[103] An KH, Kim WS, Park YS, Moon JM, Bae DJ, Lim SC, et al. Electrochemical Properties of High-Power Supercapacitors Using Single-Walled Carbon Nanotube Electrodes. Advanced Functional Materials. 2001;11(5):387-92.
[104] Chunming N, Enid KS, Robert H, David M, Howard T. High power electrochemical capacitors based on carbon nanotube electrodes. Applied Physics Letters. 1997;70(11):1480-2.
[105] Kong J, Franklin NR, Zhou C, Chapline MG, Peng S, Cho K, et al. Nanotube Molecular Wires as Chemical Sensors. Science. 2000;287(5453):622-5.
[106] Yeh M-K, Tai N-H, Lin Y-J. Mechanical properties of phenolic-based nanocomposites reinforced by multi-walled carbon nanotubes and carbon fibers. Composites Part A: Applied Science and Manufacturing. 2008;39(4):677-84.
[107] Abe H, Shimizu T, Ando A, Tokumoto H. Electric transport and mechanical strength measurements of carbon nanotubes in scanning electron microscope. Physica E: Low-dimensional Systems and Nanostructures. 2004;24(1-2):42-5.
[108] Hornbostel B, Pötschke P, Kotz J, Roth S. Mechanical properties of triple composites of polycarbonate, single-walled carbon nanotubes and carbon fibres. Physica E: Low-dimensional Systems and Nanostructures. 2008;40(7):2434-9.
[109] Xiong J, Zheng Z, Qin X, Li M, Li H, Wang X. The thermal and mechanical properties of a polyurethane/multi-walled carbon nanotube composite. Carbon. 2006;44(13):2701-7.
[110] Wang J, Xie H, Xin Z. Thermal properties of paraffin based composites containing multi-walled carbon nanotubes. Thermochimica Acta. 2009;488(1-2):39-42.
[111] Sahoo NG, Jung YC, Yoo HJ, Cho JW. Influence of carbon nanotubes and polypyrrole on the thermal, mechanical and electroactive shape-memory properties of polyurethane nanocomposites. Composites Science and Technology. 2007;67(9):1920-9.
[112] Kuan H-C, Ma C-CM, Chang W-P, Yuen S-M, Wu H-H, Lee T-M. Synthesis, thermal, mechanical and rheological properties of multiwall carbon

nanotube/waterborne polyurethane nanocomposite. Composites Science and Technology. 2005;65(11-12):1703-10.
[113] Niihara K. New design concept of structural ceramics. Ceramic nanocomposites. Nippon Seramikkusu Kyokai Gakujutsu Ronbunshi/Journal of the Ceramic Society of Japan. 1991;99(1154):974-82.
[114] Mishra RS, Mukherjee AK. Processing of high hardness-high toughness alumina matrix nanocomposites. Materials Science and Engineering A. 2001;301(1):97-101.
[115] Xiea X-L, Maia Y-W, Zhou X-P. Dispersion and alignment of carbon nanotubes in polymer

matrix: A review. Materials Science and Engineering. 2005;49:89-112.
[116] Flahaut E, Peigney A, Laurent C, Marlière C, Chastel F, Rousset A. Carbon nanotube-metal-oxide nanocomposites: microstructure, electrical conductivity and mechanical properties. Acta Materialia. 2000;48(14):3803-12.
[117] An JW, You DH, Lim DS. Tribological properties of hot-pressed alumina-CNT composites. Wear.255(1-6):677-81.
[118] Yang J, Schaller R. Mechanical spectroscopy of Mg reinforced with Al2O3 short fibers and C nanotubes. Materials Science and Engineering A. 2004;370(1-2):512-5.
[119] Harris PJF. Carbon nanotube composites. International Material Reviews. 2004;49(1):31-43.
[120] Qian D, Dickey EC, Andrews R, Rantell T. Load transfer and deformation mechanisms in carbon nanotube-polystyrene composites. Applied Physics Letters. 2000;76(20):2868-70.
[121] Ajayan PM, Stephan O, Colliex C, Trauth D. Aligned Carbon Nanotube Arrays Formed by Cutting a Polymer Resin-Nanotube Composite. Science. 1994;265(5176):1212-4.
[122] Andrews R, Jacques D, Qian D, Rantell T. Multiwall Carbon Nanotubes: Synthesis and Application. Accounts of Chemical Research. 2002;35(12):1008-17.
[123] Zhang WD, Shen L, Phang IY, Liu T. Carbon Nanotubes Reinforced Nylon-6 Composite Prepared by Simple Melt-Compounding. Macromolecules. 2004;37:256-9.
[124] Rawal S. Metal-matrix composites for space applications. JOM Journal of the Minerals, Metals and Materials Society. 2001;53(4):14-7.
[125] Kuzumaki T, Miyazawa K, Ichinose H, Ito K. Processing of carbon nanotube reinforced aluminum composite. Journal of Materials Research. 1998;13(9):2445-9.
[126] Kuzumaki T, Ujiie O, Ichinose H, Ito K. Mechanical Characteristics and Preparation of Carbon Nanotube Fiber-Reinforced Ti Composite. Advanced Engineering Materials. 2000;2(7):416-8.
[127] Kim KT, Cha SI, Hong SH, Hong SH. Microstructures and tensile behavior of carbon nanotube reinforced Cu matrix nanocomposites. Materials Science and Engineering: A. 2006;430(1-2):27-33.

[128] Chen WX, Tu JP, Wang LY, Gan HY, Xu ZD, Zhang XB. Tribological application of carbon nanotubes in a metal-based composite coating and composites. Carbon. 2003;41(2):215-22.
[129] Riedel R. Handbook of Ceramic Hard Materials. Germany: Wiley; 2000.
[130] Tjong SC. Carbon Nanotube Reinforced Composites: Metal and Ceramic Matrices. Berlin: Wiley-VCH; 2009.
[131] Becher PF, Hsueh C-H, Angelini P, Tiegs TN. Toughening Behavior in Whisker-Reinforced Ceramic Matrix Composites. Journal of the American Ceramic Society. 1988;71(12):1050-61.
[132] Marshall DB, Oliver WC. Measurement of Interfacial Mechanical Properties in Fiber-Reinforced Ceramic Composites. Journal of the American Ceramic Society. 1987;70(8):542-8.
[133] Zhan G-D, Kuntz JD, Wan J, Mukherjee AK. Single-wall carbon nanotubes as attractive toughening agents in alumina-based nanocomposites. Nat Mater. 2003;2(1):38-42.
[134] Dong SM, Katoh Y, Kohyama A, Schwab ST, Snead LL. Microstructural evolution and mechanical performances of SiC/SiC composites by polymer impregnation/microwave pyrolysis (PIMP) process. Ceramics International. 2002;28(8):899-905.
[135] Zhang S, Sun D, Fu Y, Du H. Toughening of hard nanostructural thin films: a critical review. Surface and Coatings Technology. 2005;198(1-3):2-8.
[136] Fan J-P, Zhuang D-M, Zhao D-Q, Zhang G, Wu M-S, Wei F, et al. Toughening and reinforcing alumina matrix composite with single-wall carbon nanotubes. Applied Physics Letters. 2006;89(12):121910-3.
[137] Kothari AK, Jian K, Rankin J, Sheldon BW. Comparison Between Carbon Nanotube and Carbon Nanofiber Reinforcements in Amorphous Silicon Nitride Coatings. Journal of the American Ceramic Society. 2008;91(8):2743-6.
[138] Padture NP. Multifunctional Composites of Ceramics and Single-Walled Carbon Nanotubes. Advanced Materials. 2009;21(17):1767-70.
[139] Xia Z, Riester L, Curtin WA, Li H, Sheldon BW, Liang J, et al. Direct observation of toughening mechanisms in carbon nanotube ceramic matrix composites. Acta Materialia. 2004;52(4):931-44.
[140] Zhan G, Kuntz JD, Mukherjee AK, inventors; Anisotropic thermal applications of composites of ceramics and carbon nanotubes. US. 2005.
[141] Wang X, Padture NP, Tanaka H. Contact-damage-resistant ceramic/single-wall carbon nanotubes and ceramic/graphite composites. Nat Mater. 2004;3(8):539-44.
[142] Mangsen GE, Lambertson WA, Best B. Hot Pressing of Aluminum Oxide. Journal of the American Ceramic Society. 1960;43(2):55-9.
[143] Peigney A, Flahaut E, Laurent C, Chastel F, Rousset A. Aligned carbon nanotubes in ceramic-matrix nanocomposites prepared by high-temperature extrusion. Chemical Physics Letters. 2002;352(1-2):20-5.

[144] Shen Z, Johnsson M, Zhao Z, Nygren M. Spark Plasma Sintering of Alumina. Journal of the American Ceramic Society. 2002;85(8):1921-7.
[145] Chen W, Anselmi-Tamburini U, Garay JE, Groza JR, Munir ZA. Fundamental investigations on the spark plasma sintering/synthesis process: I. Effect of dc pulsing on reactivity. Materials Science and Engineering A. 2005;394(1-2):132-8.
[146] Poyato R, Vasiliev AL, Padture NP, Tanaka H, Nishimura T. Aqueous colloidal processing of single-wall carbon nanotubes and their composites with ceramics. Nanotechnology. 2006;17(6):1770.
[147] Rul S, Laurent C, Peigney A, Rousset A. Carbon nanotubes prepared in situ in a cellular ceramic by the gelcasting-foam method. Journal of the European Ceramic Society. 2003;23(8):1233-41.
[148] Bae EJ, Choi WB, Jeong KS, Chu JU, Park GS, Song S, et al. Selective Growth of Carbon Nanotubes on Pre-patterned Porous Anodic Aluminum Oxide. Advanced Materials. 2002;14(4):277-9.
[149] de Heer WA, Châtelain A, Ugarte D. A Carbon Nanotube Field-Emission Electron Source. Science. 1995;270(5239):1179-80.
[150] Sohn JI, Kim Y-S, Nam C, Cho BK, Seong T-Y, Lee S. Fabrication of high-density arrays of individually isolated nanocapacitors using anodic aluminum oxide templates and carbon nanotubes. Applied Physics Letters. 2005;87(12):123115.
[151] Dai H, Hafner JH, Rinzler AG, Colbert DT, Smalley RE. Nanotubes as nanoprobes in scanning probe microscopy. Nature. 1996;384(6605):147-50.
[152] Montanaro L, Jorand Y, Fantozzi G, Negro A. Ceramic foams by powder processing. Journal of the European Ceramic Society. 1998;18(9):1339-50.
[153] Altinkok N, Koker R. Mixture and pore volume fraction estimation in Al2O3/SiC ceramic cake using artificial neural networks. Materials & Design. 2005;26(4):305-11.
[154] Peng HX, Fan Z, Evans JRG. Factors affecting the microstructure of a fine ceramic foam. Ceramics International. 2000;26(8):887-95.
[155] She J, Ohji T, Deng Z-Y. Thermal Shock Behavior of Porous Silicon Carbide Ceramics. Journal of the American Ceramic Society. 2002;85(8):2125-7.
[156] Moreira EA, Innocentini MDM, Coury JR. Permeability of ceramic foams to compressible and incompressible flow. Journal of the European Ceramic Society. 2004;24(10-11):3209-18.
[157] Lopes RrA, Segadaes AM. Microstructure, permeability and mechanical behaviour of ceramic foams. Materials Science and Engineering: A. 1996;209(1-2):149-55.
[158] Inui T, Otowa T. Catalytic combustion of benzene-soot captured on ceramic foam matrix. Applied Catalysis. 1985;14:83-93.
[159] Alvin MA, Lippert TE, Lane JE. Assessment of porous ceramic materials for hot gas filtration applications. American Ceramics Society Bulletin. 1991;70(9):1491–8.

[160] Boczkowska A, Konopka K, Kurzydlowski KJ. Effect of elastomer structure on ceramic-elastomer composite properties. Journal of Materials Processing Technology. 2006;175(1-3):40-4.
[161] Boczkowska A, Babski K, Konopka K, Kurzydlowski KJ. Quantitative description of ceramic-elastomer composites with percolation microstructures. Materials Characterization. 2006;56(4-5):389-93.
[162] Koza E, Leonowicz M, Wojciechowski S, Simancik F. Compressive strength of aluminium foams. Materials Letters. 2004;58(1-2):132-5.
[163] Mahdi E, Hamouda AMS, Sahari BB, Khalid YA. On the Collapse of Cotton/Epoxy Tubes under Axial Static Loading. Applied Composite Materials. 2003;10(2):67-84.
[164] Lee DG, Lim TS, Cheon SS. Impact energy absorption characteristics of composite structures. Composite Structures. 2000;50(4):381-90.
[165] Chen Y-C, Wu S. Piezoelectric composites with 3-3 connectivity by injecting polymer for hydrostatic sensors. Ceramics International. 2004;30(1):69-74.
[166] Mitsakou C, Housiadas C, Eleftheriadis K, Vratolis S, Helmis C, Asimakopoulos D. Lung deposition of fine and ultrafine particles outdoors and indoors during a cooking event and a no activity period. Indoor Air. 2007;17(2):143-52.
[167] Hillie T, Hlophe M. Nanotechnology and the challenge of clean water. Nat Nano. 2007;2(11):663-4.
[168] Li Y-H, Ding J, Luan Z, Di Z, Zhu Y, Xu C, et al. Competitive adsorption of Pb2+, Cu2+ and Cd2+ ions from aqueous solutions by multiwalled carbon nanotubes. Carbon. 2003;41(14):2787-92.
[169] Züttel A, Sudan P, Mauron P, Kiyobayashi T, Emmenegger C, Schlapbach L. Hydrogen storage in carbon nanostructures. International Journal of Hydrogen Energy. 2002;27(2):203-12.
[170] Barhate RS, Ramakrishna S. Nanofibrous filtering media: Filtration problems and solutions from tiny materials. Journal of Membrane Science. 2007;296(1–2):1-8.
[171] Wendorff JH, Agarwal S, Greiner A. Technical Applications of Electrospun Nanofibers. Electrospinning: Wiley-VCH Verlag GmbH & Co. KGaA 2012, p. 185-216.
[172] Podgórski A, Bałazy A, Gradoń L. Application of nanofibers to improve the filtration efficiency of the most penetrating aerosol particles in fibrous filters. Chemical Engineering Science. 2006;61(20):6804-15.
[173] Lee KW, Liu BYH. On the Minimum Efficiency and the Most Penetrating Particle Size for Fibrous Filters. Journal of the Air Pollution Control Association. 1980;30(4):377-81.
[174] Park SJ, Lee DG. Performance improvement of micron-sized fibrous metal filters by direct growth of carbon nanotubes. Carbon. 2006;44(10):1930-5.
[175] Park JH, Yoon KY, Na H, Kim YS, Hwang J, Kim J, et al. Fabrication of a multi-walled carbon nanotube-deposited glass fiber air filter for the enhancement of

nano and submicron aerosol particle filtration and additional antibacterial efficacy. Science of The Total Environment. 2011;409(19):4132-8.
[176] Mostafavi ST, Mehrnia MR, Rashidi AM. Preparation of nanofilter from carbon nanotubes for application in virus removal from water. Desalination. 2009;238(1–3):271-80.
[177] Akasaka T, Watari F. Capture of bacteria by flexible carbon nanotubes. Acta Biomaterialia. 2009;5(2):607-12.
[178] Kang S, Herzberg M, Rodrigues DF, Elimelech M. Antibacterial Effects of Carbon Nanotubes: Size Does Matter! Langmuir. 2008;24(13):6409-13.
[179] Arias LR, Yang L. Inactivation of Bacterial Pathogens by Carbon Nanotubes in Suspensions. Langmuir. 2009;25(5):3003-12.
[180] Li YH, Wang S, Luan Z, Ding J, Xu C, Wu D. Adsorption of cadmium(II) from aqueous solution by surface oxidized carbon nanotubes. Carbon. 2003;41(5):1057-62.
[181] Lu C, Liu C. Removal of nickel(II) from aqueous solution by carbon nanotubes. Journal of Chemical Technology and Biotechnology. 2006;81(12):1932-40.
[182] Di ZC, Ding J, Peng XJ, Li YH, Luan ZK, Liang J. Chromium adsorption by aligned carbon nanotubes supported ceria nanoparticles. Chemosphere. 2006;62(5):861-5.
[183] Luo G, Yao H, Xu M, Cui X, Chen W, Gupta R, et al. Carbon Nanotube-Silver Composite for Mercury Capture and Analysis. Energy & Fuels. 2009;24(1):419-26.
[184] Schierz A, Zänker H. Aqueous suspensions of carbon nanotubes: Surface oxidation, colloidal stability and uranium sorption. Environmental Pollution. 2009;157(4):1088-94.
[185] Rao GP, Lu C, Su F. Sorption of divalent metal ions from aqueous solution by carbon nanotubes: A review. Separation and Purification Technology. 2007;58(1):224-31.
[186] Lu C, Chiu H. Adsorption of zinc(II) from water with purified carbon nanotubes. Chemical Engineering Science. 2006;61(4):1138-45.
[187] Li YH, Zhu Y, Zhao Y, Wu D, Luan Z. Different morphologies of carbon nanotubes effect on the lead removal from aqueous solution. Diamond and Related Materials. 2006;15(1):90-4.
[188] Li YH, Di Z, Ding J, Wu D, Luan Z, Zhu Y. Adsorption thermodynamic, kinetic and desorption studies of Pb2+ on carbon nanotubes. Water Research. 2005;39(4):605-9.
[189] Lu C, Chiu H, Liu C. Removal of Zinc(II) from Aqueous Solution by Purified Carbon Nanotubes: Kinetics and Equilibrium Studies. Industrial & Engineering Chemistry Research. 2006;45(8):2850-5.
[190] Salam MA, Al-Zhrani G, Kosa SA. Simultaneous removal of copper(II), lead(II), zinc(II) and cadmium(II) from aqueous solutions by multi-walled carbon nanotubes. Comptes Rendus Chimie. 2012;15(5):398-408.
[191] Ho YS, John Wase DA, Forster CF. Batch nickel removal from aqueous solution by sphagnum moss peat. Water Research. 1995;29(5):1327-32.

[192] Liang P, Liu Y, Guo L, Zeng J, Lu H. Multiwalled carbon nanotubes as solid-phase extraction adsorbent for the preconcentration of trace metal ions and their determination by inductively coupled plasma atomic emission spectrometry. Journal of Analytical Atomic Spectrometry. 2004;19(11):1489-92.
[193] Chen C, Wang X. Adsorption of Ni(II) from aqueous solution using Oxidized multiwall carbon nanotubes. Industrial and Engineering Chemistry Research. 2006;45(26):9144-9.
[194] Tofighy MA, Mohammadi T. Adsorption of divalent heavy metal ions from water using carbon nanotube sheets. Journal of Hazardous Materials. 2011;185(1):140-7.
[195] Gui X, Wei J, Wang K, Cao A, Zhu H, Jia Y, et al. Carbon Nanotube Sponges. Advanced Materials. 2010;22(5):617-21.
[196] Lee C, Baik S. Vertically-aligned carbon nano-tube membrane filters with superhydrophobicity and superoleophilicity. Carbon. 2010;48(8):2192-7.
[197] Chen Z, Zhang L, Tang Y, Jia Z. Adsorption of nicotine and tar from the mainstream smoke of cigarettes by oxidized carbon nanotubes. Applied Surface Science. 2006;252(8):2933-7.
[198] Lam CW, James JT, McCluskey R, Hunter RL. Pulmonary Toxicity of Single-Wall Carbon Nanotubes in Mice 7 and 90 Days After Intratracheal Instillation. Toxicological Sciences. 2004;77(1):126-34.
[199] Liu S, Wei L, Hao L, Fang N, Chang MW, Xu R, et al. Sharper and Faster "Nano Darts" Kill More Bacteria: A Study of Antibacterial Activity of Individually Dispersed Pristine Single-Walled Carbon Nanotube. ACS Nano. 2009;3(12):3891-902.
[200] Sato Y, Yokoyama A, Shibata K-i, Akimoto Y, Ogino S-i, Nodasaka Y, et al. Influence of length on cytotoxicity of multi-walled carbon nanotubes against human acute monocytic leukemia cell line THP-1 in vitro and subcutaneous tissue of rats in vivo. Molecular BioSystems. 2005;1(2):176-82.
[201] Ghafari P, St-Denis CH, Power ME, Jin X, Tsou V, Mandal HS, et al. Impact of carbon nanotubes on the ingestion and digestion of bacteria by ciliated protozoa. Nat Nano. 2008;3(6):347-51.
[202] Roberts AP, Mount AS, Seda B, Souther J, Qiao R, Lin S, et al. In vivo Biomodification of Lipid-Coated Carbon Nanotubes by Daphnia magna. Environmental Science & Technology. 2007;41(8):3025-9.
[203] http://www.sigmaaldrich.com/. [cited; Available from:
[204] Baker Brachmann C, Davies A, Cost GJ, Caputo E, Li J, Hieter P, et al. Designer deletion strains derived from Saccharomyces cerevisiae S288C: A useful set of strains and plasmids for PCR-mediated gene disruption and other applications. Yeast. 1998;14(2):115-32.
[205] Kelsall R, Hamley I, Geoghegan M. Nanoscale Science and Technology: WILEY; 2005.
[206] M. WI. The Principles and Practice of Electron Microscopy. 2nd ed. Cambridge: Cambridge University Press; 1997.

[207] X-Tek. [cited; Available from: http://www.xtekxray.com/products/computed_tomography.html
[208] Mukhopadhyay K, Krishna KM, Sharon M. Fullerenes from camphor: A natural source. Physical Review Letters. 1994;72(20):3182.
[209] Kumar M, Ando Y. A simple method of producing aligned carbon nanotubes from an unconventional precursor - Camphor. Chemical Physics Letters. 2003;374(5-6):521-6.
[210] Kumar M, Ando Y. Carbon Nanotubes from Camphor: An Environment-Friendly Nanotechnology. Physics. 2007(61):643-6.
[211] Kumar M, Ando Y. Chemical Vapor Deposition of Carbon Nanotubes: A Review on Growth Mechanism and Mass Production. Journal of Nanoscience and Nanotechnology. 2010;10(6):3739-58.
[212] Dupuis AC. The catalyst in the CCVD of carbon nanotubes--a review. Progress in Materials Science. 2005;50(8):929-61.
[213] Zhao N, Cui Q, He C, Shi C, Li J, Li H, et al. Synthesis of carbon nanostructures with different morphologies by CVD of methane. Materials Science and Engineering: A. 2007;460-461:255-60.
[214] Liu K, Jiang K, Feng C, Chen Z, Fan S. A growth mark method for studying growth mechanism of carbon nanotube arrays. Carbon. 2005;43(14):2850-6.
[215] Brockner W, Ehrhardt C, Gjikaj M. Thermal decomposition of nickel nitrate hexahydrate, Ni(NO3)2·6H2O, in comparison to Co(NO3)2·6H2O and Ca(NO3)2·4H2O. Thermochimica Acta. 2007;456(1):64-8.
[216] Elrefaie FA, Smeltzer WW. Thermodynamics of nickel-aluminum-oxygen system between 900 and 1400 Electrochemical Society. 1981;128(10):2237-42.
[217] Üstündag E, Subramanian R, Dieckmann R, Sass SL. In situ formation of metal-ceramic microstructures in the Ni-Al-O system by partial reduction reactions. Acta Metallurgica et Materialia. 1995;43(1):383-9.
[218] Trumble KP, Rühle M. The thermodynamics of spinel interphase formation at diffusion-bonded Ni/Al2O3 interfaces. Acta Metallurgica et Materialia. 1991;39(8):1915-24.
[219] Calow CA, Porter IT. The solid state bonding of nickel to alumina. Journal of Materials Science. 1971;6(2):156-63.
[220] Bhaduri SB. Science and technology of ceramic foams. Advanced Performance Materials. 1994;1(3):205-20.
[221] Carty WM, Lednor PW. Monolithic ceramics and heterogeneous catalysts: honeycombs and foams. Current Opinion in Solid State and Materials Science. 1996;1(1):88-95.
[222] Twigg MV, Richardson JT. Fundamentals and Applications of Structured Ceramic Foam Catalysts. Industrial & Engineering Chemistry Research. 2007;46(12):4166-77.

[223] Malgas G, Arendse C, Cele N, Cummings F. Effect of mixture ratios and nitrogen carrier gas flow rates on the morphology of carbon nanotube structures grown by CVD. Journal of Materials Science. 2008;43(3):1020-5.
[224] Wei YY, Eres G, Merkulov VI, Lowndes DH. Effect of catalyst film thickness on carbon nanotube growth by selective area chemical vapor deposition. Applied Physics Letters. 2001;78(10):1394-6.
[225] Kumar M, Ando Y. Controlling the diameter distribution of carbon nanotubes grown from camphor on a zeolite support. Carbon. 2005;43(3):533-40.
[226] Li WZ, Wen JG, Ren ZF. Effect of temperature on growth and structure of carbon nanotubes by chemical vapor deposition. Applied Physics A: Materials Science & Processing. 2002;74(3):397-402.
[227] Harris PJF. Carbon nanotube composites. International Materials Reviews. 2004;49:31-43.
[228] Liu T, Tong Y, Zhang W-D. Preparation and characterization of carbon nanotube/polyetherimide nanocomposite films. Composites Science and Technology. 2007;67(3–4):406-12.
[229] Biron M. Thermoplastics and Thermoplastic Composites. Thermoplastics and Thermoplastic Composites Technical Information for Plastics Users Elsevier Ltd 2007.
[230] Lau K-t, Lu M, Chun-ki L, Cheung H-y, Sheng F-L, Li H-L. Thermal and mechanical properties of single-walled carbon nanotube bundle-reinforced epoxy nanocomposites: the role of solvent for nanotube dispersion. Composites Science and Technology. 2005;65(5):719-25.
[231] Pötschke P, Bhattacharyya Arup R, Janke A, Goering H. Composites of Polycarbonate with Multiwalled Carbon Nanotubes Produced by Melt Mixing. Advances in Polycarbonates: American Chemical Society 2005, p. 148-63.
[232] Zhang WD, Shen L, Phang IY, Liu T. Carbon nanotubes reinforced nylon-6 composite prepared by simple melt-compounding. Macromolecules. 2004;37(2):256-9.
[233] Zhang WD, Phang IY, Liu T. Growth of carbon nanotubes on clay: Unique nanostructured filler for high-performance polymer nanocomposites. Advanced Materials. 2006;18(1):73-7.
[234] Liu T, Phang IY, Shen L, Chow SY, Zhang WD. Morphology and mechanical properties of multiwalled carbon nanotubes reinforced nylon-6 composites. Macromolecules. 2004;37(19):7214-22.
[235] Wise KE, Park C, Siochi EJ, Harrison JS. Stable dispersion of single wall carbon nanotubes in polyimide: the role of noncovalent interactions. Chemical Physics Letters. 2004;391(4–6):207-11.
[236] Besancon BM, Green PF. Polystyrene-based single-walled carbon nanotube nanocomposite thin films: Dynamics of structural instabilities. Macromolecules. 2005;38(1):110-5.
[237] Kashiwagi T, Grulke E, Hilding J, Harris R, Awad W, Douglas J. Thermal degradation and flammability properties of poly(propylene)/carbon nanotube composites. Macromolecular Rapid Communications. 2002;23(13):761-5.

[238] Larrañaga M, Mondragon I, Riccardi CC. Miscibility and mechanical properties of an amine-cured epoxy resin blended with poly(ethylene oxide). Polymer International. 2007;56(3):426-33.
[239] Mondragon I, Fernandez-Nograro F, Valea A, Llano-Ponte R. Dynamic and mechanical properties of DGEBA/poly(propylene oxide) amine based epoxy resins as a function of stoichiometry. European Polymer Journal. 1996;32(2):257-66.
[240] Saleh NJ, Razak A, Tooma MA, Aziz M. A Study on Mechanical Properties of Epoxy Resin Cured at Constant Curing Time and Temperature with Different Hardeners. Eng & Tech Journal,. 2011;29(9):1804-18.
[241] Aziz M. A STUDY ON THE EFFECT OF HARDENER ON THE MECHANICAL PROPERTIES OF EPOXY RESIN. University of Technology, 2010.
[242] Sahoo NG, Cheng HKF, Cai J, Li L, Chan SH, Zhao J, et al. Improvement of mechanical and thermal properties of carbon nanotube composites through nanotube functionalization and processing methods. Materials Chemistry and Physics. 2009;117(1):313-20.
[243] Hocine NA, Médéric P, Aubry T. Mechanical properties of polyamide-12 layered silicate nanocomposites and their relations with structure. Polymer Testing. 2008;27(3):330–9.
[244] Zhang Y, Yang JH, Ellis TS, Shi J. Crystal structures and their effects on the properties of polyamide 12/clay and polyamide 6–polyamide 66/clay nanocomposites. Journal of Applied Polymer Science. 2006;100(6):4782-94.
[245] Sandler JKW, Pegel S, Cadek M, Gojny F, van Es M, Lohmar J, et al. A comparative study of melt spun polyamide-12 fibres reinforced with carbon nanotubes and nanofibres. Polymer. 2004;45(6):2001-15.
[246] Gojny FH, Wichmann MHG, Fiedler B, Bauhofer W, Schulte K. Influence of nano-modification on the mechanical and electrical properties of conventional fibre-reinforced composites. Composites Part A: Applied Science and Manufacturing. 2005;36(11):1525-35.
[247] Shen Z, Bateman S, Wu DY, McMahon P, Dell'Olio M, Gotama J. The effects of carbon nanotubes on mechanical and thermal properties of woven glass fibre reinforced polyamide-6 nanocomposites. Composites Science and Technology. 2009;69(2):239-44.
[248] Pillai S, Ray S. Epoxy-based carbon nanotubes reinforced composites; 2011.
[249] Brady-Estévez AS, Nguyen TH, Gutierrez L, Elimelech M. Impact of solution chemistry on viral removal by a single-walled carbon nanotube filter. Water Research. 2010;44(13):3773-80.
[250] Kanyó T, Kónya Z, Kukovecz Á, Berger F, Dékány I, Kiricsi I. Quantitative Characterization of Hydrophilic−Hydrophobic Properties of MWNTs Surfaces. Langmuir. 2004;20(5):1656-61.
[251] Huang TS, Tzeng Y, Liu YK, Chen YC, Walker KR, Guntupalli R, et al. Immobilization of antibodies and bacterial binding on nanodiamond and carbon

nanotubes for biosensor applications. Diamond and Related Materials. 2004;13(4–8):1098-102.
[252] Guan T, Yao M. Use of carbon nanotube filter in removing bioaerosols. Journal of Aerosol Science. 2010;41(6):611-20.
[253] Hinds WC. Aerosol technology : properties, behavior, and measurement of airborne particles. New York [u.a.]: Wiley; 1999.
[254] Adler J. Ceramic Diesel Particulate Filters. International Journal of Applied Ceramic Technology. 2005;2(6):429-39.
[255] Thomas R, Yumei D, Yuelong H, Le Y, Moldenaers P, Weimin Y, et al. Miscibility, morphology, thermal, and mechanical properties of a DGEBA based epoxy resin toughened with a liquid rubber. Polymer. 2008;49(1):278-94.
[256] Mylvaganam K, Zhang LC. Ballistic resistance capacity of carbon nanotubes. Nanotechnology. 2007;18(47):475701.
[257] Corté L, Beaume F, Leibler L. Crystalline organization and toughening: example of polyamide-12. Polymer. 2005;46(8):2748-57.